Ubiquitin-independent disassembly of the SDS22-PP1-Inhibitor-3 complex in PP1 biogenesis by the AAA-ATPase p97 and SEP domain adapters

Inaugural-Dissertation

zur

Erlangung des Doktorgrades

Dr. rer. nat.

der Fakultät für

Biologie

an der

Universität Duisburg-Essen

vorgelegt von

Matthias Weith

aus Lübeck

August 2018

Die der vorliegenden Arbeit zugrunde liegenden Experimente wurden in der Abteilung für Molekularbiologie I am Zentrum für Medizinische Biotechnologie der Universität Duisburg-Essen durchgeführt.

1. Gutachter: Prof. Dr. Hemmo Meyer (Universität Duisburg-Essen)

2. Gutachter: Prof. Dr. Stefan Westermann (Universität Duisburg-Essen)

3. Gutachter: Prof. Dr. Thomas Mayer (Universität Konstanz)

Vorsitzender des Prüfungsausschusses: Prof. Dr. Peter Bayer
(Universität Duisburg-Essen)

Tag der mündlichen Prüfung: 17.01.2019

DuEPublico

Duisburg-Essen Publications online

UNIVERSITÄT DUISBURG ESSEN

Offen im Denken

ub | universitäts bibliothek

Diese Dissertation wird via DuEPublico, dem Dokumenten- und Publikationsserver der Universität Duisburg-Essen, zur Verfügung gestellt und liegt auch als Print-Version vor.

DOI: 10.17185/duepublico/48038
URN: urn:nbn:de:hbz:464-20211109-073347-6

Alle Rechte vorbehalten.

Table of contents

List of figures

List of tables

Summary

Protein phosphatase-1 (PP1) is responsible for a large fraction of all phosphoserine/-threonine dephosphorylation reactions in eukaryotic cells and is as a major regulator of diverse physiological processes. It acts in conjunction with a multitude of binding partners, which serve as targeting or substrate-specifying subunits in PP1 holoenzymes. The catalytic subunit of PP1 alone has low substrate specificity and its activity needs to be restrained before specific holoenzymes are assembled. However, the processes preceding PP1 holoenzyme formation are largely unknown.

Sds22 and Ypi1 are essential interactors of PP1 in *Saccharomyces cerevisiae* and homologous proteins are present throughout eukaryotes. Both yeast and mammalian SDS22 are required for the antagonistic function of PP1 towards the Aurora B kinase during chromosome segregation in mitosis. Ypi1 is also required for this function in yeast but the role of the mammalian homolog Inhibitor-3 (I3) in mitosis was unknown until we found in an earlier study that it limits the amounts of SDS22 bound to PP1 at the kinetochore. In apparent contradiction to earlier studies, we found that SDS22-bound PP1 is inhibited in its mitotic function. Yeast Sds22 and Ypi1/I3 were recently shown to be required for the stability of the PP1-homolog Glc7. Together, these data indicated that SDS22 and I3 do not merely act as PP1 substrate-specifiers in mitosis.

Sds22, Glc7/PP1 and Ypi1/I3 form a stable trimeric complex in budding yeast and a similar complex is formed in mammalian cells by the counterparts SDS22, PP1 and I3 (SPI complex). Biochemical studies had shown that the catalytic subunit in this complex is inactive. This led us to assume that the SPI complex could serve as an intermediate in PP1 biogenesis. Indeed, the experiments presented here reveal that newly synthesized PP1 interacts transiently with SDS22 and I3 before it binds substrate-specifiers such as NIPP1 or MYPT1. We further show that PP1 remains inactive as long as SDS22 and I3 are bound. Thus, the SPI complex also serves to restrain the unspecific phosphatase activity of the newly synthesized catalytic subunit of PP1.

Release of PP1 from the SPI complex does not occur spontaneously but requires the activity of the AAA-ATPase p97. A link between p97 and PP1 was evident from studies on Shp1, an adapter of the yeast p97-homolog Cdc48. Shp1 was recently shown to be required for the stability of newly synthesized Glc7. As a Cdc48 adapter, it mediates the physical interaction between this ATPase and Glc7, Sds22 and Ypi1. Consistently, we find that p97 is recruited by three Shp1-homologous adapters, p47, p37 and UBXN2A to the SPI complex in human cells. However, while Cdc48 and Shp1 in yeast were proposed to allow Glc7 to bind Sds22 and Ypi1, our data clearly indicate that p97 disassembles the SPI complex.

Furthermore, inhibition of p97 activity or depletion of its adapters inhibited the de novo formation of NIPP1- and MYPT1-PP1 holoenzymes. In a mass spectrometry-based survey of

the PP1 interactome, we find that several interactions of PP1 are affected in conditions that inhibit or delay SPI complex disassembly. Of note, this also leads to defects in the mitotic function of PP1. Our results thus reveal a process in PP1 biogenesis, which is required for normal function and holoenzyme formation of this major phosphatase.

Although p97 is known to be recruited by ubiquitination in a plethora of processes, disassembly of the SPI complex proceeded normally despite inhibition of E1 ubiquitin-activating enzymes in cells. To better understand the mechanistic details of the process, we reconsituted SPI complex disassembly by p97 *in vitro*. We found that *in vitro*-translated PP1 can form an SPI complex in rabbit reticulocyte lysates and this complex can be disassembled by supplementation of the lysate with p37. In this setting, we identified the SEP domain in p37 as an essential element for this activity of p97.

Further experiments with purified components were performed by Jonas Seiler and Johannes van den Boom and will be published along with the data presented in this thesis. These experiments revealed direct interaction of the p37 SEP domain with I3, indicating that I3 is the direct target of p97 in the SPI complex. This interaction and disassembly of the SPI complex *in vitro* occurred in the absence of ubiquitination. SPI complex disassembly thus constitutes the first ubiquitin-independent process, in which p97 activity could be demonstrated with a defined substrate.

A range of biochemical approaches established by J. Seiler, J. v. d. Boom and Matthias Kracht showed that p97 unfolds I3 by threading it through the central pore of the hexamer. This uncovers a binding site on PP1, which is required for formation of holoenzymes with the majority of its interactors. The release of I3 allowed subsequent binding of the substrate-specifier NIPP1 and thus, SPI complex disassembly *in vitro* fully recapitulated the process observed in cells. Importantly, the SPI complex was efficiently disassembled *in vitro* with sub-stoichiometric concentrations of p97, opening an avenue for future studies of the enzymatic properties of this ubiquitous and pleiotropic ATPase.

Zusammenfassung

Protein phosphatase-1 (PP1) katalysiert einen Großteil der Dephosphorylierungsreaktionen an Phosphoserin/-threonin Aminosäureresten in eukaryontischen Zellen und reguliert so eine Vielzahl physiologischer Vorgänge. PP1 kooperiert mit vielen Bindungspartnern, die als Lokalisation- und Spezifität-bestimmende Untereinheiten in PP1-Holoenzymen dienen. Die katalytische Untereinheit alleine hat nur geringe Substratspezifität und ihre Aktivität außerhalb von Holoenzymen muss beschränkt werden. Wie diese Anforderung in der Biogenese von PP1 erfüllt wird, ist noch unbekannt.

Sds22 und Ypi1 sind essentielle Bindungspartner von PP1 in *Saccharomyces cerevisiae* und Homologe sind in allen Eukaryonten vorhanden. Sowohl in Hefe als auch in Säugetierzellen ist SDS22 für den Antagonismus zwischen PP1 und der Kinase Aurora B erforderlich, welcher die Chromosomenteilung während der Mitose steuert. Das Hefeprotein Ypi1 ist für diese Funktion von PP1 ebenfalls notwendig. In Säugetierzellen war keine Funktion des homologen Inhibitor-3 (I3) in der Mitose bekannt, bis wir in einer früheren Untersuchung zeigen konnten, dass es die Bindung von SDS22 an Kinetochor-gebundendem PP1 begrenzt. In scheinbarem Widerspruch zu vorherigen Ergebnissen fanden wir, dass PP1 in seiner mitotischen Funktion durch SDS22-Bindung inhibiert wird. In Hefezellen wurde vor Kurzem gezeigt, dass Sds22 und Ypi1/I3 für die Stabilität von Glc7/PP1 benötigt werden. Zusammen genommen sprechen diese Daten dagegen, dass die Hauptfunktion von SDS22 und I3 in der Bestimmung der Substratspezifität von PP1 in der Mitose liegt.

In *S. cerevisiae* bilden Sds22, Glc7 und Ypi1 einen stabilen trimeren Komplex und ein ähnlicher Komplex zwischen den Homologen SDS22, PP1 und I3 (SPI Komplex) existiert in Säugerzellen. Biochemische Untersuchungen haben gezeigt, dass die katalytische Untereinheit in diesem Komplex inaktiv ist. Das führte uns zu der Annahme, dass der SPI Komplex ein Übergangsstadium in der Biogenese von PP1 darstellen könnte. Tatsächlich zeigen Experimente in dieser Arbeit, dass die neusynthetisierte katalytische PP1-Untereinheit transient mit SDS22 und I3 interagiert, bevor sie Holoenzyme mit NIPP1 oder MYPT1 bildet. Wir zeigen weiterhin, dass PP1 inaktiv bleibt, solange SDS22 und I3 gebunden sind. Der SPI Komplex dient also auch dazu, die unspezifische Aktivität des neusynthetisierten PP1 zu beschränken.

Die Freisetzung von PP1 aus dem SPI Komplex erfolgt jedoch nicht spontan, sondern unter Beteiligung der AAA-ATPase p97. Eine Verbindung zwischen p97 und PP1 wurde in Studien an Shp1, einem Adapter der homologen ATPase Cdc48 in Hefe, gefunden. Vor kurzem konnte gezeigt werden, dass Shp1 benötigt wird um neusynthetisiertes PP1 zu stabilisieren. Als Cdc48-Adapter vermittelt es die direkte Bindung zwischen der ATPase und Glc7, Sds22 und Ypi1. Wir zeigen hier, dass p97 in menschlichen Zellen durch die drei Shp1-homologen Adapter p47, p37 und UBXN2A zum SPI Komplex rekrutiert wird. Während vorgeschlagen

wurde, dass Cdc48 und Shp1 die Bindung von Glc7 an Sds22 und Ypi1 ermöglichen, zeigen unsere Daten klar, dass p97 den SPI Komplex löst.

Inhibition der p97 Aktivität oder Depletion der Adapter führte außerdem zu einer geringeren Neubildung der Holoenzyme NIPP1- und MYPT1-PP1. In einer massenspektometrischen Untersuchung des PP1-Interaktoms finden wir veränderte Abundanzen mehrerer Bindungspartner in Bedingungen, die die Lösung des SPI Komplexes behindern. Wir beobachten außerdem, dass die mitotische Funktion von PP1 in diesen Bedingungen gestört ist. Unsere Ergebnisse beschreiben somit einen Vorgang in der Biogenese von PP1, der die normale Funktion und die Bildung von Holoenzymen dieser Phosphatase sicher stellt.

Obwohl bekannt ist, dass p97 in einer Reihe von Funktionen durch die Ubiquitinierung von Substraten gesteuert ist, wird die Lösung des SPI Komplexes in Zellen durch Inhibition der Ubiquitin-aktivierenden E1-Enzyme nicht beeinträchtigt. Um den Mechanismus besser zu verstehen, haben wir den SPI Komplex und seine Lösung durch p97 *in vitro* rekonstituiert. *In vitro*-translatiertes PP1 bildet in Retikulozytenlysat einen SPI Komplex und dieser kann durch Zugabe von p37 zum Lysat zur Lösung gebracht werden. Durch solche Experimente können wir zeigen, dass die SEP Domäne in p37 für die Funktion von p97 in diesem Prozess notwendig ist.

Weitere Experimente mit gereinigten Proteinen, durchgeführt von Jonas Seiler und Johannes van den Boom, werden zusammen mit den Ergebnissen dieser Arbeit veröffentlicht. Sie zeigen eine direkte Interaktion der SEP Domäne in p37 mit I3 und somit, dass I3 das direkte Substrat von p97 im SPI Komplex darstellt. Diese Interaktion sowie die Lösung des Komplexes *in vitro* sind ohne Ubiquitin möglich. Somit ist die Lösung des SPI Komplexes der erste Ubiquitin-unabhängige Prozess, in dem die Funktion von p97 an einem definierten Substrat gezeigt wurde.

Mittels biochemischer Methoden, die von J. Seiler, J. v. d. Boom und Matthias Kracht etabliert wurden, zeigen wir, dass I3 von p97 durch die zentrale Pore gezogen und dabei entfaltet wird. Dadurch wird eine Bindungsstelle an PP1 frei gelegt, die zur Bildung von Holoenzymen mit der Mehrzahl der PP1-Bindungspartner benötigt wird. Die Freisetzung von I3 ermöglichte gleichzeitig die Bindung von NIPP1 und somit wird der in Zellen beobachtete Prozess durch die *in vitro* Rekonsitution vollständig nachvollzogen. Die Lösung des SPI Komplexes *in vitro* erfolgte effizient bei sub-stöchiometrischen Konzentrationen von p97 und könnte so in Zukunft enzymkinetische Studien dieser ubiquitär exprimierten, pleiotropen ATPase ermöglichen.

I Introduction

I. 1: Protein phosphatase-1 (PP1)

I.1.1 Classification of protein phosphatases

Phosphorylation is the most abundant post-translational modification (PTM) of proteins, predicted to occur on 90 % of the expressed human proteome (Sharma et al., 2014). It is a major mode of cellular signaling, since the attachment of a negatively charged phosphate can change many properties of the target, such as its conformation, activity and interactions. Furthermore, crosstalk with other PTMs such as ubiquitination can affect turnover, localization and other properties (Hunter, 2007). Although regulatory phosphorylation also occurs on lipids, carbohydrates and other molecules, this aspect will not be further discussed here. The number of human genes encoding protein kinases, which transfer the γ-phosphate of ATP to their targets, is estimated to be 538 (Chen et al., 2017). To balance these activities, the human genome contains 189 genes encoding protein phosphatases.

Phosphatases are a vast group of enzymes able to catalyze the hydrolytic removal of phosphate groups from modified amino acids but also from non-protein substrates. The most widely studied phospho-modification of proteins occurs on the residues serine (Ser), threonine (Thr) and tyrosine (Tyr), yielding the phosphorylated residues pSer, pThr and pTyr, which account for 84.1 %, 15.5 % and 0.4 % of the *O*-linked phosphoproteome, respectively (Sharma et al., 2014). Most phosphatases show either specificity for pSer and pThr, with some preference for one or the other, or for pTyr (see below). Nitrogen-linked phosphorylation on histidine is a pivotal mechanism of regulation in prokaryotes but has only recently been implicated in eukaryotic signaling cascades (Klumpp and Krieglstein, 2009). Other amino acids are also subject to phosphorylation but seem to play minor roles. Consistently, phosphatases specific for Ser, Thr, Tyr and His account for the largest part of the human protein phosphatase repertoire (Chen et al., 2017).

A widely used classification scheme for protein phosphatases is based on the catalytic mechanism and associated amino acid sequence motifs at the catalytic site (see Figure 1 for an overview). Evolutionary conservation-based classification is less informative, owing to the fact that many phosphatase enzymes underwent convergent evolution (Moorhead et al., 2009). Furthermore, comparison of structural folds of phosphatases in a recent study resulted in similar grouping as the established scheme (Chen et al., 2017).

Despite the low fraction of pTyr in the phosphoproteome, the largest superfamily of phosphatases are the protein tyrosine phosphatases (PTPs), which are encoded by 111 human genes (Chen et al., 2017) and employ covalent attachment of phosphate to a catalytic cysteine residue to remove it from substrates. Some members of this family are also able to dephosphorylate Ser or Thr residues, resulting in their classification as “dual specificity

phosphatases". The haloacid dehydrolases (HAD), encoded by 17 human genes, also display activity towards both groups of phosphorylations. Enzymes in this family contain one magnesium atom in the catalytic center and employ covalent attachment of phosphate to an aspartate residue during dephosphorylation reactions (Seifried et al., 2013). On the other hand, there are two superfamilies of phosphatases, which only display specific activity towards pSer and pThr. The metal-dependent protein phosphatases (PPMs) are an evolutionary diverse family comprising 20 genes in humans. They share a similar structure and catalytic mechanism with the fourth family, the "phosphoprotein phosphatases" (PPP). This family includes protein phosphatase-1, -2A and -2B (PP1, PP2A and PP2B, which is also called calcineurin or PP3) as well as PP4 through PP7, being encoded by 15 genes in total. Both PPMs and PPPs contain two metal ions at their active site. These metals generate hydroxide from one of two bound water molecules, which then performs a nucleophilic attack on the substrate phosphorous atom to release it as inorganic phosphate, without formation of a covalent bond with the enzyme as seen in the PTP and HAD families (Jackson and Denu, 2001; Swingle et al., 2004; Zhang et al., 1996).

The two most abundant members of the PPP family, PP1 and PP2A together account for a substantial part of the total cellular protein phosphatase activity, with estimates running as high as 90 % (Bollen et al., 2010). This is in sharp contrast to only 5 genes encoding these enzymes, including all isoforms. This imbalance to the number of kinases has in the past been interpreted to signify that protein phosphatases work as non-specific counterparts opposing the specific activity of kinases. While the catalytic subunit indeed has the ability to accommodate a wide variety of substrates, it is now established that both PP1 and PP2A are obligate multimeric enzymes and approaches to understand or modulate their function have advanced to acknowledge the regulator-driven specificity of these enzymes (Brautigan, 2013; Virshup and Shenolikar, 2009).

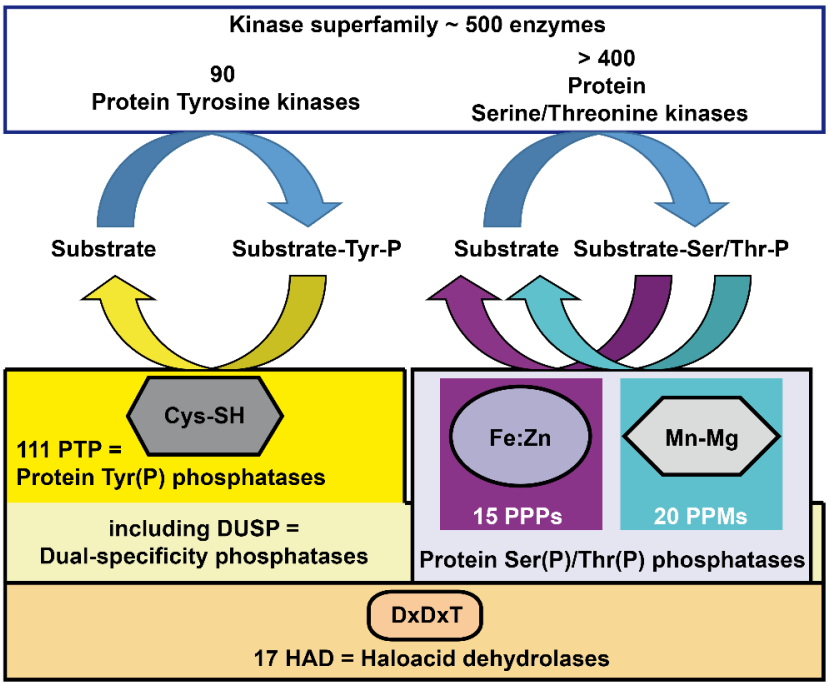

Figure 1: Relationship between protein kinase and phosphatase gene numbers.
Classification scheme for phosphatases based on characteristics of the catalytic sites, see text for details. PPM: metal-dependent protein phosphatases; PPP: phosphoprotein phosphatases;Cys-SH: Cystein residue in the catalytic center; Fe:Zn: iron and zinc; Mn-Mg: mangenese and magensium; DxDxT: consensus amino acid sequence in Haloacid dehydrolases. Adopted from Brautigan et al. 2013.

I.1.2 Discovery and functions of PP1, an obligate multimeric enzyme

The discovery of protein phosphatase-1 can be attributed to the work of Philip Cohen and co-workers, who accomplished the separation of what was formerly thought of as a single, 35-kDa enzyme that enabled dephosphorylation of phosphorylase kinase, into separate fractions of enzymatic activity (Ingebritsen et al., 1980). One fraction of an extract generated from rabbit skeletal muscle was able to specifically dephosphorylate the β-subunit of phosphorylase kinase and its activity was inhibited by two proteinaceous phosphatase inhibitors, called inhibitor-1 (I1) and inhibitor-2 (I2)(Huang and Glinsmann, 1976). This fraction was termed “protein phosphatase-1” as opposed to the second fraction, which displayed specific activity towards the α-subunit of phosphorylase kinase. Whereas the second fraction, initially termed “protein phosphatase-2”, turned out to be a diverse group of phosphatases including PP2A, PP2B and members of the PPM family, protein phosphatase-1 (PP1) proved to be a single enzyme. Interestingly, in size-exclusion chromatography, the peak containing PP1 eluted with an apparent molecular weight between 75 and 80 kDa (Antoniw and Cohen, 1975), whereas after precipitation with 80 % ethanol and subsequent re-extraction, a 35 kDa protein was observed (Brautigan, 2013). This gave a first hint that the catalytic subunit of the phosphatase is mainly found in complex with other proteins.

Whereas in the yeast *Saccharomyces cerevisiae (S. cerevisiae)* there is only one isoform of PP1, encoded by the gene *GLC7*, the catalytic subunit in mammals has four main isoforms, namely PP1α, PP1β (also termed PP1δ), PP1γ_1 as well as the tissue-specific splice variant

PP1γ_2 (Cohen, 2002). Except PP1γ_2, which is rather specifically expressed in sperm and plays an essential role during its maturation (Silva et al., 2014), all isoforms are present throughout studied tissues but are differentially expressed (Heroes et al., 2013). The amino acid (aa) sequences of the isoforms are more than 85 % identical, but the C-terminal ~30 aa residues show strong variations between the isoforms. These residues, together with less severe differences at the N-terminus can contribute to isoform-specific interactions (Bollen et al., 2010; Terrak et al., 2004) and their conservation in mammals indicates functional significance (Andreassen et al., 1998).

PP1 was found to regulate glycogen metabolism and smooth muscle tone, where its activities were studied first (Alessi et al., 1992; Stralfors et al., 1985). However, it was soon recognized that it has much broader roles in cellular physiology. Analysis of hypomorphic mutants of the single yeast homolog of PP1, Glc7, revealed extensive networks of negative genetic interactions (Costanzo et al., 2016; Logan et al., 2008). Important PP1-regulated events were found in cell cycle progression by reversal of checkpoints (Cannon, 2010), in several mitotic processes (see I.2.2), cytoskeleton regulation and epithelial polarization (Grusche et al., 2009; Rodrigues et al., 2015), cellular differentiation and motility (Van Dessel et al., 2015), growth factor signaling (Bennett and Alphey, 2002), vesicular fusion (Peters et al., 1999), gene expression (Rebelo et al., 2015), splicing and spliceosome formation (Llorian et al., 2004; Novoyatleva et al., 2008; Renvoise et al., 2012), DNA damage and general stress response (Connor et al., 2001; Isono et al., 2017; Shimada and Nakanishi, 2013), apoptosis (Djouder et al., 2007) and many more.

It is sometimes helpful to simplify and integrate these highly diverse cellular functions into more general paradigms. For example, in intermediary metabolism protein phosphorylation often activates catabolic and deactivates anabolic pathways. In this context, the function of PP1 is to enhance the storage of nutrients while their supply is plentiful (Ingebritsen and Cohen, 1983a). Similarly, in regulation of cellular survival, PP1 seems to set balancing thresholds by promoting activity of pro-apoptotic signals when mTOR is activated by growth factors, while lack of mTOR signaling promotes inhibition of PP1 by binding to the mitochondria-localized interactor “unconventional RPB5 interactor 1” (URI1), which sequesters PP1 and thereby promotes survival (Djouder et al., 2007). Taking this approach further, Mathieu Bollen assigned to PP1 a general function as a “cellular economizer and reset button” (Ceulemans and Bollen, 2004).

I.1.3 Regulation of PP1 by interacting proteins

Soon after the discovery of the phosphatase enzyme itself, researchers noticed that it was present in high molecular weight complexes such as a 137 kDa complex present on glycogen particles in rabbit muscle, which was composed of the catalytic subunit and a “G” (for glycogen-targeting) subunit. This complex was more active in dephosphorylation of

glycogen phosphorylase than the free catalytic subunit (Stralfors et al., 1985; Tang et al., 1991). These observations were combined by Michael Hubbard and Philip Cohen into a paradigm of regulation, proposing that the activity of PP1 is directed by interactors, which target the catalytic subunit to specific sites or enhance its enzymatic activity towards substrates (Hubbard and Cohen, 1993).

This paradigm has evolved in the following years with the discovery of a plethora of interactors, which specifically bind to PP1 via several conserved interaction motifs. Most of these PP1-interacting proteins (PIPs), contain a variation of the so-called “RVXF” motif, which was shown to serve as an anchor for initial binding, since it provides a rather strong interaction (Heroes et al., 2013; Wakula et al., 2003). A similar function is served in some PIPs by the “SILK” motif. In addition, secondary interactions are established by motifs like “MyPhoNE”, which is present in myosin phosphatase targeting subunit 1 (MYPT1) and allows this substrate-specifier to extend around the catalytic subunit and reach close to the active site, which is distant from the RVXF binding groove (Hendrickx et al., 2009; Terrak et al., 2004; Wakula et al., 2003)(see Figure 2 for an overview). MYPT1 also establishes strong interactions by wrapping its ankyrin repeats around the C-terminus of PP1 (Terrak et al., 2004)(Figure 2B). This kind of interaction is expected to determine isoform-specific interactions of some PIPs.

The overall number of validated PP1 interactors is around 200 (Heroes et al., 2013) and a few examples are shown in Figure 2A. This plethora of interactions serves to regulate PP1 activity in several ways, including its localization to specific cellular compartments or structures. Recruitment by “targeting subunits” can lead to local dephosphorylation of a multitude of substrates or can be regulated by interactors, which narrow down the intrinsically broad substrate range of PP1 (Bollen et al., 2010; Cohen, 2002). Interactors like MYPT1 or spinophilin were shown to provide enhanced interaction surfaces for the substrate, while binding of non-substrates is sterically blocked (Ragusa et al., 2010; Terrak et al., 2004). These interactors are therefore called “substrate-specifiers”. In a number of cases, including for example the centrosomal kinase Nek2, it was observed that interactors themselves are dephosphorylated and vice versa, substrates are also regularly found to bind PP1 via so-called “docking motifs” (Bollen, 2001; Roy and Cyert, 2009).

Broadly, the complexes formed by PP1 with substrate-specifiers or targeting subunits can be referred to as “holoenzymes”, and form the basis for clearly specific activities. This insight into phosphatase function has now fully replaced a way of thinking, which assigned a “bulk” or “housekeeping” role to phosphatases, as opposed to specific activities of kinases (Brautigan, 2013). This view is also rebuttled by two further observations: firstly, dephosphorylation often does not directly follow phosphorylation but depends on specific signals (Sullivan and Morgan, 2007) and second, substrate ranges of kinases are in some cases equal to or even broader than those of phosphatases or their holoenzymes, illustrated

for example by the DNA damage-responsive kinases ATM and ATR, which have hundreds of substrates (Smolka et al., 2007).

A consequence of this mode of regulation is that PP1 functions have to be studied in conjunction with its regulators, which complicates the clarification of PP1-dependent pathways and thus, the specific substrates of many holoenzymes have not been revealed so far. The use of mass spectrometry-based techniques such as label-free quantification and phosphoproteomics is just beginning to fill this gap (Yadav et al., 2017).

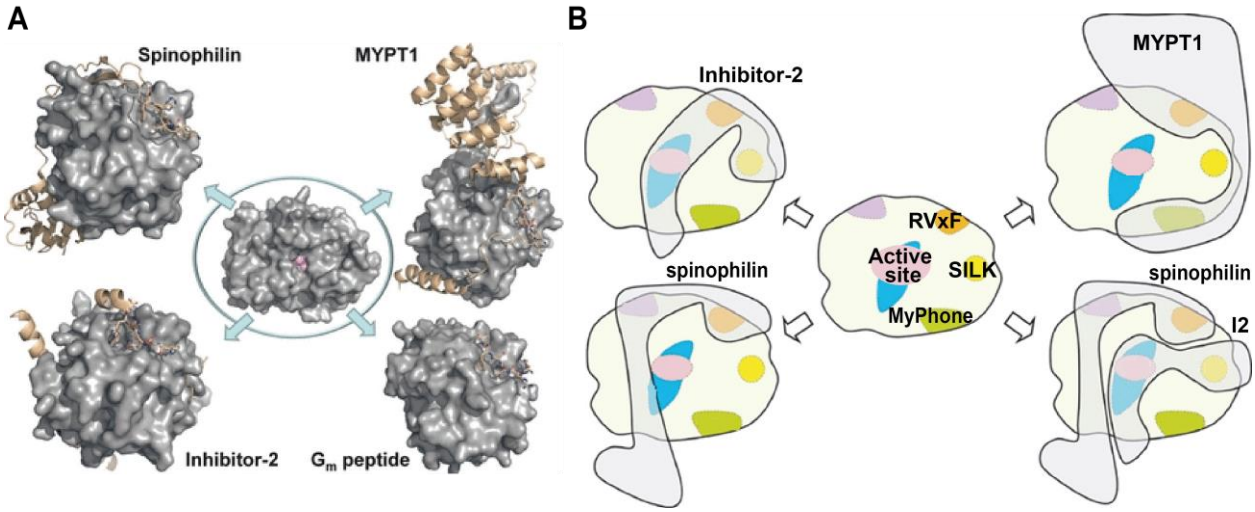

Figure 2: Regulation of PP1 by interacting proteins (PIPs) involves various interaction motifs and complex binding mechanisms.
(**A**) Exemplary PP1 holoenzyme structures. Center: Catalytic subunit of PP1, with active site metal ions depicted as pink spheres (PDB id: 3EGG). Upper left: The spinophilin-PP1 holoenzyme (spinophilin is shown in beige ribbons). Lower left: The I2-PP1 holoenzyme (I2 is shown in beige). Upper right: The MYPT1-PP1 holoenzyme (MYPT1 is shown in beige). Lower right: Complex between an RVxF motif-containing peptide of the G subunit with PP1 (the RVxF peptide is shown in beige). Adopted from (Peti et al., 2013) (**B**) Illustration of binding sites for various interaction motifs on the PP1 catalytic subunit. ("The PP1 binding code" (Heroes et al., 2013)). Only the binding sites for docking motifs discussed in the main text (RVxF, SILK, MyPhoNE) are specified, while others are only indicated by colored areas (SpiDoC, purple and IDoHA, blue). The complexes of spinophilin, I2 and MYPT1 (from lower left to upper right) illustrate that most PIPs interact via several PP1 docking sites, whereas the trimeric complex spinophilin-PP1-I2 (lower right) shows another option to form unique PP1 holoenzymes. PDB: Protein Data Bank. Adopted from (Heroes et al., 2013).

I.1.4 Interactions serve to restrain unspecific activity of the catalytic subunit of PP1

Another aspect of the control of PP1 by regulatory proteins is illustrated by the consequences of unrestrained activity of the catalytic subunit. In contrast to many kinases, which recognize defined peptides by specific interactions at their active site, the active site of PP1 is shallow and able to accompany a broad range of substrates (Heroes et al., 2013; Peti et al., 2013). In yeast, Glc7 overexpression is known to be lethal (Liu et al., 1992) and in human U2OS cells, blocking the PP1-PIP interface with a synthetic peptide has cytotoxic effects (Chatterjee et al., 2012), presumably due to the release of free catalytic subunit. In line with these results, PP1 interacting proteins (PIPs) were reported to be in molar excess to the catalytic subunit (Heroes et al., 2013).

Clearly, these results show that unrestrained activity of free catalytic subunit is harmful to the cell. Another way to interpret these findings is that an important function of PIPs is to keep the activity of the catalytic subunit in check. Therefore, when assessing PP1 activity towards a specific substrate, most PP1-PIP complexes, which are also referred to as “holoenzymes”, show lower activity than a free, unbound catalytic subunit. This is also the case for the classic and still most widely used assay for PP1 activity, which measures its ability to dephosphorylate active, phosphorylated glycogen phosphorylase (designated “phosphorylase *a*”), which is a substrate of phosphorylase kinase and an important effector in glycogen metabolism. The full activity of preparations containing complex-bound PP1 is only observed after a limited digest with trypsin, which releases the trypsin-insensitive catalytic subunit from its interactors. This method is widely used to compare the amounts of catalytic subunit, measured as phosphatase activity, between different preparations independent of incorporation in complexes with varying specific activity towards phosphorylase *a*.

Apart from the specificity gained by interaction with substrate-specifiers, the activity of the catalytic subunit is also controlled by a range of “inhibitors”. It is necessary to distinguish these designated inhibitors from substrate-specifiers by criteria such as occlusion of the active site of the phosphatase. This has been demonstrated for the interactions of I2 and CPI-17 with PP1. While I2 interacts in its unphosphorylated form with PP1 and occludes the active site (Hurley et al., 2007)(see also Figure 2B), CPI-17 acts as a pseudosubstrate via a phosphorylated peptide, which is structurally protected from dephosphorylation (Eto et al., 2007). Interestingly, these inhibitory interactors were in some cases observed to form trimeric complexes with the catalytic subunit, such as MYPT1-PP1-CPI-17, spinophilin-PP1-I2 or GADD34-PP1-I1 (Heroes et al., 2013) (see also Figure 2B).

I. 2: Essential functions of PP1 are regulated by SDS22 and Inhibitor-3 (I3)

I.2.1 Data regarding essential functions of yeast PP1 homologs

As mentioned before, PP1 is required for the storage of glycogen via direct regulation of glycogen synthase, glycogen phosphorylase and the upstream phosphorylase kinase (Ingebritsen and Cohen, 1983b). Accordingly, the single homolog of PP1 in *S. cerevisiae* was first identified in 1990 in the labs of Erwin Reimann and Robert Trumbly in a glycogen accumulation-deficient strain, carrying a mutant version of the gene *GLC7* (for “glycogen-7”)(Feng et al., 1991; Peng et al., 1990).

One year earlier, the group of Mitsuhiro Yanagida published their characterization of the *Schizosaccharomyces pombe* (*S. pombe*) gene *dis2*+, which they found in a screen for mutations resulting in chromosome disjoining phenotypes, together with a counteracting gene, “suppressor of *dis2”*, *sds21*+ (Ohkura et al., 1989). They found that both genes encoded homologs of rabbit PP1α, with 82 % identity in the case of dis2+ and 74 % in the

case of sds21+. They also identified a homologous coding sequence in *S. cerevisiae* by southern hybridization and called it "*DIS2S1"*. Subsequently, the identity of *DIS2S1* and *GLC7* was noted and the involvement of this *S. cerevisiae* gene in glycogen accumulation was confirmed (Clotet et al., 1991). However, in the same publication by Clotet and co-workers, the authors also noted that they observed a lethal phenotype in *dis2S1/glc7* mutants, which was more likely to be caused by functions similar to those described for the *S. pombe* homologs.

It is not surprising that mutants of PP1 homologs in yeast would result in several defects, due to the plethora of functions of the phosphatase. In order to interpret results of genetic interaction studies, a greater understanding of the direct cause for the observed phenotype of *glc7* mutants would be beneficial. This is complicated by the fact that different mutations result in different but also overlapping phenotypes. Since many of the studied mutations occur in surface-exposed residues, they affect interactions with Glc7 regulators rather than the catalytic activity, resulting in pathway-dependent effects (Ramaswamy et al., 1998) and often mixed phenotypes since many interactors share common binding sites. This is exemplified in the case of the *glc7-129* mutant, which results in reduced glycogen accumulation and deficient sporulation but also causes arrest in mitosis due to chromosome congregation defects (Bloecher and Tatchell, 1999). Further illustrating these difficulties, MacKelvie and co-workers reported a mitosis-specific arrest of the mutant *glc7-12*, whereas *glc7-10* resulted in arrest at an earlier cell cycle stage and *glc7-13* resulted in a random arrest (MacKelvie et al., 1995). However, the *glc7-10* mutant was reported by others to cause chromosome instability and confer a mitotic arrest, indicating that strain-specific defects occur for at least some *glc7* mutants (Sassoon et al., 1999). Moreover, unlike canonical cell cycle deficient "cdc" mutants, which were characterized by their uniform phenotype (Hartwell et al., 1973), the mitotic arrest only affected ~ 50 % of the cells with the *glc7-12* mutation (MacKelvie et al., 1995). This could be a consequence of the pleiotropic effects of a perturbed function of the phosphatase, which can cause simultaneous arrest at different phases of the cell cycle as well as secondary effects originating from functions in cell cycle-relevant processes such as the DNA damage response (Shimada and Nakanishi, 2013).

However, as in the case of *dis2*+, an essential aspect of Glc7 function clearly relates to the regulation of mitotic processes. This has been established not only for the yeast PP1 enzyme but also for homologues in higher eukaryotes and can be at least partially explained by their antagonism towards the kinase Ipl1 and its homologues Aurora A and Aurora B, which is introduced in the next section.

I.2.2 Balanced activities of Aurora kinases and PP1 orchestrate mitosis

Faithful segregation of sister chromatids during mitosis requires correct attachment of spindle microtubules to the kinetochore structure formed at the centromere on mitotic chromosomes.

The centromere is a chromatin region, defined by specific DNA sequences in yeast, and by the presence of specific histone variants within centromeric nucleosomes in metazoans (Black and Cleveland, 2011; Joglekar et al., 2006). A proteinaceous structure called the "constitutive centromere-associated network" (CCAN) is present at these sites in mitosis and interphase and constitutes the inner kinetochore. The CCAN provides the anchoring point for formation of the outer kinetochores upon entry into mitosis (Hori et al., 2008). These highly organized structures are made up of a network of multimeric protein complexes, together called the "KMN network". It consists of the KNL1 (kinetochore null protein 1)-, Mis12 (missegregation 12)- and Ndc80 (nuclear division cycle 80)-complexes (Figure 3A). Microtubule attachment to the kinetochore in metazoans occurs mainly via Ndc80 and the SKA (spindle- and kinetochore-associated) complex (Foley and Kapoor, 2013; Welburn et al., 2009), whereas yeast possess a complex called DASH/Dam1, which was recently shown to assemble into a ring to encircle microtubule ends (Jenni and Harrison, 2018).

The KMN network also functions as an organizing center for processes involved in the surveillance of attachments between the kinetochores and microtubules (Foley and Kapoor, 2013). Two important processes that contribute to this surveillance are those of "error correction" as well as the "spindle assembly checkpoint" (SAC). The error correction process depends on the activity of kinases, which phosphorylate kinetochore substrates such as Ndc80. The main kinase responsible for this phosphorylation is Aurora B, which is localized to centromeres, as part of the chromosomal passenger complex (CPC) (Carmena et al., 2012). Phosphorylation generally reduces the attachment strength between kinetochores and microtubules, thereby providing a means of destabilizing incorrect attachments (Foley and Kapoor, 2013; Musacchio, 2015). On the other hand, force transmission during chromatid segregation requires stabilization of the kinetochore-microtubule interface and therefore, destabilizing phosphorylation has to be removed before entry into anaphase. Therefore, a mechanism has to be in place to establish the correct balance between kinase and phosphatase activities. An attractive model explains this balance with the distance of kinetochore substrates from centromere-localized Aurora B (Lampson and Cheeseman, 2011; Welburn et al., 2010). In this model, Aurora B-mediated phosphorylation functions as a sensor for the distance or tension between kinetochores, which are pulled away from the kinase when correct attachments are established. This leads to a net dephosphorylation of kinetochore components, since phosphatases are recruited directly to kinetochores (Figure 3B).

Both PP2A phosphatase, together with B56 subunits as well as PP1 have been implicated as antagonists of Aurora B-mediated phosphorylation at kinetochores (Foley et al., 2011; Liu et al., 2010). Consistent with a prominent role of PP1 in this function, kinetochores extracted from *glc7-10* mutants in budding yeast have lower microtubule binding affinity than those extracted from wild-type cells (Sassoon et al., 1999). The antagonistic function of PP1

towards Aurora B depends on PP1 recruitment to the kinetochore. The main anchor for PP1 at kinetochores is KNL1 (Liu et al., 2010), which contains an RVxF motif within its first 100 N-terminal residues. Recruitment of PP1 to kinetochores via KNL1 is subject to regulation and is reduced by Aurora B-dependent phosphorylation of the RVxF motif (Liu et al., 2010). This is just one example for a range of feedback mechanisms, which contribute to the kinase-phosphatase balance that regulates attachments (Funabiki and Wynne, 2013).

Interestingly, the antagonistic role of Aurora B on interactions with PP1 has recently been extended to other RVxF motif-containing proteins (Nasa et al., 2018). These include CDCA2 (also called Repo-Man), which targets PP1 to chromatin in ana- and telophase, Ki67, UBR5 and others that may recruit PP1 during mitosis, but also chromatin- or DNA-associated factors such as RIF1 and BRCA1 that do not have known functions in mitosis (Nasa et al., 2018).

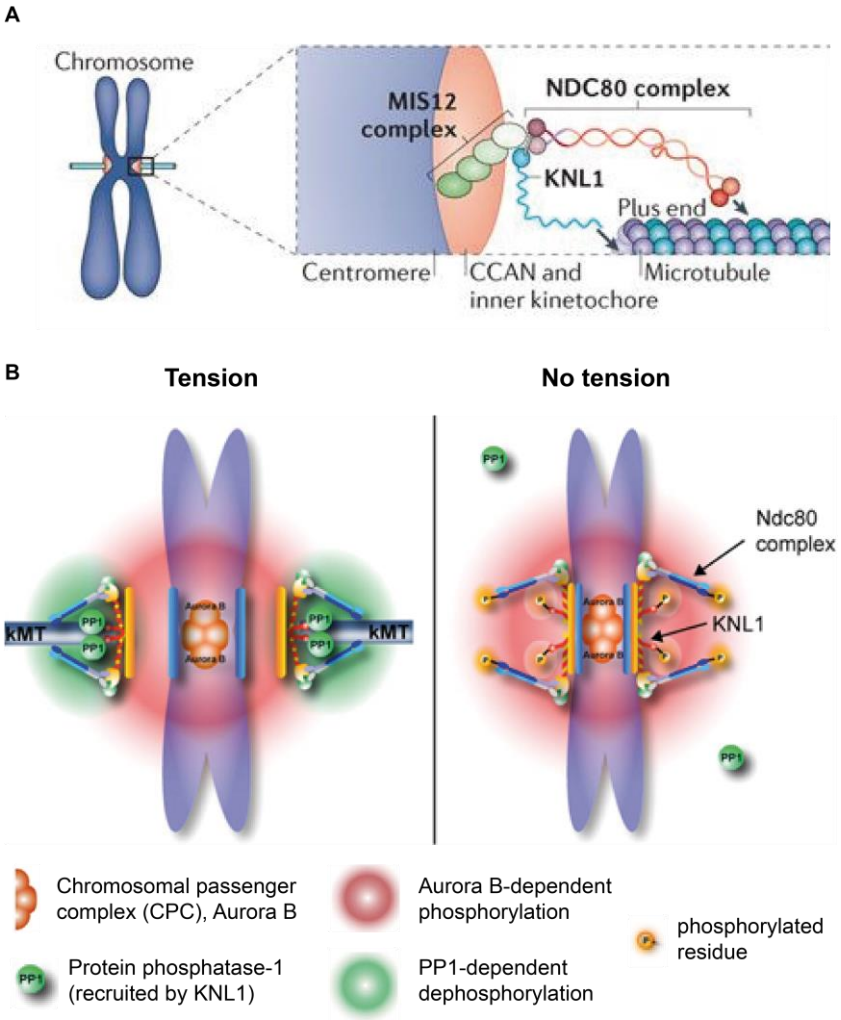

Figure 3: Architecture of microtubule attachment sites on mitotic chromosomes and error correction mediated by opposing activities of Aurora B and PP1.
(**A**) Schematic illustration of complexes at the kinetochore formed on mitotic chromosomes. Shown are the KMN (kinetochore null protein 1 (KNL1)–missegregation 12 (MIS12) complex–nuclear division cycle 80 (NDC80) complex) network, including the four-subunit MIS12 complex, which bridges KNL1 and the NDC80 complex to the constitutive centromere-associated network (CCAN) and centromeric chromatin. Microtubule binding depends on the NDC80 complex, KNL1 and the SKA complex (not shown) and is indicated with arrows. Adapted from (Foley and Kapoor, 2013). (**B**) Tension-based model for the error correction process, which regulates microtubule-kinetochore attachments.

Aurora B, localized as part of the Chromosomal passenger complex (CPC) to centromeres, weakens microtubule attachment via phosphorylation of kinetochore substrates. Increased distance of Aurora B from these substrates due to increased distance between kinetochores and the centromere at correctly attached chromosomes favors dephosphorylation of kinetochores by phosphatases such as PP1 and PP2A (not shown). Adapted from (Liu et al., 2010).

Another major process for the regulation of mitotic progression is the SAC, which also operates at kinetochores. Like the error correction process, it monitors the correctness of kinetochore-microtubule attachments. It is activated by unattached or tension-less kinetochores and prevents premature entry into anaphase. The effector of the SAC is the mitotic checkpoint complex (MCC), which consists of MAD2, BUBR1, BUB3 and CDC20 (Foley and Kapoor, 2013). Recruitment of the crucial SAC-promoting proteins BUB1 and MAD1 to kinetochores depends on phosphorylation events. These are thought to be regulated by the same pool of Aurora B as the error correction process (Musacchio, 2015). Phosphorylation of unattached kinetochores by Aurora B activates a downstream kinase called MPS1, which then phosphorylates a repetitive sequence on KNL1 to generate a platform for MCC formation (Musacchio, 2015)(Figure 4A).

The MCC serves to sequester CDC20 and prevent it from activating the anaphase promoting complex / cyclosome (APC/C). The activity of the APC/C as a ubiquitin E3 ligase is required for degradation of securin, an inhibitory interactor of the protease Separase, which cleaves the sister chromatid-linking protein cohesin. APC/C further targets cyclin B for destruction, which is a second hallmark event at the entry into anaphase (Sudakin et al., 1995). Therefore, a kinetochore-localized process generates a diffusible signal in form of the MCC, which suppresses the degradation of securin and Cyclin B (Figure 4B).

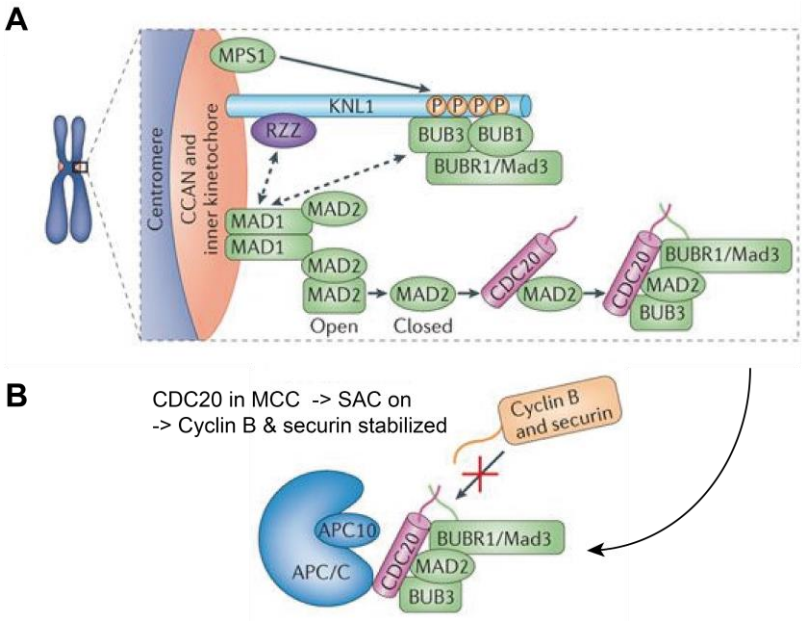

Figure 4: Mechanism of the Spindle assembly checkpoint (SAC) by formation of the Mitotic checkpoint complex (MCC).
(**A**) Unattached kinetochores are phosphorylated by checkpoint kinases including MPS1, which leads to the recruitment of several checkpoint proteins to KNL1 (see main text). These in turn promote the recruitment of MAD1 and MAD2. MAD2 is converted at the kinetochore from an “Open” to a “Closed”

conformation, favoring its interaction with CDC20 and formation of the MCC, consisting of BUBR1, MAD2, BUB3 and CDC20. (**B**) CDC20 and the MCC can bind to the Anaphase promoting complex/Cyclosome (APC/C) but prevent the interaction with Cyclin B and securin, which depends on free CDC20 bound to the APC/C. Adapted from (Foley and Kapoor, 2013).

As for the error correction mechanism, PP1 has been implicated as a major balancing factor, counteracting Aurora B-dependent phosphorylation of kinetochore substrates involved in SAC regulation (London et al., 2012). Consistently and crucially, the initiation of anaphase following satisfaction of this checkpoint requires PP1 (Meadows et al., 2011; Rosenberg et al., 2011; Sivakumar et al., 2016).

Apart from the antagonism towards Aurora B, PP1 has also been shown to counteract Aurora A, which is a master regulator of centrosome maturation - the process which prepares the organizing centers for the mitotic spindle (Barr and Gergely, 2007; Lim et al., 2009) - and further mitotic spindle-associated processes (Carmena et al., 2009). PP1 is able to remove the activating phosphorylation from T-loop residue threonine-288 of Aurora A, at least *in vitro* (Littlepage et al., 2002), whereas more indirect connections have also been found *in vivo* (Xiao et al., 2011). An important regulator of the PP1-Aurora A balance is Inhibitor-2 (I2), which was found to both inhibit PP1-mediated dephosphorylation of Aurora A but also to directly stimulate Aurora A activity (Satinover et al., 2004).

The precise function of many PP1-PIP complexes during mitosis awaits further clarification, but it is becoming increasingly clear that the phosphatase plays central roles in diverse processes with many partners to orchestrate the correct division of the genetic material and subsequent exit from mitosis (Grallert et al., 2015; Nasa and Kettenbach, 2018; Rogers et al., 2016).

I.2.3 Functional genetic analysis of Sds22 and Ypi1/I3 in yeast

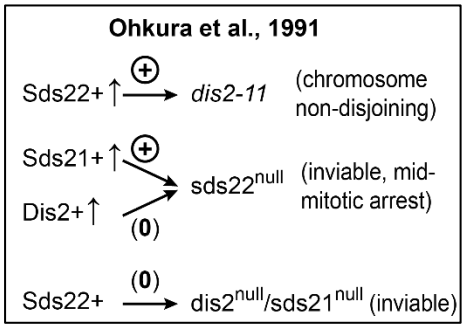

Figure 5: Data visualization (Ohkura et al., 1991)
Symbols are as follows: upward arrow: overexpression; downward arrow: depletion; arrow with "+" in circle: positive genetic interaction or rescue; arrow with "(+)": partial rescue; arrow with "(0)": no genetic interaction; arrow with "−" in circle: negative genetic interaction or synthetic lethality. See text for details.

Together with the sds21+ phosphatase-encoding gene in fission yeast, another gene, sds22+, was found to be able to suppress the chromosome non-disjoining phenotype of the mutant *dis2-11* when overexpressed (Ohkura et al., 1989). However, it did not rescue the double-null mutant of both PP1 homologs dis2+ and sds21+, indicating that it is not another phosphatase enzyme (Figure 5). Ohkura and co-workers later characterized the gene product as a 30 kDa protein, containing 11 leucine-rich repeats of 22 aa residues each and found that it was enriched in the nuclear fraction of *S. pombe* homogenates (Ohkura and Yanagida, 1991). They also studied the consequences of disruption of the sds22+ gene either by loss of a

rescue plasmid in a double-negative diploid background or by germination of heterozygous diploids and found a partial metaphase arrest phenotype, which was rescued by overexpression of sds21+ but not dis2+. Although sds22+ seemed to be closely linked to the function of the PP1 homologs sds21+ and dis2+, they found that overexpression of sds22+ did not result in an increase of the overall phosphatase activity towards glycogen phosphorylase.

In a later study by Stone *et al.* (Stone et al., 1993) in the same lab, a first hint to a potential pathway-specific function of sds22+ was found by testing phosphatase activity towards phosphorylase *a* but also with the additional substrate histone H1. Only in the case of histone H1, sds22+-associated phosphatase was active (Figure 6). Employing a temperature-sensitive mutant of *sds22*, this study again revealed a mitotic arrest phenotype, which affected roughly half of the cells. The overall phosphatase activity, measured after immunoprecipitation with a dis2+- and sds21+-bi-specific antibody, decreased over time at the non-permissive temperature along with an apparent decrease of the levels of these phosphatases as detected by Western Blot. These results led the authors to suggest two explanations: Either sds22+ functions as a substrate-specifier for mitotic targets of dis2+/sds21+ or it controls the level of these phosphatases, which then leads to the same arrest phenotype as observed with mutations affecting these genes directly, which was described before (I.2.1).

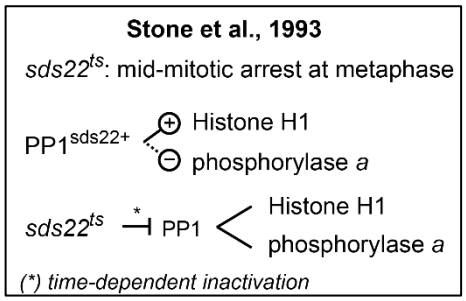

Figure 6: Data visualization (Stone et al., 1993)
"+" in circle: phosphatase activity
"-" in circle: no phosphatase activity
"ts": temperature-sensitive mutation
See text for details.

With the establishment of a model of regulator-driven function of Ser-/Thr-phosphatases (Hubbard and Cohen, 1993), it became more obvious that PP1-regulatory proteins may have substrate-specifying functions and accordingly, the idea that Sds22 plays such a role in mitosis was strengthened. Indeed, with the identification of the *S. cerevisiae*-homolog Sds22 by MacKelvie and colleagues, further evidence accumulated (MacKelvie et al., 1995). Overexpression of Sds22 was able to rescue the mitotic arrest, but not the growth deficiency of the *glc7-12* mutant at higher temperature. Arguably, the *glc7-12* mutation causes further defects, which are not rescued by Sds22 but also not penetrant at milder temperature. Furthermore, the rescue effect was allele-specific and did not extend to the random arrest phenotype observed for *glc7-13* in this study. Along the same lines, the authors also state that *glc7-10* displayed arrest at an earlier cell cycle stage and was not rescued by Sds22 overexpression. However,

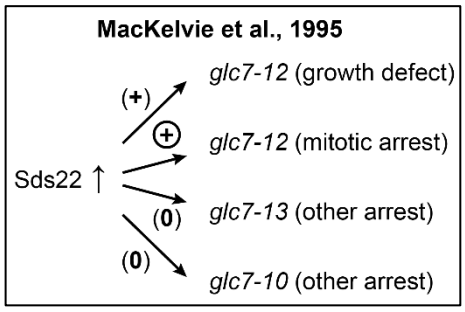

Figure 7: Data visualization (MacKelvie et al., 1995).
Symbols as in Figure 5. See text for details.

others observed chromosome segregation defects and mitotic arrest for the *glc7-10* mutation as mentioned before (I.2.1). Nonetheless, these data indicated a pathway-specific effect of Sds22 depletion (Figure 7).

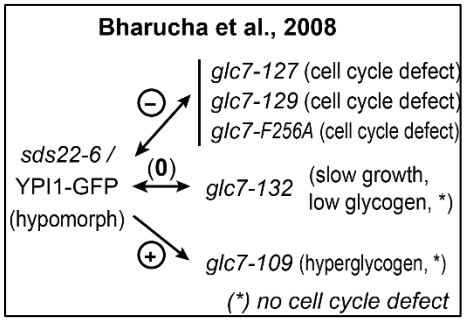

Figure 8: Data visualization (Bharucha et al., 2008)
Symbols as in Figure 5. See text for details.

Bharucha and co-workers also tested genetic interactions of different *glc7* mutants with *sds22-6* and found strong negative interactions with the cell cycle-deficient alleles *glc7-127, -129* and *-F256A.* However, they also found that accumulation of unusually high glycogen levels due to expression of *glc7-109*, indicating increased phosphatase activity in this non-mitotic pathway, was suppressed by *sds22-6* as well as by a hypomorph variant of the Ypi1 protein, which will be introduced below (Bharucha et al., 2008)(Figure 8).

In another study on Sds22 in yeast, Peggie and colleagues analyzed two temperature-sensitive alleles, *sds22-5* and *sds22-6* (Peggie et al., 2002). At the restrictive temperature, these mutations did not cause a distinct mitotic arrest. Instead, the authors observed high degrees of chromosome segregation errors. In the case of *sds22-6* the likely reason for this was loss of binding to Glc7. The *sds22-5* mutant strain was later used in a study by Pedelini and colleagues (Pedelini et al., 2007), who detected a specific arrest in mid-mitosis with a “dumb-bell”-like shape and short mitotic spindles, indicating that the outcome of Sds22 deficiency might be strain-specific as observed for *glc7* before (I.2.1). The growth deficiency of *sds22-5* and *-6* was partially suppressed by overexpression of Glc7 and, vice versa, Sds22 overexpression suppressed growth defects in *glc7* mutants at moderate temperature (Figure 9), consistent with a relieve of mitotic defects observed for *glc7-5* and *-12*.

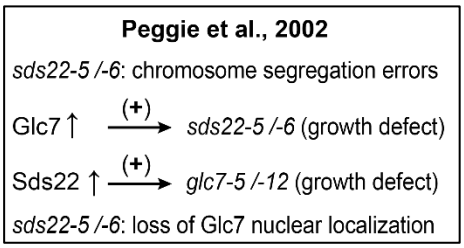

Figure 9: Data visualization (Peggie et al., 2002)
Symbols as in Figure 5. See text for details.

Another interesting observation was made using fluorescent protein fusions of Glc7. Whereas these were normally localized to the nucleus, shifting strains carrying mutants of *sds22* to the restrictive temperature led to a more equal distribution of the signal between the cytosol and nucleus. Furthermore, Peggie *et al.* detected the appearance of bright spots of fluorescence in these conditions (Peggie et al., 2002). Although these authors noted that there was no effect of Sds22 mutation on the levels of Glc7, this suggested that Sds22 might be required to keep Glc7 both correctly localized and stable.

Pedelini and co-workers clarified the identity of a phosphoprotein in a complex of Sds22 and Glc7 in budding yeast (Pedelini et al., 2007). A similar phosphoprotein had been observed in isolates of fission yeast sds22+ (Stone et al., 1993) and earlier in a complex with the

mammalian homologs SDS22-PP1 (Dinischiotu et al., 1997). Pedelini *et al.* found that this protein corresponded to Ypi1 (yeast protein phosphatase inhibitor 1), which had been identified as a homolog of a human protein called “Inhibitor-3” (I3) (Garcia-Gimeno et al., 2003). I3 had been shown to inhibit PP1 isolated from rabbit muscle (Garcia-Gimeno et al., 2003; Zhang et al., 1998) and consistently, Ypi1 inhibited glycogen accumulation upon overexpression (Garcia-Gimeno et al., 2003). Furthermore, its deletion had lethal effects, indicating an essential function in budding yeast. (Garcia-Gimeno et al., 2003).

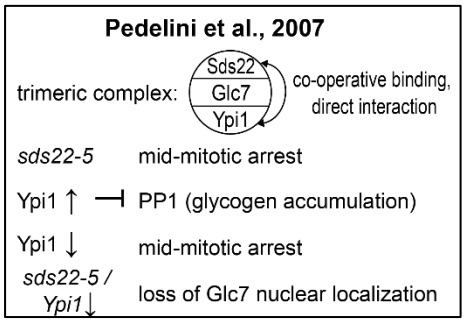

Figure 10: Data visualization (Pedelini et al., 2007).
Symbols as in Figure 5. See text for details.

Pedelini *et al.* showed in yeast-3-hybrid studies that Sds22 and Ypi1 cooperatively bind Glc7 in a trimeric complex (Pedelini et al., 2007). In addition they found a synthetic inhibitory effect of both proteins on the phosphatase activity of Glc7, measured towards para-nitrophenylphosphate (pNPP). Further analysis presented in their study, using a conditionally expressed construct, revealed that Ypi1 depletion resulted in a similar mitotic arrest as observed following loss of Sds22 (Pedelini et al., 2007; Stone et al., 1993). Interestingly, the same loss of nuclear localization of a fluorescent protein-Glc7 fusion was observed upon depletion of either protein (Pedelini et al., 2007)(summarized in Figure 10).

In the lab of Kelly Tatchell, glucose-repression was applied to downregulate Ypi1 under control of a GAL promoter and consequently, a mitotic arrest phenotype was observed (Bharucha, 2008). Consistent with a more general requirement of Ypi1 for Glc7 function, the hyperglycogen trait of *glc7-109* was suppressed by expression of non-functional *YPI1-GFP* (Bharucha et al., 2008)(Figure 8), although this might have been caused by titration of Glc7 away from its substrates.

Taken together, these yeast studies indicated that Sds22 and Ypi1 are involved in a common pathway of PP1 regulation, which appears to directly or indirectly affect the essential mitotic function of the yeast PP1 homologs but also showed effects on their nuclear localization, stability and activity in unrelated pathways. Interestingly, whereas Sds22 and Ypi1 inhibit Glc7 *in vitro* (Garcia-Gimeno et al., 2003; Pedelini et al., 2007) and Ypi1 overexpression inhibited the glycogen accumulating function of Glc7 (Pedelini et al., 2007), several observations pointed to a positive role on PP1 function. This includes the rescue of dis2+ mutation by overexpression sds22+ in fission yeast (Ohkura et al., 1989), rescue of defects of *glc7* mutants by overexpression of Sds22 (MacKelvie et al., 1995) and the loss of Glc7 nuclear localization upon depletion of Sds22 or Ypi1 in budding yeast (Pedelini et al., 2007; Peggie et al., 2002). The latter effect was recently reinvestigated by Cheng and Chen, who reported evidence that Sds22 and Ypi1 are required for the stability of Glc7 (Cheng and Chen, 2015), pointing to a more general role of these interactors for PP1.

While a general function for PP1 stability can explain many of the observations reported for Sds22 and Ypi1, it seems that the pathway-specific effects, especially regarding the requirement of both proteins in a mitotic function of Glc7 cannot easily be reconciled with such a model. Therefore, the following section will review the data obtained for the proposed function of yeast Sds22 and Ypi1 in the antagonism between Glc7 and the yeast homologue of the Aurora kinases, Ipl1.

I.2.4 Potential roles of Sds22 and Ypi1/I3 for the Glc7 - Ipl1 antagonism in yeast

The antagonism between PP1 and Aurora B was first established by genetic interaction studies with mutants of the yeast Aurora A and Aurora B-homolog Ipl1, for “increase-in-ploidy 1” (Chan and Botstein, 1993). Aurora and Ipl1 kinases serve highly conserved functions in mitosis (Biggins et al., 1999)(see also I.2.2). Starting with the observation that a truncation mutant of the PP1-homolog Glc7, *glc7-1,* was able to suppress the lethality of a temperature-sensitive mutant, *ipl1-1* (Francisco et al., 1994), the antagonism between yeast PP1 and Aurora kinases was further established by positive genetic interactions between other mutant versions of ipl1 as well as the *GLC7* mutants *glc7-1, -10, -12*, *-127* and *glc7-129* (Figure 11)(Francisco et al., 1994; Hsu et al., 2000; Peggie et al., 2002; Pinsky et al., 2006). In contrast, *glc7-109*, which is defective in a specifically cytoplasmic function, does not rescue *ipl1-2*, indicating that some alleles of *GLC7* confer defects in unrelated pathways as dicussed earlier (Hsu et al., 2000).

Direct dephosphorylation of Ipl1 by Glc7 does not seem to be the major mechanism of the antagonism in yeast, since a mutant of Ipl1 with a threonine-to-alanine exchange at residue 260, the main site which is autophosphorylated for full activation, is still rescued by *glc7* mutants. This suggests that Glc7 is rather required for the dephosphorylation of Ipl1 substrates (Pinsky et al., 2006). The antagonism between Ipl1 and Glc7 likely extends to a multitude of processes but many effects can be related to the essential processes of error correction and the SAC, which have been described earlier I.2.2).

Clearly, the disruption of a mitotic checkpoint could have detrimental consequences, since it is in place to assure the fidelity of chromosome segregation into daughter cells. However, defects in proteins required to regulate the SAC itself can be rescued by ablation of this checkpoint. In principle, this could be expected to relieve some defects caused by PP1 malfunction, since PP1 was shown to be required for silencing of the SAC (see I.2.2). However, mutants of *mad1* in budding yeast, which have no functional SAC, are synthetically lethal with *glc7* mutations (Bloecher and Tatchell, 1999). This is likely due to the high rate of chromosome loss observed in the double mutants and can be explained by the role of Glc7 in the chromosome segregation process itself (Sassoon et al., 1999). It is interesting to note that disruption of the SAC releases the mitotic arrest in a *glc7-129* mutant but subsequently leads to a delay in later mitotic phases (Bloecher and Tatchell, 1999). The observation that

glc7-129 shows reduced interaction with microtubule motors was proposed as an explanation for this delay (Peggie et al., 2002). This indicates that the antagonism between Ipl1 and Glc7 may play a role in several mitotic events, including, but not necessarily limited to chromosome-microtubule interactions and regulation of the SAC.

Similar genetic interactions as for Glc7 were found between Sds22 and Ipl1, as well as between Ypi1 and Ipl1 (summarized in Figure 11). First, Peggie *et al.* reported that the temperature-sensitivity of the *ipl1-2* mutation was suppressed by the PP1 binding-deficient *sds22-6* mutant allele (Peggie et al., 2002). Subsequently, also overexpression of Sds22 was found to suppress an *ipl1* mutation (Pinsky et al., 2006). The mechanism of the latter suppression effect remained elusive, but the authors observed similar effects upon overexpression of several RVxF motif-containing interactors, such as the peroxisome component PEX31, which are unlikely to serve specific roles during mitosis. This indicates that interfering unspecifically with Glc7 function may be sufficient to suppress *ipl1* mutant phenotypes.

Two parsimonious explanations for the rescue of the *ipl1-2* mutation by *sds22* mutants are possible based on the assumption that Sds22 is a substrate-specifier for Glc7. On this basis, Sds22 could either enhance Glc7 activity towards Ipl1 directly to regulate its activation by dephosphorylation of the T-loop, or Sds22 could support Glc7-mediated dephosphorylation of Ipl1 substrates at the kinetochore. As noted before, suppression of the mitotic defect of a T-loop mutant Ipl1 variant by mutation of Glc7 argues against a direct function of Glc7 in regulating this phosphorylation in budding yeast. Dephosphorylation of Ipl1 substrates by Sds22-Glc7 seems a more likely possibility, since it was shown in fission yeast that this phosphatase holoenzyme is active against the Cdc2-target histone H1. However, although Glc7 directly opposes Ipl1-mediated phosphorylation of histone H3 (Hsu et al., 2000) as well as the kinetochore-microtubule interface protein Dam1 (Pinsky et al., 2006)(see also I.2.2), no data regarding the effect of *sds22* mutants on these substrates in yeast were reported.

The group of Maria Garcia-Gimeno observed rescue of *ipl1-321* by overexpression of Ypi1 (Pedelini et al., 2007). This could be explained both by an inhibitory function of Ypi1 or by titrating Glc7 away from its targets at the kinetochore. On the other hand, their experiments also indicated that Ypi1 is an essential protein (Garcia-Gimeno et al., 2003) and that cells lacking Ypi1 arrest in mitosis with an active SAC (Pedelini et al., 2007).

The nature of the arrest in Ypi1-depleted cells was further investigated in subsequent studies. The group of Kelly Tatchell found that the arrest - but not the growth deficiency - could be rescued by co-deletion of Mad1 to disrupt the SAC (see I.2.2)(Bharucha et al., 2008). Conversely, Marquina and co-workers reported that Mad1 deletion did not rescue the arrest of Ypi1 depletion, whereas disruption of the morphogenesis checkpoint by deletion of the kinase Swe1 did (Marquina et al., 2012). A possible explanation for this discrepancy

would be that mitotic processes leading to the activation of both checkpoints are affected and that the specific arrest depends on the strain background or method used to deplete Ypi1.

The ability of Ypi1 to bind Glc7 via the RVxF motif is required for viability, since a *ypi1*$^{V51A/W53A}$ mutant is unable to rescue a yeast strain with genomic deletion of *ypi1* (Bharucha et al., 2008). The single mutant *ypi1*^{W53A}, which likely retains residual binding to Glc7, only rescues the deletion when overexpressed from a plasmid (Bharucha et al., 2008). Pedelini et al. found that *ypi*^{W53A} partially rescues the *ipl1-2*^{ts} mutation and simultaneously decreases the nuclear localization of both Sds22 and Glc7 (Pedelini et al., 2007).

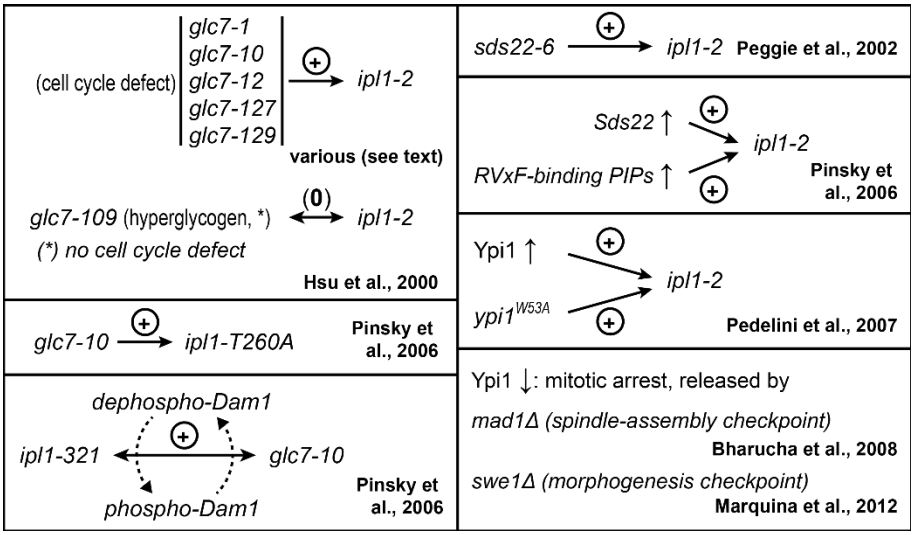

Figure 11: Genetic interaction data for *glc7*, *sds22* and *ypi1* mutants with ipl1 mutants and mitotic functions.
Symbols as in Figure 5. See text for details.

The data on the mitotic roles of Sds22 and Ypi1, as summarized in Figure 11, indicate that both are required for the antagonistic function of Glc7 towards Ipl1 in mitosis but they do not clarify the underlying mechanism conclusively. Therefore, further studies were required to distinguish between putative roles of these regulators as either substrate-specifiers, targeting subunits or stabilizing factors for the phosphatase catalytic subunit.

Notably, Tung *et al.* also reported rescue of *ipl1-2* by mutation as well as overexpression of the yeast I2 homolog, Glc8 (Tung et al., 1995). Since yeast Ipl1 is the only homolog of the mammalian Aurora A and Aurora B enzymes, this could be related to the link between I2 and Aurora A in the regulation of centrosomes (I.2.2). Although the *S. cerevisiae*-homolog Glc8 was shown to be required for full activity of Glc7/PP1 (Nigavekar et al., 2002), knockdown of I2 in mammalian cells was reported to reduce phosphorylation of the Aurora B substrate histone H3 on serine-10. This rather suggests an inhibitory role of I2 in control of PP1 activity in mitosis (Wang et al., 2008).

I.2.5 Structure and localization of mammalian SDS22 and I3

SDS22, which is also called PPP1R7 (for “PP1 regulatory subunit 7”) in mammals, contains 11 complete and one partial leucine-rich repeat (LRR), composed of 22 and 11 aa residues, respectively (Figure 12). SDS22 is prototypical of a class of LRR proteins (Kobe and Kajava, 2001). LRR domains adopt a curved fold by β-sheet interactions between the repeats. This fold leaves a concave and a convex surface exposed to the solvent. At the N- and C-terminus, LRR proteins often contain “cap” regions to shield the hydrophobic core (Bella et al., 2008). This is also the case for SDS22, since the 27 aa-long C terminus contains a sequence of 16 aa that correspond to the consensus “YRxxφxxxφPxφxxLD” (Ceulemans and Bollen, 2004; Ceulemans et al., 1999). The N-terminal 77 aa residues of SDS22 are not conserved through evolution but likely to be required for its stability (Stone et al., 1993). The interaction of yeast Sds22 with several proteins, including the AAA-ATPases Rvb1 and Rvb2, which was found in a large scale study (Ho et al., 2002), was attributed to the 25 N-terminal residues (Ghosh and Cannon, 2013; Ho et al., 2002) but this sequence is not well conserved in human SDS22 (Figure 12E).

The LRR domain is known to be involved in many protein-protein interactions, which usually occur at the concave side (Bella et al., 2008). The interaction between SDS22 and PP1 has also been mapped to residues exposed at the concave surface of the SDS22 LRR domain (Ceulemans et al., 2002b)(Figure 12A). On the PP1 side, the interaction was reported to occur at the “α-4/-5/-6” helix triangle, close to the active site. This interaction is not isoform-specific, since the region in PP1 isoforms is conserved and SDS22 interacts with all isoforms in *in vitro* assays (Ceulemans et al., 2002b) as well as in cells (Posch et al., 2010). In contrast to most other validated PIPs (Heroes et al., 2013), SDS22 does not contain an RVxF motif. Since the RVxF motif contributes a high affinity binding site as an anchor for many PIPs (Wakula et al., 2003), its vacancy in the SDS22-PP1 interaction suggests that trimeric complexes might be formed with SDS22 and other PP1-interactors (Verbinnen et al., 2017).

Sds22 in yeast as well as its counterpart in mammals were shown to localize both to the cytoplasm and the nucleus (Lesage et al., 2007; Posch et al., 2010; Stone et al., 1993). Deletion of the C terminus abolished nuclear localization but this is probably an indirect effect due to destabilization upon loss of the LRR cap region (Ceulemans et al., 1999; Stone et al., 1993). While Sds22 was reported to localize to the nucleus independent of its binding to PP1 (Stone et al., 1993), a definite NLS has not been detected (Peggie et al., 2002). Moreover, Bharucha and co-workers observed that nuclear localization of Sds22 was strongly reduced in yeast expressing Ypi1 from a *ypi1*^{W53A} mutant allele (Bharucha et al., 2008).

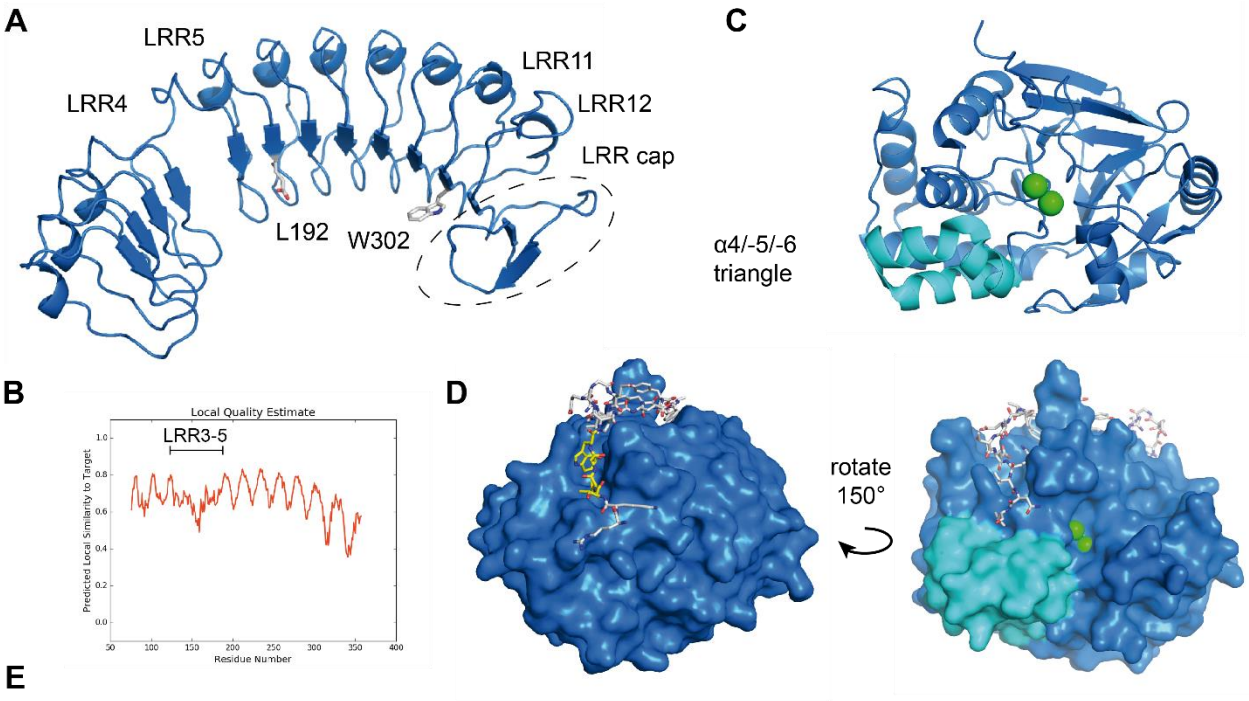


```
Sds22_Hs 1   MAAERGAGQQQSQEMMEVDRRVESEESGDEEGKKHSSGIVADLSEQSL-KDGEERGEEDPEEEHELPV--------- 67
                                                 :.:.|: ||.||:     :|.|::.|
Sds22_Sc 1   ----------------------------------------MDKNSVNKDSEEK-----DERHKIEVVDDTNPDFI 30

Sds22_Hs 68  --DME-TINLDRDAEDVDLNHYRIGKIEGFEV--LKKVKTLCLRQNLIKCIENLEEL--QSLRELDLYDNQIKKI-E 136
               |.| |.:|..|.|.:||.|.:|..:|...:  .|.:|.||||||||:.|..:|.|  ..:.:||.|||:||.| .
Sds22_Sc 31  TADSELTQDLPDDVEVIDLVHLKIKSLEDLNLYRFKNLKQLCLRQNLIESISEVEVLPHDKIVDLDFYDNKIKHISS 107

Sds22_Hs 137 NLEALTELEILDISFNLLRNIEGVDKLTRLKKLFLVNNKISKIENLSNLHQLQMLELGSNRIRAIE--NIDTLTNLE 211
             |:..||:|..||:|||.:::|:.::.||.|:.|:.|.|.||||||||.|..|:.||||.|::.:||  :.:.|:|||
Sds22_Sc 108 NVNKLTKLTSLDLSFNKIKHIKNLENLTDLENLYFVQNSISKIENLSTLKSLKNLELGGNKVHSIEPDSFEGLSNLE 184

Sds22_Hs 212 SLFLGKNKITKLQNLDALTNLTVLSMQSNRLTKIEGLQNLVNLRELYLSHNGIEVIEGLENNNKLTMLDIASNRIKK 288
             .::|||||.|.:|.||..|.||.:||:|||:|.|||.|:.|.||.|||||||.|..|||||.|.|||.||:.||:|..
Sds22_Sc 185 EIWLGKNSIPRLINLHPLKNLKILSIQSNKLKKIENLEELTNLEELYLSHNFITKIEGLEKNLKLTTLDVTSNKITS 261

Sds22_Hs 289 IENISHLTELQEFWMNDNLL-ESWSDLDE-LKGARSLETVYLERNPLQKD--PQYRRKVMLAL-PSVRQIDATFVRF 360
             :||::||:.|.:.|.:.|.: :|:..|.| |.....|||:|||.||:|.:  ..||||:.:.| ||:::|||||:|.
Sds22_Sc 262 LENLNHLSNLTDIWASFNKIDQSFESLGENLSALSRLETIYLEGNPIQLENKTSYRRKLTMNLPPSLQKIDATYIRG 338
```

Figure 12: Overview of SDS22 structure, interaction with the PP1 catalytic subunit and conservation between human and yeast variants.
(**A**) A model for the structure of human SDS22 was generated using the SWISS-MODEL workspace (Waterhouse et al., 2018) with the LRR domain of the Chlorobium tepidum Roco protein (Guaitoli et al., 2016) as template. The model comprises SDS22 residues 76 - 357 and is shown in cartoon representation, highlighting α-helices and β-sheets. A gap between LRR4 and LRR5 likely resulted from poor sequence homology with the template in this region. This is reflected in the quality estimate diagram shown in (**B**). The C terminus of the model, including LRR11, -12 and the LRR cap, also has poor quality. The residues L192 and W302, which have been shown to be involved in the interaction with the PP1 catalytic subunit (Ceulemans et al., 2002b), are shown in stick-representation. (**C**) The catalytic subunit of human PP1α (residues 7-300; PDB id: 4mp0, chain A) is shown in cartoon representation with two manganese ions in the active site shown in green and the α-4/-5/-6-helix-triangle highlighted in cyan. (**D**) The same model as in (**C**) is shown in surface representation from two different angels. In addition, residues 394-433 of rat PNUTS (PDB id: 4mp0, chain B) are shown in stick representation with the RVXF-motif residues (398-TVTW-401) highlighted in yellow. (**E**) Pair-wise sequence alignment between human SDS22 (Hs_SDS22) and budding yeast Sds22 (Sc_Sds22), generated using the Needleman-Wunsch algorithm (EMBOSS, https://www.ebi.ac.uk/).

Inhibitor-3 or PPP1R11 consists of 126 aa, of which 20 are positively charged and another 19 are negatively charged (31 %) at physiological pH. It has a theoretical mass of 14 kDa but behaves anomalously in SDS-PAGE with an apparent mass of about 24 kDa. Secondary

structure prediction shows a few regions with potential for β-sheet formation in the first half of the protein but the second half appears to be completely unstructured. This is also reflected by a very low proportion of predicted buried residues between 8 % and 13 %, depending on the algorithm used, and a high likelihood of disorder for most of its sequence (Figure 13A to C). I3 shares these biophysical characteristics with a group of small, heat-stable proteins with inhibitory function towards PP1, which includes Inhibitor-1, DARPP-32 and I2 (Eto et al., 2003; Garcia-Gimeno et al., 2003; Zhang et al., 1998; Zhang et al., 2008). The interaction of I3 with PP1 was shown to occur via a "KKVEW" sequence at positions 39 to 43, which conforms to the RVxF consensus. The occurrence of an acidic residue in this sequence is noteworthy, because negative charges usually reduce the binding strength of RVxF peptides to PP1. This is the basis for the negative regulation of PP1 binding by the attachment of phosphates, for example within the RVxF motif of KNL1 (Nasa et al., 2018). Another interaction domain residing roughly 22 residues C-terminal to the RVxF motif was proposed, based on the observation that it was required for the inhibitory effect of I3 on PP1 activity towards phosphorylase *a* (Zhang et al., 2008)(see also Figure 13A). The structure of the related PP1 interactor I2 shows a direct interaction with the active site of PP1 (Hurley et al., 2007) via a region with a similar spacing from the RVxF motif. However, the putative second binding site does not seem to be required for the interaction between yeast Ypi1 and Glc7, for which the N-terminal 93 residues were sufficient (Pedelini et al., 2007)(see also Figure 13D).

Although the interaction of I3 with the β-isoform of the PP1 catalytic subunit seems to be weaker than with the α- and γ-subunits (Huang and Lee, 2008; Huang et al., 2005), several high throughput studies detected PP1β in I3-isolates and vice versa (Boldt et al., 2016; Ewing et al., 2007; Hein et al., 2015; St-Denis et al., 2016; Wan et al., 2015), indicating that I3 can interact with all PP1 isoforms.

Yeast Ypi1 and mammalian I3 show moderate sequence conservation (Figure 13D). Data on both proteins indicate a predominantly nuclear localization (Lesage et al., 2007; Pedelini et al., 2007). Additionally, I3 was also observed to accumulate in nucleoli and at centrosomes by the group of Ernest Lee (Huang et al., 2005), using immunofluorescence to visualize the endogenous protein in HEK293 cells. However, the centrosomal localization was not observed with a GFP-I3 fusion protein in the same study. The authors identified a basic stretch, 33-RKRK-36, which functions as a nuclear localization signal (NLS) and another stretch, 94-HRKGRRR-100, which upon deletion in the mutant GFP-I3(1-93) abrogated the nucleolar accumulation (Huang et al., 2005)(see also Figure 13A). The same group reported later that I3 contains a site for Caspase-3-mediated cleavage and that upon apoptosis, I3 together with PP1γ relocalizes first from nucleoli to the nucleus and finally to the cytoplasm (Huang and Lee, 2008).

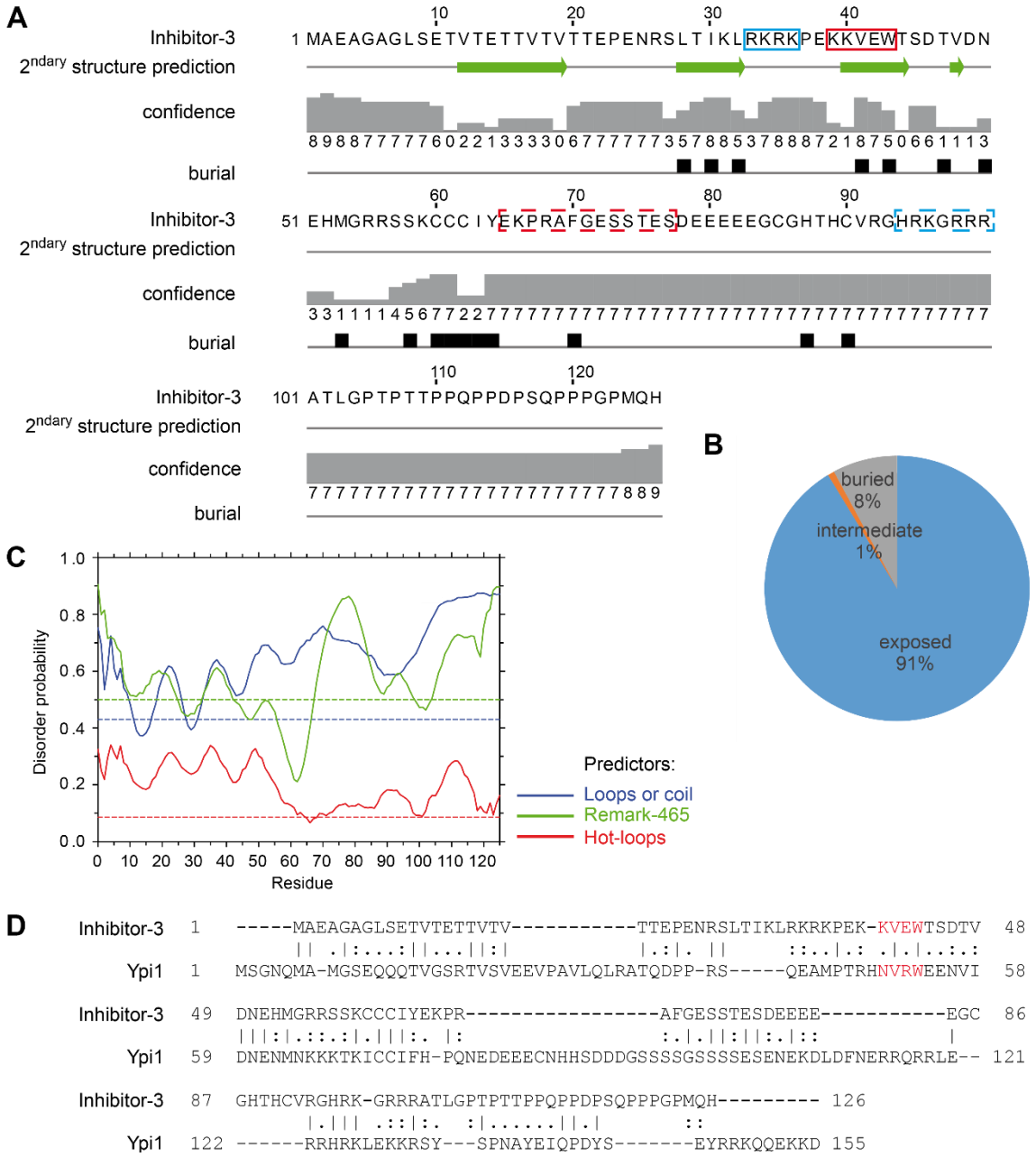

Figure 13: Inhibitor-3 secondary structure and disorder prediction and homology to yeast Ypi1. (**A**) Secondary structure of I3 (β sheets shown as green arrows) and buried amino acid residues (burial) were predicted based on the sequence of the human protein using the Jnet algorithm incorporated in JPred 4.0 (Drozdetskiy et al., 2015). The RVxF consensus sequence "KKVEW" (rectangle) and a potential second PP1-interaction site (dashed lines) are highlighted in red (Zhang et al., 2008). Sites reported to mediate nuclear (rectangle) and nucleolar (dashed lines) localization are highlighted in blue (Huang et al., 2005). (**B**) Prediction of solvent-exposed and buried residues of I3 using the PROFsec algorithm (Predictprotein Server)(Rost et al., 2004) (**C**) Prediction of disordered regions of I3 using the DisEMBL algorithm (Linding et al., 2003). "Loops and Coils" estimates are derived from secondary structure prediction, "Remark 465" score is based on missing sequences in protein structure databases, indicating flexibility and "Hot loops" are predicted coiled regions with high calculated thermodynamic flexibility. Dashed lines indicate threshold for disorder based on statistical likelihood for each method. This prediction shows high likelihood of disorder for most regions in I3. (**D**) Sequence alignment for human I3 and budding yeast Ypi1 as in Figure 12E.

I.2.6 Functional characterization of SDS22 and I3 in metazoans

Studies in the eukaryotic model system *Drosophila melanogaster* found roles for Sds22 in epithelial polarity (Grusche et al., 2009), likely via PP1-dependent dephosphorylation of

Merlin and Moesin, two linker proteins between cytoskeleton and plasma membrane (Yang et al., 2012). Furthermore, both Sds22 as well as the two essential PP1 homologs PP1α87B and PP1β9C were required for maintenance of epithelial integrity and to prevent cell invasion (Grusche et al., 2009), in line with a previous report that regulation of nonmuscle myosin and actin organization is the essential function of PP1β in *Drosophila* (Vereshchagina et al., 2004). Similar to studies on the function of Sds22 in yeast, these observations were largely consistent with both a substrate-specifying function, but also with a general requirement of SDS22 for PP1 stability or activity.

In mammalian cells, SDS22 has been implicated as a substrate-specifier in maintenance of epithelial polarity and in relaxation of the polar actin cytoskeleton during mitosis via regulation of ezrin/radixin/moesin (ERM) complex components (Grusche et al., 2009; Kunda et al., 2012; Rodrigues et al., 2015). These studies mainly employed depletion experiments. However, artificial recruitment of SDS22 to the cortical cytoskeleton, which was achieved by Rodrigues *et al.* using an optogenetic approach (Kennedy et al., 2010), induced localized relaxation in the illuminated region (Rodrigues et al., 2015). While this shows that SDS22 can recruit PP1 to locally dephosphorylate cytoskeleton-regulatory substrates, this approach did not definitely show that it is a complex of SDS22 with PP1, which is active in this function. Indeed, other reports found that PP1-MYPT1 is the specific phosphatase complex involved in the regulation of ERM proteins (Eto et al., 2005; Jin et al., 2006). It is at least conceivable that PP1 is first recruited by SDS22 to the membrane but that SDS22 is then replaced by other PIPs. To test this more conclusively, a fusion of SDS22 with PP1 would have been a possible approach.

Other studies assigned substrate-specifying functions to SDS22 in processes such as dispatch of endosomes from the mitotic spindle (Loubery et al., 2017), but also did not address whether PP1 function was generally impaired in SDS22-deficient conditions. There is also a lack of data on direct interactions between SDS22-PP1 and proposed substrates in mammalian cells, although in many cases physical interaction of PP1 with its substrates is rather stable (Virshup and Shenolikar, 2009). More detailed data were obtained for the involvement of SDS22 in mitotic regulation of PP1 and will be discussed in a later section (I.2.8).

Compared with SDS22, data on the function of I3 are more scarce. It was originally identified as the product of a cDNA encoding the “hemochromatosis candidate gene V” (HCGV) with unknown function and was found to be an inhibitory interactor of PP1 in a phosphorylase *a* phosphatase assay (Zhang et al., 1998). Its localization to the nucleus, nucleoli and centrosomes was interpreted to predict a role in cytokinesis or nucleolar events (Huang et al., 2005), which is in some agreement with its implication in mitotic functions in yeast (I.2.4). However, these initial reports have not been confirmed by data on any of these processes in metazoans.

Instead, unrelated functions have been assigned to I3, including a role in the regulation of apoptosis as mentioned before (Huang and Lee, 2008) (I.2.5) and a function in inhibiting PP1-mediated dephosphorylation of STAT3 (Li et al., 2017). In this study, expression of I3 was found to be under control of the microRNA MIR34a. This regulatory mechanism was activated by hypoxia-inducible factor 1α (HIF1α) and required functional p53. As a consequence of expression of I3 and activation of STAT3 due to inhibition of PP1, epithelial-mesenchymal transition could be induced in hypoxic conditions in p53-deficient colorectal cancer cells (Li et al., 2017).

Another recent report found that I3 acts as an E3 ligase in toll-like receptor signaling (McKelvey et al., 2016). However, the putative RING finger domain does not conform to the consensus of this family. RING finger domains contain two motifs, each of which coordinates a zinc ion by cysteine and histidine residues in a typical arrangement with variable spacing (Borden and Freemont, 1996). Although the authors state that the putative RING domain in I3 could contain non-canonical zinc-finger motifs, the spacing of the putative zinc-binding residues histidine-52 and cysteine-60 through -62 in the first of two zinc fingers is very untypical for a RING finger domain, since zinc-coordinating cysteine and histidine residues are found with a minimum distance of two residues each in these domains. Furthermore, this arrangement does not conform to any of the known zinc-binding motifs (Krishna et al., 2003).

I.2.7 A stable, inactive complex can be formed by SDS22, PP1 and I3

The first studies on fission yeast sds22+ already reported the co-elution of a phosphoprotein of roughly 25 kDa (Stone et al., 1993) and a protein of similar size was soon discovered in a complex with SDS22 isolated from rabbit skeletal muscle (Dinischiotu et al., 1997). These homologous proteins in yeast and mammals were identical with Ypi1 and I3, respectively (see also I.2.3). Interestingly, before the interactor of SDS22 in this complex was identified, a bioinformatics-based analysis of the evolutionary conservation of PP1-interacting proteins indicated that SDS22 and I3 are the two most ancient partners of the catalytic subunit (Ceulemans et al., 2002a). Indeed, SDS22, PP1 and I3 co-migrate in gel filtration experiments using HeLa extracts and immunoprecipitation (IP) of endogenous I3 revealed binding of SDS22 (Lesage et al., 2007).

Two-hybrid experiments indicated that yeast Ypi1 and Sds22 interact directly (Pedelini et al., 2007), which required the C-terminal ~60 residues of Ypi1. The interaction of Ypi1 with Sds22 further depended on the C-terminal 22 residues in Sds22, which were however not sufficient in isolation and may have been required for protein stability since they contain the LRR cap (I.2.5). A region of 40 N-terminal residues of Sds22 was dispensable, which agreed with the requirement for interaction of Sds22 with Glc7. Although mammalian SDS22 and I3 were also observed to interact directly in yeast-2-hybrid experiments, pulldown of tagged proteins did not support this finding (Lesage et al., 2007). On the other hand, combined

expressions of Sds22 and Ypi1 or I3 together with Glc7/PP1 in both yeast-3-hybrid as well as pulldown experiments consistently led to more efficient interactions than any pairwise combination (Lesage et al., 2007; Pedelini et al., 2007). These results show that a trimeric complex of SDS22, PP1 and I3 (SPI complex) is the most stable configuration and indicate cooperative binding between SDS22 and I3. This could either be mediated by a direct interaction between these two or by induction of a conformational change in PP1. Indeed, an influence on PP1 conformation has been reported for SDS22, as will be discussed below.

How does this trimeric complex relate to the observed roles of SDS22 and I3 alone, which were discussed before? One line of evidence suggested that both proteins function as inhibitors of the PP1 catalytic subunit. This was shown by *in vitro* experiments for yeast Sds22 and Ypi1 using pNPP as a substrate (Pedelini et al., 2007). In these assays, an additive effect of both proteins on PP1 activity was observed. This was not the case for mammalian SDS22 and I3 when added to PP1 in an assay for phosphorylase *a*-phosphatase activity, although both proteins inhibited PP1 individually with IC_{50}-values of about 50 nM (Lesage et al., 2007). This inhibition appeared to be substrate-dependent, since PP1 activity towards casein was also inhibited, whereas myelin basic protein and histone H2A were dephosphorylated despite the presence of up to 400 nM SDS22 or I3. This was in line with early findings on Sds22+-associated phosphatase in fission yeast, which was active against histone H1 (Stone et al., 1993).

Interestingly, in addition to the substrate-dependent inhibition, SDS22 causes a time-dependent inactivation of PP1, affecting its activity towards all of these substrates and rendering the catalytic subunit sensitive to digestion by trypsin (Lesage et al., 2007). This effect indicated an influence of SDS22 on PP1 conformation, as had been observed before in the case of I2 (Bollen and Stalmans, 1992; Yang et al., 1981). It occurred at lower concentrations of SDS22 than required for the inhibition of PP1 and importantly, PP1 isolated by co-immunoprecipitation of endogenous I3 from Cos1 cells or by co-elution with GST-tagged SDS22 or I3 displayed very little trypsin-revealed phosphorylase *a*-phosphatase activity compared to PP1 associated with NIPP1 (nuclear inhibitor of PP1), a substrate-specifier involved in gene expression regulation (Van Dessel et al., 2015). These results indicated that SDS22- and I3-associated PP1 is inactive *in vivo*, likely due to the conformational change exerted in PP1 by incubation with SDS22 (Lesage et al., 2007).

Although the data obtained with defective mutants of Sds22 and Ypi1 in yeast indicated that both are required for essential mitotic and potentially other roles of Glc7, it appears unlikely that the trimeric complex has substrate-specifying functions because of the inactivation effect of Sds22 and because Ypi1 would compete with targeting subunits at kinetochores such as KNL1, which bind Glc7 via an RVxF motif. A potential function for the trimeric complex may be to assist or bring about the nuclear localization of the catalytic subunit. This is in line with the requirement of both interactors for nuclear localization of Glc7. The main factor driving

correct localization of the complex appears to be I3, as indicated by the dependence of Sds22 nuclear localization on Ypi1 (Bharucha et al., 2008) and the presence of localization signals in I3 but not SDS22 (Figure 13). However, it is unclear how this would translate to mitosis in higher eukaryotes, which disassemble the nucleus upon entry into mitosis.

I.2.8 A model for the function of SDS22 and I3 towards PP1

A widely held conception of SDS22 function in mammals is that it serves as a substrate-specifier in the mitotic role of PP1 (Nasa and Kettenbach, 2018). This has been investigated in some detail by the group of Jason Swedlow, who found that SDS22 was required to promote dephosphorylation of Aurora B at the T-loop residue Threonine-232 (T232) by PP1 (Posch et al., 2010). On the other hand, depletion of SDS22 caused decreased phosphorylation of PP1 substrates at kinetochores, indicating that other subunits are responsible for directing PP1 activity in opposing Aurora B-mediated phosphoregulation of kinetochore substrates. In contrast, Wurzenberger and co-workers implicated SDS22 along with another PP1 interactor, Repo-Man, in the dephosphorylation of Dsn1 by PP1 in anaphase (Wurzenberger et al., 2012). Mps1 was also proposed to be a direct substrate of PP1 activity at kinetochores in *Drosophila* and depletion of Sds22 resulted in a similar increase of Mps1 phosphorylation as depletion of PP1-87B (Moura et al., 2017).

Posch *et al.* in the Swedlow group detected localization of an overexpressed GFP-SDS22 fusion to kinetochores during metaphase and to the central spindle and midbody in later phases of mitosis, consistent with direct opposition of SDS22-PP1 towards Aurora B (Posch et al., 2010). On the other hand, the authors concede that they failed to detect the endogenous protein via immunofluorescence. Starting with the observation that SDS22 was readily detectable at kinetochores only upon depletion of I3, Annika Eiteneuer and Jonas Seiler in our lab investigated the interplay between the members of the trimeric SPI complex and its potential role in mitosis (Eiteneuer et al., 2014). They found that depletion of both SDS22 as well as I3 led to increased chromosome misalignments in metaphase, delayed mitotic progression, increased Aurora B activity (determined by measuring autophosphorylation of T232), increased phosphorylation of the PP1 substrate Dsn1 and activation of the SAC. While these observations upon depletion of SDS22 were consistent with a substrate-specifying function, the same effects upon depletion of I3 coincided with excessive accumulation of SDS22 at kinetochores as well as on a soluble KNL1-construct together with PP1 (Eiteneuer et al., 2014). Moreover, while the free catalytic subunit of PP1 efficiently dephosphorylated Aurora B at residue T232, addition of SDS22 led to a dose-dependent inhibition of PP1 in this assay, clearly contradicting the notion that SDS22 is a substrate-specifier for Aurora B-directed PP1 activity (Eiteneuer et al., 2014).

Shortly after publication of these results, a study by Cheng and Chen provided additional insight into Sds22 and Ypi1 function in yeast (Cheng and Chen, 2015). They found that both

proteins are required for the stability of the Glc7 catalytic subunit. Previous observations of “fluorescent spots” and loss of Glc7 nuclear localization by others had already suggested this, but this study was the first to define these spots as aggregates with participation of heat-shock proteins. These data assigned to Sds22 and Ypi1/I3 a role in the stabilization rather than pathway-specific regulation of PP1.

Our earlier findings, together with the effects of SDS22 overexpression presented in this thesis, led us to propose a hypothetical model for the functions of SDS22 and I3 in the regulation of PP1. It assumes an activating role of SDS22 and I3 towards PP1, which is required in a step preceding localization of the catalytic subunit to the kinetochore. This step likely involves the trimeric SPI complex. Prior to recruitment by factors such as KNL1, both SDS22, which would otherwise inhibit PP1, as well as I3, which blocks RVxF-motif-mediated binding, have to be dissociated (Figure 14).

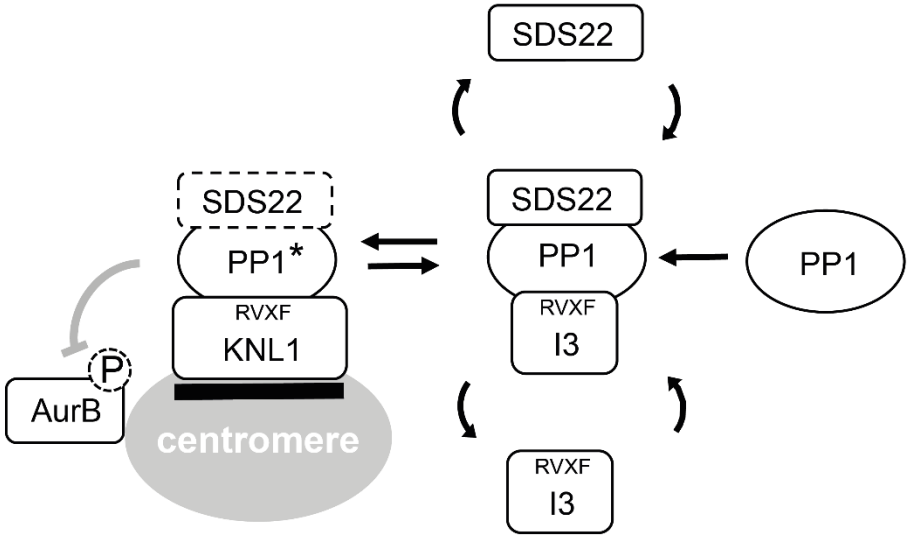

Figure 14: Model for the roles of mammalian SDS22 and I3 in the regulation of PP1 at kinetochores

SDS22 and I3 bind inactive, possibly newly synthesized PP1 in a putative activation step. However, PP1 remains inactive while held in this SPI complex. At this or also at later stages of the PP1 life cycle, I3 binds SDS22-PP1 in solution, thereby preventing association of SDS22-bound PP1 with KNL1 at the kinetochore, which would otherwise interfere with PP1 functions. Sequestration of SDS22-PP1 by I3 thus assures binding of active, SDS22-free PP1 to the kinetochore. The asterisk flags active PP1. (Eiteneuer et al., 2014). AurB: Aurora B.

This model was derived based on data from mitotic cells, but might also extend to other contexts of PP1 function. It provides an explanation for the apparently paradox observations that both depletion of SDS22 as well as forced localization with PP1 at kinetochores reduces the ability of PP1 to balance Aurora B activity (Eiteneuer et al., 2014). The activating role of I3 for PP1 function and to limit SDS22 association with PP1 at kinetochores is also well explained by the proposed role of the trimeric SPI complex as an intermediate step. This model furthermore has the potential to explain and to reconcile similar observations for Sds22 and Ypi1 in yeast, which were described before (I.2.3).

Data on the biogenesis of the related phosphatase PP2A might provide further hints on processes occurring during the activation of multimeric phosphatase enzymes. In the case of PP2A, a catalytic C subunit forms an obligate dimer with a scaffolding A subunit, which is complemented by a variable regulatory B subunit to form trimeric holoenzymes (Sents et al., 2013). Since the free PP2A catalytic subunit lacks specificity and poses a risk to the cell, it is critical that its activity is kept in check before holoenzymes are assembled (Hombauer et al., 2007). Kong and co-workers in the group of Craig Thompson found a stabilizing role of the conserved PP2A interactor α4, deletion of which leads to progressive loss of PP2A complexes (Kong et al., 2009). The interaction of α4 with PP2A C was increased at higher temperatures, concomitant with a reduced interaction of PP2A C with the scaffolding subunit, indicating that α4 stabilizes the C subunit under conditions of stress. Consistently, in proteasome-inhibited conditions, ubiquitinated forms of the catalytic subunit accumulated in α4-depleted cells. Kong *et al.* further observed that the overexpression of PP2A C is enhanced by co-expression of α4 (Kong et al., 2009). These results strongly implicated α4 in the biogenesis of PP2A. However, whether the function of α4 is confined to regulation of PP2A stability is debated since it was also observed to target PP2A to dephosphorylate substrates and recruit it to microtubules (Sents et al., 2013). Interestingly, a microtubule-localized ubiquitin E3 ligase, Mid1, was shown to modify α4 by monoubiquitylation, which regulates the stability of the PP2A C-α4 complex (Watkins et al., 2012).

Other factors involved in the biogenesis of PP2A are “target of rapamycin signaling pathway regulator-like 1” (TIPRL1), which can form a complex with PP2A and α4, and “phosphatase 2A phosphatase activator” (PTPA), which might be required for loading of the catalytic subunit with metal ions (Guo et al., 2014). The role of TIPRL1 has not been extensively studied, but it might serve to stabilize the PP2A-α4 complex or to inhibit the catalytic subunit in this complex (Sents et al., 2013). Arguably, the α4-PP2A C-TIPRL1 complex resembles the SPI complex, since SDS22 and I3 also stabilize and inhibit the PP1 catalytic subunit. This led to the proposition that the role of the PP2A biogenesis factors might be taken over in a similar manner in the case of PP1, where SDS22 could replace α4, I3 might have a function comparable to TIPRL1 and I2 would be required for metal loading in analogy to PTPA (Verbinnen et al., 2017). Of note, structural studies of the interaction of I2 with PP1 indeed showed contacts between I2 and the metal residues inside the active site of PP1 (Hurley et al., 2007).

Our model prompted us to evaluate the putative role of SDS22 and I3 as factors involved in the early life cycle of PP1. Moreover, the observation in a recent study by Cheng and Chen, that similar destabilizing effects on Glc7 are found upon mutation of the yeast protein Shp1, especially regarding the newly synthesized catalytic subunit, indicated another layer of regulation in the context of Sds22 and Ypi1 (Cheng and Chen, 2015). Shp1 was identified as an activator of yeast PP1 by genetic interaction studies (Zhang et al., 1995). However, it was

soon recognized to act in conjunction with a hexameric ATPase called “Cdc48” in budding yeast and “p97” in mammals. Since a major aim of this thesis was to clarify the functional connection between p97 and PP1 that involves the SPI complex, the next sections will introduce the ATPase itself and its putative link to regulation of PP1, which likely depends on homologs of yeast Shp1.

I. 3: The AAA-ATPase p97 and its potential roles in the regulation of PP1

I.3.1 Structure and activity of the AAA-ATPase p97

In a screen for cold-sensitive cell-division-cycle (*cdc*) mutants, Moir and co-workers identified the protein Cdc48 (Moir et al., 1982), whose mutation led to arrest in mid-mitosis. In vertebrate cells, the homolog “p97” was first detected accidentally, as the protein that contained a peptide called “Valosin”, which was thought to be an active peptide with effects on the intestine (Koller and Brownstein, 1987). Later, the same “Valosin-Containing Protein” (VCP) was found by Jan-Michael Peters and co-workers, who looked for novel particles in the “S100” (supernatant of 100.000 x g-centrifugation) fraction of *Xenopus laevis* oocyte extracts. They found a hexameric particle of 570 kDa, which displayed a barrel shape around a central core in negative stain electron microscopy (EM). Since the protomers had a molecular weight of 97 kDa, the authors assigned to them the name “p97” (Peters et al., 1990).

Homologs of p97 have subsequently been found throughout the eukaryotic kingdom, as well as in archaea. It is a highly abundant and ubiquitously expressed protein, which belongs to the family of AAA+-ATPases (ATPases associated with diverse cellular activities). These enzymes are characterized by a conserved AAA motif, which forms an ATPase domain of 230-270 aa residues. The domain contains the “Walker” motifs, which participate in the binding (Walker A) as well as the hydrolysis (Walker B) of ATP, which in all members of the family is Mg^{2+}-dependent. Although AAA motifs are found in a variety of enzymes that use the energy of ATP to generate mechanic force, such as motor proteins, ATP-binding cassette enzymes or helicases, a group of “classical AAA-ATPases” including p97 is further defined by a “second region of homology”, positioning an arginine finger to make intersubunit contacts in oligomeric assemblies, as well as by an α-helical domain C-terminal to the AAA motif (Erzberger and Berger, 2006; Ogura and Wilkinson, 2001; Patel and Latterich, 1998; Wendler et al., 2012). The members of the classical AAA-ATPase family form hexameric ring structures around a central pore. These rings may consist of a single layer of ATPase domains or can be stacks of adjacent AAA motif-containing domains within the protomers.

Since p97 forms a stack of two hexameric rings, consisting of the “D1” and “D2” ATPase domains, it belongs to the type II hexameric AAA-ATPases (Zhang et al., 2000b). In addition to the two ATPase domains, p97 has an N-terminal domain of about 200 residues arranged

in a psi-barrel fold forming an N-terminal sub-domain (Nn) and a β-barrel fold in a C-terminal subdomain (Nc), connected by a short linker (Figure 15A). The N- and D1-domains are connected by a longer, 22 aa linker, which provides flexibility to the arrangement of the N domain. The N domain was shown to adopt two main conformational states, depending on the nucleotide-binding status of p97. It was found to be in plane with the D1 domain in an ADP-bound state of the hexamer, forming the so-called “down”-conformation. Loading p97 with ATP (or the non-hydrolyzable analog ATPγS) induces an “up”-conformation (Figure 15B). These conformational changes are likely involved in substrate handling (van den Boom and Meyer, 2018) but will not be further detailed here. There is also a short linker between the D1- and D2-domains and a flexible tail at the C-terminus.

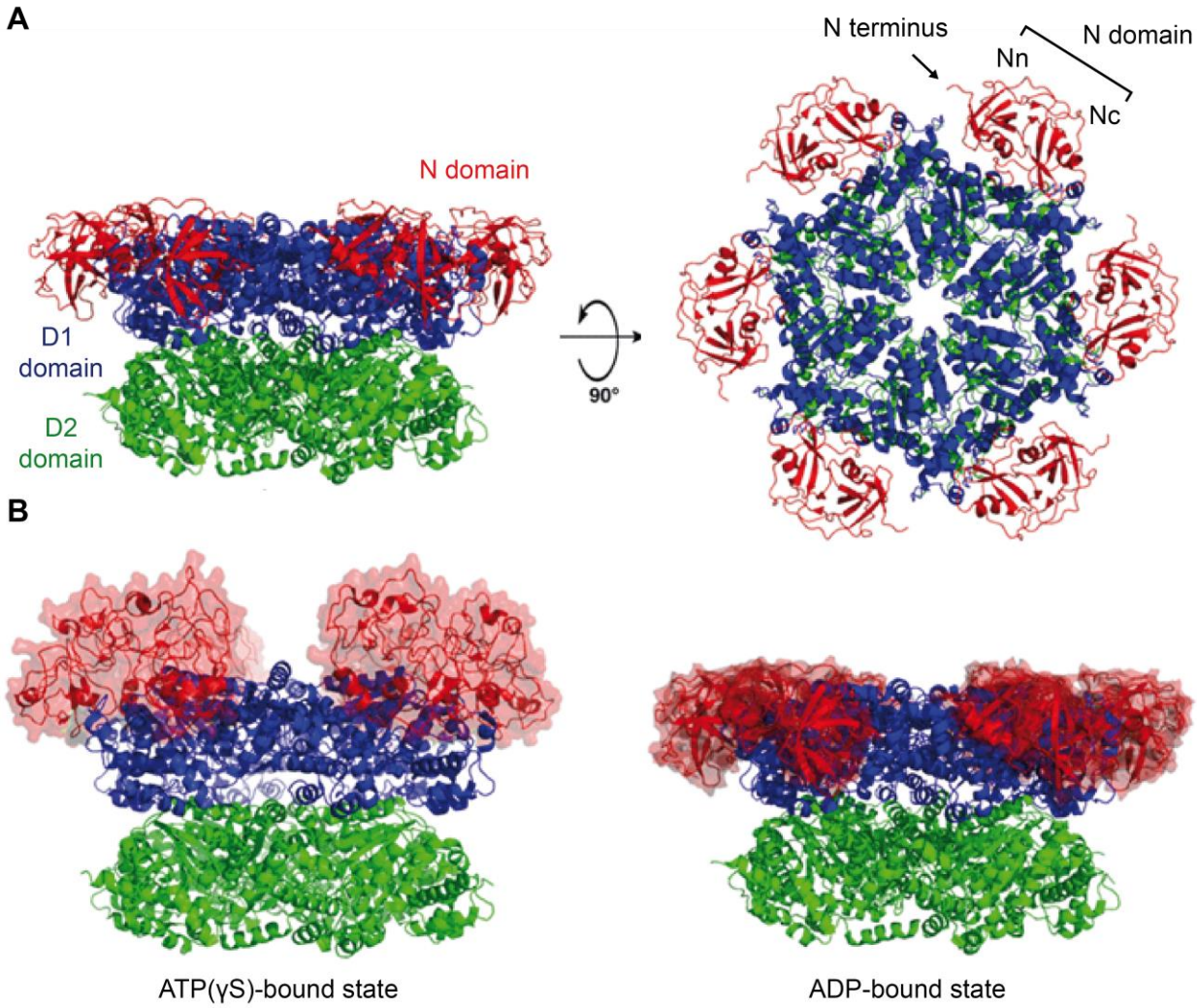

Figure 15: Structure of the AAA-ATPase Cdc48/p97
(**A**) Yeast Cdc48 and its human homolog p97 form homohexameric assemblies around a central pore. Each protomer comprises an N-terminal domain (red), which contains the two subdomains Nn and Nc, and two ATPase domains called D1 and D2. (**B**) The N domains of Cdc48/p97 are flexible due to the linker to the D1 domain. In the ATP or ATPγS-bound state (left) they are found in a so-called “up conformation”, in which they are positioned above the D1 ring (PDB id: 5FTN). Upon hydrolysis of ATP to ADP, they move to the “down conformation”, which is co-planar with the D1 ring (ADP-bound state, PDB id: 5FTK, right). Adopted from: (Bodnar and Rapoport, 2017a).

Interestingly, the C-terminal tail of p97 contains an “HbYX” motif, which is also present in the 19S regulatory particle (RP) of the proteasome (Smith et al., 2007) and serves to dock the Rpt subunits of the 19S RP onto the 20S core peptidase, forming the 26S proteasome. The Rpt subunits themselves belong to the classical AAA-ATPase family and form a heterohexameric ring structure on top of the proteolytic, barrel-shaped chamber of the 20S peptidase (Voges et al., 1999). The AAA-ATPases in this proteasome complex serve to recognize and unfold substrates, which are then channeled into the proteolytic chamber (Tomko et al., 2010; Voges et al., 1999). This arrangement is present in all kingdoms of life. In further support of an evolutionary connection between the 19S RP and p97, functional assemblies of yeast Cdc48 as well as the archaeal homolog VAT with the respective 20S proteasomes have recently been reported (Barthelme et al., 2014; Barthelme and Sauer, 2012), although the physiological role in yeast still awaits clarification (Esaki et al., 2018) and conservation in higher eukaryotes has not been shown. Nonetheless, it has been a long-standing proposition that the main role of p97 was to prepare folded proteins for final degradation by the proteasome (Dai et al., 1998).

Although proteolytic enzymes such as the bacterial ATP-dependent FtsH protease belong to the classical AAA-ATPase superfamily and other proteases such as Lon are closely related (Wendler et al., 2012), the unifying characteristic of ATP-dependency distinguishes them from ATP-independent proteases. This hints to a fundamental difference in function, since the expense of energy is not required for the actual proteolytic process but rather reflects the requirement of processing of folded or complex-bound substrates (Baker and Sauer, 2012; Esser et al., 2004; Sauer et al., 2004). In line with this thought, the hexameric AAA-ATPase ClpA can cooperate with the protease ClpP in *Escherichia coli* as a functional equivalent of the proteasome but is also a bona-fide chaperone (Weber-Ban et al., 1999). Together with heat-shock proteins, it is part of the Clp/Hsp100 family in yeast, which overlaps with the classical AAA-ATPases (Schirmer et al., 1996; Wendler et al., 2012). Similarly, the Lon protease also recognizes misfolded substrates for degradation (Gur and Sauer, 2008).

Chaperone-related activities have also been attributed to the ATPase function of p97. An early report implicated yeast Cdc48 in the release of the transcription factor Spt23 from membranes resulting in its activation rather than degradation (Hoppe et al., 2000; Rape et al., 2001). Furthermore, p97 was found to be required in the process of endoplasmic reticulum-associated degradation (ERAD) but its direct role lies in the extraction not the degradation of the substrates of this protein quality control pathway (Ye et al., 2001). These and further reports led to the view that p97 functions as a “segregase” to extract client proteins from complexes, membranes or other structures and argued against a function limited to protein degradation (Meyer et al., 2012). However, until very recently, the precise mechanism of action by which p97 allows proteins to be removed from tight bonds remained elusive. This aspect of p97 function will be discussed in more detail below (I.3.6).

On the other hand, p97 is undoubtedly involved in proteolytic activities and an extensive body of evidence has accumulated, linking it to the Ubiquitin-Proteasome System (Jentsch and Rumpf, 2007; Meyer et al., 2012; Ye, 2006). Ubiquitination is a post-translational modification catalyzed by an enzymatic cascade that comprises a ubiquitin-activating enzyme (E1), a ubiquitin-conjugating enzyme (E2) and a ubiquitin ligase (E3). This cascade transfers the small globular protein ubiquitin onto a lysine residue of the target selected by the specific E3 ligase. Ubiquitin comprises 76 aa residues including seven lysine residues, onto which further ubiquitin moieties can be transferred to generate polyubiquitin chains with different linkage types. It has been recognized that ubiquitination is not simply a signal for protein degradation but can have a variety of outcomes, depending on the interaction that is promoted by the modification (Chen and Sun, 2009). The outcome was also shown to depend on the specific linkage type of the polyubiquitin chain. Whereas K48-linked polyubiquitin chains are usually a signal to target the substrate for proteasomal degradation, the outcome of polyubiquitination with other linkage types is more diverse (Komander, 2009). The prominent role of p97 in the ubiquitin system is easily recognized upon RNAi-mediated depletion, which leads to strong accumulation of poly-ubiquitinated protein species, suggesting that p97 plays a role in the turnover of a large number of proteins (Wojcik et al., 2004). However, this observation does not preclude other non-degradative outcomes of p97-mediated processing of ubiquitinated proteins as described above. This may again be dependent on the linkage type and consequently on the recruitment of p97 via different adapters, which have been found to be essential to target the ATPase to ubiquitinated substrates (Meyer et al., 2012) (see also I.3.2). Figure 16 shows a model for the involvement of p97 in pathways involving ubiquitinated substrates.

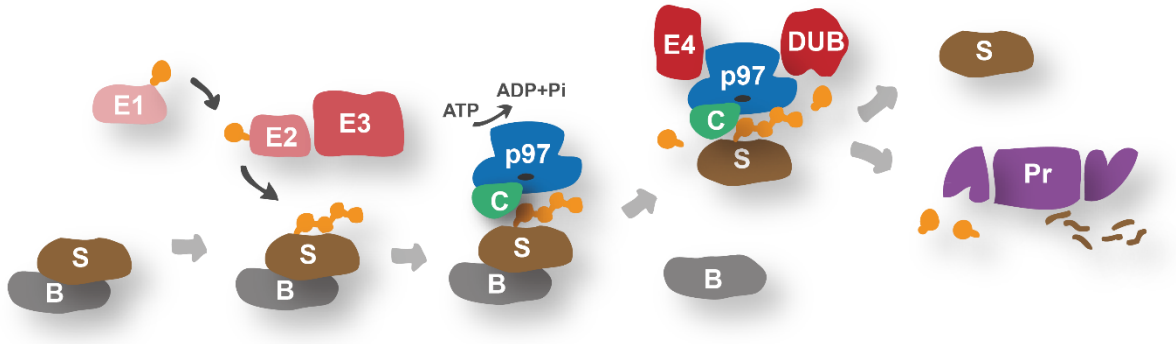

Figure 16: General model for the function of p97 in substrate segregation and ubiquitin chain editing.
A substrate (S) is targeted by the cascade of ubiquitination involving E1, E2 and E3 enzymes as introduced in the main text. Recognition of ubiquitinated substrates is mediated by a biquitin-binding p97 cofactor (C). The ATPase activity of p97 generates mechanical force that structurally remodels the substrate to segregate it from binding partners (B) or cellular surfaces. Ubiquitin chain extension enzymes (E4) or deubiquitinases (DUB) may be co-recruited by p97 to modulate the ubiquitination state of the substrate. p97-mediated processing can either release the substrate in a native form or target it for degradation by the proteasome (Pr). Adopted from (Meyer et al., 2012).

Similar to this prototypical function of p97, the 19S particle in eukaryotes was also found to primarily recognize ubiquitinated proteins to target them for degradation. This forms the basis for degradation by the canonical 26S proteasome in the ubiquitin-proteasome system (UPS), which is the principal mechanism for the turnover of short-lived proteins in eukaryotes (Pickart, 1997). However, since the ClpA-ClpP protease in prokaryotes shares the structural arrangement of the proteasome but bacteria lack a general degradative signal like ubiquitin (Voges et al., 1999), it appears clear that substrate recognition by the bacterial "proteasome" has to proceed by other mechanisms. This was shown to include direct recognition of the substrate by ClpA (Flynn et al., 2003) and binding of substrate adapters (Dougan et al., 2002). Interestingly, ubiquitin-independent degradation of substrates such as ornithine decarboxylase, IκBα, c-Jun, calmodulin and troponin C has been observed in eukaryotes (Benaroudj et al., 2001; Pickart, 1997). Systematic evaluation of the ubiquitin-dependence of proteasomal degradation indicated that degradation of substrates in the absence of ubiquitination exists in eukaryotes but may be an evolutionary remnant of a "pre-ubiquitin world" (Erales and Coffino, 2014).

In the case of p97, the N domain seems to be the essential region for substrate recognition activities. An earlier study found that it can make direct contact with ubiquitin chains containing at least 3 to 4 ubiquitin moieties (Dai and Li, 2001), although this has not been confirmed subsequently. It was also reported that the N domain directly contacts unmodified stretches in the substrate (DeLaBarre and Brunger, 2005; Meyer et al., 2012) and a study on the archaeal p97 homolog VAT proposed that the N domain on its own is able to stabilize unfolded proteins or act in a chaperone-like manner in folding or unfolding of substrates (Golbik et al., 1999). Consistently, the N domain of Cdc48 recognizes non-native proteins (Thoms, 2002). On the other hand, a vast body of work implicated adapter proteins as the actual substrate-engaging entities in p97 complexes (Buchberger et al., 2015). It has also been shown that many of these adapters possess domains for the recognition of ubiquitin and this seems to be the major mode by which p97 is recruited in its various functions (Meyer et al., 2012). Although some p97 adapters lack a ubiquitin-binding domain, formation of heterooligomeric complexes with ubiquitin-binding adapters provides an alternative possibility for the involvement of ubiquitin in processes governed by p97 adapters such as p37, which do not harbor ubiquitin-binding domains. The adapter protein p37 mediates p97 function in the only example of a putatively ubiquitin-independent process so far, which is the interphase maintenance of ER and Golgi (Uchiyama et al., 2006). However, the direct substrate and mode of recognition in this context have not been described.

In sum, it has been shown that a prominent function of p97 is to support cellular proteostasis by facilitating the turnover of poly-ubiquitinated proteins, although other outcomes of processing by p97 are also possible. Due to the multitude of interacting proteins, which direct the function of p97 to diverse cellular roles, it seems likely that other modes of recruitment,

involving variable ubiquitin modifications and perhaps even ubiquitin-independent modes of recruitment may exist. This will be further discussed in connection with the diversity of p97 functions in the next section.

I.3.2 Regulation of a broad diversity of cellular p97 functions by adapter proteins

In vertebrate cells, p97 makes up an estimated 1 % of the cytosolic protein content (Peters et al., 1990; Ye, 2006). However, it is also found inside the nucleus and associated with membranes (Ye, 2006). Despite its original identification as a cell-cycle deficient mutant in yeast (I.3.1), one of the first functions assigned to a p97 homolog was membrane fusion activity, in which p97 was first implicated due to its similarity with another classical hexameric AAA-ATPase, N-ethylmaleimide-sensitive factor (NSF) (Peters et al., 1990). NSF mediates the reformation of the Golgi apparatus by ATPase activity-dependent disassembly of wound-up SNAREs (soluble NSF attachment protein receptor) in the fragmentation phase in early mitosis to prime them for further membrane fusion events and by an ATP-independent mechanism during mitotic exit (Muller et al., 2002). The existence of a p97-dependent pathway of membrane fusion was later confirmed in ER and Golgi reassembly after mitosis (Latterich et al., 1995; Rabouille et al., 1995) as well as in nuclear envelope reassembly (Hetzer et al., 2001).

In the first isolations of p97, a protein of 47 kDa was prominently co-eluted and was found to be involved in the membrane fusion activity of p97 (Kondo et al., 1997). This protein, which was termed “p47”, is one of the main interactors of p97 but a similarly abundant complex is formed by the proteins Ufd1 (“Ubiquitin-fusion degradation 1”) and Npl4 (“Nuclear protein localization 4”) with p97. The Ufd1-Npl4 complex and p47 were found to bind p97 in a mutually exclusive manner (Meyer et al., 2000). A large number of interactors has since then been identified (Buchberger et al., 2015) and include a range of proteins that can be viewed as adapters, which direct the ATPase activity of p97 to a specific context, but also include a variety of enzymes, which themselves provide catalytic functions. It has been observed that some adapters influence the ATPase activity of p97 (Meyer et al., 1998) and it has even been proposed that they participate in the transmission of mechanical force to the substrate, as will be discussed later (I.3.6). Therefore, the term “cofactor” has been used broadly to refer to interactors of p97, which may or may not have catalytic activity on their own. Consistent with a prominent role of p97 in ubiquitin-mediated processes, many interacting enzymes have ubiquitin chain-extending, -modifying or -removing activities (Meyer et al., 2012)(see also Figure 16). However, p97 does not simply function as a scaffold protein but applies its ATPase activity in a plethora of processes.

Adapters bind mostly to the N domain via a range of interacting motifs, including a prominent Ubiquitin Regulatory X (UBX), and a similar UBX-like (UBX-L) domain, which is present in a range of proteins in mammals and defines these as bona-fide p97 interactors (Kloppsteck et

al., 2012). Other interaction motifs that bind to the N-terminus include the VCP-interacting and VCP-binding motifs (VIM and VBM) and a SHP box or Binding Site 1 (BS1) motif. In contrast, PUB and PUL domains make contact to the C-terminal flexible tail of p97 (Buchberger et al., 2015).

Although p97-adapter complexes are likely to have diverse topologies, some so-called "major" cofactors were shown to interact in a mutually exclusive manner. These include Ufd1-Npl4 and p47 but also UBXD1, a UBX-domain containing protein. These core complexes may then recruit accessory adapters or co-factors (Meyer et al., 2012), forming intricate networks, which have only begun to be understood by recent application of mass spectrometry methods (Raman et al., 2015).

The core complex formed by p97 with Ufd1-Npl4 has been most extensively studied in processes that require the extraction of ubiquitinated proteins. This includes the prominent role of p97 in ERAD, as mentioned before, but also the non-degradative function in mobilization of Spt23 from the ER membrane (see I.3.1). In addition to ER-localized processes, Ufd1-Npl4 also targets p97 to extract proteins from chromatin, as will be discussed further below, and from the outer mitochondrial membrane, although in this context the interactor Vms1 might replace Ufd1 in the complex with Npl4 (Heo et al., 2010). This mechanism is part of a similar quality control mechanism as compared to ERAD. Furthermore, Ufd1-Npl4 also targets p97 to soluble proteins including HIF1α (Alexandru et al., 2008) or protein complex members such as IκBα (Li et al., 2014) (see also Figure 17).

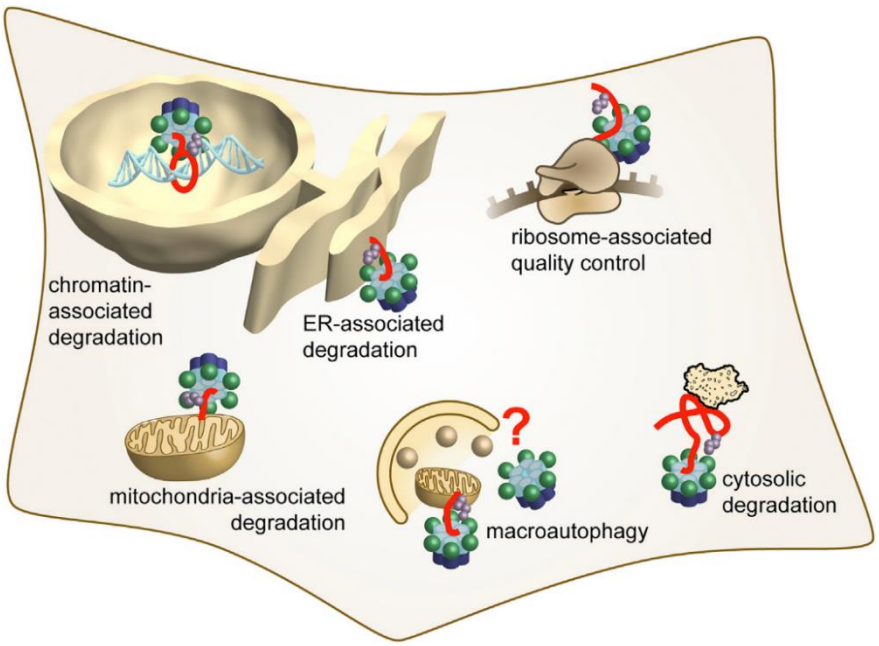

Figure 17: Prominent examples of p97-mediated pathways.
As discussed in the text, p97 was shown to handle ubiquitinated substrates at various cellular structures, including the endoplasmic reticulum (ER), mitochondria, ribosomes but also chromatin. A paramount function of p97 is the retrotranslocation of misfolded ubiquitinated proteins from the ER into the cytosol for degradation (ER-associated degradation; ERAD). It was also implicated in selective macroautophagy of damaged organelles through unknown mechanisms and might assist cytosolic degradation processes. Substrates of p97 are depicted in red, ubiquitin chains in violet. Adopted from (van den Boom and Meyer, 2018).

In general, p97 seems to play an important role for cellular proteostasis, especially with regard to quality control of ER-localized proteins. This is supported by the strong induction of an Unfolded Protein Response (UPR) upon pharmacological inhibition of p97 activity and subsequent activation of the intrinsic pathway of apoptosis (Kothe et al., 2005; Meyer et al., 2012). Whether a similar role of p97 exists in the maintenance of proteostasis in the cytosol is still unclear, although the quality control in the ER and cytosol are closely linked (Buchberger et al., 2010). We recently established another function of p97 in the regulation of the so-called “Integrated Stress Response” (ISR)(Pakos-Zebrucka et al., 2016) by facilitating the degradation of the PP1-interactor CReP (Constitutive Repressor of eIF2α Phosphorylation)(Hülsmann et al., 2018). This PP1 complex is required to balance the activity of stress kinases towards the regulator of translation, eIF2α, and degradation of CReP is known to mediate the cellular response to various stress conditions, including accumulation of unfolded proteins in the ER (So et al., 2015).

The other core complexes, p97-p47 and p97-UBXD1 have also been implicated in processes where a segregase function is required, for example during sorting of membrane-bound proteins in the endolysosomal pathway, which requires UBXD1 (Ritz et al., 2011). Recently, our group identified a prominent role for p97-UBXD1 in the response to damage occurring in lysosomes following treatment with the peptide LloMe (Papadopoulos et al., 2017). In addition to UBXD1, another interactor called PLAA and the deubiquitinating enzyme (DUB) YOD1 are part of the p97 complex, illustrating the additional layers of regulation that can occur in p97-mediated processes. These two studies also further established a link between p97 and lysosomal degradation. Interestingly, links were also found with a third major degradative pathway operating in the cytosol, which is autophagy. Here, p97 may be required in a maturation step via an unknown mechanism (Meyer et al., 2012).

In analogy to the disassembly of SNARE complexes by NSF (Sollner et al., 1993), p97-p47 has been proposed to have a disassembling function towards SNAREs, but its direct substrate has not been identified (see I.3.5). Although it is clear that p97 together with p47 is required for the reassembly of the Golgi and for ER network formation (see I.3.5), both the Ufd1-Npl4 adapter complex and p47 were required for the reformation of the nuclear envelope following mitosis (Hetzer et al., 2001). With the discovery that Ufd1 and Npl4 are required for p97-mediated extraction of the mitotic kinase Aurora B from chromatin during mitotic exit (Ramadan et al., 2007), it became clear that p47 has a specific role during the membrane fusion process, whereas Ufd1-Npl4 are required to counteract Aurora B, which otherwise inhibits membrane fusion. However, in addition to p97-p47, a complex formed with the p47-related adapter p37 has also been implicated in p97-mediated membrane fusion as will be discussed below (I.3.5). The p97-p47 core complex also differs from p97-Ufd1-Npl4 in terms of the ubiquitin signal responsible for its recruitment. Whereas Ufd1-Npl4 has high

affinity for K48-linked ubiquitin chains, p97-p47 has high affinity for monoubiquitin, as will also be discussed below (I.3.5).

Apart from its prominent function in proteostasis and membrane fusion, p97 has been shown to be involved in a plethora of other cellular functions, including signaling during the hypoxia response and apoptosis but also during the DNA damage response, which showcases its ability to extract proteins not only from membranes but also from chromatin. For example, it has recently been shown by our group that p97 together with Ufd1-Npl4 extracts sterically trapped Ku80 following double-strand breaks (van den Boom et al., 2016). It was also shown that p97 can interact directly with further DNA damage response-regulatory proteins, including Breast Cancer Antigen 1 (BRCA1)(Zhang et al., 2000a).

It seems possible that the p97 ATPase module in all of these processes fulfils the same molecular function. However, an alternative idea is that different complexes lead to different modes of translation between ATP consumption and the mechanical force exerted by p97 on its substrates. For example, it was suggested that the UBA domain of p47 could act as a mediator of the mechanical force (Beuron et al., 2006). Given the diversity of functions fulfilled by p97, it is crucial to understand the underlying mechanism of action. This requires the availability of suitable assays, some of which have recently emerged for the study of the Ufd1-Npl4 cofactor complex and will be discussed in a later section (I.3.6). However, our understanding of p97 function will also require assays for the other core complexes, as well as a better understanding of their cellular roles.

I.3.3 Roles of yeast Cdc48 and mammalian p97 in cell cycle regulation

In budding yeast, Cdc48 was found to have a role in passing the G1-S transition (Start) by facilitating the degradation of Far1 (Fu et al., 2003). Another recent study on this function of Cdc48 assigned it to a role in determining the fate of the G1 cyclin Cln3, although this function awaits further verification (Parisi et al., 2018). Such involvement in the regulation of the cell cycle extends the repertoire of p97 even further and is consistent with the arrest observed for the *cdc48-1* mutant that initially led to its identification in budding yeast (Moir et al., 1982). It has also been shown in mammalian cells that p97 has cell cycle-regulatory functions. One of them occurs at the G2/M transition, where p97 together with Ufd1-Npl4 is required for robustness of the G2/M checkpoint in response to DNA damage. This results from the role of p97 in facilitating the degradation of Cdc25A, a phosphatase that promotes entry into mitosis (Riemer et al., 2014).

Although these functions impact cell cycle progression, they cannot fully explain the mid-mitotic arrest phenotype in *cdc48* mutants in budding yeast. However, roles of the ATPase during mitosis have also been identified. For example, it was reported that spindle disassembly at mitotic exit requires Cdc48 together with Ufd1-Npl4 (Cao et al., 2003) and that the mutant *cdc48-3* arrests at mitotic exit. However, the *cdc48-1* mutant analyzed earlier

had a large-budded phenotype with the chromatin positioned at the bud neck, typical of a metaphase arrest (Moir et al., 1982). A later report also found several mitotic defects after integration of the *cdc48-3* mutation in a different strain background (W303) (Cheng and Chen, 2010) compared to the earlier study by Cao *et al.* (strain MLY1640 (Latterich et al., 1995)). The mitotic defects of *cdc48-3* in the W303 background included a SAC-dependent metaphase arrest, defects in chromosome separation and spindle and pole body defects (Cheng and Chen, 2010).

It appears that p97 can influence mitotic progression in several ways (Meyer and Popp, 2008), but one prominent line of evidence places p97 in an antagonistic function to Aurora kinases. This antagonism was observed in yeast, where hyperphosphorylation of a substrate of Ipl1, Dam1, is restored by combination of the *ipl1-132* mutant with a *cdc48-3* mutation (Cheng and Chen, 2010). However, the combined strain still grew poorly, likely due to defects in unrelated Cdc48 functions (Cheng and Chen, 2010). The adapter implicated in the Ipl1-antagonistic function of Cdc48/p97 in yeast is called Shp1 for “Suppressor of high-copy PP1”. A mutation in *shp1* was able to restore growth of the *ipl1-132* mutant (Cheng and Chen, 2010). This is likely due to its essential function in the regulation of the Ipl1-opposing phosphatase Glc7, as will be discussed below (I.3.4).

In mammalian cells, however, the Shp1 homolog p47 was not implicated in the regulation of Aurora B. Conversely, the function of Ufd1-Npl4 in the extraction of Aurora B from chromatin following ubiquitination of the kinase during mitotic exit (Ramadan et al., 2007), hinted at the possible involvement of this regulation also at earlier mitotic stages. Indeed, such an antagonistic function has been unraveled by a study in our group (Dobrynin et al., 2011), including the finding that RNAi-mediated depletion of Ufd1-Npl4 alleviates the chromosome congression defects of low-dose inhibition of Aurora B with the drug hesperadin.

I.3.4 Function of the yeast Cdc48/p97 substrate adapter Shp1

In an attempt to find further regulatory subunits of the yeast PP1 phosphatase Glc7, Zhang *et al.* performed a screen based on suppression of its high-copy lethality phenotype (see also I.1.4) (Zhang et al., 1995). Thereby, two mutants of the same gene were obtained, which the authors termed “suppressor of high copy PP1” mutants, *shp1-1* and *shp1-2*.

The gene product, Shp1 (also called Ubx1 in budding yeast), is a 423 aa protein with a molecular weight of about 47 kDa. It contains an N-terminal ubiquitin-associated (UBA) domain, a SEP domain, for “Shp1, eyes-closed, p47” (all of which contain homologous domains) and a C-terminal Ubiquitin Regulatory X (UBX) domain. The UBX domain is structurally similar to ubiquitin and known to mediate the interaction of a group of seven proteins, Ubx1 or Shp1 through Ubx7, with the AAA-ATPase Cdc48/p97 in budding yeast (Schuberth et al., 2004). However, the interaction between Shp1 and Cdc48 does not depend entirely on the UBX domain, since mutation of a short motif between the UBX and

SEP domains, termed BS1 (“binding site 1”) or SHP box, in addition to mutation or deletion of the UBX domain was necessary to fully abolish Cdc48 binding (Bohm and Buchberger, 2013). Interestingly, another potential BS1 motif was found N-terminal of the SEP domain (Bohm and Buchberger, 2013). The function of the SEP domain in Shp1 is unknown, although formation of homooligomers is attributed to the equivalent domain in mammalian homologs, as will be discussed below (I.3.5). Finally, the UBA domain is responsible for the reported ability of Shp1 to interact with poly-ubiquitinated proteins (Schuberth et al., 2004).

Although subsequent studies firmly established that Shp1 functions are mediated by binding to Cdc48 (Cheng and Chen, 2010; Hartmann-Petersen et al., 2004; Schuberth et al., 2004), Shp1 apparently has profound roles as an interactor of Glc7 (see Figure 18 for a summary).

Zhang *et al.* investigated the two mutant *shp1* strains with respect to PP1-related phenotypes and found that they accumulated less glycogen than wild-type and were unable to form spores (Zhang et al., 1995), which was similar to the effects of a temperature-sensitive *glc7* mutant employed in the same study and those of the *glc7-1* mutation (Cannon et al., 1994). Zhang and co-workers found a general reduction of PP1 activity in *shp1*-mutant yeast as determined by a phosphorylase *a* phosphatase activity assay (Zhang et al., 1995) (see I.1.4 for an explanation of this assay). Wilson *et al.* later confirmed that phosphorylase *a* phosphatase activity was reduced in a yeast strain with *shp1* mutation and attributed this to a role of Shp1 as an activator of Glc7 (Wilson et al., 2005). However, these studies did not perform trypsin-mediated release of interacting proteins, which target and restrict the activity of Glc7*,* leaving the possibility that the observed reduced activity actually stems from a shift in Glc7 holoenzymes. The mitotic role of Glc7 seemed to be unaffected in this first study of the *shp1-1* and *shp1-2* mutants (Zhang et al., 1995). Therefore, the results implicated Shp1 as a general activator for PP1, whose mutation would result in glycogen accumulation and sporulation defects overlapping with *glc7* mutation-induced defects.

More recently, however, an approach by Cheng and Chen using a conditional promoter revealed a metaphase arrest and defects in the separation of a fluorescently labeled chromosome upon depletion of Shp1 (Cheng and Chen, 2010). These defects were similar to those observed for the *cdc48-3* mutant, which was introduced earlier (I.3.3), although they were milder. The authors related this phenotype to the Glc7-Ipl1 balance (see I.2.2), since depletion of Shp1 partially rescued growth in an *ipl1-132* mutant strain (Cheng and Chen, 2010). Their observation that the *cdc48-3* mutation did not rescue growth of *ipl1-132* mutants indicated that Shp1 regulated a specific Cdc48-dependent pathway that antagonizes Ipl1. This study further investigated the Ipl1-substrate Dam1 and found that its phosphorylation, which is lost in *ipl1-132,* is rescued by co-depletion of Shp1 (see also I.2.4 and I.3.3). These results, which were largely confirmed by a study in Alexander Buchberger’s lab (Bohm and Buchberger, 2013), implicated Shp1 in regulation of the mitotic function of Glc7.

Cheng and Chen further noticed that the nuclear localization of Glc7 is impaired without functional Shp1 (Cheng and Chen, 2010), although this was not the case in the study conducted by Böhm *et al.* (Bohm and Buchberger, 2013). Importantly, a study in the group of Kelly Tatchell detected similar effects of mutations in *sds22, ypi1* as well as *shp1* on the nuclear localization of Glc7. Furthermore, they found that *shp1-105*, which is unable to bind Cdc48, also abolished the nuclear localization of Sds22 (Robinson et al., 2012). This indicated that a direct connection might exist between Shp1 and the PP1-regulators Sds22 and Ypi1, which had been strongly linked to the mitotic function of Glc7 earlier (see I.2.4).

The study by Böhm et al. further corroborated the role of Shp1 as a mediator between Cdc48 and Glc7. They constructed a *shp1* mutant allele, *shp1-a1,* which was defective in binding to Cdc48 due to mutations in the BS1 motif C-terminal to the SEP domain. This mutant led to a metaphase arrest as observed for Shp1 depletion and also showed positive genetic interaction with the *ipl1*-321 mutation (Bohm and Buchberger, 2013). Although Böhm and co-workers reported a physical interaction between Shp1 and Glc7, Shp1 does not appear to be a typical targeting or substrate-specifying interactor of the phosphatase, since it lacks the commonly observed interaction motifs for PP1-binding (I.1.3). Therefore, a more indirect mode of regulation is more likely and probably involves Cdc48. However, the mechanistic underpinning that would explain the involvement of Cdc48 in this function was not clarified by these studies.

Böhm and Buchberger also detected synthetic lethality between *shp1-7* and *sds22-6* (Bohm and Buchberger, 2013). Together with the earlier results on the effect of a *shp1* mutant on the nuclear localization of Sds22 (Robinson et al., 2012), this supported the notion that Shp1 and Sds22 functions could be linked. Importantly, a direct interaction between Cdc48-Shp1 and Sds22-Glc7-Ypi1 was reported recently in another study conducted by Cheng and Chen (Cheng and Chen, 2015). This study furthermore revealed the role of Sds22, Ypi1 and of Shp1 in preserving the stability of Glc7 and showed that Shp1 was specifically required for the stability of the newly synthesized catalytic subunit. These data, together with our own model for the role of SDS22 and I3 in mitosis (I.2.8) helped to establish a model for the functional link between p97 and PP1, which will be introduced in a later section (I.3.7).

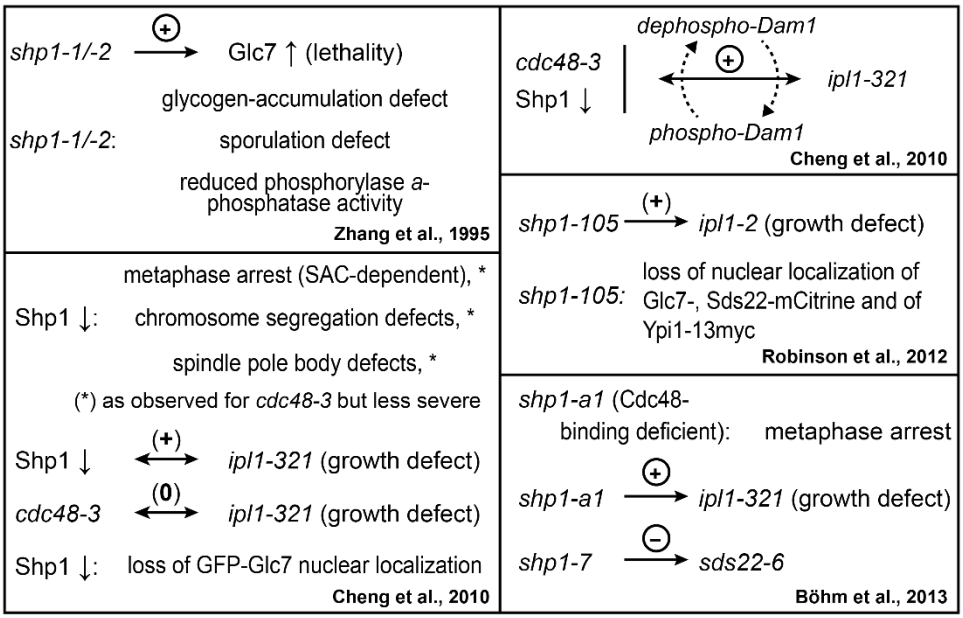

Figure 18: Summary of *shp1* mutant phenotypes and regulatory roles towards Glc7.
Symbols as in Figure 5 (see section I.2.3). See text for details.

Other studies found Shp1 to be required for glucose-dependent activation of Glc7 as well as degradation of Fructose-1,6-bisphosphatase in the vacuole, both processes being part of the glucose repression pathway (Castermans et al., 2012; Cui et al., 2004). In *Candida albicans*, Shp1 was found to be required for fundamental Glc7-dependent functions such as morphogenesis, cell cycle progression and the DNA damage response (Hu et al., 2012). Interestingly, activation of the cell morphogenesis checkpoint was also observed to cause the mitotic arrest phenotype of *ypi1* mutants (see I.2.4). In line with this pleiotropic involvement in cell physiology, *shp1* mutants in yeast were also found to be sensitive to various stresses (Zhang et al., 1995).

Even more diverse functions were found when looking at Shp1 from a different angle, namely as an adaptor protein for Cdc48. In this respect, the fission yeast homolog Ubx3 was found to be involved in the degradation of poly-ubiquitinated substrates and its mutation was synthetically lethal with the proteasome substrate-adapter Pus1/Rpn10 (Hartmann-Petersen et al., 2004). Mutation of *ubx3* also increased the sensitivity of yeast cells to proteotoxic stress and this phenotype could only be rescued by Shp1 constructs with intact UBA and UBX domains (Hartmann-Petersen et al., 2004). Further strengthening its assumed role in Cdc48- and polyubiquitin-dependent functions, Schuberth and co-workers found that Shp1 was required for degradation of the model substrate Ubiquitin-Proline-β-galactosidase (Ub-P-βGal) in budding yeast and a strain with the genetic deletion *Δshp1* was sensitive to proteotoxic stress (Schuberth et al., 2004). On the other hand, *shp1* mutants lacking the UBA domain behaved like the wild-type with regard to the antagonism towards Ipl1 (Bohm and Buchberger, 2013).

Interestingly, Glc7/PP1 was found to be required for membrane fusion in the regulation of vacuoles as well as vesicular transport (Peters et al., 1999) but the relevant PP1-interactor

remained unknown. A role for yeast Cdc48-Shp1 in a membrane fusion event was found during starvation-induced autophagy, where Shp1 interacted with Atg8 (Krick et al., 2010), which was apparently mediated by a region between the UBA and the SEP domain and thus ubiquitin-independent. However, another study on the role of Cdc48 during autophagy stated that Cdc48 function is not required for starvation-induced autophagy (Tresse et al., 2010). Therefore, the role of Shp1 in autophagy or other membrane fusion events awaits further confirmation.

The same can be said for a potential function of Cdc48 and Shp1 in a novel quality control pathway operating in the nucleus, termed “inner nuclear membrane-associated degradation” (INMAD). Shp1 (called Ubx1 in this study) might participate in this process as a Cdc48 adapter to extract the integral membrane protein Asi1 (Pantazopoulou et al., 2016).

Given the diversity of Shp1 functions, it will be necessary to dissect its roles as a Glc7 regulator from those as a Cdc48 adapter. This is complicated by the fact that both enzymes have highly diverse roles, but the apparent expandability of the UBA domain in the Glc7-regulatory role of Shp1 might help to guide such efforts. Interestingly, the mammalian homologs of Shp1, which will be introduced next, differ exactly in this structural feature.

I.3.5 The mammalian family of SEP domain-containing p97 adapters

In two studies on the involvement of p97 in the process of Golgi reformation, performed in Graham Warren’s laboratory, an unknown protein was first observed as an apparent contaminant in isolations of p97 from rat liver cytosol (Rabouille et al., 1995). Subsequently, it was recognized that this protein is required for the NSF-independent Golgi reformation pathway that is mediated by p97 (Kondo et al., 1997). This adapter was called “p47” due to its molecular size according to SDS-PAGE separation.

p47 shows homology to yeast Shp1 (26 % identity and 44 % similarity, see below, Figure 20) and both have identical domain structures with an N-terminal UBA domain, followed by an unstructured region, a SEP domain, a linker that contains a p97-binding SHP box motif (Bruderer et al., 2004) and a C-terminal UBX domain, which is also involved in binding to p97. The interaction of the UBX domain with p97 was found to occur via a conserved loop that inserts in a hydrophobic pocket in the N domain of p97 (Dreveny et al., 2004). This is similar to the binding mode of another p97 adapter, FAF1, which is shown in Figure 19A. As in the case of Shp1, mutation of the residues in this loop of the UBX domain strongly reduces but does not abolish binding to p97. This could be attributed to contacts made by other regions of the UBX domain. On the other hand, as is the case for Shp1 (Bohm and Buchberger, 2013), the SHP box motif might also contribute substantially to the interaction of p47 with p97. The structure of the SHP box motif in Ufd1 bound to the p97 N domain was recently determined (Le et al., 2016) and the SHP box in p47 is likely to interact in a similar manner with p97 (Figure 19B and C).

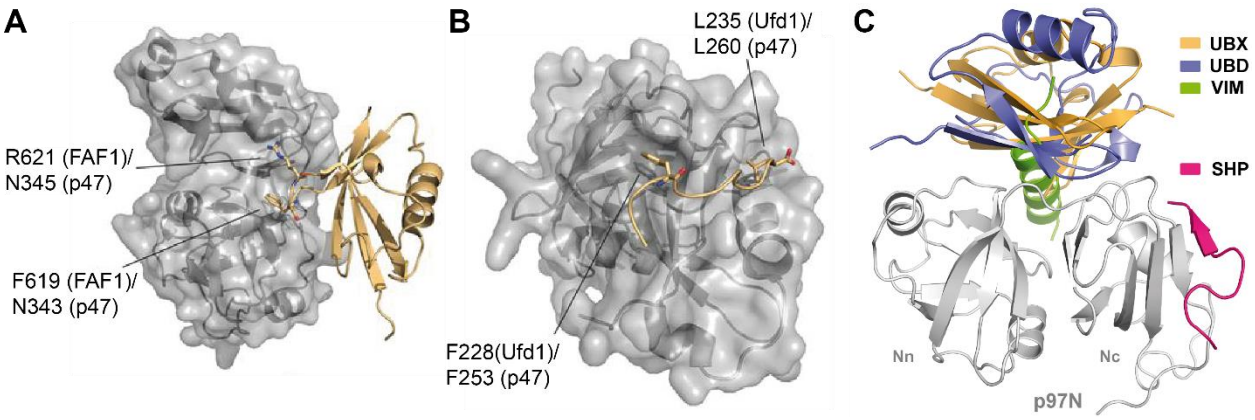

Figure 19: Structure of p97-binding elements in p47 and localization on the p97 N domain. (**A**) Structure of the UBX domain of FAF1 (beige cartoon) bound to p97 N (grey surface). The loop that protrudes from the UBX domain of FAF1 into the groove between p97 Nn and Nc subdomains is shown in stick representation and conserved residues in p47 are indicated along with those in FAF1. (**B**) Structure of the Ufd1-SHP box motif (beige) bound to the Nc subdomain of p97 N (grey surface). Conserved residues between Ufd1 and p47 are indicated and shown as sticks. (A) and (B) adopted from (Stach and Freemont, 2017) (**C**) Location of the p97-binding sites of p47 (UBX domain and SHP motif) in comparison with other typical p97 binding motifs on the p97 N domain. Adopted from (Le et al., 2016).

Trimerization of p47 was first suggested due to its apparent mass of 140 kDa in gel filtration experiments and because the p97-p47 complex differed by about 140 kDa from the size of the pure p97 hexamer in light scattering and gel filtration experiments (Kondo, 1997). The behavior of p47 as a trimer and its stoichiometry of binding to p97 were debated, since NMR (Nuclear Magnetic Resonance) experiments indicated that p47 loses the trimeric state upon binding to p97 (Yuan et al., 2004). However, a later study by the same group employed a more diverse set of experiments including isothermal titration calorimetry, which indicated that p47 bound to p97 at a ratio of 0.5, equal to 3 molecules of p47 binding to a p97 hexamer (Beuron et al., 2006). The potential of p47 to self-associate in solution was mapped to a fragment comprising the SEP domain (aa 171-246), the subsequent linker and the UBX domain (aa 286-370) (Yuan et al., 2004). The SEP domain itself behaved as a monomer upon removal of the adjacent C-terminal 24 residues from a fragment comprising aa 171-270 (Yuan et al., 2004), suggesting that the SEP domain itself is not sufficient for trimerization. Nonetheless, this study assigned a role to β sheet contacts formed by the SEP domain in the trimerization of p47, judging from shifts in NMR profiles. In addition, the authors stated that the regions adjacent to the SEP domain were also likely to be involved.

The UBA domain of p47 is required for binding to poly-ubiquitinated proteins. However, whereas yeast Shp1 was implicated in facilitating protein degradation in concert with Cdc48, the binding efficiency of p47 for bulk polyubiquitin was shown to be much lower than that of a Ufd1-Npl4 complex with p97 (Meyer et al., 2002). Conversely, p47 was shown to bind a fusion of ubiquitin with GST (Ub-GST) efficiently, suggesting that it has the ability to bind monoubiquitinated substrates. Interestingly, binding to the Ub-GST fusion by p47 required complex formation with p97, whereas the UBA domain of p47 alone was able to compete

with the p97-p47 complex for binding to Ub-GST. This hints at a negative regulation of ubiquitin binding by this domain in apo-p47, which is somehow relieved by binding to p97 (Meyer et al., 2002).

Somewhat contradictory, a recent publication reported a p97-independent role of p47 in targeting poly-ubiquitinated NEMO, a regulatory subunit of the IκB kinase complex, for lysosomal degradation (Shibata et al., 2012). This study also proposed that p47 bound lysine-63 (K63)-linked as well as linear polyubiquitin chains more efficiently than lysine-48 (K48)-linked chains.

In the Golgi reformation pathway, p47 is required to recruit p97 to the t-SNARE Syntaxin-5, a common component in the membrane fusion pathways of both NSF and p97 (Rabouille et al., 1998). A recent study found that Syntaxin-5 is monoubiquitinated during mitosis, which reduces its interaction with the v-SNARE Bet1 and concurrently increases the interaction with p47 (Huang et al., 2016). Co-recruitment of the deubiquitinating enzyme (DUB) VCIP135 (valosin-containing protein interacting protein of 135 kDa) by p97-p47 to Syntaxin-5 causes deubiquitylation and allows Syntaxin-5 to interact with Bet1, thus promoting the fusion of Golgi membranes by this pair of SNAREs. Interestingly, dissociation of a complex formed by p97 and p47 with Syntaxin-5 on beads required energy but the exact mechanism remained unclear (Uchiyama et al., 2002).

Cdc48 also functions in the fusion of ER membranes in yeast (Latterich et al., 1995). However, the relevant adapter has not been determined and a role in membrane fusion comparable to that of p47 was not evident for Shp1 as noted before (I.3.4). Moreover, Golgi fragmentation and reformation during mitosis are limited to animal cells (Warren, 1993), which precludes any direct comparison of yeast Cdc48 and mammalian p97 in this process. In *Drosophila* however, a p47-homolog may also be required for membrane fusion pathways (Sang and Ready, 2002).

A different function of p47 was indicated by the observation that it inhibits the ATPase activity of p97 *in vitro* by up to 85 % (Meyer et al., 1998). A recent reinvestigation of this feature of p47 indicated a biphasic behavior with inhibition of p97 ATPase activity at a p47 concentration below ~10 nM (measured with 4.2 nM of p97 hexamer), whereas at higher concentrations, ATPase activity recovered and was increased in the presence of more than ~50 nM p47 (Zhang et al., 2015). The authors attributed the strongest inhibition to a situation where the concentration of p47 was below the K_D for trimer formation, which they determined to be 6.9 nM, indicating that monomeric p47 would inhibit, whereas trimeric p47 would stimulate p97 activity. However, to date no functional consequence of the inhibitory potency of p47 has been reported.

Overall, Shp1 and p47 share a similar structure and display sequence homology but their reported functions appear to be more divergent than overlapping. Conservation of the essential role of Shp1 in the regulation of mitotic function, stability or nuclear localization of

PP1/Glc7 has not been observed for p47. Therefore, it seems likely that other proteins, which share sequence homology and structural elements with Shp1, could possess similar roles in higher eukaryotes.

Indeed, three other p97 adapters contain a SEP domain besides p47. This family of p47-related p97 adapters contains p37 (also called UBXN2B), UBXN2A (or UBXD4) and the more distantly related Socius (UBXD5) (Schuberth and Buchberger, 2008). While the N-terminal sequences seem rather divergent between the SEP domain-containing proteins and Shp1, the region starting from the SEP domain is more conserved (Figure 20). Socius is an exception to this, since Shp1 sequence conservation is comparable but rather low across the whole protein. Importantly, while both p37 and UBXN2A contain a C-terminal UBX domain and a SHP box in addition to the SEP domain, neither contains the N-terminal UBA domain present in p47 and Shp1 (Figure 20).

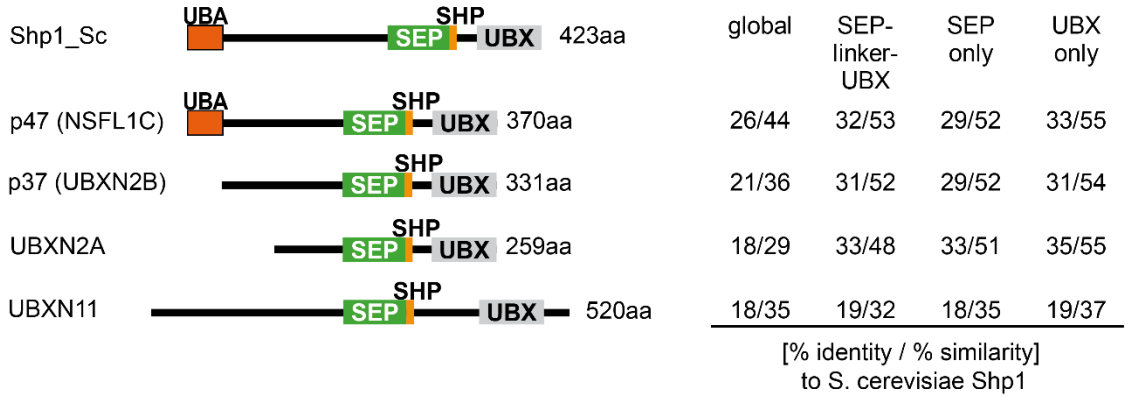

Figure 20: Domain structures of yeast Shp1 and human SEP domain-containing proteins.
Domain structures of Shp1 from *S. cerevisiae* (Shp1_Sc) and homologous human SEP domain-containing proteins were drawn based on annotated domains in Uniprot (https://www.uniprot.org/) and in (Yuan et al., 2004) and (Hanzelmann and Schindelin, 2016). Sequence identity and similarity were calculated based on pairwise sequence alignments of indicated protein regions using the Needleman-Wunsch algorithm (EMBOSS, https://www.ebi.ac.uk/).

Another common characteristic of p37 and UBXN2A is their low expression level in comparison to p47, which in U2OS cells differs almost 100-fold, according to a mass spectrometry survey (Beck et al., 2011). The subcellular localization of p47, which is predominantly nuclear owing to two nuclear localization signals (NLS), also differs from that of p37 and UBXN2A, which were found to localize to the ER and the Golgi apparatus (Rezvani et al., 2009; Uchiyama et al., 2006).

In accordance with its high sequence similarity to p47, p37 has also been implicated in the fusion of Golgi and ER membranes. In line with their different subcellular localizations, p47 appears to be the main factor for reformation of these organelles during mitotic exit, whereas p37 has more prominent roles in their maintenance during interphase. Importantly, this function appears to be independent of ubiquitination since p37 does not have a UBA domain and because only recruitment but not the deubiquitinating activity of VCIP135 is required (Uchiyama et al., 2006).

p47 and p37 were shown to compete for binding to p97 and immunoprecipitation of p37 from rat brain cytosol did not result in co-purification of p47, suggesting that they form distinct p97-cofactor complexes *in vivo* (Uchiyama et al., 2006). However, an experiment that specifically tests mutually exclusive binding instead of competition, such as those performed for Ufd1-Npl4 and p47 (Meyer et al., 2000), would be required to definitely exclude possibilities like mixed oligomers or binding to different subunits of the p97 hexamer in a common complex.

Another context apart from the maintenance of organellar membranes, in which p47 and p37 might cooperate, is in the antagonism towards the kinase Aurora A (see also I.2.2). A recent study showed that p37 is required for limiting centrosomal recruitment of Aurora A kinase in prophase, thereby regulating centrosome maturation and spindle positioning. Furthermore, although depletion of p47 alone showed no defects on spindle positioning and centrosome maturation, it aggravated these phenotypes when co-depleted with p37 (Kress et al., 2013). However, comparing p47 or p37 in this function to Shp1 is difficult, since mutants of Ipl1, the single Aurora homolog in budding yeast, do not show any defects in spindle or pole body organization (Biggins et al., 1999). However, the spindle pole body defect reported for *cdc48-3* is consistent with conservation of this function of p97 in yeast (Cheng and Chen, 2010)(see also I.3.4).

Another regulatory function of p37 in mitosis indicates a connection to the regulation of protein phosphatase-1. The PIP Repo-Man has been shown to be the substrate-adapter for PP1-mediated dephosphorylation of histone 3 residue threonine-3 (H3T3) to limit the presence of Aurora B on chromosome arms during mitosis (Qian et al., 2011). However, a recent study implicates PP1-Repo-Man in the regulation of NuMA (Nuclear and Mitotic Apparatus), which is involved in recruitment of dynein to the cell cortex during mitosis and necessary for correct function of the mitotic spindle (Lee et al., 2018). In this study, p37 was proposed to negatively regulate the PP1-Repo-Man complex in metaphase by an unknown mechanism (Lee et al., 2018).

Data on UBXN2A are rather scarce and only one function was reported repeatedly, which is the regulation of the α3-Containing Nicotinic Acetylcholine Receptors (nAChRs) (Rezvani et al., 2009). However, this function may be indirect, since UBXN2A was later found to regulate the activity of the E3 ligase CHIP, which ubiquitinates nAChRs and facilitates their degradation (Teng et al., 2015). Finally, it seems unlikely that UBXD5, which thus far has been only implicated in cytoskeleton-regulatory functions (Katoh et al., 2002), has conserved roles related to Shp1.

Altogether, conservation of the PP1-regulatory role of Shp1 in the human SEP domain-containing family of p97 adapters has not been sufficiently addressed to date. However, given the essential role of Shp1 in the regulation of PP1 and its dependency on Cdc48 (I.3.4), it is likely that a link between p97 and PP1 is also present in higher eukaryotes. Indeed, a mass spectrometry survey of the p97 adapters conducted by the Harper group

revealed that p37 and UBXN2A interact with all components of the trimeric SDS22-PP1-I3 complex (Raman et al., 2015).

Apart from addressing the putative conservation of the functional link between yeast Cdc48 and Glc7 in human cells, understanding the mechanism by which p97 would act on components of the SDS22-PP1-I3 complex was another aim of this study. Thus, some key aspects of the general mechanism of action of p97 will be discussed below.

I.3.6 Mechanism of action of p97

A central unanswered question in the study of p97 regards the molecular mechanism of action, by which it fulfils the plethora of functions it has been linked to. Until recently, a major hurdle to answering this question was the lack of a suitable *in vitro* substrate (van den Boom and Meyer, 2018). The first successful reconstitutions of substrate processing were achieved with the archaeal p97 homolog VAT, although truncation and replacement of the pore residue in the D1 domain was necessary (Barthelme and Sauer, 2013). Nevertheless, these modifications led to the first evidence that a p97 homolog would be capable of unfolding a substrate by channeling it through its central pore. This mechanism is the same as that applied by the proteasomal ATPases in pre-processing of substrates before entry into the 20S peptidase chamber and indeed, it was also possible to couple VAT with the archaeal proteasome (Barthelme et al., 2014).

At first, passing of substrates through p97 seemed surprising since structural investigations of the pore opening in the D1 domain indicated that it was too small to accommodate a peptide chain (van den Boom and Meyer, 2018). However, the development of assays using *in vitro*-ubiquitinated fluorescent proteins, which can be processed *in vitro* by a p97-Ufd1-Npl4 complex (Blythe et al., 2017; Bodnar and Rapoport, 2017b), allowed this hypothesis to be more explicitly tested without extensive modification of p97. Bodnar and co-workers applied two approaches to conclusively show that a poly-ubiquitinated model substrate is processed by moving through the pore of the hexamer[236]. First, they replaced residues facing the inside of both the D1 and the D2 pores with UV-inducible cross-linking residues and found that the substrate makes contact with both pore residues in an ATP-dependent manner. Since this would still be consistent with the substrate moving into but not passing through the channel entirely, they employed a second approach by fusing the bacterial hexameric FtsH protease to the C-terminus of p97. In this configuration, the protease was only accessible to proteins exiting the p97 ATPase on the C-terminal end of the pore. Indeed, the substrate was degraded in an ATP-dependent manner and in the same conditions in which cross-linking to the pore loop residues was possible[236].

These studies provided solid evidence that p97 can handle its substrates by moving them through its central channel, which results in their unfolding. Therefore, it can be assumed that at least one and likely the most prominent mode of action in p97-mediated processes

involves unfolding at the expense of ATP and using a channeling mechanism (Figure 21A)(van den Boom and Meyer, 2018).

Similar to the channeling mechanism, it is also theoretically possible that some substrates enter the pore from the D1 domain but are subsequently expelled again (Figure 21B). However, the central role of ATPase activity in the D2 domain of p97 rather suggests that substrates would have to reach the D2 domain to be processed efficiently (Brunger and DeLaBarre, 2003).

Somewhat surprisingly, this contrasts with the mode of action of the closely related AAA-ATPase NSF, to which p97 had been compared to in its “early days”. NSF was found to be required for the release of wound-up SNARE complexes after membrane fusion, to allow Golgi reformation after mitosis and in other contexts (Muller et al., 2002). In the case of NSF, a spring-loaded mechanism was recently described (Ryu et al., 2015; Zhao et al., 2015). NSF acts together with a family of proteins termed “SNAPs” (soluble NSF attachment proteins), which mediate binding of NSF to membrane-localized SNARE complexes (Zhao et al., 2015). NSF in its ATP-bound state binds the SNARE-SNAP assembly and the resulting complex is referred to as the “20S” particle. This particle is stable in the absence of magnesium, which is required for ATP hydrolysis in NSF. Ryu *et al.* found that NSF is released in a single burst upon addition of magnesium, resulting also in the disassembly of the SNARE complex (Ryu et al., 2015). As suggested by the cryo-EM structures obtained by Zhao *et al.*, this likely involves rotational movement and transmission of torque force, possibly via the SNAP adapters, to unwind the SNAREs (Zhao et al., 2015).

Implication of both NSF and p97 in membrane fusion pathways supported the idea that p97 might transfer force onto its substrates via the adapters (Figure 21C). Such a model was proposed by Beuron *et al.* based on EM reconstitutions of the complex of p97-p47 in the presence of either AMP-PNP or ADP (Beuron et al., 2006). Although these reconstitutions did not provide high resolution, the authors interpreted differences in the observed densities as a movement of the UBX domains and the SEP-UBX linker of p47. Speculating further, they proposed that ATP hydrolysis in p97 would also cause movement of the UBA domains, which could provide a means of transferring the force generated by ATP consumption onto a substrate.

A fourth model for the mechanism of p97 proposes that substrates enter via the C-terminal opening into the D2 domain (Figure 21D). This was initially suggested following the observation that the D1 pore was not wide enough for substrates to enter from the N-terminal side (Zhang et al., 2000b). Although the ability of the D1 pore to accommodate ubiquitinated substrates was proven by recent data, the model might still hold in the case of p97 adapters like UBXD1, which differ from Ufd1-Npl4 in binding the C-terminus of p97 instead of the N domain (van den Boom and Meyer, 2018).

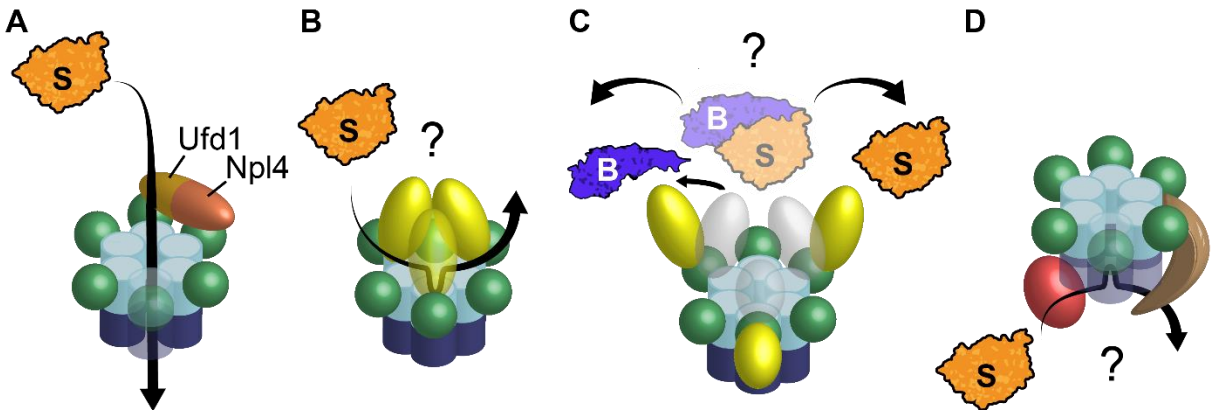

Figure 21: Overview of verified or proposed models of p97 activity.
(**A**) Established model for substrate (S) unfolding by p97-Ufd1-Npl4 complex, which involves threading them through the central pore. The arrow indicates the path of the substrate. (**B**) Hypothetical model for substrate processing for p97 by incomplete threading and release (indicated by arrow). Alternative cofactors such as p47 (shown as a trimer, yellow), could direct p97 activity in this manner. (**C**) Hypothetical model for transfer of mechanical force via the adapter (yellow), to release a substrate from a binding partner (B), akin to NSF-mediated unfolding of SNARE complexes (see text). (**D**) Hypothetical model for substrate processing by p97 together with C terminus-binding cofactors (red and brown), such as UBXD1. Local substrate unfolding in the D2 pore could proceed without complete threading (indicated by arrow). Adopted from (van den Boom and Meyer, 2018).

In sum, our knowledge on the mechanism of action of p97 has deepened substantially following the *in vitro* reconstitution of the unfolding mechanism. However, there are still many open questions. Importantly, it can be argued that a major uncertainty rests in the diversity of p97 holoenzymes, which may or may not employ the same mechanism of substrate handling as the p97-Ufd1-Npl4 complex (van den Boom and Meyer, 2018). Therefore, *in vitro* reconstitution of substrate handling by alternative p97-cofactor complexes would help to evaluate whether passage through the central channel and unfolding holds true as a generic mechanism or is restricted to Ufd1-Npl4.

Apart from these questions regarding the general mode of processing, the requirements for recognition and positioning of substrates for entry into the channel will require further study. Regarding the recognition aspect, the recently reported *in vitro* reconstitutions have supported the notion that p97 requires ubiquitination of its substrates (Blythe et al., 2017; Bodnar and Rapoport, 2017b). From both approaches, it could be concluded that a minimum chain length of 5 ubiquitin molecules is required for unfolding. Longer and branched chains enhance the efficiency of unfolding, although this seems to be in contradiction to the observation that the diameter of the channel would be insufficient to accommodate a branched chain, which entails passage of several peptides at the same time. Perhaps underscoring this difficulty, both reconstitution approaches required the use of superstoichiometric amounts of the p97 complex. Simultaneous processing of the substrate by the action of deubiquitinating enzymes might be required to achieve efficient movement through the p97 pore (Bodnar and Rapoport, 2017b; van den Boom and Meyer, 2018).

Parallels to the function of the 19S RP of the proteasome may provide some hints on the requirements for substrate recognition and for the initiation of unfolding. One aspect of this

comparison is that proteasomal degradation of folded, ubiquitinated proteins seems to require a stretch of unstructured peptide. This was not observed for p97-mediated processing of the poly-ubiquitinated model substrates and it was even suggested that p97 would pre-process a class of proteins, which do not possess the unstructured regions required for direct proteasomal degradation (van den Boom and Meyer, 2018).

To approach these and further open questions, *in vitro* reconstitution of p97-mediated processing of other substrates or in conjunction with other adapters might proof beneficial. Furthermore, structural studies based on high-resolution cryo-EM (Bodnar et al., 2018) and other methods, which are beyond the scope of this introduction, might help to clarify further mechanistic details.

I.3.7 A working model for regulation of the SDS22-PP1-I3 complex by p97

Genetic interactions between Shp1 and Glc7 in yeast as well as the requirement for binding to Cdc48/p97 to allow Shp1 to sustain Glc7 function (I.3.4) represent two important points of evidence for a link between p97 and PP1. This link was recently underscored by the study of Cheng and Chen, who observed aggregation and instability of a GFP-Glc7 fusion upon depletion of Shp1 (Cheng and Chen, 2015). Interestingly, Cheng *et al.* reported that formation of GFP-Glc7 aggregates depended on ongoing translation, indicating that specifically the newly synthesized catalytic subunit was destabilized.

It would be conceivable that the role of p97 is somehow linked to the degradation of the unbound catalytic subunit. This is reminiscent of a function in which it has recently been implicated and which was termed “Unassembled Soluble Protein Degradation” (Xu et al., 2016). This proposed quality control mechanism targets unassembled components of oligomeric complexes, which display otherwise buried hydrophobic surface patches, and was shown to operate on the prototypic substrate Ubl4A and subunits of several unrelated complexes, which are marked by the E3 ligase HUWE1 for p97-mediated degradation (Xu et al., 2016). Similarly, unassembled subunits of the fatty acid synthase complex require Cdc48 for degradation (Scazzari et al., 2015). This might be of special relevance in the case of PP1 due to the toxicity caused by unrestrained activity of the catalytic subunit (I.1.4).

Sds22-Glc7-Ypi1 in yeast as well as the human homologs SDS22-PP1-I3 are known to form trimeric complexes, which might be required for the stability of the catalytic subunit at a stage preceding holoenzyme formation (I.2.7). Consistently, Cheng *et al.* observe destabilizing effects of the temperature-sensitive *sds22-6* mutant as well as upon depletion of Ypi1 on GFP-Glc7 (Cheng and Chen, 2015). They propose that prior to formation of the Sds22-Glc7-Ypi1 complex, Cdc48/p97-Shp1 acts as a chaperone to prevent aggregation of unassembled Glc7, which might be caused by unshielded hydrophobic surface patches such as that forming the RVXF-binding groove. In this view, the role of p97 would reside in the assembly of the Sds22-Glc7-Ypi1 complex.

The aforementioned involvement in cytosolic quality control mechanisms as well as reports that the p97 N domain is capable of stabilizing unfolded proteins, which were cited earlier (I.3.1), would support this assumption. On the other hand, several pieces of evidence argue against this notion. First, Cdc48 physically interacts with all three components of the Sds22-Glc7-Ypi1 complex. This was shown by Cheng *et al.* using a substrate-trapping mutant, $Cdc48^{QQ}$, which increased binding to Sds22, Glc7 and Ypi1 (Cheng and Chen, 2015). The authors interpret this finding as a transient interaction of the chaperone with the assembled complex. However, the higher affinity of the substrate-trapping for the complex indicates that the ATPase activity of p97 would lead to a reduction in the interaction. This would be inconsistent with a role in assembling the complex. Furthermore, it is difficult to rationalize how the unfolding activity of p97 would relate to this function.

As mentioned before, it seems possible that p97 helps to degrade the unassembled catalytic subunits. However, such quality control would rather be important in the case of an imbalance in the synthesis of the complex subunits and would not explain the induction of Glc7-containing aggregates, which was observed upon depletion of Shp1 in the presence of functional Sds22 and Ypi1 (Cheng and Chen, 2015; Raman et al., 2015).

Therefore, we favored an alternative explanation for the observation that Shp1, Sds22 and Ypi1 are required for the stability and activity of Glc7. We further based our hypothesis on the model derived by our earlier study on the regulation of human PP1 by SDS22 and I3 during mitosis (Eiteneuer et al., 2014). As described before, this model implied that SDS22 and I3 are required to stabilize PP1 in an early life-cycle stage but have to be dissociated for the catalytic subunit to become fully active (I.2.8). Given the ability of p97 to extract proteins from cellular structures, such as membranes and chromatin, as well as its role in the degradation of protein complex subunits such as IκBα (Li et al., 2014), we anticipated that its role towards the SDS22-PP1-I3 complex would conform to this general role as a segregase. Therefore, our model as presented below (Figure 22) proposes a role for p97 in the disassembly of the SDS22-PP1-I3 complex in order for the catalytic subunit to become active.

This would reconcile our data on the regulation of the mitotic function of PP1 by SDS22 and I3 with the fact that Shp1 is required for the mitotic functions of Glc7 in yeast. We also considered the possibility that the SDS22-PP1-I3 complex could be a more general transitional state of newly synthesized PP1. Given the obligate multimeric state of PP1, it is unlikely that the catalytic subunit would be released from the SPI complex in a free form. Whereas for the mitotic function it would be expected that p97 releases PP1 from the SPI complex specifically for binding to KNL1, this could also extend to other PP1-PIP complexes in the biogenesis of PP1 (Figure 22).

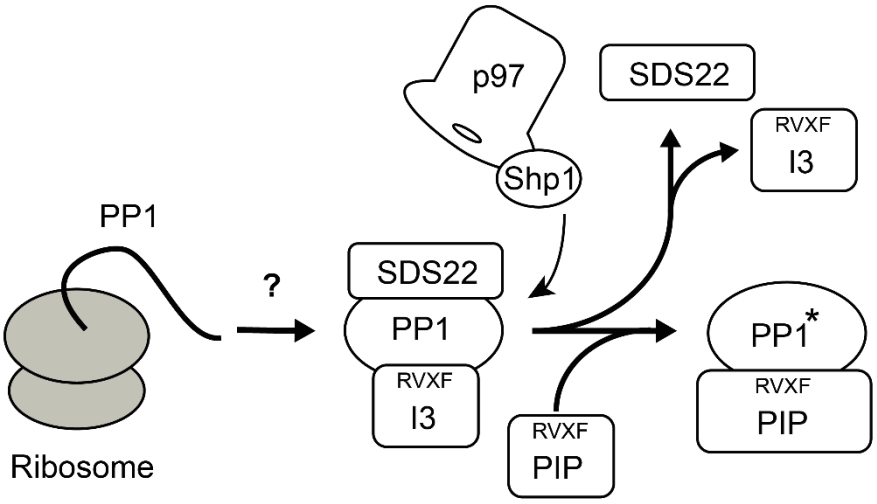

Figure 22: Model for p97 activity towards PP1 and the SPI complex.
Newly synthesized PP1 is bound by SDS22 and I3, potentially following prior, undefined steps in its biogenesis ("?"). The SPI complex is targeted by p97, together with Shp1-homologous adapters (Shp1) and processed by an unknown mechanism to release SDS22 and I3. This reveals the RVxF binding site of PP1 for binding by other PIPs. In agreement with biochemical data (Lesage et al., 2007), PP1 in the SPI complex is expected to be inactive, whereas mature holoenzymes contain active PP1 (denoted by an asterisk).

I. 4: The aims of this thesis

Protein phosphatase-1 (PP1) acts as a regulator of physiological processes as diverse as smooth muscle relaxation, glycogen metabolism but also cellular differentiation, proliferation and survival (Ceulemans and Bollen, 2004). Both PP1 and the second major serine/threonine-phosphatase PP2A are obligate multimeric enzymes (Virshup and Shenolikar, 2009) and the model of regulator-driven function of PP1, first proposed by Michael Hubbard and Philipp Cohen in the early 1990s (Hubbard and Cohen, 1993), is now firmly established. However, an ongoing effort is to classify the interactors of PP1, which likely exceed 200 proteins, into functional categories, such as substrate-specifiers, targeting subunits or inhibitors (Heroes et al., 2013). Furthermore, while recent studies on PP2A have revealed intricate regulatory processes during its biogenesis (Sents et al., 2013), surprisingly little is known about the ordered assembly of PP1 holoenzymes.

Among the interactors of PP1, SDS22 and I3 stand out in several ways. They were reported to be the most ancient binding partners of PP1 (Ceulemans et al., 2002a) and early reports on sds22+ in fission yeast indicated that it is essential for PP1 activity (Stone et al., 1993). Null mutants of *sds22* and *ypi1* in budding yeast are inviable and depletion of both Sds22 and Ypi1 leads to a similar mitotic defect phenotype as observed for *glc7*/PP1 mutant alleles (Bharucha et al., 2008; MacKelvie et al., 1995; Pedelini et al., 2007). The fundamental role of Sds22 and Ypi1 for PP1 function in yeast is further illustrated by the observation that both are required for the nuclear localization (Pedelini et al., 2007; Peggie et al., 2002) and for the stability of the Glc7 catalytic subunit (Cheng and Chen, 2015).

In human cells, SDS22 was found to be required for the antagonistic function of PP1 towards Aurora B in mitosis (Posch et al., 2010; Wurzenberger et al., 2012). While there were no previous reports on a mitotic function of I3, biochemical studies showed that a trimeric complex composed of SDS22, PP1 and I3 (SPI complex) exists in cells but is inactive (Lesage et al., 2007). My colleagues Annika Eiteneuer and Jonas Seiler further studied SDS22 and I3 in mitosis and found that I3 is required to keep inactive SDS22-PP1 in solution (Eiteneuer et al., 2014). According to the model derived from these data, SDS22 and I3 first interact with PP1, in a step that is required for PP1 activation, but have to dissociate subsequently. Our first aim in this study was to interrogate this model and to further clarify whether and how the activity of PP1 in human cells depends on SDS22 and I3. With our finding that newly synthesized PP1 indeed forms a transient complex with SDS22 and I3, we then set out to study how this event is regulated.

Indications for a link between p97 and SDS22, PP1 and I3 were found in budding yeast. The Cdc48/p97-adapter Shp1 was first identified due to its requirement for Glc7/PP1 activity (Zhang et al., 1995). In addition, *shp1*-mutant strains display mitotic defects reminiscent of *sds22* and *ypi1* mutants (Bohm and Buchberger, 2013; Cheng and Chen, 2010). Finally,

Shp1 was recently shown to mediate the physical interaction of Cdc48 with Sds22, Glc7 and Ypi1, and to be required for the stability of newly synthesized Glc7 by an unknown mechanism (Cheng and Chen, 2015). Mass spectrometry experiments in human cells indicated that the p97-adapters p37 and UBXN2A interact with SDS22, PP1 and I3 (Raman et al., 2015). Similar experiments in our laboratory (J. Hülsmann) confirmed this and also found an interaction with p47. These adapters are homologous to and share a so-called SEP domain with Shp1. However, they differ with respect to their ability to bind ubiquitin, since the UBA domain of Shp1 is only conserved in p47.

We set out to investigate the role of p97 and these adapters in the regulation of the SPI complex formed with newly synthesized PP1. We found that this complex does not dissociate spontaneously but requires p97, which is recruited by the three SEP domain-containing adapters in a redundant manner. Therefore, we further probed the mechanistic details of this process, and asked whether in this case p97 recruitment depends on ubiquitination. This question touches a fundamental aspect of the p97 system, since in most pathways regulated by p97, interactors like Ufd1-Npl4 serve as ubiquitin-adapters (Meyer et al., 2012). Disassembly of the SPI complex would be the first example for ubiquitin-independent processing of a defined substrate by p97 and our next aim was to establish assays for biochemical reconstitution of this p97-mediated process.

Finally, our results concerning the role of p97 and its adapters in SPI complex disassembly provided the necessary tools to investigate how the SPI complex regulates PP1 function. We hoped to clarify whether the essential roles of Sds22 and Ypi1 in yeast are reflected by the observed biogenesis process in human cells or rather hint to the existence of yet undefined pathways.

II Results

II. 1 SDS22 and Inhibitor-3 (I3) form a transient complex with protein phosphatase-1 (PP1) during biogenesis

The first section of the results presented here was a contribution to the work of my colleagues Annika Eiteneuer and Jonas Seiler, who had studied the roles of SDS22 and I3 in the regulation of the mitotic function of PP1. This investigation, which we published in 2014 (Eiteneuer et al., 2014), centered on the antagonism between PP1 and Aurora B in the surveillance of microtubule-kinetochore attachments or “error correction” (I.2.2). The balance of kinase and phosphatase activity in this pathway is essential for the process of chromosome congression at the metaphase plate and for the faithful segregation of chromosomes into daughter cells.

Depletion of both SDS22 and I3 led to increased chromosome misalignments in metaphase and prolonged duration of mitosis (Eiteneuer et al., 2014). Whereas a substrate-specifying function for PP1 at the kinetochore had been assigned to SDS22 (Posch et al., 2010), the role of I3 in mitosis had not been studied before. Annika Eiteneuer’s and Jonas Seiler’s work led to the conclusion that I3 was required to limit the amounts of SDS22 bound to PP1 at the kinetochore (Eiteneuer et al., 2014). Contrary to the previous report from Jason Swedlow’s group (Posch et al., 2010), they found that SDS22 acted as an inhibitor towards PP1 in this context and that increased levels of SDS22 at the kinetochore were likely causative for the inhibitory effect of I3 depletion on the mitotic function of PP1. I contributed to the work of my colleagues by performing experiments with overexpression of SDS22 (II.1.1), which mimicked the effect of I3 depletion by forcing SDS22 to localize with PP1 at kinetochores.

Based on these data regarding the effects of direct or indirect perturbations of SDS22 and I3 levels for the mitotic function of PP1, we proposed a model to reconcile the observation that both PP1 interactors are required for PP1 activity at the kinetochore but have negative effects when present at artificially increased concentrations. This model held that SDS22 and I3 serve a function in the activation of PP1, presumably by direct interaction, but need to be dissociated subsequently (Eiteneuer et al., 2014)(I.2.8).

Further investigation of the roles of SDS22 and I3, which makes up the first part of the results presented in this thesis, started by interrogating this model. A possible manifestation of it is that SDS22 and I3 interact transiently with PP1 during an event in the early life cycle of the phosphatase. This was directly addressed and confirmed by radiolabeling of newly synthesized PP1 (II.1.2). The subsequent sections focus on the role of the AAA-ATPase p97, which we show to be required in this process (II.2), as well as elucidation of the adapters that direct its activity towards PP1 (II.3). I will present an approach to reconstitute the observed events in a cell-free system using rabbit reticulocyte lysate (II.4) as well as an in-depth

investigation of the downstream effects in cells using mass spectrometry and flow cytometry (II.5).

II.1.1 SDS22 overexpression in HeLa cells inhibits PP1-mediated dephosphorylation of Aurora B in metaphase and activates the spindle assembly checkpoint (SAC)

Data gathered by Annika Eiteneuer and Jonas Seiler showed that increased binding of SDS22 to PP1 at kinetochores in cells depleted of I3 led to higher levels of Aurora B activation (Eiteneuer et al., 2014). The activity level of the kinase was determined by staining with an antibody specific for Aurora B, phosphorylated at threonine-232 (pAurB). Direct dephosphorylation of this amino acid residue by PP1 was demonstrated *in vitro* with purified components by Jonas Seiler. Importantly, this Aurora B-directed activity of PP1 was inhibited by SDS22 (Eiteneuer et al., 2014).

As an alternative approach to investigate the regulation of PP1 activity at kinetochores, SDS22 was overexpressed by transient transfection of mCherry-tagged fusion constructs. As controls, mCherry alone as well as the PP1 binding-deficient mutants SDS22^{E192A} and SDS22^{W302A} were transfected in parallel. pAurB and total Aurora B on metaphase chromosomes were detected by immunofluorescence microscopy (Figure 23A) and quantified (Figure 23B).

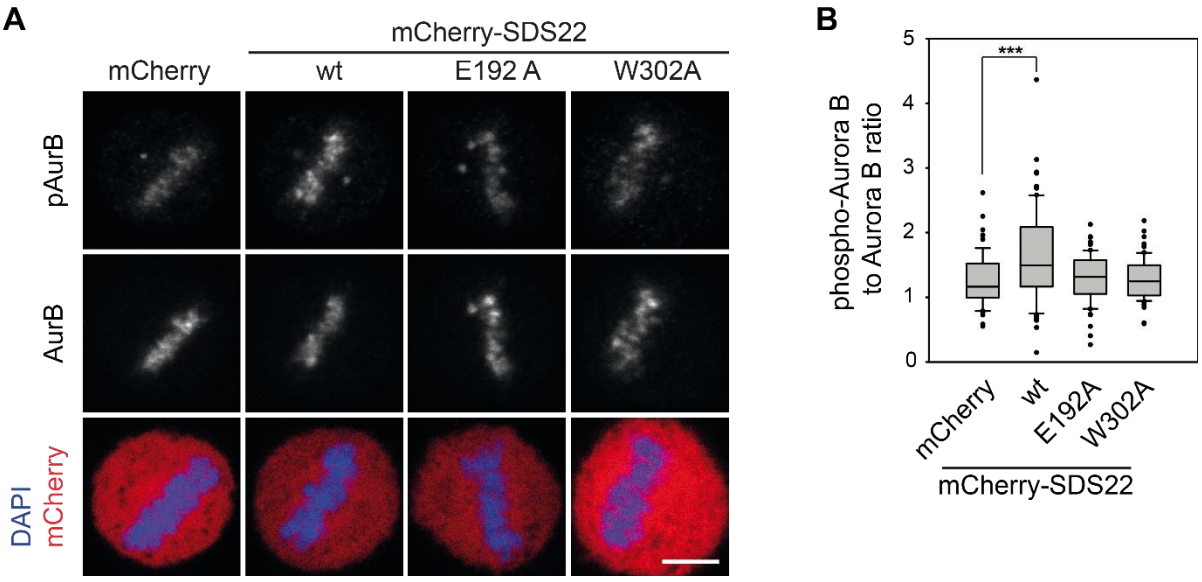

Figure 23: Immunofluorescence imaging of Aurora B and pAurB on metaphase chromatin following overexpression of SDS22 wild-type (wt) or PP1 binding-deficient mutants.
(A) Representative confocal micrographs of HeLa cells in metaphase after transient transfection to express mCherry-tagged SDS22 wild-type (wt) or either of the indicated PP1 binding-deficient mutants E192A or W302A (mCherry singal in red). Cells were fixed and stained with anti-pT232 Aurora B (pAurB) and anti-Aurora B (AurB)-antibodies and DAPI (blue). Note unspecific centrosomal staining with the pAurB antibody. Scale bar, 5 µm. **(B)** Quantification of experiments as in (A). The pAurB and AurB signal intensities on metaphase chromatin were quantified using the software CellProfiler. Box plots show median, lower and upper quartiles (line and box), 10th and 90th percentiles (whiskers) and outliers (black dots). P-values were calculated using Mann-Whitney U test (***, $p < 0.001$). Data from three independent experiments with 25 cells per condition.

Overexpression of SDS22 wild-type but not PP1-binding deficient mutants led to an increased ratio of active (phospho-)Aurora B to total Aurora B on metaphase chromatin. This supported the data of my colleagues (Eiteneuer et al., 2014), indicating that SDS22 has an inhibitory effect on PP1 at the kinetochore and reduces its ability to dephosphorylate and thereby inactivate Aurora B.

Imbalances of Aurora B kinase and PP1 phosphatase activities at kinetochores are expected to perturb kinetochore-microtubule attachments. Therefore, recruitment of BubR1 was investigated as a measure for activation of the SAC (I.2.2, Figure 24A and B).

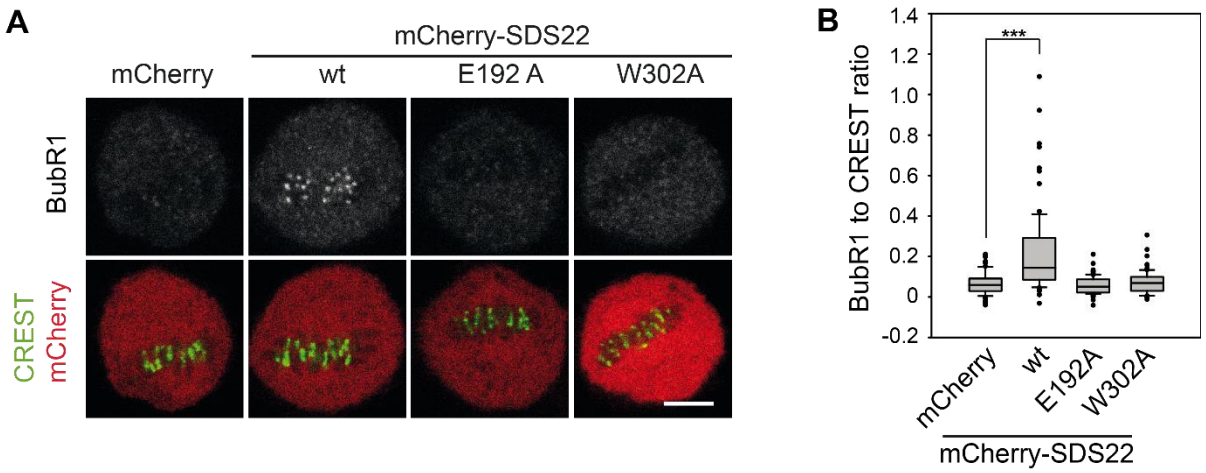

Figure 24: IF imaging of BubR1 on metaphase kinetochores following overexpression of SDS22 wild-type and mutants.
(A) Representative images of cells transfected as in Figure 23 after fixation and staining with CREST (centromere antiserum, green) and anti-BubR1 antibodies. **(B)** Quantification of (A). BubR1 and CREST signals on kinetochores (defined by CREST staining outlines). Box plots as in Figure 23B with data from three independent experiments with 25 cells per condition.

Consistent with the expectation that the imbalance caused by increased Aurora B kinase activity would cause perturbations during chromosome alignment, overexpression of SDS22 led to recruitment of BubR1 to metaphase kinetochores (Figure 24), indicating that the SAC was activated.

II.1.2 SDS22 and I3 but not NIPP1 are early interactors of the newly synthesized PP1 catalytic subunit (PP1c*)

The model that we derived based on our study of SDS22, I3 and the mitotic function of PP1 reconciles the observation that both are required for PP1 activity but subsequently need to dissociate for PP1 to become fully active (Eiteneuer et al., 2014) (I.2.8). Based on this model, we hypothesized that a direct interaction of SDS22 or I3 with PP1 occurs in an early life cycle event. To test this prediction, we employed a metabolic labeling approach with radioactive amino acids (^{35}S-L-methionine and -L-cysteine) to enable specific detection of all proteins translated in the presence of the label. Presumably, this would include the newly synthesized

catalytic subunit of PP1. PP1 occurs in three isoforms (introduction I.1.2), which differ in molecular weight by only 0.5 kDa and cannot be separated by SDS-PAGE. Therefore, regarding pulse-chase experiments, all isoforms of the newly synthesized catalytic subunit are commonly referred to hereafter as PP1c*.

To identify the radioactive signal attributable to PP1c*, synthesis of all PP1 isoforms was down-regulated by a short RNAi treatment before pulse labeling. Following isolation of either the γ-isoform of the catalytic subunit of PP1 or one of the interactors SDS22, I3 or NIPP1 by immunoprecipitation (IP), the presence of the signal for PP1c* was investigated with or without RNAi treatment (Figure 25). Short RNAi treatment was also used to identify signals of newly synthesized species of SDS22, I3 and NIPP1 (Figure 25).

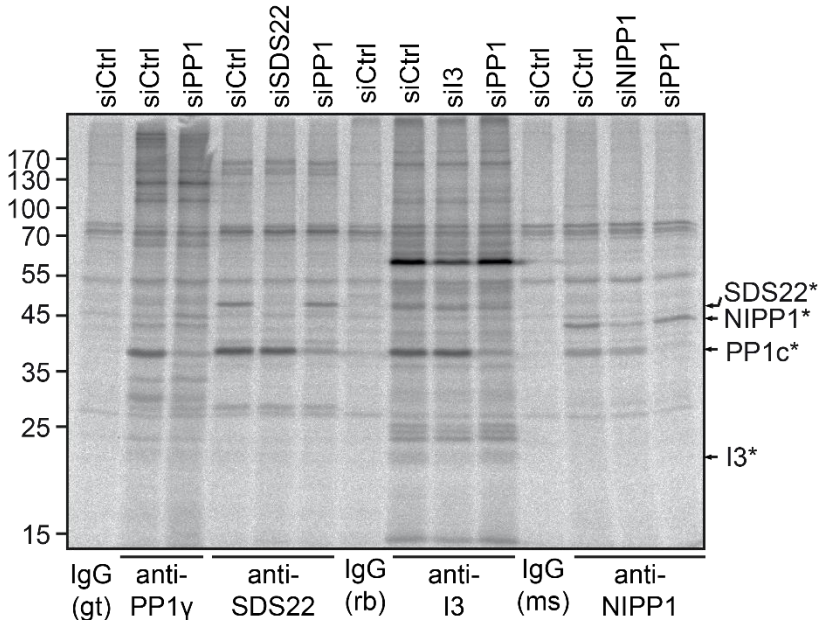

Figure 25: Short RNAi treatment to identify newly synthesized PP1 (PP1c*), SDS22, I3 and NIPP1 in pulse-chase experiments.
HeLa cells were treated with indicated siRNAs (siPP1: 6-oligo pool, siSDS22: oligo s2, siI3: oligo s2, siNIPP1: oligo s1) for 14 h prior to pulse labeling. After labeling with radioactive amino acids for 30 min, cells were either harvested directly and processed for IP with indicated antibodies or first chased for 2 hours for subsequent NIPP1-IP. Dried SDS-PAGE gels of IP samples were analyzed by autoradiography. Note specific reduction of the signal attributable to the newly synthesized PP1 catalytic subunit (PP1c*) in all IPs and of indicated signals for other newly synthesized protein species upon treatment with indicated siRNAs. gt = goat; rb = rabbit; ms = mouse.

In PP1γ-, SDS22-, I3- and NIPP1-specific IPs, we observed a radioactive protein band between 35 kDa and 45 kDa, corresponding well to the molecular weight of about 37 kDa of the catalytic subunit of PP1, which disappeared following short RNAi treatment with PP1-specific oligos (Figure 25, lanes 3, 6, 10 and 14). Similarly, bands at positions corresponding to the molecular weights of SDS22, I3 and NIPP1 were observed in respective IPs and disappeared following short, specific RNAi treatments (Figure 25, lanes 5, 9 and 13).

As stated before, the PP1 isoforms contributing to the signal of PP1c* cannot be distinguished by this method. SDS22 and I3 have been observed to interact with all isoforms of the catalytic subunit (Posch et al., 2010; St-Denis et al., 2016) (I.2.5). Potential differences

in these interactions could not be further investigated in this study due to lack of isoform-specific tools. A PP1γ antibody suitable for IPs was available and therefore, PP1γ was used as a proxy for all PP1 isoforms in experiments using direct immunoisolation of PP1 in this study.

After confirmation of the signal identity for these proteins of interest, we performed pulse-chase experiments to follow the interaction of SDS22, I3 or NIPP1 with PP1c* over time. To this end, newly synthesized proteins were again labeled with ^{35}S-L-methionine and -L-cysteine for 30 min. We then chased the radioactively marked proteins, including PP1c*, by replacing the labeling medium with medium supplemented with non-radioactive L-methionine and L-cysteine. PP1γ, SDS22, I3 or NIPP1 were isolated by IP from cells harvested either directly after the pulse labeling period or at various time-points during the chase. The amounts of PP1c* in these IPs were visualized by autoradiography (Figure 26).

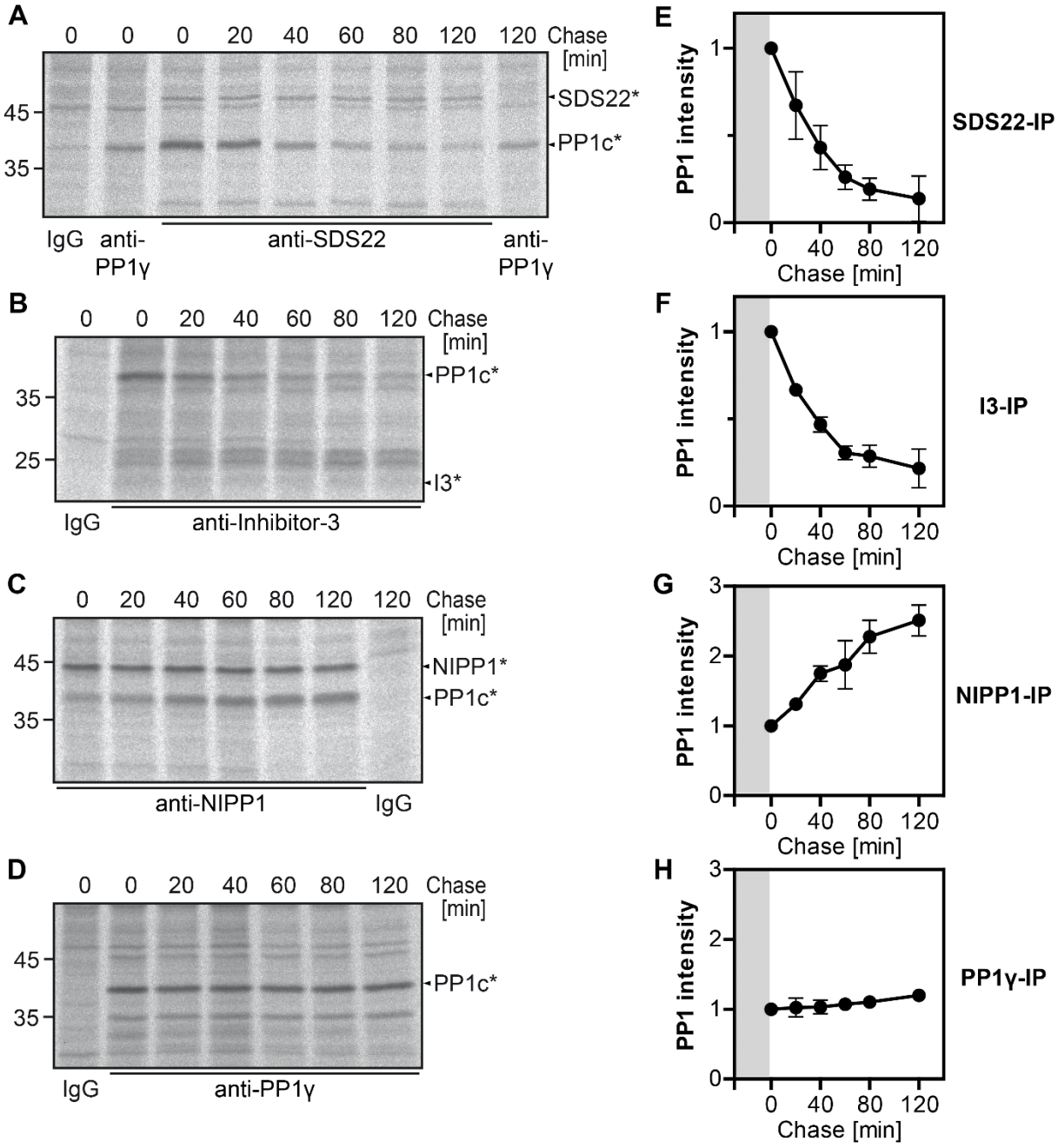

Figure 26: Time-course of PP1c* interactions with SDS22, I3 and NIPP1 after pulse labeling.
(A-D) HeLa cells were pulse-labeled as in Figure 25 and either harvested directly or first chased by washout of the label. Cells were processed for IP of indicated proteins. Dried SDS-PAGE gels of IP samples were analyzed by autoradiography and the band corresponding to PP1c* was detected. Note that SDS22-, I3- and NIPP1-IPs also contain newly synthesized species of these proteins, labeled with an asterisk (SDS22*, I3*, NIPP1*). For verification of signal identities, see Figure 25. **(E-F)** Quantification of signal for PP1c* in IPs as in (A-D). PP1c* was quantified by plotting of signal intensities using ImageJ. Background was subtracted and signals were then normalized to t = 0 min of each individual experiment. The grey area illustrates the duration of labeling. Data from n = 3 experiments. Shown are means +/- SD.

The signal corresponding to PP1c* was observed in SDS22- and I3-IPs from lysates harvested directly after 30 min labeling and decreased at successive time-points during the chase period (Figure 26A and B). Conversely, increasing amounts of PP1c* co-precipitated with NIPP1 during the 2-hour chase period (Figure 26C). PP1γ-IPs at different time-points contained comparable signals for PP1c*, indicating that the newly synthesized catalytic

subunit, by generalization from the γ-isoform, is stable over the observed time-frame (Figure 26D).

Taken together, these pulse-chase experiments show that both SDS22 and I3 interact early and transiently with PP1c*, in agreement with the previously proposed model (Eiteneuer et al., 2014). In contrast, the substrate-specifier NIPP1 interacts later with PP1c* without detectable reduction of the interaction within a 2-hour chase.

II.1.3 Pulse-chase without prior starvation shows similar interactions of PP1c* with SDS22 and NIPP1

Since the pulse-chase radiolabeling method applied before includes an amino acid-starvation period prior to pulse labeling, it was necessary to rule out starvation as an explanation for the observed interaction dynamics of PP1c* (II.1.2). To this end, starvation was omitted prior to pulse labeling and IPs of NIPP1 and SDS22 from labeled and chased cell lysates were performed at different time-points followed by detection of the signal for PP1c* by autoradiography (Figure 27).

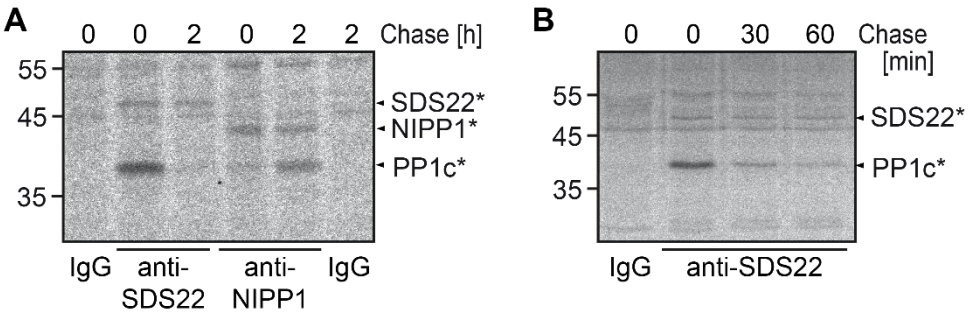

Figure 27: Pulse-chase experiments without prior starvation followed by IP of SDS22 and NIPP1.
Pulse-chase experiments with HeLa cells were done without a starvation period before labeling. Instead, radioactive amino acids were added directly to the growth medium, followed by incubation for 30 min and initiation of chase as before (Figure 26). Subsequently, SDS22- and NIPP1-IPs were done from lysates prepared at the indicated time-points. Co-precipitated PP1c* was detected by autoradiography.

As observed before, there was a strong interaction between SDS22 and PP1c* directly after pulse labeling, which decreased over time and was almost undetectable after 2 hours of chase (Figure 27A and B). PP1c* was associated with NIPP1 after 2 hours chase, but barely detectable directly after the pulse. Together, this indicates that the early and late interactions of SDS22 and NIPP1, respectively, with newly synthesized PP1 are not a consequence of starvation.

II.1.4 Depletion of I3 delays dissociation of PP1c* from SDS22 and association with NIPP1

Several reports showed that SDS22 and I3 can form a trimeric complex with the catalytic subunit of PP1 (Cheng and Chen, 2010; Lesage et al., 2007; Pedelini et al., 2007). Given that the observed time-courses of the interaction of SDS22 and I3 with PP1c* are highly

similar (II.1.2), we assumed that these interactions also occur in a common complex with the newly synthesized catalytic subunit.

In our previous study, Annika Eiteneuer observed that depletion of I3 leads to increased binding between SDS22 and PP1γ at the kinetochore (Eiteneuer et al., 2014). This prompted us to test whether the interaction between SDS22 and PP1c* in pulse-chase experiments is also influenced by RNAi-mediated depletion of I3 (Figure 28A-C). Furthermore, we tested how this treatment would affect binding of PP1c* to its substrate-specifier NIPP1 (Figure 28D).

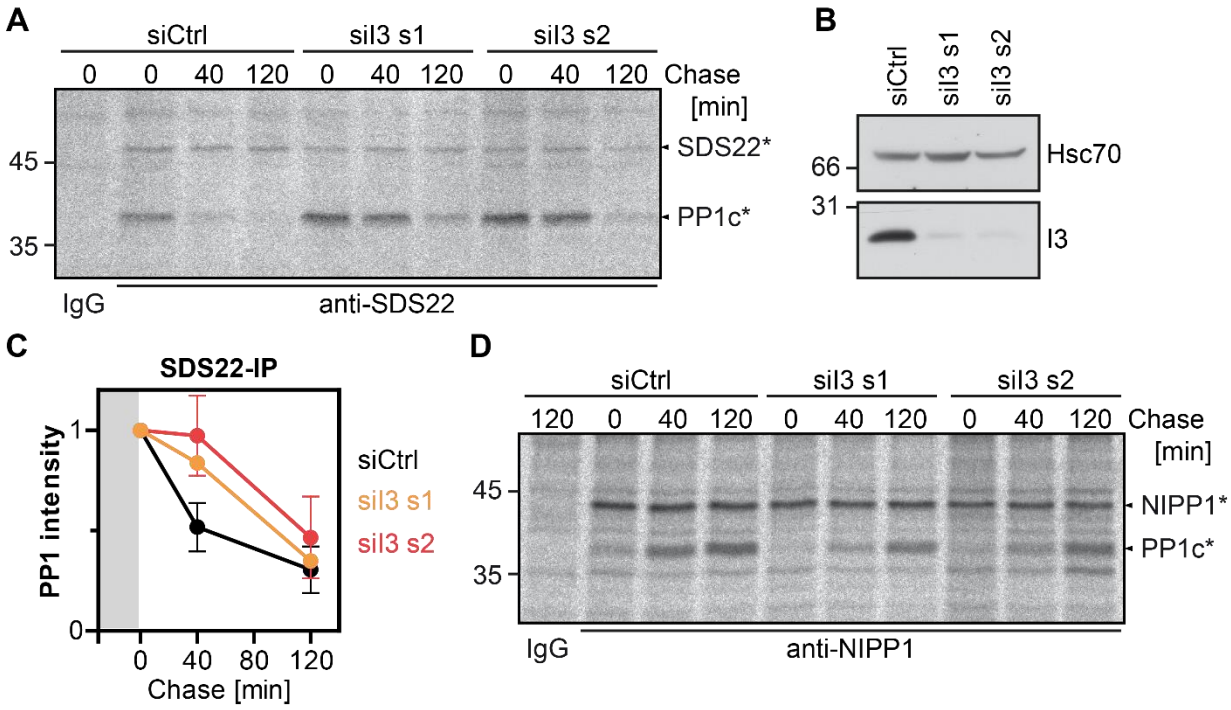

Figure 28: Time-course of PP1c* interaction with SDS22 and NIPP1 after depletion of I3.
HeLa cells were treated for 48 h by RNAi against I3 (oligos s1 or s2). **(A)** Time-course of SDS22-IPs after pulse-chase and detection of co-precipitated PP1c* as in Figure 26. **(B)** Western Blot for verification of depletion efficiency. **(C)** Quantification of PP1c* intensity in experiments as in (A). PP1c* signal intensities were normalized to the intensity at t = 0 min of each condition (n=3 for s2, n=1 for s1; means +/- SD). **(D)** Experiments as in (A) but followed by detection of PP1c* in NIPP1-IP instead of SDS22-IP.

Isolation of SDS22 by IP showed that the interaction with PP1c* persisted longer in cells depleted of I3 (Figure 28A and C). The increase of the PP1c* signal co-precipitated with SDS22 in I3-depleted samples was very prominent at the 40 min time-point of the chase, and PP1c* was still clearly detectable after 2 hours (Figure 28A and C). This indicates that I3 is required for the timely dissociation of PP1c* from SDS22 and further supports the assumption that a trimeric SDS22-PP1-I3 (SPI) complex is formed during biogenesis and subsequently dissociated.

We also observed that the association of PP1c* with NIPP1 is delayed by depletion of I3 (Figure 28D). This hints at a potential dependency of PP1 holoenzyme formation with substrate-specifiers on prior dissociation of the trimeric SPI complex, which is further investigated below (II.2.3).

II.1.5 Depletion of SDS22 affects expression or solubility of PP1

We next asked how the presence or absence of SDS22 would influence the interaction between I3 and PP1c*. This was addressed by RNAi-mediated depletion of SDS22, followed by pulse-chase experiments and isolation of I3 or PP1γ by IP (Figure 29).

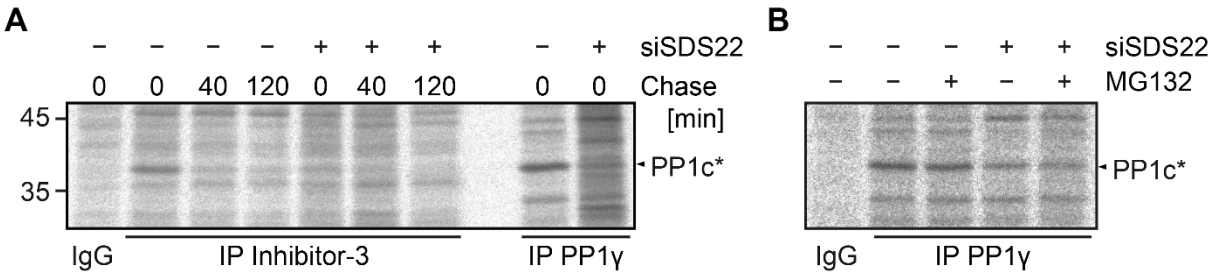

Figure 29: IP of I3 and PP1γ in pulse-chase experiments after depletion of SDS22.
HeLa cells were treated for 48 h by RNAi against SDS22 (oligo s2). **(A)** IP of I3 and PP1γ after pulse-chase as in Figure 26. Note the reduction of PP1c* signal in all IPs from SDS22-depleted cells. **(B)** IP of PP1γ from SDS22- versus control depleted cells after pulse labeling in the presence of MG132 (10 µM) or DMSO alone (−). Note reduction of the PP1c* signal by depletion of SDS22 and no rescue by addition of MG132.

Depletion of SDS22 by RNAi led to reduced signal of PP1c* in IPs of I3 as well as in direct IPs of the γ-isoform of PP1 (Figure 29). In contrast, the signal intensity of unspecifically bound proteins was not reduced, arguing against an inhibitory effect of SDS22 depletion on translation in general. Strong reduction of PP1c* in I3-IP could be due to lack of formation of the SPI complex. However, the same effect observed in PP1γ-IP suggests that depletion of SDS22 affects the newly synthesized catalytic subunit more directly. To test whether the lack of SDS22 leads to degradation of PP1c*, the proteasome inhibitor MG132 was added during pulse labeling. However, in this setting the addition of 10 µM MG132 did not rescue the amount of PP1c* detectable in IPs from SDS22-depleted cells (Figure 29B).
In contrast to I3, which seems to be mainly required for the dissociation of PP1c* from SDS22, the absence of SDS22 might have a more fundamental impact on the stability, solubility or expression of the PP1 catalytic subunit. However, more detailed experiments are required to differentiate between these possibilities.

II. 2 The AAA-ATPase p97 is required for dissociation of PP1c* from SDS22 and I3 and for association with the substrate-specifiers NIPP1 and MYPT1

The previous experiments supported a model, which assigns a role to SDS22 and I3 in the early life-cycle of PP1 and led to the conclusion that these interactors form a trimeric complex with newly synthesized PP1c. We next asked, whether and how this complex is regulated. Importantly, mass spectrometry experiments in our lab (Hülsmann et al., 2018) showed a physical interaction between the AAA-ATPase p97 and all three components of the SPI complex. In the following, the role of p97 in the regulation of this trimeric complex will be addressed.

II.2.1 Interaction of SDS22, PP1 and I3 with p97 and a substrate-trapping mutant

To investigate a potential role of p97 towards newly synthesized PP1, we first aimed to confirm physical interaction of p97 with SDS22, I3 and PP1, which form the SPI complex. To this end, HEK293 FlpIn T-REx cell lines were induced to express either p97 wild-type (wt) or the substrate-trapping mutant p97 E578Q. The E578Q mutation reduces the ATPase activity of p97 and was shown to stabilize interactions with its substrates (Hülsmann et al., 2018; Ye et al., 2003). Both proteins were expressed as fusions with a C-terminal myc-strep-epitope tag allowing isolation based on streptactin-affinity (Figure 30).

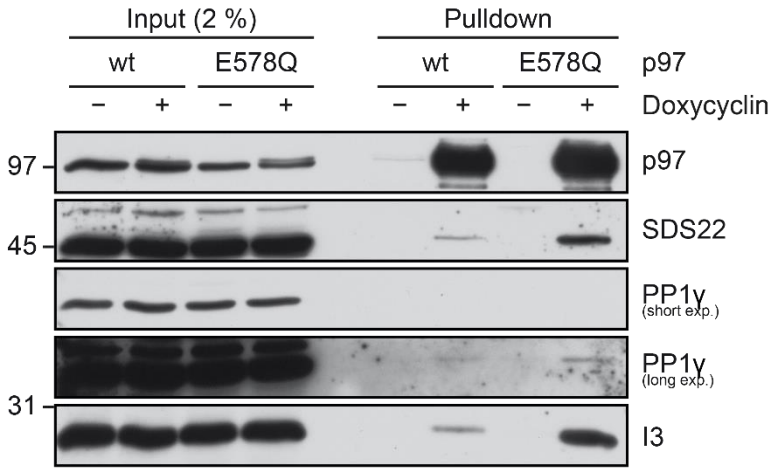

Figure 30: Affinity isolation of p97 wt and the substrate-trapping E578Q mutant from HEK293T cells.
HEK293T FlpIn cell lines were induced for 24 h to express either p97 wild-type (wt) or the E578Q-mutant, followed by isolation of the overexpressed protein by streptactin-based affinity isolation. Note co-isolation of the endogenous p97 protein due to hexamer formation. Detection of the SPI components SDS22, PP1γ and I3 by Western Blotting.

Detection of SDS22, PP1γ and I3 in streptactin-isolates from induced but not from uninduced cells confirmed the presence of a physical interaction with p97-myc-strep (Figure 30). Comparison of intensities revealed increased binding of the SPI complex to the p97 mutant E578Q compared to p97 wt, indicating that the SPI complex is a substrate of p97.

II.2.2 Inhibition or depletion of p97 stabilizes the interaction of PP1c* with SDS22 and I3

We next asked whether p97 activity is related to dissociation of the SPI complex containing newly synthesized PP1. In a first approach, small chemical inhibitors of p97 ATPase activity, NMS-873 or CB-5083 (Magnaghi et al., 2013; Zhou et al., 2015), were added during the chase period of pulse-chase experiments followed by IP of SDS22 (Figure 31A-C) or I3 (Figure 31E-F). MG132 was added in a parallel pulse-chase experiment as a control (Figure 31D).

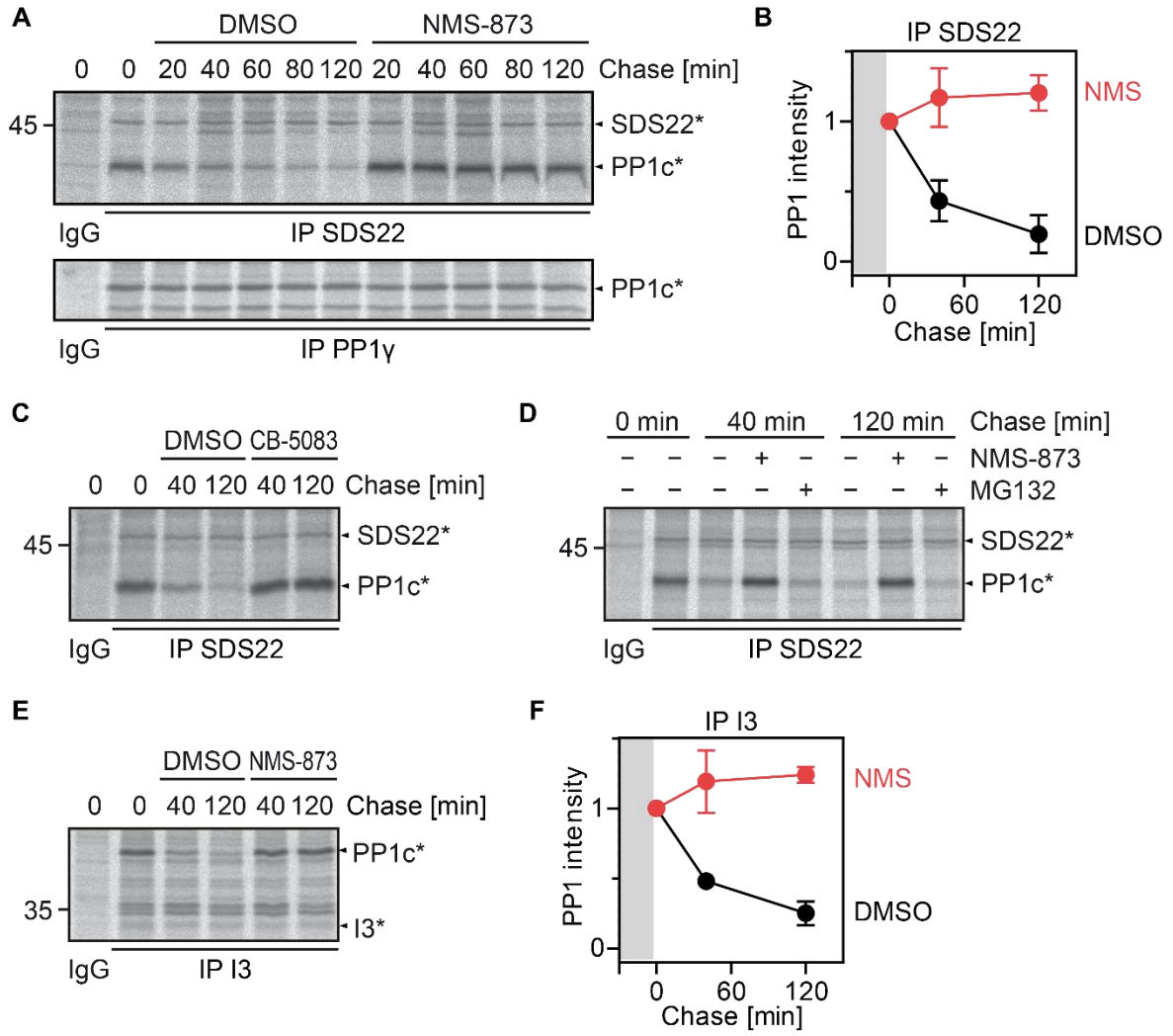

Figure 31: Pulse-chase experiments to follow SDS22- and I3-interactions with PP1c* during inhibition of p97-ATPase activity or inhibition of the proteasome.
HeLa cells were subjected to pulse-chase experiments as in Figure 26. **(A)** Addition of NMS-873 (10 µM) or DMSO alone to the chase medium and IP of SDS22 or PP1γ as a control at indicated times. Detection of PP1c* by autoradiography. **(B)** Quantification of experiments as in (A) but with only three time-points. PP1c* signal intensities were normalized to the intensity at t = 0 min of each condition (n=3; means +/- SD). **(C, D)** Experiments as in (A) but with CB-5083 (5 µM) or MG132 (10 µM) instead of NMS-873. **(E)** Pulse-chase with addition of NMS-873 as in (A) but followed by IP of I3. **(F)** Quantification of (E) as in (B).

Inhibition of p97 activity stabilized both the SDS22-PP1c* and I3-PP1c* interactions over the entire chase period (Figure 31A-C and E-F). In contrast, treatment with MG132 did not affect the dissociation of PP1c* from SDS22 (Figure 31D). Stabilization of both interactions with PP1c* by inhibition of the ATPase activity of p97 indicates that an enzymatic disassembly step is required to release PP1c* from the trimeric complex with SDS22 and I3.

In another set of experiments, RNAi-mediated depletion of p97 was employed to interfere with p97 function. Pulse-chase experiments followed by SDS22-IP were performed and the interaction with PP1c* was analyzed by autoradiography (Figure 32).

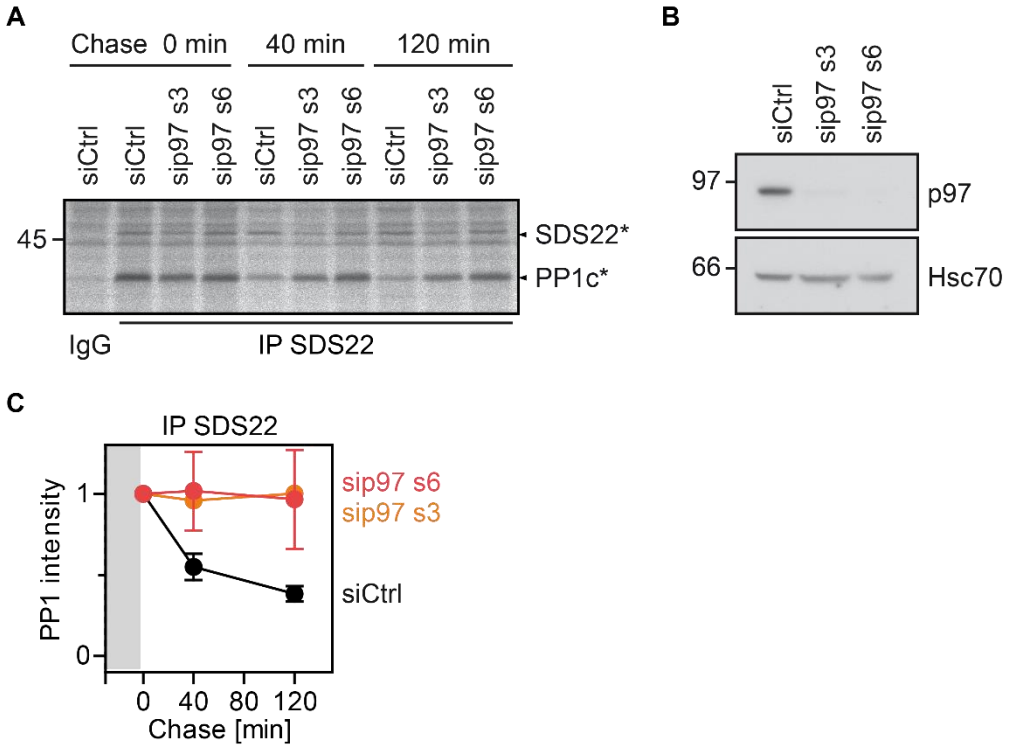

Figure 32: Pulse-chase experiments to follow PP1c* interaction with SDS22 after depletion of p97.
HeLa cells were treated for 48 h by RNAi against p97 (oligos s3 or s6). **(A)** Time-course of SDS22-IP after pulse-chase and detection of co-precipitated PP1c* as in Figure 26. **(B)** Western Blot for verification of depletion efficiency. **(C)** Quantification of PP1c* intensity in experiments as in (A). PP1c* signal intensities were normalized to the intensity at t = 0 min of each condition (n=3 for s6, n=1 for s3; means +/- SD).

Similar to chemical inhibition of its ATPase activity, siRNA-mediated depletion of p97 strongly stabilized the interaction of SDS22 with PP1c* during the 2-hour chase period (Figure 32A and C), further strengthening the conclusion that p97 is required for the disassembly of the SPI complex containing newly synthesized PP1.

Furthermore, we observed that association of PP1c* with SDS22 is not affected by depletion of p97. This is in contrast to the role assigned by a recent report (Cheng and Chen, 2015) to the yeast homolog of p97, Cdc48. The authors investigated the stability of Glc7/PP1 and found that it depends on the presence of Sds22 and Ypi1/I3. Given that the stability of Glc7 also depended on Cdc48 and the adapter Shp1, which interact with Sds22, Glc7 and Ypi1, they assumed that the role of Cdc48 is to allow assembly of the Sds22-Glc7-Ypi1 complex (Cheng and Chen, 2015). In contrast, the data presented here clearly indicate that p97 is required for disassembly but not assembly of the SPI complex.

II.2.3 Inhibition of p97 abolishes the association of PP1c* with NIPP1 and MYPT1

Our observation that the SPI complex containing PP1c* is stabilized by inhibition of p97 raised the question whether other interactions of PP1c* are affected downstream. We hypothesized that the SPI complex sequesters PP1c* and therefore, inhibiting its disassembly by NMS-873 treatment would decrease holoenzyme formation of PP1c* with

other regulatory subunits. In a first step, we tested a range of antibodies for their ability to immunoprecipitate known interactors of PP1. We detected newly synthesized PP1 by autoradiography in IPs of MYPT1 and Inhibitor-2 (I2) in addition to the interactions described so far (Figure 33A and B, other IPs not shown - see IV.3 for a full list of tested antibodies). NIPP1 and MYPT1 antibodies were then used for IPs following pulse-chase experiments with the p97 inhibitor NMS-873 (Figure 33C-F).

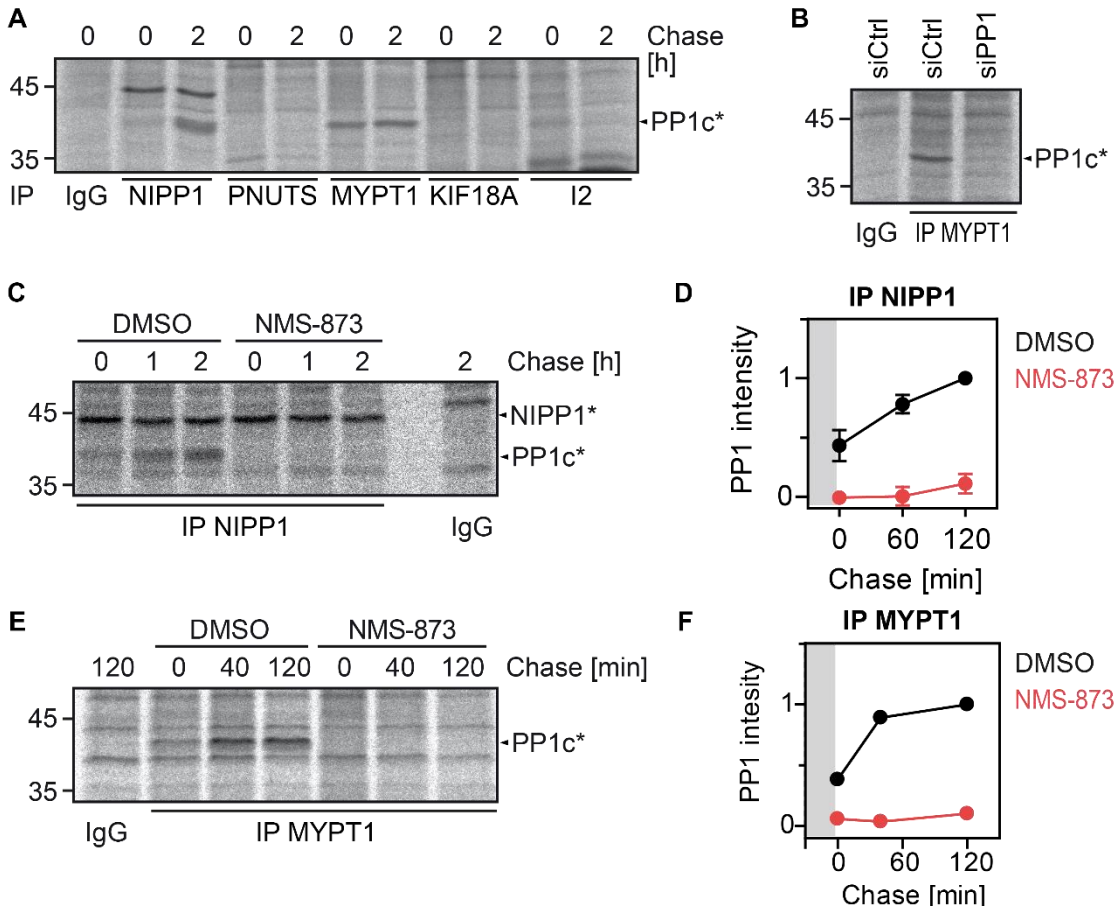

Figure 33: Pulse-chase experiments followed by IP of known PP1 interactors and effect of NMS-873 on association of PP1c* with NIPP1 and MYPT1.
(A) Pulse-chase experiments as in Figure 26, followed by IP of indicated PP1 interactors and detection of PP1c* by autoradiography. Note co-IP of PP1c* with NIPP1 after 2 h chase, at both time-points with MYPT1 and directly after pulse-labeling with Inhibitor-2 (I2). **(B)** Pulse-labeling after depletion of PP1 isoforms as in Figure 25 to verify PP1c* signal in MYPT1-IP. **(C)** Experiments as in Figure 31A, but with addition of NMS-873 (10 µM) already during the pulse, followed by IP of NIPP1. Detection of NIPP1-associated PP1c* by autoradiography. **(D)** Quantification of PP1c* intensity in experiments as in (C). PP1c* signal intensities were normalized to the intensity at t = 2 h of the DMSO control (n=3; means +/- SD). **(E)** Experiments as in (C) but followed by IP of MYPT1 and detection of MYPT1-associated PP1c* by autoradiography. **(F)** Quantification of PP1c* intensity in experiments as in (E). PP1c* signal intensities were normalized to the intensity at t = 2 h of the DMSO control (n=2; means without SD).

Under control conditions, the signal for PP1c* in NIPP1- and MYPT1-IPs increased substantially from the beginning to the end of a 2-hour chase (Figure 33C-F). PP1c* in MYPT1-IPs seemed to increase more rapidly compared to NIPP1-IPs, possibly due to different cellular localization of these PP1 interactors. I2-IP contained a weak signal for PP1c* after pulse labeling, which disappeared after the 2-hours chase, indicating a similar

interaction pattern as observed for SDS22 and I3 (Figure 33A). Addition of NMS-873 during pulse labeling prevented binding of PP1c* with the substrate-specifiers NIPP1 and MYPT1, indicating that p97 activity is required to allow formation of these holoenzymes (Figure 33C-F). This result is consistent with the notion that the newly synthesized catalytic PP1 subunit is sequestered in the SPI complex and requires release by p97 (Figure 31).

II.2.4 The effects of NMS-873 on early life-cycle interactions of PP1 are reversible

Binding of PP1c* with NIPP1 and MYPT1 was prevented in the presence of NMS-873 (II.2.3). This is consistent with sequestration of PP1c* in the SPI complex but could also be explained by destabilization or degradation of PP1c*. To investigate whether PP1c* remained stable in the presence of NMS-873, we performed washout experiments: during the labeling step, p97 was inhibited by addition of NMS-873. PP1c* was then chased and its interactions were followed by IP of SDS22, NIPP1 or MYPT1. NMS-873 was left out during the chase as a first washout, which served to evaluate whether the association of PP1c* with NIPP1 and MYPT1 can be recovered. In an alternative chase condition with NMS-873, disassembly of the SPI complex was further inhibited (see II.2.2). The final washout of NMS-873 (2nd chase) served to test the possibility to resume SPI complex disassembly after prolonged inhibition of p97 (Figure 34).

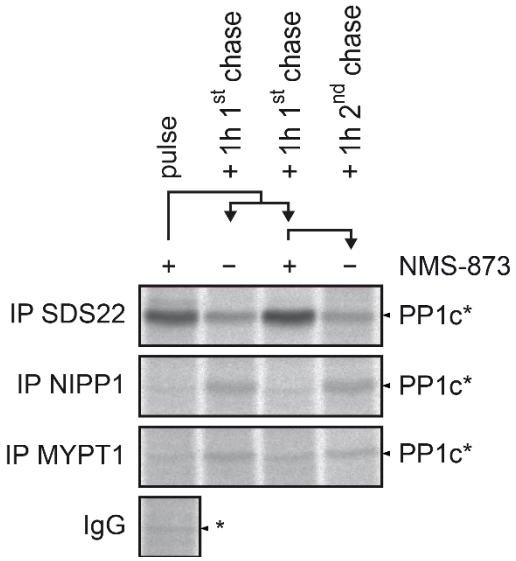

Figure 34: Washout of NMS-873 after pulse labeling, followed by isolation of SDS22, NIPP1 or MYPT1.
HeLa cells were treated with NMS-873 (10 µM) during the labeling step of radioactive pulse-chase experiments. One sample was harvested directly after labeling and subjected to IP of indicated proteins ("pulse"). From two samples, radioactive label and NMS-873 were washed out after 30 min and replaced by chase medium containing NMS-873 (10 µM) or DMSO alone (−), followed by incubation for 1 h ("1st chase") and harvest. Another sample was treated with NMS-873 during the first chase and then subjected to another 1 h chase after washout of NMS-873 ("2nd chase").

As observed before (II.2.3), addition of NMS-873 during pulse labeling reduced the signal for PP1c* in NIPP1- and MYPT1-IPs to background levels (Figure 34, lane 1). However, after

1 hour of chase without the drug, PP1c*-binding was recovered (lane 2), indicating that the catalytic subunit was not destabilized but rather sequestered in the presence of NMS-873. SDS22-IP from cells harvested directly after labeling contained substantial amounts of PP1c* (lane 1), which remained stable when treatment with NMS-873 was continued during the subsequent chase (lane 3) but not when it was washed out (lane 2). Washout of NMS in the second chase resulted in a similar reduction of PP1c* in SDS22-IP within 1 h as compared to washout in the first chase (lane 4). Thus, the effects of NMS-873 were fully reversible regarding both association of PP1c* with substrate-specifiers as well as dissociation from SDS22.

II.2.5 Induced expression of PP1γ followed by cycloheximide chase recapitulates successive binding of interactors

We next wanted to test the effects of interfering with SPI complex disassembly on the catalytic subunit of PP1 itself. To this end, an inducible HeLa FlpIn cell line was established for expression of PP1γ fused to a C-terminal strep tag. This allowed specific isolation of the newly synthesized protein for downstream analysis. In a first line of experiments, the interactions of induced PP1γ-strep were examined. We found that a short, 1-hour induction with doxycycline, followed by a chase in the presence of cycloheximide (CHX) to inhibit further translation, recapitulated interactions observed with newly synthesized PP1 in pulse-chase experiments (II.1.2). In this setup, we tested addition of NMS-873 during the CHX chase to study the influence of p97-inhibition on the interactions of newly synthesized PP1γ-strep (Figure 35).

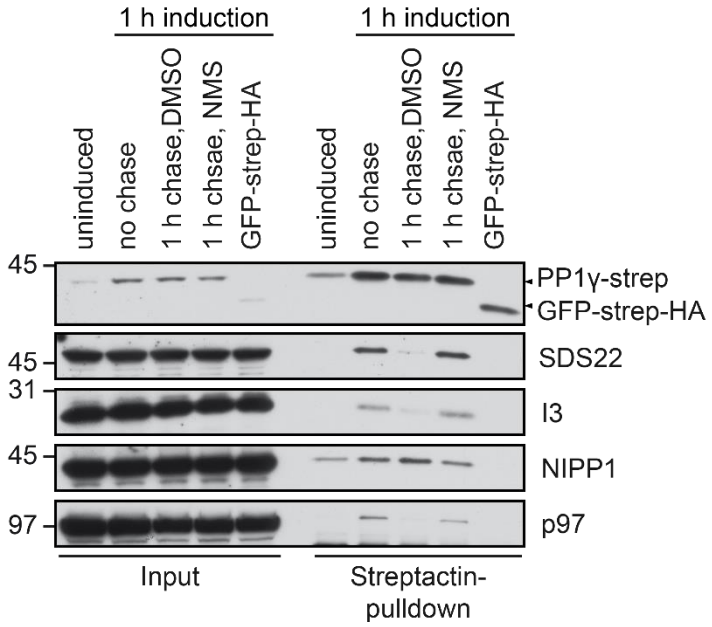

Figure 35: Short induction of PP1γ-strep and cycloheximide (CHX) chase in the absence or presence of NMS-873.
HeLa FlpIn cell lines were induced with doxycycline for 1 h to express PP1γ-strep or GFP-strep-HA. An uninduced sample of the cell line expressing PP1γ-strep was included to control for background expression and was harvested together with the “no chase” and GFP samples. Two other samples

were subjected to a subsequent chase in the presence of CHX (100 µg/ ml) combined with NMS-873 (5 µM) or DMSO alone. Samples were processed for pulldown of strep-tagged proteins using streptactin-coupled beads. Bound proteins were detected by Western Blotting with indicated antibodies.

Isolation of the exogenous PP1γ-strep after induction for 1 hour resulted in co-elution of SDS22 and I3 (Figure 35), consistent with formation of an SPI complex as observed for PP1c* (II.1.2). Co-elution of NIPP1 was increased but was already detectable in streptactin-isolates from uninduced cells. PP1γ-strep was also readily detected in the absence of doxycycline induction, indicating leakiness of the TET-On System or accumulation of weakly expressed protein due to the long half-life of PP1 in cells (see also Figure 46A).

Importantly, inhibition of further protein translation by treatment with CHX led to complete dissociation of SDS22 and I3 from PP1γ-strep within 1 hour. Simultaneously, we observed a reproducible increase of the amount of NIPP1 isolated with PP1γ-strep. These two opposing processes - reduction of SDS22- and I3-binding to PP1 versus increase of NIPP1 binding - were not detectable when NMS-873 was added together with CHX during the chase. This indicates that p97 activity is required to allow the recombinant PP1γ catalytic subunit to establish interactions with substrate-specifiers and to release it from a complex with SDS22 and I3, recapitulating the previously observed processes involving endogenous PP1c*. Consistently, we observed co-isolation of p97 with PP1γ-strep after 1 h induction, as well as after chase in the presence of NMS-873 but not with PP1γ-strep that was chased without the inhibitor and thereby lost its interactions with SDS22 and I3 (Figure 35).

II.2.6 Induced PP1γ-strep requires p97-dependent processing to become active

In the previous section, I described conditions that recapitulate disassembly of the SPI complex and formation of holoenzymes with inducibly expressed PP1γ-strep. We now used this model system to study the effect of p97-inhibition on the activity of the newly synthesized catalytic subunit after its isolation.

A study conducted in Mathieu Bollen's group (Lesage et al., 2007) suggested that the SPI complex is in an inactive state *in vivo*. We thus hypothesized that shortly induced PP1γ-strep, which is not released from SDS22 and I3 by p97, would be less active. To test this, PP1γ-strep was isolated from HeLa FlpIn cells after applying the conditions described before (II.2.5) and its activity towards phosphorylase *a* was measured with our without prior treatment with trypsin to remove interacting proteins (Figure 36).

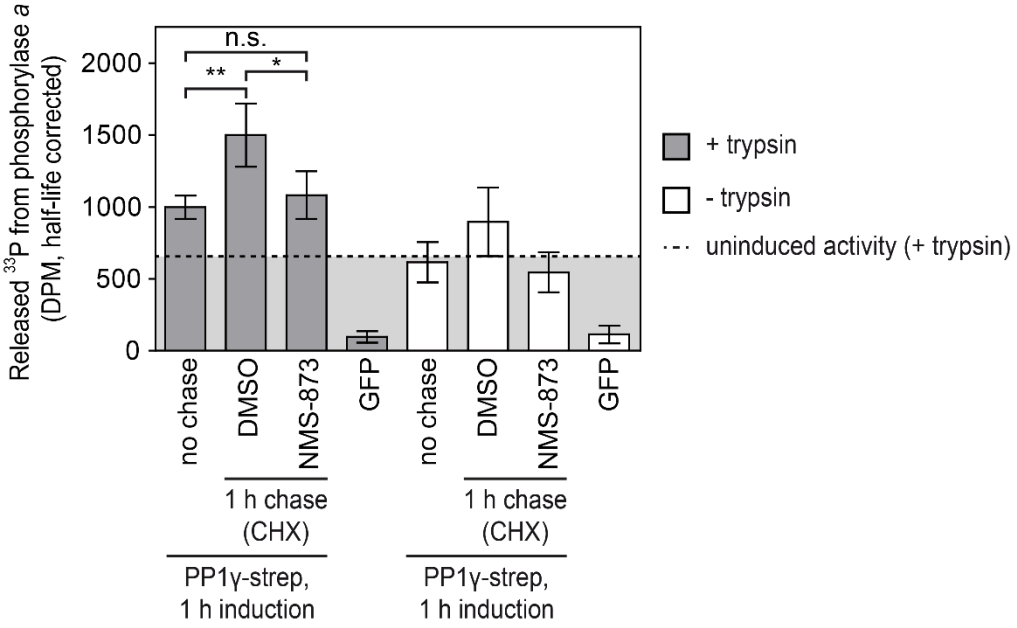

Figure 36: Phosphorylase *a* phosphatase activity of shortly induced, CHX-chased PP1γ-strep with or without trypsin-mediated removal of interactors.
HeLa FlpIn cell lines were induced (or not induced) to express PP1γ-strep or GFP-strep-HA and directly harvested or subjected to CHX chase as in Figure 35. Following isolation on Streptactin-coupled beads, tagged proteins were eluted with biotin. The eluates were split into two samples, which were treated (grey columns) or not treated (white columns) with trypsin to remove interactors from the catalytic subunit. After addition of soybean trypsin-inhibitor, the PP1 activity present in each sample was determined in assays using ^{33}P-labeled phosphorylase *a* as a substrate (DPM = decays per minute). Dotted line indicates fraction of activity attributed to background expression of PP1γ-strep (see also Figure 35). Shown are means +/- s.e.m. (n=5, *P< 0.05; **P < 0.01 as determined by Repeated Measures ANOVA and Bonferroni's Multiple Comparisons post-hoc-test).

Measurement of the trypsin-revealed phosphatase activity of PP1γ-strep after 1 hour induction showed a release of roughly 1000 DPM (998 +/- 81 DPM s.e.m.) of ^{33}P from phosphorylase *a*. Further incubation of the HeLa FlpIn cells for 1 hour in the presence of CHX led to significantly increased activity of isolated PP1γ-strep, resulting in 1500 DPM (1500 +/- 220 DPM, $p < 0.01$) released from phosphorylase *a.* Further translation during the chase can be excluded by comparison of the isolated levels in Figure 35. Of note, this increase of activity was abolished by addition of NMS-873 during the CHX chase (1082 +/- 166 DPM, $p < 0.05$). Reflecting results obtained by Western Blot (Figure 35), isolates from uninduced cells of the PP1γ-strep cell line contained substantial phosphatase activity (615 +/- 134 DPM), compared to the virtually inactive isolates from cells expressing GFP-SH (84 +/- 41 DPM). Activity measurements without trypsin-mediated removal of PP1 interactors showed similar tendencies (Figure 36).

The measured activity after 1 hour induction by doxycycline can be explained by background expression of PP1γ-strep and partial activation of newly translated species. However, the majority of the induced PP1γ-strep required p97 activity to become active during the subsequent CHX chase period. Taken together with the observation that the SPI complex is stabilized by addition of NMS-873 during the chase period (Figure 35), this strongly suggests

that a major part of the newly synthesized PP1 catalytic subunit is initially held in an inactive SPI complex.

II. 3 p97 is targeted to the SPI complex by a family of direct substrate adapters, without the need of ubiquitination

The results presented in Part 2 suggest that p97 disassembles the SPI complex to allow subunit exchange on PP1c* from SDS22 and I3 to substrate-specifiers such as NIPP1 and MYPT1. Our next aim was to clarify the identity of the p97 adapters involved in this function. In yeast, the Cdc48/p97-adapter Shp1 was recently shown to mediate the direct interaction between Cdc48 and the homologs of the SPI complex members, called Sds22, Glc7/PP1 and Ypi1/I3 (Cheng and Chen, 2015). Shp1 also interacts with Glc7 genetically and is essential for its activity (Bohm and Buchberger, 2013; Zhang et al., 1995) and stability (Cheng and Chen, 2015). Therefore, Shp1-homologous p97-adapters in human cells were good candidates and their role in mediating the interaction with the SPI complex was confirmed as shown below. A common characteristic of these adapters is the conservation of the “SEP” domain present in Shp1 (I.3.5).

II.3.1 The SEP domain-containing adapters p47, p37 and UBXN2A target p97 to the SPI complex

Mass spectrometry experiments in our lab (D. Ritz, J. Hülsmann) and in the Harper group (Raman et al., 2015) indicated a physical interaction between the p97 adapters p47, p37 and UBXN2A and the SPI complex. Transient transfection and pulldown experiments (J. Seiler) confirmed interaction of p47, p37 and UBXN2A but not another SEP domain-containing p97 adapter, Socius/Ubxn11 or the ubiquitin adapter Ufd1, with SDS22, PP1 and I3.

To test the dependency of SPI complex disassembly on these adapters, we first established a method to efficiently remove all three candidate proteins from HeLa cells. Since p47 is the most abundant of these adapters and was not completely depleted by RNAi (Figure 37A), knockout (KO) cell lines were established using a commercial CRISPR/Cas9 system (Santa Cruz), which introduces a Puromycin-resistance cassette by homologous recombination at the p47 genomic locus. Cells were selected by Puromycin for integration of the cassette and p47 KO was verified by Western Blot (J. Seiler, see also IV. 4).

To confirm that these three SEP domain-containing adapters mediate the interaction with the SPI complex and to assess their individual contributions, endogenous p97 was isolated by IP from native or p47 KO-HeLa cells, which were additionally depleted of p37, UBXN2A or both by RNAi. Subsequently, the interaction of p97 with SDS22 was evaluated by Western Blot (Figure 37B).

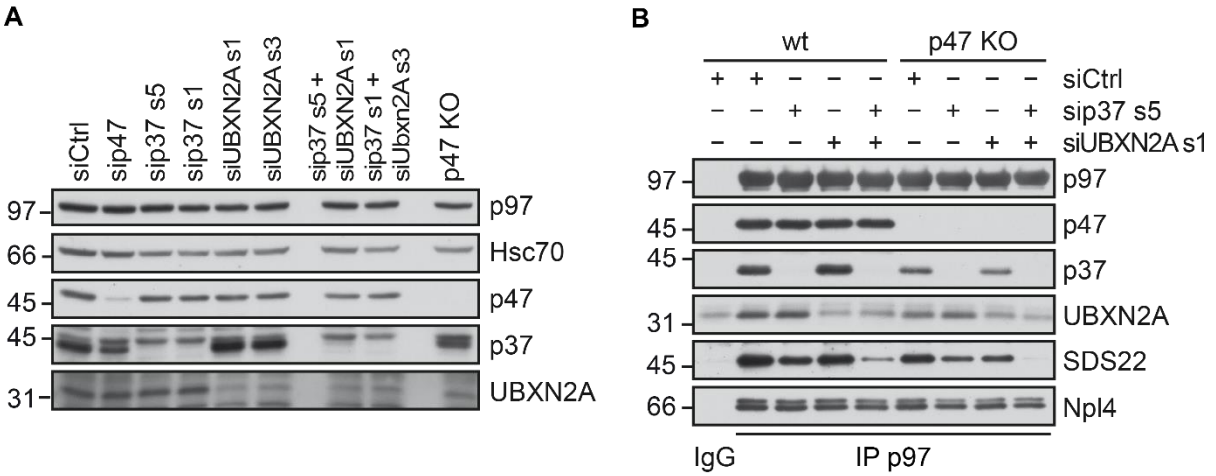

Figure 37: Effects of p47 KO and p37- or UBXN2A-depletion alone or in combination on co-IP of the SPI complex with p97.
(A) Verification of individual knockout (KO) of p47 (clone 42) and single and combined depletion of p37 and UBXN2A with two different oligos in HeLa cells. **(B)** Parental, wild-type (wt) HeLa cells or the p47 KO cell line (clone 42) were treated for 48 h with indicated siRNAs targeting p37 or UBXN2A individually or in combination. Endogenous p97 was isolated by IP and bound proteins analyzed by Western Blot staining with indicated antibodies. Npl4 was probed as an alternative adapter control.

IP of endogenous p97 led to detectable co-isolation of SDS22 (Figure 37B). I3 could not be detected with a polyclonal antibody due to cross-reactive staining of the light chain of the p97-antibody used for immunoprecipitation. Staining of PP1γ resulted in very low signal strength, which was not reproducible in repeated experiments and was therefore omitted in this figure. We thus interpreted the interaction with SDS22, which was reproducible in repeated experiments, as an approximation for binding of p97 with the whole SPI complex.
Single depletion or knockout of any of the SEP domain-adapters, p47, p37 or UBXN2A, only partially reduced the interaction of p97 with SDS22, with p37-depletion having the strongest effect (Figure 37B, lane 3). Double knockdown of p37 together with UBXN2A in native HeLa cells reduced the interaction further, as indicated by clear reduction of the SDS22 signal (lane 5). This effect was further enhanced by combination of p37- and UBXN2A-depletion with p47 KO, which reduced the interaction to undetectable levels (last lane).

II.3.2 Combined loss of p47, p37 and UBXN2A inhibits disassembly of the SPI complex

The combined loss of p47, p37 and UBXN2A had the strongest effect on binding of p97 to SDS22, and was therefore applied to assess p97 activity in the regulation of the transient biogenesis complex composed of SDS22, PP1c* and I3. This approach complements chemical inhibition of p97 (II.2.2) and avoids interfering with p97 functions in other complexes.
Two different clonal HeLa cell lines after KO of p47 or native HeLa cells as control were treated by RNAi to deplete p37 and UBXN2A. Subsequently, pulse-chase experiments followed by isolation of SDS22 or I3 at different time-points were performed as described

previously (II.1.2). Co-isolated PP1c* was measured by autoradiography and quantified (Figure 38).

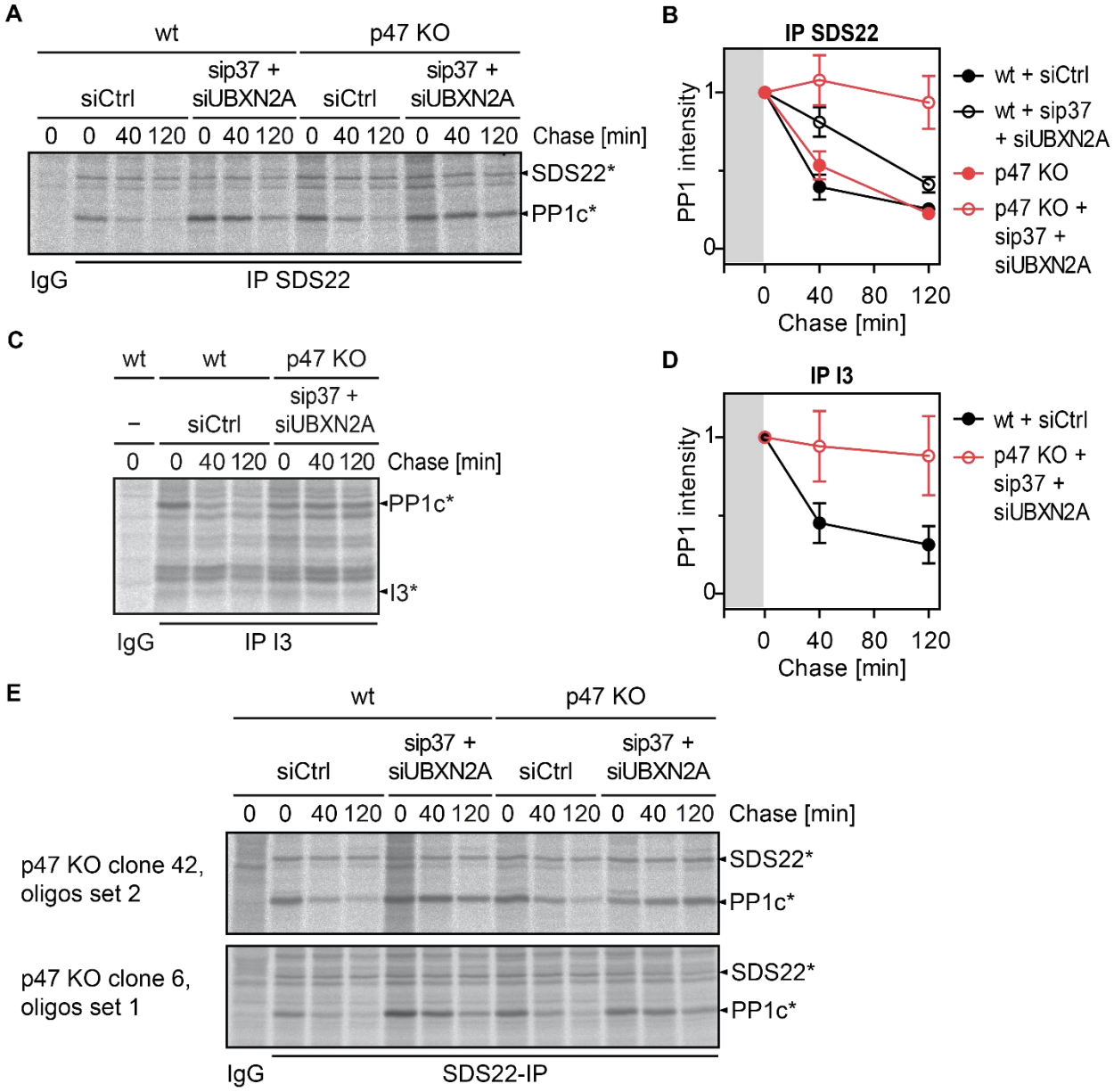

Figure 38: Pulse-chase experiments to follow the interaction of PP1c* with SDS22 and I3 after KO of p47 and/or knockdown of p37 and UBXN2A.
(A) Parental, wild-type (wt) HeLa cells or p47 KO cell line (clone 42) were treated for 48 h with siRNA targeting p37 (s5) and UBXN2A (s1) or control siRNA. Pulse-chase experiments were performed as in Figure 26 and PP1c* was detected by autoradiography in SDS22-IPs at different time-points. **(B)** Quantification of experiments as in (A). PP1c* signal intensities were normalized to the intensity at t = 0 min of each condition (n=3; means +/- SD). **(C)** Experiments as in (A) but with less conditions as indicated. PP1c* was detected by autoradiography in I3-IPs at different time-points. **(D)** Quantification of experiments as in (C). PP1c* signal intensities were normalized to the intensity at t = 0 min of each condition (n=3; means +/- SD). **(E)** Parental, wild-type (wt) HeLa cells or two different clonal p47 KO cell lines were treated for 48 h with siRNA targeting p37 and UBXN2A (oligos set 1: p37 s5 + UBXN2A s1; set 2: p37 s1 + UBXN2A s3) or control siRNA (see Figure 37). Pulse-chase experiments were performed as in Figure 26 and PP1c* was detected by autoradiography in SDS22-IPs at different time-points.

As observed before (II.1.2), the signal for PP1c* decreased in SDS22- and I3-IP from native HeLa cells treated by control RNAi within the 2-hour chase period to low residual levels.

RNAi-mediated depletion of p37 and UBXN2A led to slower release of PP1c* from SDS22, consistent with a prominent role of p37 and UBXN2A in targeting p97 towards the SPI complex (Figure 38A and B). Compared to wild-type HeLa cells, both p47 KO cell lines (clone 6 and clone 42) showed similar rates of decrease of the PP1c* signal in SDS22-IP during the chase period (Figure 38E). However, combination of p47 KO with depletion of p37 and UBXN2A led to strong stabilization of the PP1c* signal in SDS22-IP over the duration of the chase (Figure 38A, B and E). A very similar stabilizing effect of the combined KO and depletion was observed on the interaction of PP1c* with I3 (Figure 38C and D). This synergistic effect of p47 KO with p37 and UBXN2A depletion is in line with results from interaction experiments (II.3.1), indicating that all three adapters within this family of SEP domain-containing proteins are involved in the disassembly of the SPI complex by p97.

II.3.3 Combined loss of p47, p37 and UBXN2A delays PP1c*-NIPP1 association

Inhibition of p97 ATPase activity was previously shown to prohibit association of newly synthesized PP1 with NIPP1 and MYPT1 (II.2.3). We next asked whether this effect could also be observed upon depletion of the p97 adapters involved in SPI complex disassembly. To this end, p47 KO and depletion of p37 and UBXN2A were applied, followed by pulse-chase experiments, isolation of NIPP1 by IP and detection of co-precipitated PP1c* (Figure 39).

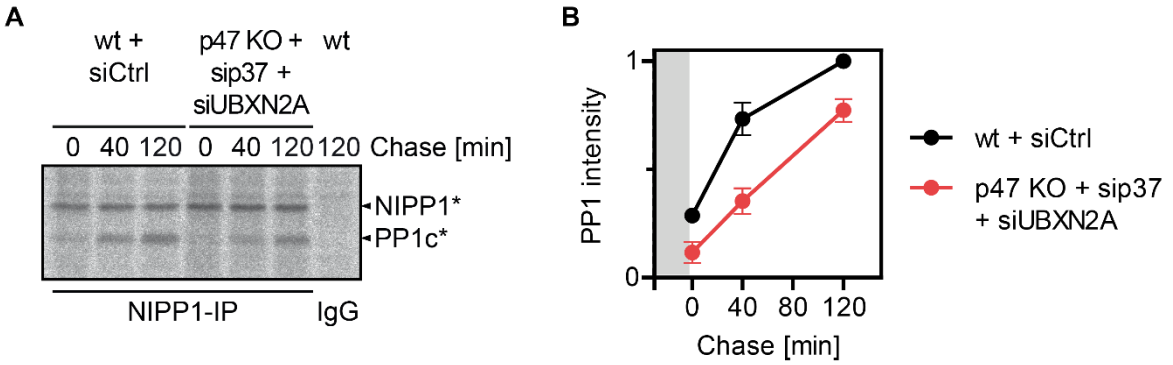

Figure 39: Influence of combined depletion of SEP domain-adapters on association of PP1c* with NIPP1 in pulse-chase experiments.
(A) Parental, wild-type (wt) HeLa cells or p47 KO cells (clone 42) were treated by siRNA against p37 (s5) and UBXN2A (s1) and subjected to pulse-chase experiments as in Figure 38A, but followed by IP of NIPP1. NIPP1-associated PP1c* was detected by autoradiography. **(B)** Quantification of experiments as in (A). PP1c* signal intensities were normalized to the intensity at t = 2 h of the control siRNA condition in parental HeLa cells (n=3; means +/- SD).

NIPP1-IPs contained increasing amounts of PP1c* over the time-course of the chase, as observed before (II.1.2). Increase of the signal for PP1c* in NIPP1-IPs from p47 KO cells after depletion of p37 and UBXN2A was still apparent, but clearly delayed (Figure 39). Together with the inhibitory effect of combined loss of the adapters on the dissociation of PP1c* from SDS22 and I3 (II.3.2), this result provides further evidence that the lack of

association of PP1c* with substrate-specifiers is caused by perturbed SPI complex disassembly by p97.

II.3.4 Ubiquitination is dispensable for dissociation of PP1c* from SDS22 by p97

p97 is recruited to its substrates by ubiquitination and ubiquitin adapters like Ufd1-Npl4 in a number of pathways (I.3.2), but neither p37 nor UBXN2A contain a known ubiquitin-interacting domain. We thus asked whether recruitment of p97 to the SPI complex during PP1 biogenesis was dependent on ubiquitination. To study this, we made use of the inhibitor TAK-243 that interferes with ubiquitin activation by both E1 enzymes, UAE and Uba6 (Hyer et al., 2018). Total cellular ubiquitin conjugates and the ubiquitin-dependent degradation of Cdc25A phosphatase (Riemer et al., 2014) were used as readouts to establish the active concentration of TAK-243 in HeLa cells (Figure 40A and B). Subsequently, efficient treatment conditions were applied before pulse-chase experiments to test whether dissociation of PP1c* from SDS22 depends on ubiquitination (Figure 40C).

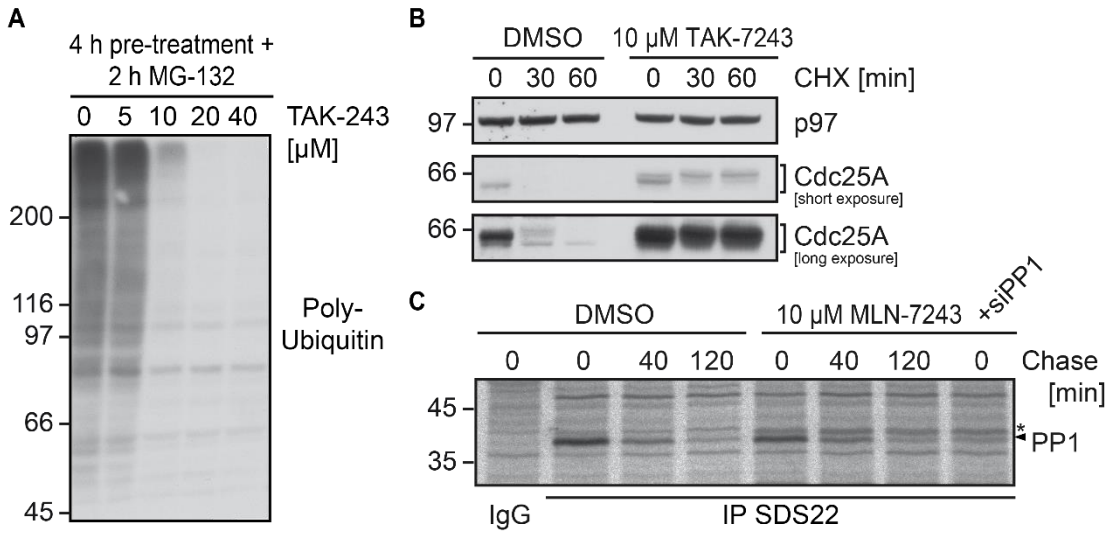

Figure 40: Inhibition of ubiquitin-activating enzymes using TAK-243 in an assay for CDC25A degradation and in pulse-chase experiments to study dissociation of PP1c* from SDS22.
(A) HeLa cells were treated for 4 hours with the E1 inhibitor TAK-243 at indicated concentrations and then subjected to another 2-hour treatment with TAK-243 in the presence of MG132 (10 µM) to accumulate polyubiquitinated proteins. The cell lysis buffer was supplemented with N-ethylmaleimide (NEM, 1.5 mg/ml). Samples were analyzed by Western Blot staining with a ubiquitin chain-reactive antibody (Sigma U5379). **(B)** HeLa cells were pre-treated with 10 µM TAK-243 or DMSO alone for 4 hours, followed by addition of cycloheximide (CHX, 100 µg/ml) and incubation for the indicated times before harvest and lysis. CDC25A and p97 as loading control were stained after Western Blotting. **(C)** HeLa cells, pre-treated with TAK-243 or DMSO as in (B) were used in pulse-chase experiments as in Figure 33 in the presence of TAK-243 or DMSO alone, followed by IP of SDS22 and detection of radiolabeled PP1c*. Short RNAi treatment against PP1 was applied as in Figure 25 to verify PP1c* band identity (+siPP1). Thereby, a signal appearing in the TAK-243 conditions was attributed to an unknown contaminant (marked by *).

Treatment of HeLa cells with 10 µM TAK-243 for 4 hours led to strong reduction of the signal obtained with a polyubiquitin-reactive antibody in Western Blot (Figure 40A and B). This treatment also markedly slowed down the degradation of a p97-Ufd1-Npl4 substrate, Cdc25A, confirming that ubiquitination of this cell cycle-regulatory phosphatase is a

prerequisite for its degradation (Figure 40C) (Riemer et al., 2014). Conversely, dissociation of PP1c* from SDS22 proceeded apparently normal when E1 ubiquitin-activating enzymes were blocked by addition of TAK-243 for 4 hours before pulse labeling (Figure 40D). This result indicates that ubiquitination is not a prerequisite for the p97-mediated disassembly of the SPI complex.

II. 4 p97 mediates dissociation of *in vitro* translated PP1γ from SDS22 and I3

Our results in HeLa cells indicated that SPI complex disassembly is an intermediate step in the maturation of PP1. In order to better understand this process, we aimed for reconstitution in simpler systems. As a first step, we chose rabbit reticulocyte lysate (RRL) as a cell-free system to express PP1 and to study or manipulate its further processing. If it allows recapitulation of the formation and subsequent disassembly of the SPI complex, this would enable us to dissect the minimal requirements for this process more precisely than our previous experiments in cells.

II.4.1 A stable complex of SDS22, I3 and *in vitro* translated PP1γ is formed in rabbit reticulocyte lysate (RRL)

We first asked whether human PP1γ expressed by coupled transcription-translation in RRL forms a complex with SDS22 and I3 and whether this complex is further processed in the lysate. Initial experiments were done by supplementing RRL with radioactive ^{35}S-L-methionine, followed by IP of endogenous rabbit SDS22. However, addition of recombinantly expressed human SDS22 (purified from insect cells by J. Seiler) increased the amount of PP1γ in SDS22-IP (Figure 41A). I chose to study the SDS22-PP1γ interaction by Western Blot, which was possible because the antibody for human PP1γ did not recognize rabbit PP1. Dissociation of PP1γ from SDS22 was assessed by inhibiting translation after expression of PP1γ, followed by SDS22-IPs at various time-points (Figure 41B). Endogenous rabbit I3 was also immunoprecipitated to test for formation of the trimeric complex with PP1γ and SDS22 (Figure 41C).

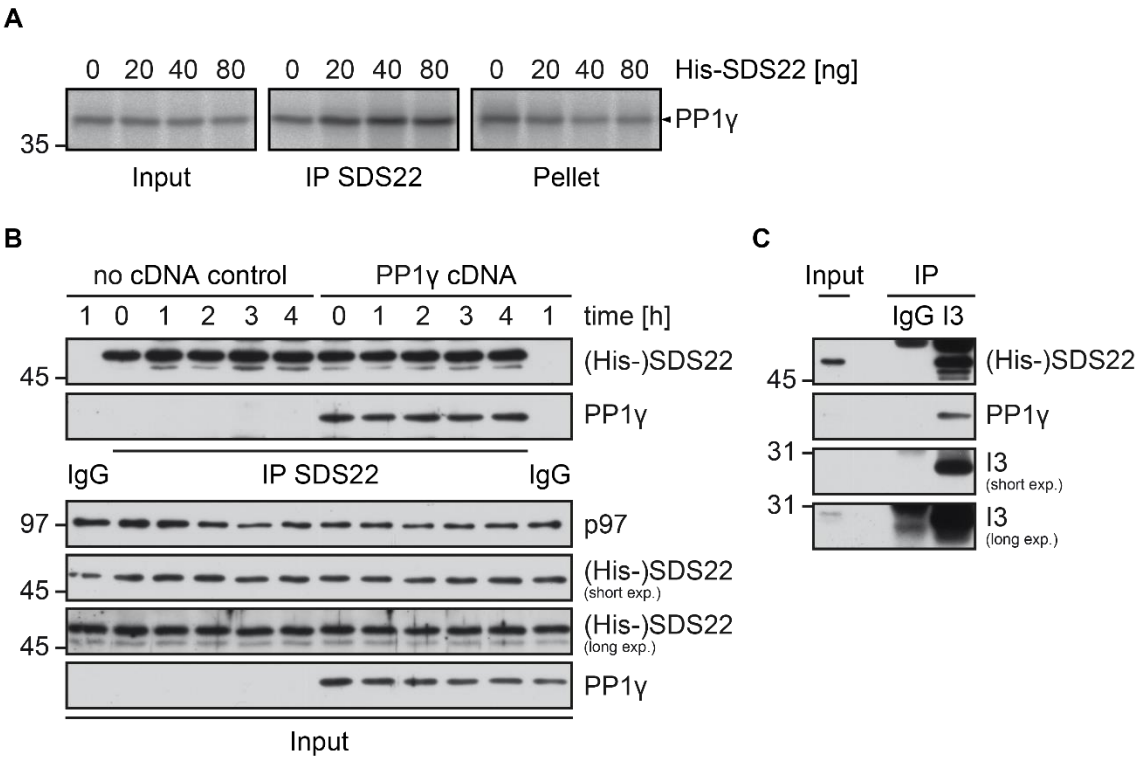

Figure 41: Expression of PP1γ in RRL and formation of a complex with His-tagged SDS22 and endogenous I3.
(A) RRL reactions (5 µl each), supplemented with ^{35}S-labeled L-methionine were set up to express PP1γ in the presence of the indicated amounts of purified human His-SDS22. After expression for 1 h, reactions were diluted with lysis buffer and subjected to centrifugation (17.000 g, 15 min, 4 °C). Pellets were resuspended and boiled in sample buffer. SDS22 was isolated from supernatants by IP and the amount of PP1γ in SDS22-IP and pellet from each condition was measured by autoradiography of dried SDS-PAGE gels. Note the increase of PP1γ in SDS22-IPs and decrease in the pellet fraction after addition of up to 40 ng (8 ng/ µl) His-SDS22. **(B)** RRL reactions supplemented with non-radioactive L-methionine and 5 ng/ µl His-SDS22 were set up with or without cDNA to express PP1γ. After expression for 30 min, further translation was inhibited by addition of cycloheximide (500 µg/ml) and RNase A (80 µg/ml). Samples were removed during further incubation at 30 °C at the indicated times. SDS22-bound PP1γ was detected by Western Blotting of SDS22-affinity-isolates. **(C)** Expression of PP1γ in RRL as in (B) followed by IP of I3 and Western Blot staining with indicated antibodies.

Addition of His-tagged human SDS22 to RRL increased the stability of recombinantly expressed PP1γ beyond improving the yield of PP1γ co-IP with SDS22, since the radioactive signal in pellet fractions of RRL reactions supplemented with His-SDS22 was reduced (Figure 41A).

IPs of both SDS22 (which enriched both the endogenous and the exogenous species) and endogenous I3 from RRL contained the expressed PP1γ, indicating that the SPI complex can be formed (Figure 41B and C). There was no signal in samples without addition of cDNA coding for PP1γ, showing that the antibody used for Western Blot staining does not or only weakly recognize endogenous rabbit PP1 (Figure 41B).

Notably, SDS22-IPs over a time-course of 4 hours contained unchanged amounts of PP1γ, indicating that the SPI complex is not disassembled by further incubation in the lysate (Figure 41B).

II.4.2 The RRL-derived SPI complex can be disassembled in *Xenopus laevis* Egg Extract (XEE)

To test whether the SPI complex formed with RRL-expressed PP1γ was amenable to subsequent disassembly, we made use of extracts prepared from *Xenopus laevis* eggs in the presence of cytostatic factor (CSF) (Minshull et al., 1991) as a source of potentially required additional components and / or enzymatic activity. The SPI complex in RRL was generated with addition of ^{35}S-L-methionine, which was necessary in this case because the anti-PP1γ antibody showed cross-reactivity with *Xenopus* PP1 (not shown). Samples of the RRL reaction after expression of PP1γ were transferred to freshly prepared XEE (J. v. d. Boom) and incubated further, with or without addition of the p97 inhibitor NMS-873. Following SDS22-IP at different time-points as indicated, complex-bound amounts of PP1γ were revealed by autoradiography (Figure 42).

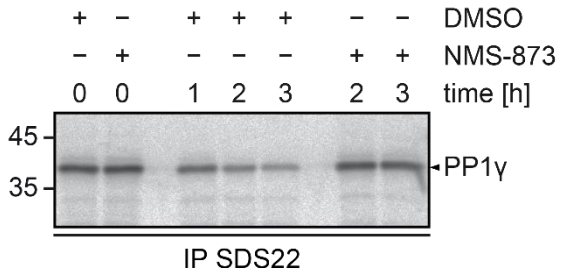

Figure 42: p97-dependent disassembly of RRL-derived SPI complex in *Xenopus* Egg Extract.
RRL, supplemented with ^{35}S-L-methionine and 5 ng/ µl His-SDS22 was set up to express PP1γ. After expression for 1 hour, 2.5 µl of RRL per reaction were transferred to 50 µl XEE, supplemented with NMS-873 (36 µM) or DMSO alone, and incubated further at 22 °C for the indicated times. Reactions were diluted 1:10 with cold CSF-XB buffer + 0.5 % Triton X-100 and subjected to IP of SDS22. SDS22-bound amounts of radiolabeled PP1γ were analyzed by autoradiography of dried gels.

SDS22-IP from RRL samples incubated in XEE in the presence of DMSO alone contained decreasing amounts of PP1γ at successive time-points. This indicates that transfer to XEE allows disassembly of the SPI complex. In contrast, addition of NMS-873 abolished dissociation of PP1γ from SDS22 (Figure 42). This result showed that the RRL-derived SPI complex can be disassembled in a p97-dependent manner, likely assisted by an unknown component present in XEE that is lacking in RRL (II.4.1).

II.4.3 Supplementation of RRL with p37 initiates disassembly of the SPI complex

The previous result indicated that the RRL-derived SPI complex can be disassembled and that this process requires p97, consistent with our results in HeLa cells (II.2.2). The observation that disassembly of the RRL-derived SPI complex was possible in XEE but not in RRL indicated that one or several factors were missing. We therefore attempted to supplement RRL with elements involved in SPI complex disassembly. This included an ATP-regenerating system (IV. 14) to provide energy for p97 function as well as recombinant (His-tagged) p97 itself (purified from insect cells by J. v. d. Boom). Furthermore, we added p37 as

a p97 adapter (purified from *E. coli* by J. Seiler), since its depletion had the strongest effect on binding of p97 to the SPI complex (II.3.1). We also hypothesized that adding (His-tagged) NIPP1 (purified from *E. coli* by D. Hönig) as an alternative RVxF-motif-containing interactor for PP1 might influence the disassembly process.

PP1γ was again expressed in a RRL reaction in the presence of His-SDS22. Aliquots were then supplemented with the indicated components, usually including the ATP-regenerating system except in reactions with addition of ATPγS. We also tested p97-dependency by addition of NMS-873 to the reaction. After incubation for 1 hour, SDS22 was isolated by IP and bound PP1γ was analyzed by Western Blot (Figure 43).

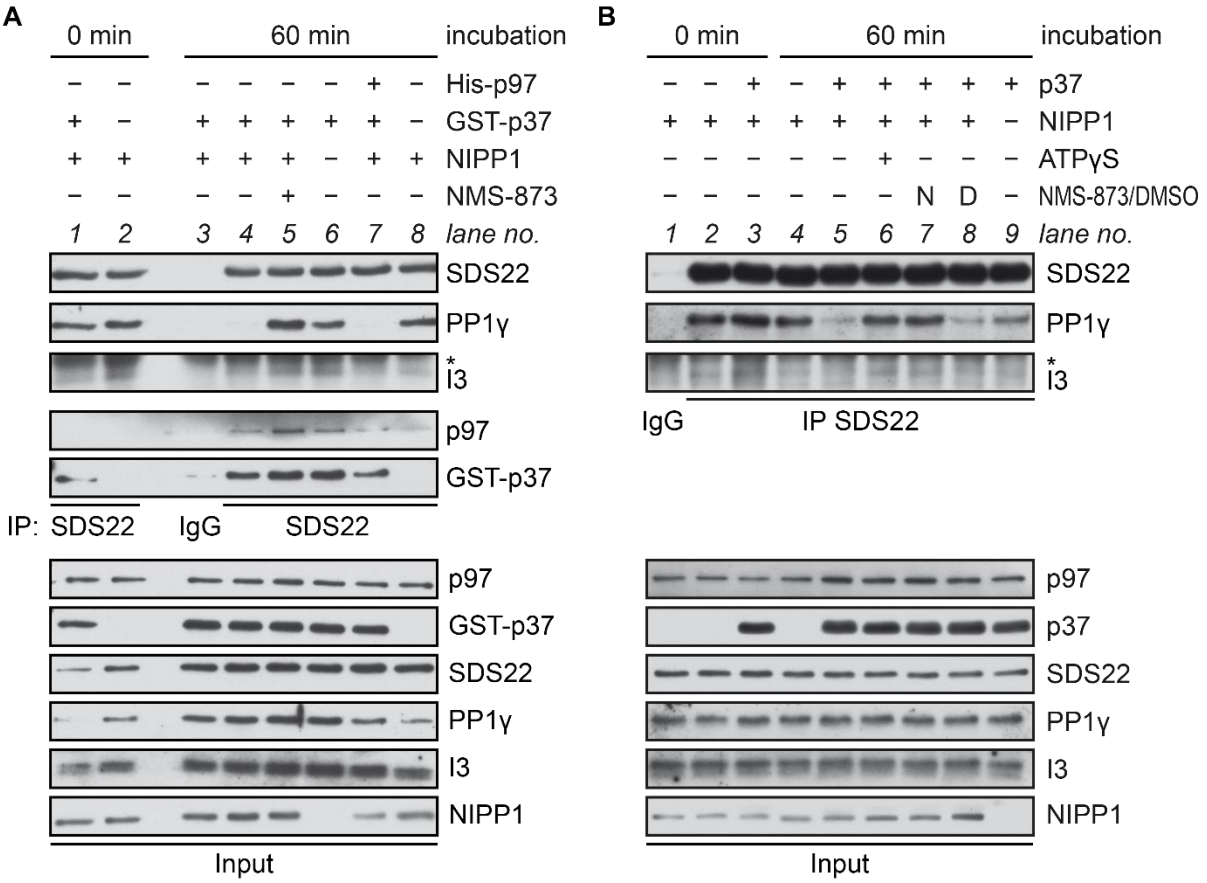

Figure 43: Supplementation of RRL to disassemble the complex of SDS22, I3 and expressed PP1γ.
(A) A RRL reaction was set up as in figure Figure 41B to express PP1γ for 1 hour. Aliquots of 5 µl each were then supplemented with an ATP-regenerating system and indicated recombinant proteins (0.1 µM of His-p97 and GST-p37, 0.24 µM His-NIPP1). One reaction was additionally supplemented with NMS-873 (0.5 µM). Before or after 1 hour incubation at 30 °C, reactions were diluted 1:30 with cold reaction buffer + 1 % Triton X-100 and subjected to SDS22-IP. SDS22-bound proteins were analyzed by Western Blot staining with indicated antibodies. **(B)** Setup of RRL reaction as in (A) and supplementation with indicated recombinant proteins (0.1 µM p37, 0.24 µM His-NIPP1), 2 µM ATPγS instead of the ATP-regenerating system and 0.5 µM NMS-873 or DMSO alone as indicated. SDS22-IP and Western Blot analysis as in (A).

The experiments shown in Figure 43 demonstrate that the SPI complex established in RRL can undergo disassembly when the lysate is supplemented with specific components. The essential protein component for this disassembly was p37. In the absence of p37 or GST-p37, the amount of PP1γ co-isolated with SDS22 remained unchanged during 60 min

incubation (Figure 43A, compare lanes 2 and 8, Figure 43B, lanes 2 and 4). Addition of p37 led to a reduction of PP1γ in SDS22-IP after 60 min (Figure 43A, compare lanes 1 and 6, Figure 43B, lanes 3 and 9). However, the interaction was completely lost when another PP1γ interactor, NIPP1, was added as an acceptor for the catalytic subunit after disassembly (Figure 43A, lane 4 and Figure 43B, lane 5), whereas NIPP1 alone did not displace I3 or PP1γ from SDS22 (Figure 43A, lane 8, Figure 43B, lane 4). Supplementation of RRL with recombinant His-p97 was also tested (Figure 43A, lane 7), but was not necessary for SPI disassembly.

Dissociation of PP1γ from SDS22 was energy-dependent, since replacing the energy-regeneration system with non-hydrolyzable ATPγS led to stabilization of the SDS22-PP1γ interaction (Figure 43B, lane 6). The disassembly was again inhibited by addition of NMS-873 but not DMSO alone (Figure 43B, lanes 7 and 8), indicating that activity of endogenous, rabbit p97 was required. Co-IP of p97 with SDS22 in the presence of GST-p37 indicated that, like in HeLa cells, p37 was required as an adapter for targeting of p97 to the SPI complex (Figure 43A).

II.4.4 p47 does not fully substitute for p37 to disassemble the SPI complex in RRL

Experiments in HeLa cells indicated that three SEP domain-containing p97 adapters - p47, p37 and UBXN2A - had partially redundant functions in the recruitment and activity of p97 towards the SPI complex (II.3.2). Next, it was tested whether (GST-tagged) p47 (purified from *E. coli* by C. Brasseur) was able to substitute for p37 to allow dissociation of RRL-expressed PP1γ from SDS22 (Figure 44).

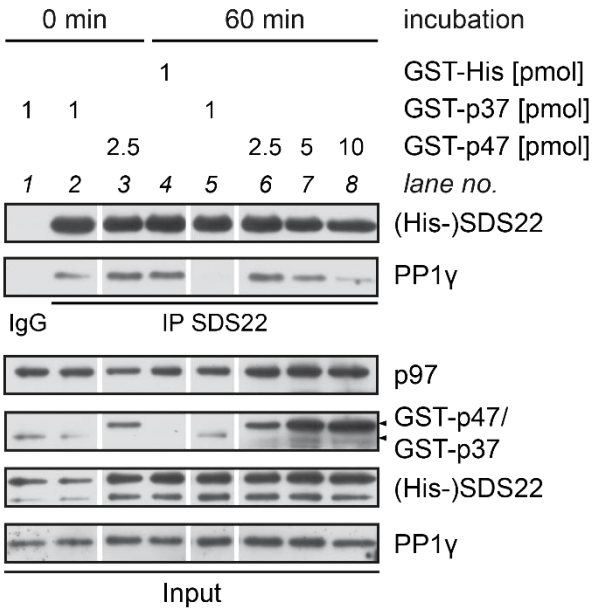

Figure 44: Substitution of GST-p47 for GST-p37 to dissociate PP1γ from SDS22 in RRL.
A RRL reaction was set up as in Figure 43 to express PP1γ. After 1 hour, aliquots were supplemented with indicated recombinant proteins (1 pmol equals 0.1 µM final concentration in the reaction). SDS22 was isolated and IPs were analyzed by Western Blot as before. Three lanes showing IP with IgG control were cut for simplicity (white spaces).

As observed before (Figure 43), addition of 1 pmol or 0.1 µM GST-p37 led to dissociation of PP1γ from SDS22 after 60 min incubation of supplemented RRL (Figure 44, compare lanes 5 and 2), whereas the complex remained stable after addition of GST-His (lane 4). Addition of 2.5 pmol GST-p47 did not affect PP1γ co-IP with SDS22, and 5 or 10 pmol GST-p47 only led to a partial reduction (compare lanes 6 to 8 and 3). Since SDS22-IP at the t = 0 min time-point was only included for the condition with 2.5 pmol GST-p47, it could not be excluded that higher amounts of GST-p47 led to destabilization rather than p97-mediated disassembly of the SPI complex. Since the process was in the meantime also reconstituted with purified components, no further experiments with different p97 adapters were conducted in RRL.

II.4.5 Mapping of p37 structural requirements reveals an essential role of the SEP domain in SPI complex disassembly

The dependency of SPI complex disassembly on supplementation of RRL with p37 enabled further studies to compare truncation- or point-mutants with the wild-type protein to determine the required structural elements in p37 for this activity. Mutant and wild-type p37 were recombinantly expressed in *E. coli* as fusion proteins with a GST-tag, which was subsequently cleaved off during purification (J. Seiler). The purified proteins were then compared regarding their ability to assist disassembly of the SPI complex established in RRL (Figure 45).

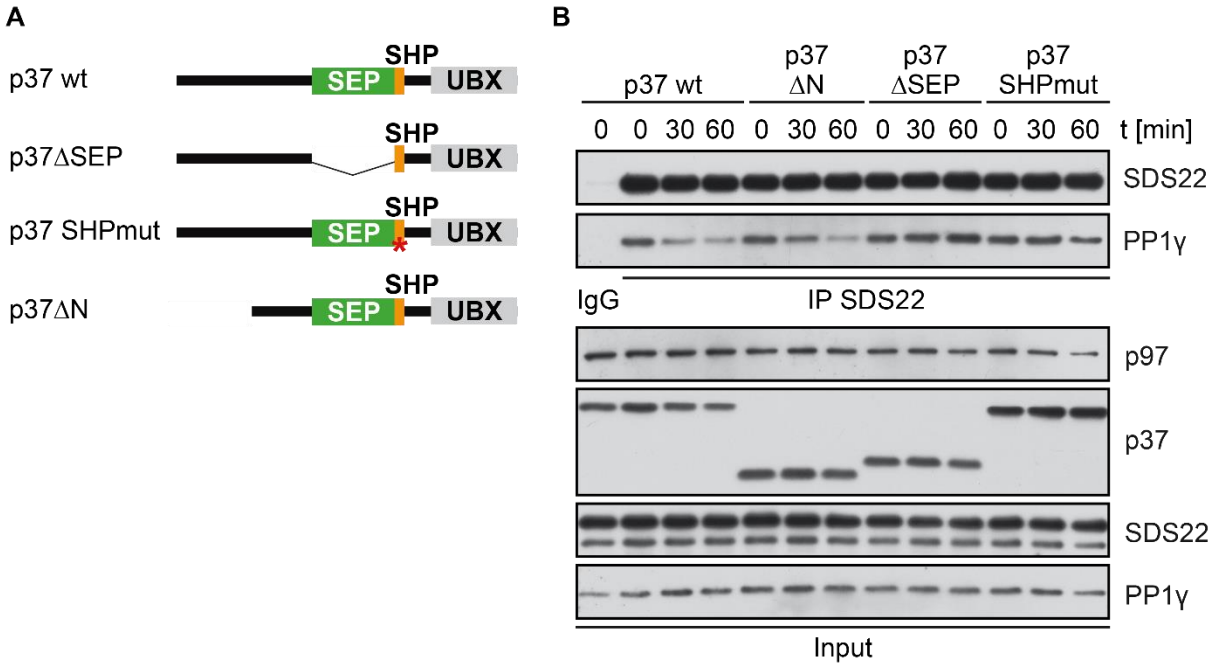

Figure 45: Comparison of the ability of p37 wild-type and mutants to mediate disassembly of the SPI complex in RRL.
(A) Schematic representation of p37 wild-type (wt) and mutants (ΔSEP = ΔAA140-206; SHPmut = F215A/E218A/QKL220-222AAA; ΔN = ΔAA2-81) **(B)** A RRL reaction was set up as in Figure 43 to express PP1γ. After 1 hour, aliquots were supplemented with indicated p37 variants (0.1 µM) and incubated at 30 °C for the indicated times. SDS22 was isolated by IP and bound PP1γ was analyzed by Western Blot as before.

Supplementation of RRL with wild-type p37 led to time-dependent release of PP1γ from SDS22. A similar effect was observed when RRL samples were supplemented with a p37 mutant lacking amino acids 2 - 81 ("ΔN") but not when adding the truncation mutant "ΔSEP", lacking the SEP domain (AAs 140 to 206), nor after addition of p37 "SHPmut", carrying mutations within the SHP-box motif (Figure 45A and B). These results indicate that the SHP box motif, which is required for p97 binding (I.3.5), as well as the SEP domain are required for p37-mediated disassembly of the SPI complex. Conversely, the N-terminal region, which is weakly homologous to the ubiquitin-associated (UBA) domain in p47, was not required. This supports the notion that recruitment of p97 to the SPI complex by p37 is ubiquitin-independent (see also II.3.4). Importantly, the SEP domain in p37 appears to facilitate the recruitment of p97 as a direct substrate-binding domain. *In vitro* and pulldown experiments (J. Seiler) indicated that p97-binding by p37 is another prerequisite for interaction with the SPI complex, possibly hinting at a non-linear binding interface (see also III. 5).

II. 5 Inhibition of p97 and depletion of SEP domain-adapters change the PP1 interaction landscape and affect mitosis

The previous results indicated that upon inhibition of p97 activity or in SEP domain adapter-depleted conditions, SPI complex disassembly and the formation of holoenzymes with newly synthesized PP1 are strongly compromised (II.2 and II.3). To assess the influence of interfering with disassembly of the SPI complex on the general regulation of PP1 holoenzyme composition, we wished to compare the interactome of PP1γ between conditions which allow or prohibit SPI disassembly. To achieve this, we applied label-free quantification mass spectrometry (LFQ-MS) to compare interactors in PP1γ-IPs from NMS-873- against DMSO-treated HeLa cells as well as after depletion of p47, p37 and UBXN2A in comparison to native, control-depleted cells.

II.5.1 Two experimental approaches to compare PP1γ interactomes following inhibition of SPI complex disassembly

Treatment of HeLa cells with NMS-873 was shown to efficiently block both SPI complex disassembly as well as formation of NIPP1- and MYPT1-holoenzymes with newly synthesized PP1 (II.2). However, downstream effects of this perturbation can be expected to depend on the half-life of PP1 holoenzymes. To obtain an estimate of its half-life, we compared pulse-labeled PP1 in PP1γ-specific IPs over a chase of several days. This indicated a half-life between 24 h and 48 h (Figure 46A). We therefore expected prolonged inhibition of p97 to be necessary to detect downstream effects of interfering with de-novo PP1 holoenzyme formation. This led us to evaluate treatment with NMS-873 for 16 h or 24 h prior to IP of PP1γ (Figure 46B). As expected, treatment with 5 µM NMS-873 compared to

DMSO for 16 h led to increased co-IP of SDS22 and I3 with PP1γ. The 24 h-treatment led to high numbers of apoptotic cells and the interactions with SDS22 and I3 seemed less stable. Optimization of elution conditions finally resulted in the MS experiment setup for 16 h NMS-873 treatment, as shown in Figure 46C (MS1).

In a second approach to determine downstream effects of perturbed SPI disassembly, interactions of PP1γ in HeLa cells depleted of p47, p37 and UBXN2A by combined KO and RNAi-treatment for 48 h II.3.2) were compared to interactions in control-depleted parental HeLa cells by IP of PP1γ and LFQ-MS analysis of its interactors. After confirming that the treatment resulted in the expected increase of SDS22- and I3-binding to PP1γ (Figure 46D), a similar experimental setup was adopted for MS analysis as for experiments with NMS-873 treatment (Figure 46E, MS2).

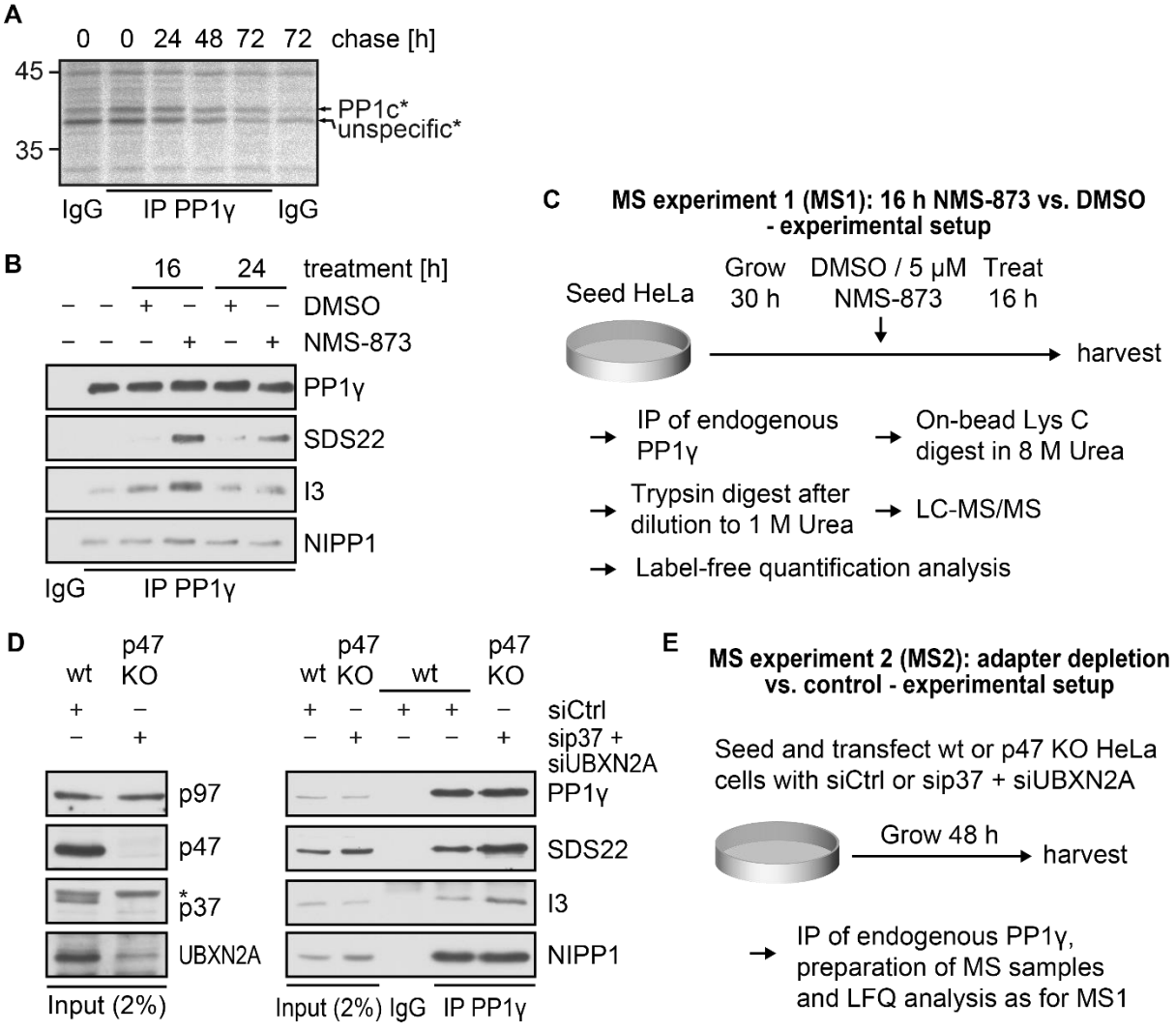

Figure 46: Evaluation of conditions for MS analysis of the PP1γ-interactome after NMS-873 treatment or depletion of SEP domain-containing adapters.
(A) Determination of PP1γ turnover. HeLa cells were seeded at low density to allow continued growth for at least 3 days. 24 hours after seeding, cells were pulse-labeled as before (Figure 26) and chased for indicated times. PP1γ was isolated by IP from complete lysates, which retained similar amounts of total radioactive label (not shown). The amount of radiolabeled species of PP1 (PP1c*) remaining at each time-point was determined by autoradiography. **(B)** Evaluation of 16 h or 24 h treatment with NMS-873 (5 µM). HeLa cells were treated as indicated and subjected to IP of PP1γ, followed by Western Blot analysis of bound proteins by indicated antibodies. **(C)** Workflow for MS analysis after

treatment with NMS-873. **(D)** Parental, wild-type (wt) HeLa cells were treated with non-targeting control siRNA (siCtrl), whereas p47 KO cells (clone 42) were treated with siRNAs targeting p37 (oligo s5) and UBXN2A (oligo s1) for 48 hours. Knockout and knockdown efficiencies were verified by Western Blot (lower panel, asterisk indicates unspecific staining by the p37 antibody). Endogenous PP1γ was isolated by IP and bound proteins were analyzed by staining with indicated antibodies. **(B)** Workflow for MS analysis after depletion of SEP domain-adapters.

II.5.2 Analysis of known PP1 interactions upon perturbation of SPI complex disassembly

After completion of MS experiments, data were first filtered for known contaminants and spurious assignments, followed by a step to reduce the data sets to proteins specifically enriched in PP1γ-IPs over control IPs with goat IgG (IV.16). Next, known PP1 interactors (Heroes et al., 2013) were annotated. MS analysis resulted in identification of an almost identical set of 30 or 31 known PP1 interactors in both approaches, with the exception of N-Cor, which was only identified in the first set of MS runs to assess the effect of NMS-873 treatment (MS1). The following diagrams (Figure 47) visualize fold changes of interactor LFQ intensities between PP1γ-IPs from NMS-873- or DMSO-treated cells (MS1) and between PP1γ-IPs from cells depleted of p47, p37 and UBXN2A or native mock-depleted cells (MS2).

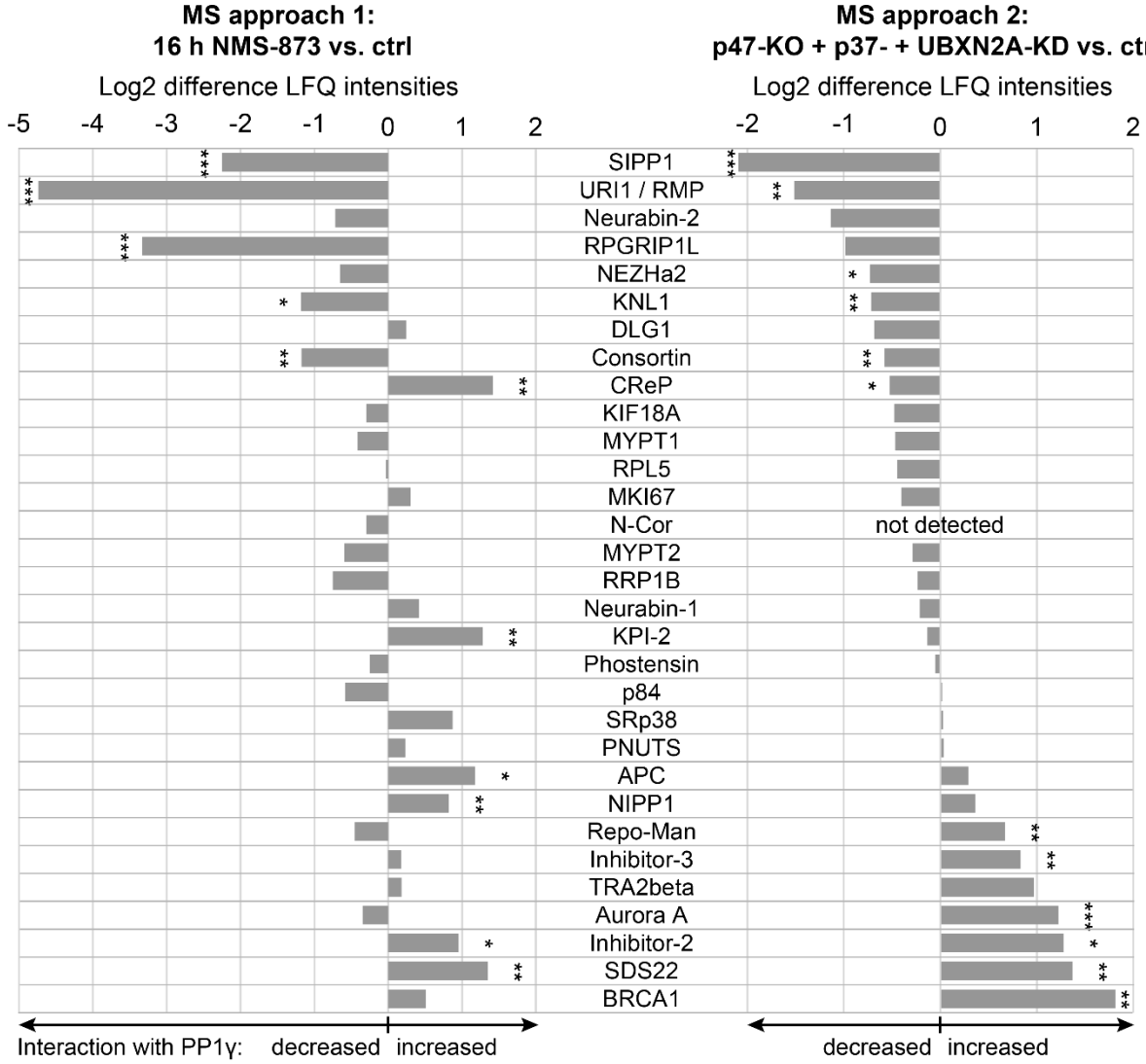

Figure 47: Effects of two approaches of inhibiting SPI complex disassembly on binding of known interactors to PP1γ.
LFQ intensities of interactors of PP1γ in both MS approaches (1: 16 h treatment with 5 µM NMS-873 and 2: combined knockout of p47 and RNAi mediated depletion of p37 and UBXN2A compared to control depletion, see II.5.1) were compared using the Perseus software to perform Student's t-test for each protein between the treatment and control runs, followed by a correction for multiple testing based on permutation (FDR = 0.05, S0 = 0.1, 250 permutations; * $p < 0.05$, ** $p < 0.01$, *** $p < 0.001$). Data are displayed with respect to the treatment conditions compared to control ("increased" indicates higher LFQ intensity in NMS-873-treated or SEP domain adapter-depleted cells). To facilitate direct comparison, results for PP1 interactors from both approaches are depicted in the order of fold changes in the depletion experiment (MS2).

Confirming the results of pre-tests conducted for both approaches by Western Blotting, interaction of SDS22 and I3 with PP1γ was found upregulated upon interfering with SPI complex disassembly (Figure 46 and Figure 47). These increases were significant with the exception of the interaction of I3 with PP1γ after 16 h treatment with NMS-873, which was only slightly increased. As also observed in Western Blot, NIPP1 was not reduced in either treatment (Figure 46 and Figure 47, see also III. 8).

In general, both treatments resulted in a similar pattern of effects for most PP1 interactors. The most severely affected interactions were those of SIPP1 and URI1 / RMP with PP1γ, which were strongly reduced by both treatments. The interaction with URI1 was subsequently investigated in more detail (see II.5.4). Another consistently decreased interaction was that of PP1γ with the kinetochore protein KNL1 (see below).

Interestingly, apart from SDS22 and I3, Inhibitor-2 (I2) was among the interactors with increased abundance in PP1γ-IP in both treatment conditions. In addition, the I2-interactor KPI-2, for "Kinase/Phosphatase/I2" (Wang and Brautigan, 2002), was significantly stronger associated with PP1γ upon NMS-873 treatment. The kinase Aurora A, which has also been reported to directly interact with I2 (Satinover et al., 2004) was increased in the second MS approach but not upon treatment with NMS-873. Similarly, Repo-Man was only found to interact more strongly with PP1γ upon depletion of SEP domain-adapters (see also III. 8).

To verify shifts of interactions between PP1γ and some of the known regulatory subunits in cells deprived of the SEP domain-adapters, IP of PP1γ was repeated and co-precipitated proteins were detected by Western Blotting (Figure 48). This experiment largely confirmed the data obtained by LFQ-MS for interactions with URI1, SIPP1, KNL1 and I2 in addition to the expected behavior of SDS22, I3 and NIPP1. In the case of MYPT1, Western Blotting indicated a decrease, which was not assigned significance in the MS analysis.

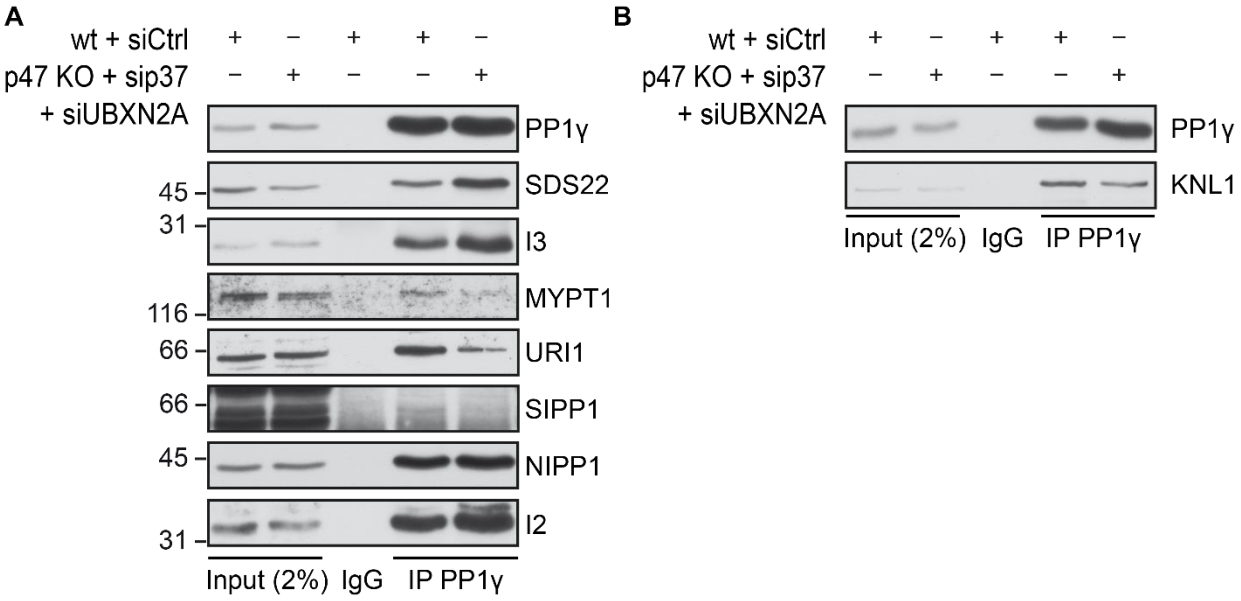

Figure 48: Verification of LFQ-MS analysis results for some exemplary PP1γ interactors in SEP domain-adapter-depleted versus control HeLa cells.
(A) and (B) Parental, wild-type (wt) HeLa cells or HeLa cells after knockout of p47 (clone 42) and siRNA mediated depletion of p37 and UBXN2A were treated as described in Figure 46, followed by IP with goat control IgG or specific antibodies for PP1γ. Co-precipitated proteins were stained with specific antibodies to detect interactors of PP1γ. In (B), a lower percentage gel was used to achieve more efficient transfer of KNL1 during wet blotting.

II.5.3 Pathway analysis of shifted PP1 interactions after SEP domain-adapter depletion

The effects on interactions of PP1γ with known regulatory subunits described so far were part of more general shifts of interactions caused by the combined KO and depletion of p47, p37 and UBXN2A. Some of these shifts may be representative of specific pathways involving PP1 activity. As an approach to decipher the pathways affected by the lack of SEP domain-adapters, some known complexes were extracted from the MS data, as shown in Figure 49.

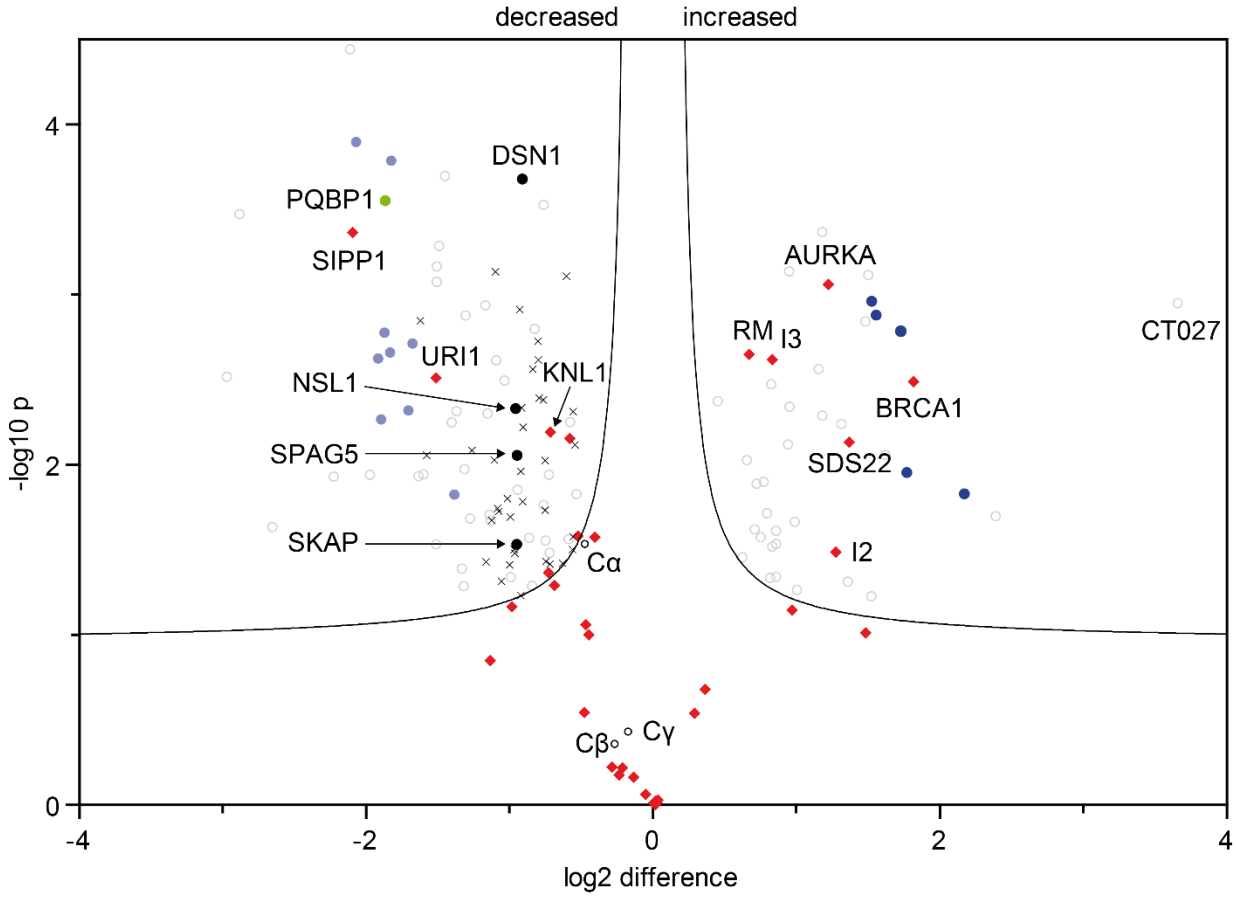

Figure 49: Shifts in the interactome of PP1γ upon loss of SEP domain-adapters with regard to known complexes and pathways.
Data from LFQ analysis of PP1γ interactors upon depletion of SEP domain-adapters (MS2, II.5.1), compared by Student's t-test as described in Figure 47 ("increased" indicates higher LFQ intensity in SEP domain-adapter-depleted cells). Open circles (grey): previously not described as interactors of PP1, significantly affected by loss of SEP domain-adapters; diamonds (red): known interactors of PP1 (Heroes, 2013); open circles (black): PP1 catalytic subunits; filled circles (black): kinetochore-associated proteins; filled circle (green): PQBP1; filled circles (light blue): R2TP/prefoldin-like complex (URI1-associated); filled circles (dark blue) BRCA1-A complex. Crosses: ribosomal subunits. Non-significantly affected interactions except known PIPs are hidden. Cα, -β, -γ = PP1 catalytic subunit α, β, γ; SKAP = Small kinetochore-associated protein; SPAG5 = Sperm-associated antigen 5; RM = Repo-Man; AURKA = Aurora kinase A; CT027 = C20orf27

As mentioned before, URI1 was among the most strongly reduced interactions of PP1γ after depletion of the SEP domain-adapters. URI1 is a component of the R2TP/prefoldin-like complex, which acts as a Hsp90 cochaperone (Mita et al., 2013). The MS data on this complex are further detailed in the following section (II.5.4). SIPP1 and its interactor PQBP1, both of which were also strongly reduced, play a role in pre-mRNA splicing (Llorian et al., 2004; Mizuguchi et al., 2014). PQBP1 interacts with the U5-15 kD protein, a component of the spliceosomal U5 complex, which in turn was implicated as a substrate of the R2TP/prefoldin-like machinery (Cloutier et al., 2017).

Another group of negatively affected interactions were those with known interactors or substrates of PP1 at kinetochores. These include the kinetochore-anchor KNL1 (Liu et al., 2010) (Figure 48B) as well as the PP1 target DSN1 (Eiteneuer et al., 2014; Wurzenberger et al., 2012) (Figure 49). In addition, NSL1, which is a component of the MIS12 complex, was

similarly downregulated. The interactions with spindle- and kinetochore-associated proteins Astrin / SPAG5 and Kinastrin / SKAP, which are subject to regulation by Aurora B (Schmidt et al., 2010), were found to be reduced. Mitosis-related kinesin motor proteins (Wordeman, 2010) were also affected (not shown in Figure 49), with KIF14 (log2 difference = -0.73; $p < 0.05$) among the down-regulated interactors, whereas KIF22 interacted more strongly with PP1 (log2 difference = +0.82; $p < 0.01$) in SEP domain adapter-depletion. To investigate whether these changes are correlated with cell cycle abnormalities, we performed flow cytometry-based analyses (I.5.4).

A range of RNA-binding proteins were detected among the downregulated interactors of PP1γ (not indicated in Figure 49), such as the spliceosome component RBM28 (Damianov et al., 2006)(log2 difference = -1.32; $p < 0.05$) and FTSJ3, which has a role in pre-rRNA processing (Morello et al., 2011)(log2 difference = -1.60; $p < 0.05$). Some PP1 substrates have reported regulatory functions in conjunction with ribosomes, such as the ribosomal protein S6 (RPS6), which is involved in binding of the 5'-methyl cap of mRNA and is dephosphorylated by PP1, thereby reducing cap-dependent mRNA translation (Hutchinson et al., 2011). RPS6 was also found in the MS data and this interaction was significantly downregulated following loss of the SEP domain-adapters (log2 difference = -0.54; $p < 0.01$). Furthermore, a large number of ribosomal proteins were among the downregulated interactors (crosses in Figure 49).

Increased interactions upon loss of the SEP domain adaptors were less numerous overall. The most strongly increased interaction with PP1γ was detected for the protein C20orf27, for which no functional data is available. Apart from specific increases of some known interactors, which were reported in the previous section, it may be worth noting that a complex surrounding the BRCA1/BARD1 ubiquitin ligase was found in the MS analysis. This further included the complex members Abraxas, RAP80, BABAM1 and the interacting E3 ligase RNF169, all of which are involved in DNA damage responses (Poulsen et al., 2012; Solyom et al., 2012). A fragment was detected for complex member BRCC3, but this interaction was unaffected by the treatment (not shown).

A few proteins related to splicing or RNA-binding were also found among interactors with increased abundance in PP1γ-IP upon depletion of SEP domain-adapters. These included RBM14(Yuan, 2014) (log2 difference = +0.71; $p < 0.05$) as well as heterogeneous nuclear ribonucleoprotein (hnRNP)(Krecic and Swanson, 1999) complex members HNRNPL (log2 difference = +1.50; $p < 0.001$) and HNRNPUL1 (log2 difference = +1.18; $p < 0.001$), whereas the interaction of HNRNPM with PP1γ was slightly reduced (log2 difference = -0.53; $p < 0.05$).

II.5.4 Depletion of SEP domain-adapters or I3 and inhibition of p97 affect PP1γ-URI1 interaction

Findings published in the literature point to a connection between PP1, URI1 and nutrient-sensing as well as apoptosis pathways (Djouder et al., 2007; Gstaiger et al., 2003). However, more recent MS experiments also detected a connection between PP1 and the R2TP co-chaperone (Yadav et al., 2017). The finding that interactions of PP1γ with URI1 as well as further members of the prefoldin-like and R2TP complexes were significantly downregulated by both ways of perturbing SPI disassembly made this connection interesting to explore. First, the results obtained by LFQ-MS experiments upon depletion of SEP domain-adapters on the PP1γ-URI1 interaction were validated by Western Blotting (Figure 50A and B, Figure 48A). Subsequently, we tested depletion of I3 as well as short and prolonged inhibition of p97 for their effect on this interaction (Figure 50C to E)

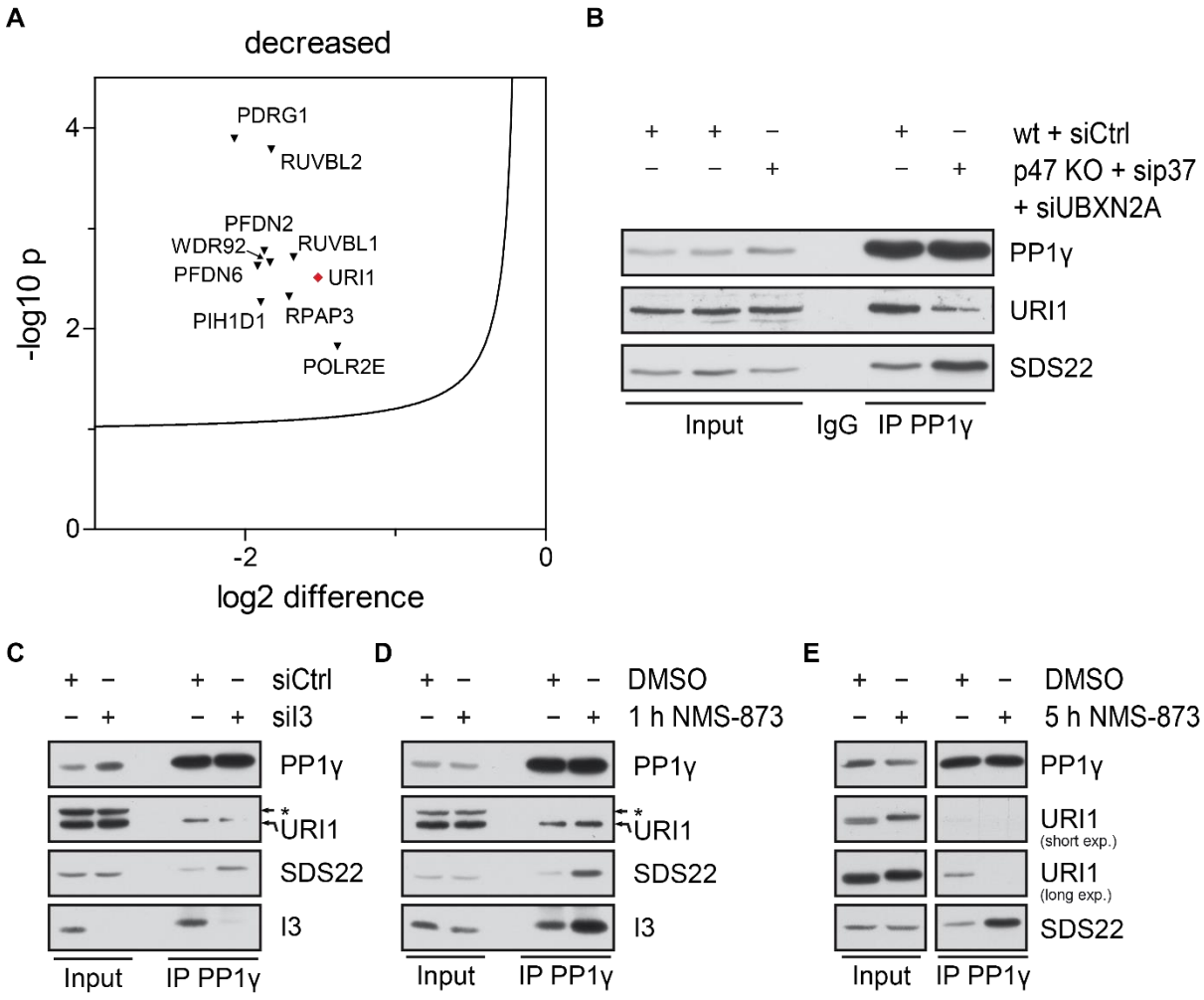

Figure 50: Interaction of PP1γ with URI1 upon depletion of SEP domain-adapters, I3 or upon treatment with NMS-873.
(A) Data from LFQ analysis of the PP1γ interactome after depletion of SEP domain-adapters as in Figure 49, limited to known members of the R2TP/Prefoldin-like co-chaperone complex (triangles), including the known PP1-interactor URI1 (diamond). **(B)** Verification of reduced interaction between PP1γ and URI1 upon depletion of p97 adapters. Western blot data as shown in Figure 48. **(C - E)** IP of PP1γ from HeLa cells after depletion of I3 for 48 h (C, siI3, oligo s2), or treatment with NMS-873 for 1 h (D, 10 µM) or 5 h (E, 5 µM). Western Blot staining with indicated antibodies.

Western Blotting confirmed reduced interaction between PP1γ and URI1 in cells depleted of SEP domain-adapters by combined KO and RNAi (Figure 50B). Since SPI disassembly in this condition is perturbed, the lack of interaction with URI1 might be due to competition for the RVXF motif, which is occupied by I3 in the SPI complex. However, upon depletion of I3, the interaction of PP1γ with URI1 was similarly decreased, whereas SDS22 was bound more strongly, as expected (Figure 50C). Although a 1-hour inhibition of p97 activity by NMS-873 is sufficient to strongly enrich SDS22 and I3 on PP1γ, it did not reduce the interaction of PP1γ with URI1 (Figure 50D), whereas prolonged treatment (5 h, Figure 50E) led to a reduction, which was also observed by LFQ-MS analysis following 16 h treatment.

II.5.5 Analysis of cell cycle distribution of SEP domain adapter-depleted cells by flow cytometry

Our MS analysis of HeLa cells after knockout of p47, combined with depletion of p37 and UBXN2A for 48 hours (MS2, II.5.1), indicated reduced interactions between PP1γ and several known interactors in mitosis, including the main PP1-binding protein at the kinetochore, KNL1 (II.5.3) (Liu et al., 2010). A potential confounding factor to this analysis would be a shift in the cell cycle caused by the treatment. More specifically, a reduced fraction of cells in mitosis would likely cause mitotic interactions of PP1 to appear less frequent. On the other hand, reduced interactions of PP1 in mitosis might also lead to defects downstream of PP1 dysfunction. Mitotic defects would likely activate the SAC and lead to increased duration of mitosis, causing a shift in the opposite direction with higher fractions of cells in mitosis.
To discriminate between these possibilities, we performed cell cycle analysis by staining the mitotic marker histone H3 phospho-serine 10 (pH3S10)(Hans and Dimitrov, 2001) together with propidium iodine (PI) staining to assess total DNA content (Figure 51).

Flow cytometry analysis indicated that neither the combined depletion of p37 and UBXN2A, nor KO of p47 alone had a significant impact on the mitotic index (the percentage of all counted cells displaying pH3S10 intensity above the threshold as indicated in Figure 51). However, combined KO and depletion of the SEP domain adapters led to a highly significant, roughly 2-fold increase in the percentage of cells stained positively by the mitotic marker pH3S10.

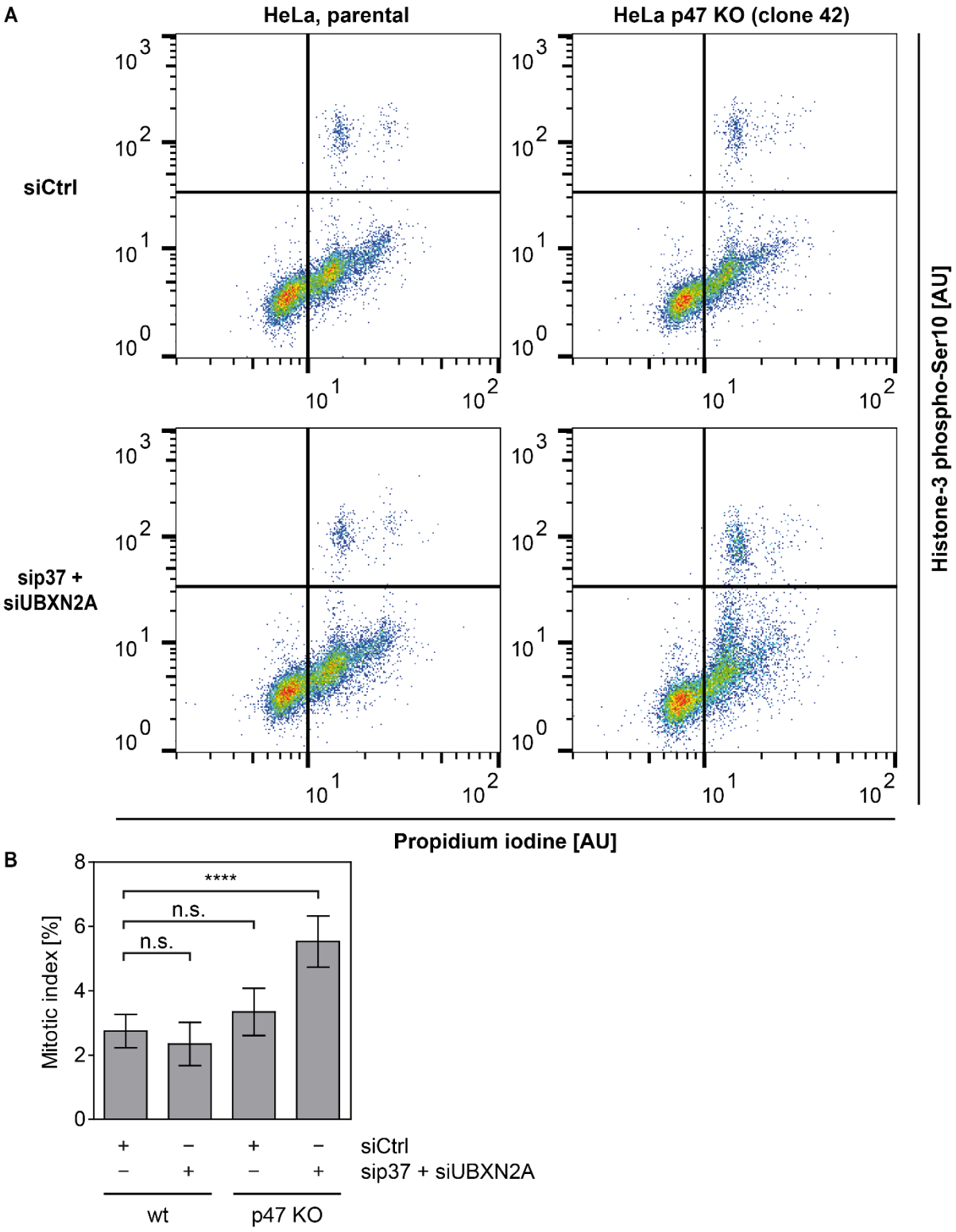

Figure 51: Flow cytometry analysis of the mitotic index of parental, wild-type HeLa or p47 KO cells after mock depletion or depletion of p37 and UBXN2A.
Parental, wild-type (wt) HeLa cells or p47 KO cells (clone 42) were treated with non-targeting control siRNA (siCtrl) or siRNAs targeting p37 (oligo s5) and UBXN2A (oligo s1) for 48 hours. Formaldehyde-fixed and permeabilized cells were stained with specific antibodies for pH3S10 and PI and analyzed by flow cytometry. **(A)** After gating for single cells, pH3S10 and PI signal intensities were plotted to identify mitotic cells (high PI, high pH3S10). Thresholds were set manually as indicated. **(B)** Quantification of the percentage of mitotic cells (mitotic index) in repeated experiments. Statistic analysis was done using a One-Way repeated measures ANOVA with Bonferroni post-hoc test. n = 3; **** $p < 0.0001$.

III Discussion

The results presented here and in our related publication (Weith et al., 2018), which was still under revision when this thesis was concluded, describe a process occurring in the early life cycle of the serine-/threonine-phosphatase PP1. We reveal that SDS22 and I3 form an intermediate complex with the newly synthesized PP1 catalytic subunit (SPI complex) during PP1 biogenesis. This complex keeps the catalytic subunit in an inactive state before it is released to form holoenzymes with other interaction partners. PP1 requires the AAA-ATPase p97 to be released from the SPI complex. The mechanistic details of this function of p97 enhance our conception of the roles of this important protein remodeling enzyme. Following a short overview, I will discuss the results that reflect these processes.

Several studies in yeast and mammalian cells implicated the PP1 interactors SDS22 and I3 in mitotic functions of PP1 (Cheng and Chen, 2010; Posch et al., 2010). On the other hand, the proposed roles of SDS22 and I3 as substrate-specifiers are complemented by reports that the yeast homologs Sds22 and Ypi1/I3 have more general roles in the stabilization, activity and localization of Glc7/PP1 (Cheng and Chen, 2015; Pedelini et al., 2007; Stone et al., 1993). Our own investigation of the function of human SDS22 and I3 in mitosis (Eiteneuer et al., 2014) led us to propose a premature stage, in which SDS22 and I3 are required for activation of PP1. Subsequently, SDS22 and I3 need to dissociate for PP1 to become fully active (I.2.8). We show here that the newly synthesized catalytic subunit of PP1 indeed interacts transiently with SDS22 as well as I3. Dissociation of both precedes in time and is required for the subsequent formation of at least a subset of PP1 holoenzymes (III. 1).

The role of the SPI complex can be further rationalized based on two observations. First, experiments with PP1 isolated from inducible cell lines show that the catalytic subunit of PP1 is inactive in the SPI complex. This satisfies the requirement to restrain the unspecific activity of the newly synthesized catalytic subunit (Verbinnen et al., 2017). Second, several pieces of evidence indicate that SDS22 is required for the stability of PP1, consistent with data on yeast Sds22 (Cheng and Chen, 2015)(III. 2).

A recent publication pointed to regulation of a complex comprising yeast Sds22, Glc7/PP1 and Ypi1/I3 by the p97 homolog Cdc48 and its adaptor protein Shp1 by an unknown mechanism (Cheng and Chen, 2015). Our data establish energy-dependent release of the SPI complex, which requires the AAA-ATPase p97. Inhibiting p97 activity stabilized the interactions of SDS22 and I3 with newly synthesized PP1 and abolished de novo formation of NIPP1- and MYPT1-PP1 holoenzymes (III. 1 and III. 2). This function of p97 further depends on its interaction with a previously undefined group of adapters, which share a SEP domain with yeast Shp1. We show by a combined KO and depletion approach that p47, p37 and UBXN2A participate in SPI complex disassembly by p97 in a redundant manner, consistent with partial conservation of the role of Shp1 in each of these adapters (III. 4).

While p97 was found to be recruited to ubiquitinated substrates in the majority of its cellular functions (I.3.2), its activity in the pathway of SPI complex disassembly does not require ubiquitination. Pulse-chase experiments with E1-activating enzyme inhibitors, which efficiently suppressed ubiquitination in cells, showed no effect on SPI complex disassembly. Furthermore, we were able to reconstitute the SPI complex in rabbit reticulocyte lysates and in this system, addition of exogenous p37 was required to recruit p97. These experiments allowed identification of the SEP domain as a novel substrate-interaction element of the p37 adapter protein (III. 5).

Furthermore, these experiments laid the ground for reconstitution of SPI complex disassembly by p97-p37 with purified components, which will be described in our publication (J. Seiler)(Weith et al., 2018). *In vitro* binding of p97 and p37 to the SPI complex as well as cross-linking via the SEP domain of p37 unequivocally demonstrate that I3 is the direct target of p97 activity (III. 6). The mechanistic details of this process were elucidated via elegant approaches applied by Jonas Seiler, Johannes van den Boom and Matthias Kracht. Our findings support the model that p97 acts as an unfoldase, which extracts proteins from cellular structures by channeling them through its central pore (Bodnar and Rapoport, 2017b).

We further demonstrate that NIPP1 can replace I3 on PP1 following disassembly of the SPI complex in reticulocyte lysates or with purified components. This corroborates the data obtained in cells and demonstrates hand-over of the catalytic subunit from the SPI complex to specific holoenzymes. We find that dissociation of SDS22 is closely coupled to the release of I3 but the mechanistic basis requires further study (III. 7).

We expected that lack of PP1 holoenzyme formation due to inhibition of SPI complex disassembly would have severe downstream effects on PP1-mediated pathways and on cellular viability in general. Mass spectrometry-based comparisons between the interactome of PP1γ in conditions that permit SPI complex disassembly and conditions that block or delay the disassembly process show prominent effects on several interactions of PP1 III. 8). This might indicate a general perturbation of holoenzyme homeostasis or could indicate differential dependency of PP1 holoenzymes on this biogenesis pathway.

Consistent with data that implicated yeast Shp1 in regulation of the mitotic function of Glc7 (Bohm and Buchberger, 2013; Cheng and Chen, 2010), the loss of all three adapters furthermore led to an increase in the mitotic index. Excessive activation of Aurora B in these conditions suggests that the activity of PP1 at kinetochores is impaired (J. Seiler)(Weith et al., 2018)(III. 9).

Future investigations might reveal whether p97-mediated regulation of the SPI complex is limited to the biogenesis of PP1 or extends to later phases of its life cycle and should assess the importance of this pathway for all or a subset of PP1 holoenzymes and the downstream effects on cellular physiology (III. 8 III. 10).

III. 1 Newly synthesized PP1 forms a transient complex with SDS22 and I3

A number of studies on the fission and budding yeast orthologs of SDS22 and I3 implicated both in the regulation of PP1 function during mitosis (I.2.4). The observed rescue of Ipl1-substrate phosphorylation levels by mutations in *sds22* and *ypi1* furthermore supported assignment of functions as substrate-specifiers to these PP1 interactors (Bharucha et al., 2008; Peggie et al., 2002). On the other hand, the mitotic phenotype caused by these mutations could also be an indirect effect. Several observations are consistent with a dependency of general PP1 activity on SDS22 and I3. First, mutation of sds22+ in fission yeast decreased the total activity of the PP1 homologs dis2+ and sds21+ towards glycogen phosphorylase *a* (Stone et al., 1993). Second, non-functional Sds22 suppressed the effect of Glc7 overexpression in budding yeast (Ghosh and Cannon, 2013). Third, *sds22* and *ypi1* mutants suppressed excessive glycogen accumulation caused by the *glc7-109* mutant (Bharucha et al., 2008), demonstrating effects in non-mitotic pathways.
In mammalian cells, SDS22 was implicated as a substrate-specifier for PP1 function at the kinetochore (Posch et al., 2010; Wurzenberger et al., 2012) and in the relaxation of the cortical actin cytoskeleton (Rodrigues et al., 2015). No data were available for a function of I3 in mammalian mitosis. Our previous study confirmed that SDS22 is required for the antagonistic function of PP1 towards Aurora B in mitosis (Eiteneuer et al., 2014) but we observed similar defects by overexpression of SDS22 (see also II.1.1). The study further showed that I3 is required to limit the level of SDS22 bound with PP1 to the kinetochore component KNL1. Strikingly, SDS22 inhibited dephosphorylation of Aurora B by PP1 *in vitro* (Eiteneuer et al., 2014). Thus, both SDS22 and I3 were required for PP1 activity in mitosis but unbalanced localization of SDS22 with PP1 at kinetochores inhibited the phosphatase.

The results presented in this thesis allow us to reconcile these seemingly contradictory observations. We define a process that occurs during PP1 biogenesis and involves SDS22 and I3. This process is essential for the formation of PP1 holoenzymes and for normal PP1 function. Its implications for the mitotic function of PP1 will be discussed later (III. 9).
First, we observed early binding and subsequent release of the newly synthesized catalytic subunit of PP1 (PP1c*) from SDS22 and I3 (II.1.2). We further found that depletion of I3 led to prolonged binding of PP1c* to SDS22 (II.1.4). This suggested that dissociation of PP1c* from both interactors happens not only simultaneously, as indicated by very similar time-courses of the observed interactions, but is also directly linked. These data were consistent with formation of a transient SDS22-PP1-I3 (SPI) complex in the early life cycle of PP1. In contrast, binding of newly synthesized PP1 to the unrelated interactors NIPP1 and MYPT1 increased with time and was detected later than binding to SDS22 and I3 (II.1.2 and II.2.3).

Thus, we could show for the first time that SDS22 and I3 differ from other PP1 interactors with regard to the life cycle stage, in which they preferentially interact with PP1.

Importantly, we found that the release of the catalytic PP1 subunit from the SPI complex is not a spontaneous process but requires the activity of the AAA-ATPase p97 (II.2.2). Pulse-chase experiments with an inhibitor of p97 ATPase activity showed that p97 is not only required for disassembly of the SPI complex but also for interactions of PP1c* with the substrate-specifiers NIPP1 and MYPT1 (II.2.3). We also found delayed NIPP1-PP1 holoenzyme formation following the depletion of adapters that recruit p97 to the SPI complex (II.3.3), supporting the notion that the formation of this holoenzyme depended directly on a function of p97 towards the SPI complex.

After reconstituting disassembly of the SPI complex in reticulocyte lysates, we were able to test the effect of adding exogenous NIPP1 during this process and found that it supported the release of PP1c* from SDS22 (II.4.3). This observation suggests that disassembly of the SPI complex might be directly followed by hand-over of the catalytic subunit to substrate specifiers like NIPP1. This was further corroborated by experiments with purified proteins, in which the exchange between I3 and NIPP1 can be observed after isolation of PP1 (J. Seiler)(Weith et al., 2018). This hand-over mechanism will be further discussed later (III. 7).

We also observed a strong impact of interfering with SPI complex disassembly on at least a subset of PP1 holoenzymes in MS experiments. These experiments relied on long-term treatment and probed interactions for the whole pool of cellular PP1 (holoenzyme homeostasis) instead of those formed with the newly synthesized catalytic subunit (de novo holoenzyme formation). Since this has fundamentally different premises, the data will be discussed separately (III. 8).

Taken together, these results indicate that the SPI complex is an obligate intermediate during de novo formation of at least two major PP1 holoenzymes. NIPP1 binds a large fraction of the PP1 catalytic subunit in the nucleus (Jagiello et al., 2000), whereas MYPT1 interacts with PP1 in the cytosol and on the cytoskeleton (Eto et al., 2005). While this suggests that the process is not restricted to interactors with a specific localization, it did not allow us to claim general dependency of holoenzyme formation on SPI complex disassembly. To test which fraction of the newly synthesized PP1 catalytic subunit is bound in the SPI complex, we attempted to deplete SDS22 from HeLa lysates, which were pulse-labeled in the presence of p97 inhibitors. Repeated rounds of SDS22 IP reduced the signal for newly synthesized PP1 in subsequent direct isolation of PP1γ compared to mock depletion of lysates with pre-immune IgG antibodies (data not shown). However, technical difficulties such as incomplete depletion of SDS22 prevented a final assessment of these results. We also approached the question whether the mitotic function of PP1 depends on this process. This was evaluated in cells depleted of the p97 adapters and will be discussed later (III. 9).

III. 2 The SPI complex can fulfill several requirements of phosphatase biogenesis

The catalytic subunits of the major serine-/threonine-phosphatase enzymes PP1 and PP2A have low intrinsic substrate specificity, implying that their occurrence in unbound form poses a risk to the cell (I.1.4). Furthermore, the free catalytic subunits are instable or prone to aggregation. This notion is supported by the role of the scaffolding subunit and the proposed role of chaperones in PP2A biogenesis (Sents et al., 2013)(I.2.8). In the case of PP1, stabilizing roles have been assigned to Sds22 and Ypi1 in yeast (Cheng and Chen, 2015). Another aspect that requires regulation is the localization of the catalytic subunit and yeast Sds22 and Ypi1 were shown to support correct nuclear localization of Glc7 (Cheng and Chen, 2010; Pedelini et al., 2007).

Our observations on the function and properties of the SPI complex suggest that it is well suited to fulfill the demands of phosphatase biogenesis and holoenzyme formation.
First, the trimeric complex can provide a storage pool for the formation of holoenzymes. As described earlier (I.1.4), PP1 interactors exist in excess over the catalytic subunit. An intermediate complex would provide a means for regulating the de novo formation of holoenzymes in a directed manner. As stated before, disassembly of the SPI complex requires the activity of the AAA-ATPase p97. This is consistent with the role of p97 as a segregase in the extraction of substrates from cellular structures (I.3.1). Therefore, release of PP1 from the SPI complex is an active process, which could be subject to extensive regulation.
It is noteworthy that disassembly of the SPI complex occurred at the expense of ATP, since replacing ATP with the non-hydrolyzable analog ATPγS inhibited the reconstituted process in rabbit reticulocyte lysates (II.4.3) and *in vitro* (Weith et al., 2018). Energy-dependent remodeling of protein complexes has been shown for example in the case of wound-up SNARE complexes, which are released by the p97-related ATPase NSF (I.3.6). In this view, the energy requirement of SPI complex disassembly might point to high-affinity interactions formed between the complex components, which would be consistent with tight constraints on the newly synthesized catalytic subunit that is sequestered in this complex.
Second, the SPI complex can serve to keep the unspecific activity of PP1 in check. A pulse-chase approach for strep-tagged PP1γ, which was expressed shortly in an inducible cell line (pulse) and subsequently chased in the presence of cycloheximide to inhibit further translation (II.2.5), recapitulated the interactions of newly synthesized endogenous PP1. It also confirmed that p97 activity is required to release PP1 from the SPI complex for interaction with NIPP1 (II.2.5). A phosphorylase *a* phosphatase assay on isolated PP1γ-strep indicated that p97 activity is required for PP1 activation, likely brought about by release of PP1 from the SPI complex. The results were similar with or without removal of PP1

interactors by a limited tryptic digest, suggesting that the catalytic subunit itself became more active after release from the SPI complex and transfer to interactors such as NIPP1. This conclusion is supported by biochemical data reported by Bart Lesage and co-workers, who found that the trimeric complex contains inactive PP1 *in vivo* (Lesage et al., 2007).

Considering the effects of mutations in sds22+ in fission yeast (Stone et al., 1993) and *shp1* mutants in budding yeast (Zhang et al., 1995), it could be asked whether global PP1 activity is also affected in mammalian cells when a component of the biogenesis pathway is missing or the progression to holoenzyme formation is blocked. However, our attempts to test PP1 activity in the phosphorylase *a* phosphatase assay after depletion of p97 adapters led to irreproducible results (data not shown). This was likely due to technical difficulties, including the long treatment duration required due to the long half-life of PP1 (II.5.1), isolation of untagged PP1 by immunoprecipitation with a polyclonal antibody and performing phosphatase assays with PP1 immobilized on beads.

Third, we find evidence for a stabilizing function of the SPI complex and more directly, for SDS22 towards PP1. SDS22 has the potential to induce a conformational change in PP1, which renders PP1 sensitive to trypsin (Lesage et al., 2007). However, recent studies in yeast (Cheng and Chen, 2015) indicate that Sds22 is required for the stability of Glc7. This is further evidenced by the notoriously difficult recombinant expression of PP1 in bacteria, which results in high fractions of insoluble protein, and also by low yields after expression in insect cells (Peti et al., 2013). Our own observations indicate that the yield of recombinantly expressed PP1 from the *Spodoptera frugiperda* Sf9 cell line is greatly enhanced by co-expression of SDS22 and I3 (J. Seiler). It could be imagined that SDS22 binds to a partially folded form of PP1 and stabilizes it. Consistently, we found increased binding of SDS22 after transient transfection and isolation of two destabilized mutants of PP1 (GFP-tagged PP1 D64N and -PP1 H125A, data not shown). In radioactive metabolic labeling experiments, depletion of SDS22 led to strong reduction of the amounts of newly synthesized PP1 retrieved by PP1γ-specific IP, whereas global protein expression was not affected (II.1.5). Absence of SDS22 might have rendered PP1c* instable, followed by sequestration in insoluble aggregates.

Yeast data further indicate that Ypi1/I3 can facilitate transport of the catalytic subunit of PP1 to the nucleus, consistent with the presence of a nuclear localization signal close to its N-terminus (Huang et al., 2005), while no such signal is found in SDS22 (Peggie et al., 2002). Several studies reported that mutation of *sds22* as well as *ypi1*/I3 resulted in a loss of Glc7 nuclear localization (Pedelini et al., 2007; Robinson et al., 2012). In the case of I3, this would be consistent with a direct role in targeting PP1 to the nucleus, while loss of SDS22 might have a secondary effect: Destabilization of the catalytic subunit could prevent the formation of a complex with I3. Consistently, we observed loss of interaction between newly synthesized PP1 and I3 after metabolic labeling of SDS22-depleted cells (II.1.5). We could

not assess the impact of SPI complex disassembly on the localization of endogenous PP1 due to lack of antibodies suitable for IF experiments. We attempted to study localization of GFP-tagged PP1γ using an inducible HeLa cell line (data not shown). However, pharmacological inhibition of p97 during expression of GFP-PP1γ did not result in the expected accumulation of SDS22 and I3 in GFP-PP1γ immunoisolates. Although we observed accelerated nuclear localization of GFP-PP1γ, which was already evident after 3 hours (data not shown), we cannot relate this to an influence of the SPI complex, since it was not formed correctly.

Our results provide indications that the SPI complex has an essential role in sequestering and stabilizing the catalytic subunit of PP1 and keeping its activity in check before hand-over to substrate-specifiers takes place. We cannot exclude the possibility that this complex also forms or that a fraction is persistent beyond biogenesis, as will be discussed in a later section (III. 10). The lack of phosphatase activity and occupation of the RVxF binding site by I3 renders it unlikely that the SPI complex serves substrate-targeting functions. In the case of SDS22-PP1, cytoskeleton-associated proteins were recently proposed as substrates and artificial targeting of SDS22 to the cortical cytoskeleton induced blebbing due to local PP1 activity (Rodrigues et al., 2015). However, we could not confirm the effect of SDS22 depletion on the phosphorylation level of moesin reported earlier by the same group in Kc cells from *Drosophila* (Kunda et al., 2012)(data not shown). We cannot exclude the possibility that SDS22-PP1 has substrate-specific activity in this or other pathways (Loubery et al., 2017) but reduced PP1 activity in any context could also be caused by compromised biogenesis. To approach this in more detail, we investigated the impact of interfering with SPI complex disassembly on downstream processes as discussed in a later section (III. 8 and III. 9).

III. 3 The AAA-ATPase p97 and Shp1-homologous adapters are required for PP1 function by disassembling the SPI complex

Strong indications for an involvement of p97 in the regulation of several aspects of PP1 function were found in studies on the yeast homolog Cdc48. The Cdc48/p97 adapter Shp1 has originally been identified as a general activator of Glc7 (Zhang et al., 1995). With subsequent reports also demonstrating a role of Shp1 and its association with Cdc48 in the mitotic function of Glc7 (Bohm and Buchberger, 2013; Cheng and Chen, 2010), a similar picture emerged as in the case of Sds22 and Ypi1/I3. However, the regulatory role of Shp1 towards Glc7 cannot be attributed to a substrate-specifying function since this protein contains domains typical of Cdc48 adapters but does not contain any of the interaction motifs typically present in PP1 interactors (Heroes et al., 2013)(see also I.1.3 and I.3.4).

During the course of this study, Cheng and Chen published their investigation of the role of Cdc48 and Shp1 towards Glc7 in budding yeast (Cheng and Chen, 2015). Following depletion of Shp1, they observed reduced nuclear localization of a GFP-Glc7 fusion protein and accumulation of the fluorescence signal into foci, whose numbers increased upon inhibition of the proteasome. Importantly, they showed this effect to be limited to newly synthesized GFP-Glc7, since a temperature-sensitive *shp1*^{ts} mutation only led to accumulation of foci at the restrictive temperature with ongoing translation but not when translation was inhibited by addition of cycloheximide (Cheng and Chen, 2015). Loss of nuclear localization and aggregation of GFP-Glc7 was also detected with the temperature-sensitive s*ds22-6* allele and upon depletion of Ypi1 but the authors did not report whether this required ongoing translation. They concluded that the Sds22-Glc7-Ypi1 complex stabilizes the catalytic subunit and allows its accumulation in the nucleus. Although depletion or mutation of Shp1 had very similar effects, they interpreted the limitation to newly synthesized Glc7 as an indication that Cdc48 and Shp1 are required to allow formation of the Sds22-Glc7-Ypi1 complex.

Mass spectrometry (MS) experiments (Hülsmann et al., 2018) detected physical interactions between p97 and the trimeric SPI complex, prompting us to investigate a potential role of p97 in the regulation of PP1 in mammalian cells. Since p97 was mechanistically described as a “segregase”, which extracts proteins from cellular structures by transforming the energy of ATP into mechanical force (I.3.1), we expected its function in the regulation of PP1 to involve a similar mechanism.

We found compelling evidence that p97 directly acts on PP1 by disassembling the SPI complex. This was first observed in pulse-chase experiments, since specific pharmacological inhibition of p97 blocked dissociation of PP1 from SDS22 and I3 (II.2.2). We further observed the same effect in cells depleted of p97 by two different siRNAs (II.2.2). Notably, this depletion had no detectable effect on the binding of newly synthesized PP1 to SDS22, indicating that assembly of the trimeric complex is independent of p97 activity in mammalian cells, whereas disassembly strictly depends on it. That p97 disassembles the SPI complex was also evident from reconstitution of the process in inducible, PP1γ-strep expressing cells (II.2.5), which differs from the pulse-chase approach since no prior starvation of the cells was applied. We also observed disassembly of an SPI complex containing *in vitro*-translated PP1 in both *Xenopus* egg extracts as well as reticulocyte lysates and found strict dependency on p97 activity in both systems (II.4.2 and II.4.3).

The activity of p97 towards the SPI complex depended on the presence of a family of adapters, which share a SEP domain with Shp1, as will be further discussed below (III. 4). The effect of adapter depletion on the disassembly process in cells (II.3.2) strongly suggested that the SPI complex is a direct target of p97. Finally, experiments with purified

components (J. Seiler)(Weith et al., 2018) provided unambiguous evidence that p97 together with its adapter p37 functions as a segregase towards the trimeric complex.

The conclusion that p97 disassembles the SPI complex but is not required for its assembly differs from the interpretation proposed by Cheng and Chen of their data on the role of yeast Cdc48-Shp1 towards Glc7/PP1 (see above)(Cheng and Chen, 2015). A simple explanation for the accumulation of GFP-Glc7 into “spots” upon depletion of the Cdc48 adapter Shp1 could be that the trimeric complex is prone to aggregation. However, the observation that Sds22 and Ypi1 did not co-aggregate with Glc7 upon depletion of Shp1 speaks against this (Cheng and Chen, 2015).

A different explanation can be derived from our findings from gel filtration experiments of HeLa whole cell lysates (J. Seiler, unpublished results). Here we observed that SDS22 is quantitatively shifted from a free, monomeric form into a complex-bound form upon depletion of the human homologs of Shp1 (III. 4) for 48 hours. Analogously, Sds22 might also become saturated in Shp1-depleted yeast, resulting in expression of an aggregation-prone, free catalytic subunit. Although p97 depletion was observed to have the same effect on the behaviour of SDS22 in gel filtration (J. Seiler, unpublished results) assembly of the SPI complex was unaffected as noted above. On the other hand, acute pharmacological inhibition of p97 activity during induction of recombinant PP1γ-fusion proteins in inducible HeLa cell lines prevented interaction of both PP1γ-strep as well as GFP-PP1γ with SDS22 and I3 (data not shown). Therefore, a free pool of SDS22 might be required to stabilize overexpressed PP1 in human cells, whereas unknown adaptation processes could be in place to assure assembly of the SPI complex with endogenous PP1.

Although Cheng and Chen ectopically expressed GFP-Glc7 under control of its native promoter, both the presence of the tag as well as the fact that the ectopic protein is expressed in addition to endogenous Glc7 might have affected the outcome of inhibiting SPI complex disassembly. It is possible that the function of Cdc48 in yeast differs from that of p97 but we think that the observations made by Cheng and Chen can also be reconciled with our new data.

III. 4 The Shp1-orthologs p47, p37 and UBXN2A recruit p97 to the SPI complex

Following hints from the literature (Raman et al., 2015) and MS data obtained in our lab (J. Hülsmann, unpublished data), we confirmed by pull-down experiments after transient transfection that three adapters, p47, p37 and UBXN2A can physically interact with SDS22, PP1 and I3 (J. Seiler)(Weith et al., 2018). All three adapters share sequence homology as well as the SEP domain with yeast Shp1 (Figure 52), whereas another SEP domain-containing adapter, Socius, is more distantly related (I.3.5) and did not interact with the SPI complex.

We first tested the effect of single depletions on the interaction of p97 with the SPI complex and on disassembly in pulse-chase experiments but found only mild effects. However, a triple depletion of all three adapters had a more pronounced effect on SPI complex disassembly (data not shown). Since p47 is the most abundant of the SEP domain containing adapters (Beck et al., 2011), we applied a combined strategy using CRISPR/Cas9-mediated knock-out (KO) of p47 (cell lines generated by J. Seiler) and RNAi-mediated knockdown (KD) of p37 and UBXN2A to deplete HeLa cells of all three adapters. By this approach, we could demonstrate that loss of these adapters abolishes the interaction between p97 and SDS22, which we studied as a surrogate for binding of the SPI complex (II.3.1). More importantly, this treatment strongly inhibited the disassembly process in pulse-chase experiments, comparable to depletion of p97 itself (II.3.2 and II.2.2). And finally, loss of all three adapters also resulted in a significant delay of PP1 holoenzyme formation with NIPP1 (II.3.3).

We wondered whether these adapters, in analogy to Shp1, are required for correct localization of PP1 but we were unable to test this since p37 RNAi interfered with exogenous expression of a GFP-PP1γ fusion in our inducible cell line (data not shown). However, we observed relocalization of SDS22, stained with a polyclonal antibody, from the nucleus to the cytoplasm in cells depleted of I3 (data not shown). This is consistent with reports in yeast that Ypi1/I3 is required for Sds22 nuclear localization (Bharucha et al., 2008). Interestingly, we found the same effect following depletion of the SEP domain adapters for 48 h (data not shown), also in line with data on yeast Shp1 (Robinson et al., 2012). The same was true for short (1-4 hours) but not longer treatments with NMS-873 (data not shown). Although this pointed to conservation of the observed roles of Ypi1/I3 and Shp1 in promoting nuclear localization of SDS22 and potentially also PP1, it remains unclear whether this effect is related to the role of p97 in PP1 biogenesis.

More detailed analysis of the results of our pulse-chase experiments for SPI complex disassembly indicated that knockout of the most abundant p97 adapter related to this process, p47 (Beck et al., 2011), did not have a strong impact, whereas p37 and UBXN2A seemed to be more strictly required. This was consistent with MS data (Raman et al., 2015) and our own experiments, which detected only a weak interaction of p47 with the SPI complex (J. Seiler)(Weith et al., 2018). The strongest effect on the interaction of p97 with the SPI complex was observed following depletion of p37 (II.3.1). Furthermore, supplementation of reticulocyte lysates with p37 but not with p47 enabled efficient disassembly of the SPI complex by recruitment of p97 (II.4.3 and II.4.4). Thus, p37 alone seems to be sufficient to recruit p97 to the SPI complex and to allow disassembly to proceed, while the role of p47 awaits further clarification.

Our study demonstrates conservation of the PP1-regulatory role of Shp1 in the function of three SEP domain-containing orthologs, p47, p37 and UBXN2A, which serve in a partially redundant manner to target p97 to the SPI complex. We show that these adapters are required for disassembly of the complex and for normal progression of de novo PP1 holoenzyme formation. Thus, it seems likely that the requirement of Shp1 for Glc7 function in yeast could be explained by compromised biogenesis. We also investigated the downstream effects of p97 adapter depletion on PP1 function and holoenzyme composition and found perturbations of the PP1 interactome and reduced PP1 activity in mitosis (II.5.2 and II.5.5)(Weith et al., 2018). These effects are reminiscent of the reported phenotypes of Shp1 depletion in yeast and will be further discussed below (III. 8 and III. 9).

More divergent functions of the individual adapters could still be envisaged. For example, their different subcellular localizations (I.3.5) could point to a role in regulation of SPI complex disassembly in different contexts (see also III. 10). It is tempting to speculate that this would constitute another layer of regulation to allow more controlled hand-over of the catalytic subunit of PP1 to its interactors (Figure 54). In this regard, it could be informative to determine in which sub-cellular compartment(s) disassembly of the SPI complex takes place during biogenesis.

III. 5 p97-mediated SPI complex disassembly by a ubiquitin-independent mechanism

As described in the introduction (I.3.6), until very recently no assay was available to study p97 activity with a defined substrate *in vitro*. With the development of model substrate-based assays by the groups of Raymond Deshaies and Tom Rapoport (Blythe et al., 2017; Bodnar and Rapoport, 2017b), it became clear that poly-ubiquitination of the substrate promotes recruitment of p97 by Ufd1-Npl4 (I.3.6). Subsequently, p97-mediated substrate unfolding was demonstrated to proceed via channeling the substrate through the central pore (Blythe et al., 2017; Bodnar and Rapoport, 2017b). While both previously reported assays were established to study the p97-Ufd1-Npl4 complex, disassembly of the SPI complex requires p97 in conjunction with p47-like adapters, which form alternative p97 complexes (Meyer et al., 2000).

Strikingly, the ubiquitin-binding domain (UBA) of Shp1 and p47 is not conserved in p37 and UBXN2A (I.3.5)(Figure 52) although the results described in the last section (III. 4) indicated that p37 is sufficient to recruit p97 to the SPI complex. Indeed, we found no evidence in pulse-chase experiments that ubiquitination is required as a recruitment signal for p97 to the SPI complex, since the disassembly process was not affected by blocking ubiquitination with a chemical inhibitor of E1 ubiquitin-activating enzyme function (II.3.4).

We further found that both the SHP box motif, which mediates binding of p37 to p97, as well as the presence of the SEP domain were essential for disassembly of the SPI complex. This

was determined by testing recombinantly expressed and purified wild-type p37 or truncated and mutated variants (provided by J. Seiler) for their ability to support disassembly of the SPI complex in experiments with reticulocyte lysates (II.4.5). On the other hand, an N-terminal sequence of 81 residues, which displays residual homology to p47 and the UBA domain, was not required. The choice of this truncation was based on the sequence conservation between Shp1 and the three SEP domain-containing adapters (Figure 52). The remaining sequence of p37 (aa 82-331) shows higher similarity to p47 and UBXN2A than the N-terminal region, indicating that it contains the structural elements required for the role of these adapters to recruit p97 to the SPI complex.

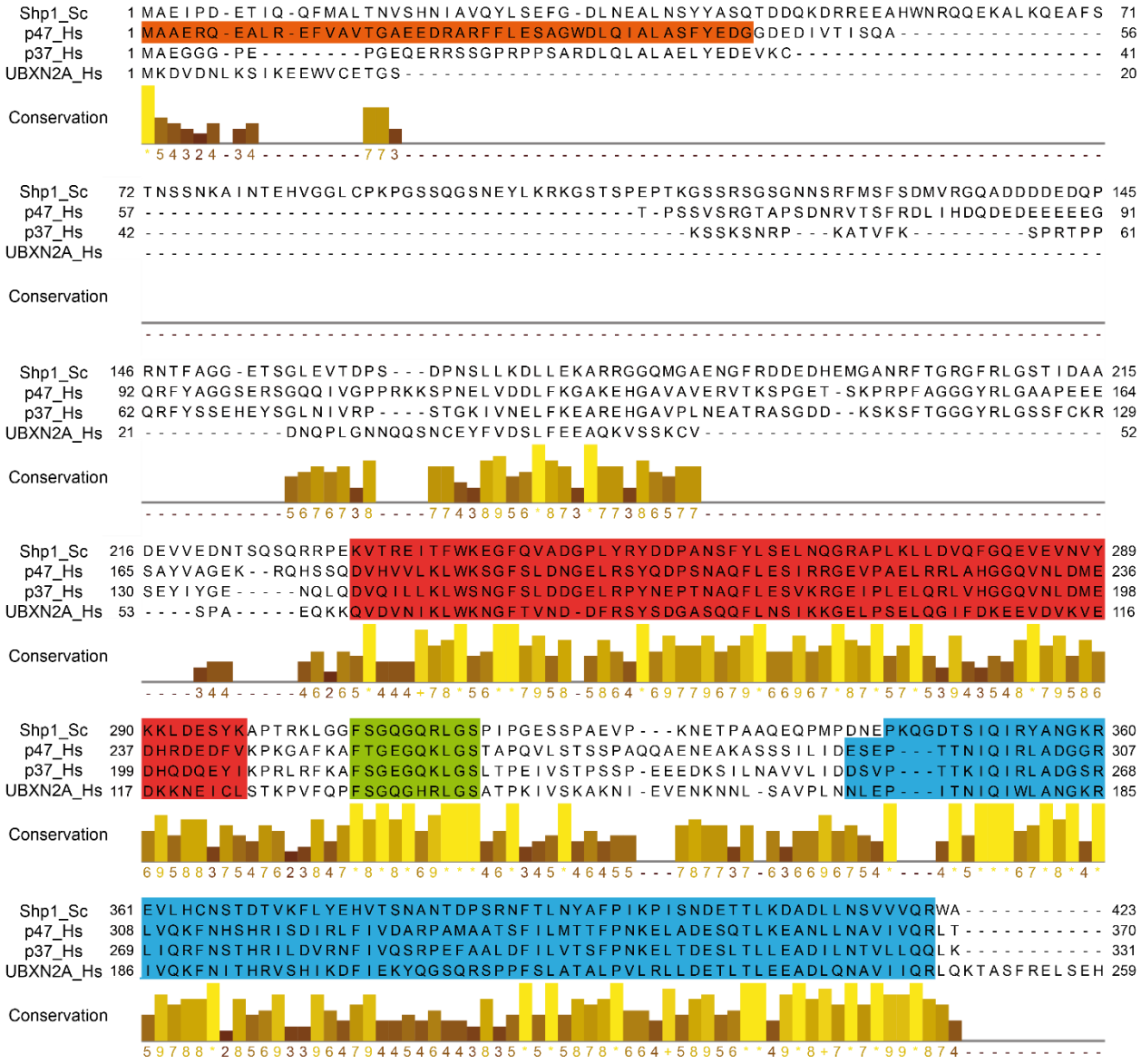

Figure 52: Multiple sequence alignment for *S. cerevisiae* Shp1 (Shp1_Sc) and human p47, p37 and UBXN2A (_Hs).
The alignment was generated using the T-Coffee algorithm with standard settings from the Jalview application. The SEP (red) and UBX (blue) domains are shown as annotated in Uniprot (https://www.uniprot.org/). The SHP box motif (Bruderer et al., 2004) is shown in green. The UBA domain of p47 (Yuan et al., 2004) is shown in orange.

Based on the observation that the SEP domain of p37 was required for SPI complex disassembly in reticulocyte lysate assays, as noted before, cross-linking experiments were set up by introduction of the modified amino acid p-benzoylphenylalanine (pBPA) in a surface-exposed position of the SEP domain (J. v. d. Boom). UV irradiation of reactions consisting of the SPI complex and p97 together with the p37 L187pBPA variant led to detectable cross-links with I3 but not SDS22 or PP1 (J. v. d. Boom)(Weith et al., 2018). No cross-links were detected in equivalent reactions with p37 F89pBPA, in which the cross-linker amino acid was introduced in the N-terminal region. *In vitro* binding experiments with p97-p37 and the SPI complex confirmed that the SEP domain was required for the interaction.

Thus, the SEP domain contributes directly to an interaction between p37 and I3, which we found to be the target of p97 activity in the SPI complex as will be further discussed below (III. 6). On the other hand, p37 alone was not able to interact with the SPI complex but required p97 (J. Seiler). This was further corroborated by investigation of p37 variants with mutations in the SHP box motif. These variants, which do not bind p97 *in vitro* (J. Seiler), were unable to mediate SPI complex disassembly in reticulocyte lysate, as noted before (II.4.5). They were also unable to bind the SPI complex in the presence of p97 *in vitro* or in cells and did not mediate SPI complex disassembly with purified components (J. Seiler)(Weith et al., 2018).

Our study of the mechanism of SPI complex disassembly by inhibition of E1-ubiquitin activating enzymes in cells and the investigation of the required elements in p37 indicated that ubiquitination was dispensable for SPI complex disassembly by p97. Thus, this could represent the first p97-mediated process with a defined, non-ubiquitinated substrate. Although a ubiquitin-independent function of p97 had been suggested previously for p37-mediated membrane fusion activity (Uchiyama et al., 2006), this could not be tested with a defined substrate. Of note, *in vitro* reconstitution of SPI complex disassembly with purified components did not require ubiquitination (J. Seiler)(Weith et al., 2018). Thus, in this work and the accompanying publication, we report for the first time unequivocal evidence for a ubiquitin-independent function of p97 (Weith et al., 2018).

On the other hand, the presence of a ubiquitin-binding domain in p47 is likely more than a remnant of evolution, as evidenced by its facilitating role for membrane fusion (Meyer et al., 2002). Possibly, ubiquitin-dependent functions of Shp1 have only been conserved in p47, but not p37 or UBXN2A, although little overlap exists between the reported roles of Shp1 and p47 (I.3.4 and I.3.5). Therefore, it remains to be shown whether specific functions of Shp1 that require the UBA domain are conserved in p47. A different path of exploration could start once more from Shp1's regulatory role towards PP1. Potentially, ubiquitination plays a role in yet undefined processes during the PP1 life cycle, such as recycling or turnover of

holoenzymes or the catalytic subunit, which might require p97. In this context, it is worth noting that ubiquitinated species of Glc7/PP1 were found in MS studies in yeast (Peng et al., 2003; Starita et al., 2012). Furthermore, the group of Kelly Tatchell recently reported accumulation of Glc7 into foci and shift of the Ipl1-Glc7 balance towards excessive kinase activity caused by mutation in the yeast ubiquitin-activating E1 enzyme Uba1 (Ravindran et al., 2018).

III. 6 SPI complex disassembly proceeds via unfolding of I3

Studies in yeast indicated that the physical interaction between Cdc48 and the Sds22-Glc7-Ypi1 complex depended on the one hand on the adapter Shp1 (Bohm and Buchberger, 2013). This was supported by our data and complemented by the observation that p37 alone does not bind the SPI complex (III. 5). On the side of the Glc7 complex in yeast, Sds22 seemed to be the essential component for the interaction with Cdc48-Shp1. It was found that the gene product of *sds22-6* did not interact with Glc7 at the non-permissive temperature (Bohm and Buchberger, 2013). In addition, in yeast expressing this mutant, the interaction between the substrate-trapping mutant $Cdc48^{QQ}$ and Shp1 with Glc7 was also suppressed (Cheng and Chen, 2015).

The cross-link experiments with p37 and the SPI complex described in the last section indicated that I3 was the direct target of p97 in mammalian cells. This was further corroborated in a set of *in vitro*-binding experiments, which indicated that the interaction of PP1 with p97 depended on the presence of I3, since a dimer of SDS22 and PP1 was not bound by p97 and its adapter p37 in the absence of I3 (J. Seiler)(Weith et al., 2018). However, I3 alone also did not bind to p97-p37 efficiently in the absence of SDS22 and PP1. This might indicate that the interaction requires contribution by contacts to PP1 and/or SDS22 in addition to those formed with I3. On the other hand, we found no direct evidence that SDS22 is required for the interaction.

An interesting possibility to explain why I3 is only targeted in the complex with PP1 emerges from the intrinsically disordered nature of I3 (Bollen et al., 2010)(I.2.5). As observed for spinophilin, I2 and MYPT1 (Choy et al., 2012), latent secondary structure elements in I3 might only be formed by binding to PP1, which could explain why those are only available for interactions with p97-p37 in an I3-PP1 complex.

While I3 was thus determined to be the essential factor for the recruitment of p97-p37, understanding how p97 actually allows PP1 to be released from the trimeric complex required more detailed investigation.

We applied previously established approaches with model substrates of p97-Ufd1-Npl4 (Bodnar and Rapoport, 2017b) to our reconstituted *in vitro* SPI disassembly assy. p97 variants with pBPA amino acids (see last section) located in the pore formed by the D1 and

D2 domains (J. v. d. Boom) were cross-linked in reactions set up for disassembly of the SPI complex. This allowed us to detect cross-links with I3, but not SDS22 or PP1, inside the central pore by Western Blot staining (J. Seiler)(Weith et al., 2018). Cross-links in the D2 domain required the presence of ATP, whereas those in the D1 pore where also formed when ATP was replaced with ATPγS, suggesting energy-dependent translocation of I3 from the D1 to the D2 pore.

In their *in vitro* assay for the p97-Ufd1-Npl4 complex, Bodnar and Rapoport were able to show that a ubiquitinated model substrate is channeled through the central pore of p97, by fusing the bacterial hexameric protease FtsH to the C-terminus of p97 (Bodnar and Rapoport, 2017b). They observed that p97 ATPase activity was required for degradation of the substrate by FtsH, demonstrating that p97 is able to channel the substrate through its central pore. Our observation that I3 moves from the D1 to the D2 domain is consistent with this mechanism but does not exclude an alternative model, which holds that the substrate is moved into the central channel from the D1 domain to the D2 domain but then exits backwards through the D1 opening (van den Boom and Meyer, 2018)(I.3.6). However, we also observed ATP-dependent cross-links between I3 and a residue positioned in a p97 sequence that is outside the pore in the C-terminal region (J. v. d. Boom, unpublished data). This supports the conclusion that a channeling mechanism also applies to the processing of I3 by p97.

The assay developed by Nicholas Bodnar and Tom Rapoport to follow p97-mediated unfolding of a model substrate by fusion to the fluorescent GFP-derivative Eos (Zhang et al., 2012) was applied to Eos-I3 by Matthias Kracht in our laboratory (Weith et al., 2018). Indeed, upon incubation of a trimeric complex of SDS22, PP1 and Eos-I3 with p97-p37, loss of the fluorescent signal over time could be observed, indicating that substrate unfolding also applies to the processing of I3 by this alternative p97 complex.

Taken together, our model of p97 activity towards the SPI complex (Figure 53, generated by J. v. d. Boom) includes ubiquitin-independent recruitment mediated by the SEP domain-containing adapters, although the equivalence of p47 and UBXN2A to p37 in this assay remains to be tested. Furthermore, the disassembly involves channeling of I3 through the central pore of the p97 hexamer and concomitant unfolding. In this aspect, the mechanism of processing by the p97-p37 complex is similar to the p97-Ufd1-Npl4 complex (Bodnar and Rapoport, 2017b).

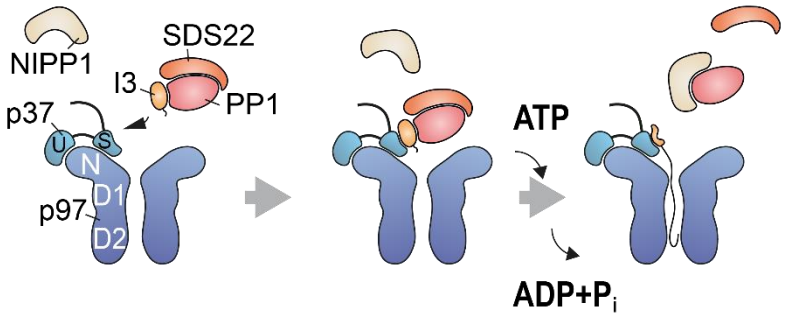

Figure 53: Model for p97-p37-mediated disassembly of the SPI complex and exchange to NIPP1.
p97 is recruited to the SDS22-PP1-I3 complex by the adapter p37. This interaction involves direct contacts between the SEP domain of p37 with I3. I3 is pulled into the central channel of the p97 hexamer and unfolded at the expense of ATP. This strips I3 from PP1 allowing substrate specifiers such as NIPP1 to bind via an RVxF motif to the RVxF binding site in PP1, which is remote from the SDS22 binding site (see I.2.5). SDS22 is displaced from PP1 by an unknown mechanism. U, UBX domain; S, SEP domain; p97 domains N, D1 and D2. (Figure created by J. v. d. Boom).

III. 7 A hand-over mechanism allows association of PP1 with NIPP1

As noted before, we observed that addition of NIPP1 to both reticulocyte lysate as well as *in vitro* disassembly reactions enhanced the release of I3 and SDS22 from PP1 (II.4.3)(Weith et al., 2018). This suggested an exchange of interactors that bind to the RVxF binding groove and is consistent with the finding that the RVxF-interactor I3 in the SPI complex is unfolded and released by p97.

Release of I3 clears the RVxF binding site in PP1 for interaction with NIPP1. The addition of NIPP1 in reticulocyte lysate reactions could thus have led to formation of the NIPP1-PP1 holoenzyme and prevent re-binding of I3. Supporting this explanation, the increase in binding of NIPP1 mirrored reduction of I3 in our *in vitro* disassembly experiments (J. Seiler)(Weith et al., 2018). Together with our pulse-chase experiments (IV.1), this supports the notion of a hand-over of the catalytic subunit from the SPI complex to other interactors. How the subsequent release of SDS22 is brought about remains elusive. We can only speculate that loss of I3 from the complex weakens the interaction with SDS22, consistent with a cooperative binding mode in the trimeric SPI complex (I.2.7). Alternatively, NIPP1 might compete sterically with SDS22 for PP1 binding (M. Bollen, personal communication). However, other PP1 interactors like KNL1 can form trimeric complexes with SDS22 (Eiteneuer et al., 2014; Verbinnen et al., 2017), which argues against steric competition as a general mechanism. Potentially, a conformational change of PP1 is caused by SDS22 in the trimeric complex Lesage (Lesage et al., 2007), and is reverted during disassembly, which could then weaken SDS22 binding. A more detailed investigation of the mechanism of SDS22 dissociation from PP1 would benefit from structural elucidation of the SPI complex. Moreover, determination of the structure of this complex together with p97 and p37 might reveal details of substrate recognition and engagement, which would greatly enhance our

understanding of p97-mediated processes in general and ubiquitin-independent recruitment in particular.

An interesting aspect of the disassembly of the SPI complex regards the fate of the processed complex. As described earlier (I.3.2), p97 acts as a facilitator for proteasomal degradation of its substrates in many ubiquitin-dependent processes, including the paramount role of p97 in ER-associated degradation. However, the apparent outcome of SPI complex disassembly on the one hand is the formation of active PP1 holoenzymes, indicating that PP1 itself is rather activated than prepared for degradation. On the other hand, the fate of its interactors in the biogenesis complex, SDS22 and I3, is less clear. We cannot formally exclude that SDS22 is also processed by p97, perhaps at a later stage than the unfolding of I3. This might have reduced the efficiency of cross-link formation to undetectable levels. However, it seems more likely that it is released without being unfolded. In the case of I3, the unfolding process would probably only revert the state of this intrinsically disordered protein (I.2.5) to the PP1-unbound form. However, we cannot exclude degradation of I3 downstream of its processing by p97 in cells.

III. 8 Potential for PP1 pathway-specific effects of perturbed SPI complex disassembly

The model for PP1 biogenesis proposed here holds that the SPI complex is an intermediate stage, which requires p97 for release of the catalytic subunit and subsequent PP1 holoenzyme formation. This raises the question how perturbation of the disassembly process would affect the function of PP1. The results discussed so far, concerning the activity of the catalytic subunit as well as formation of NIPP1- and MYPT1-PP1 holoenzymes were limited to investigation of newly synthesized PP1. On the other hand, determining whether SPI complex disassembly affects PP1 in a general manner required an approach to test the effect of perturbations of this process on the whole cellular pool of PP1. As described in earlier sections, the subcellular localization and total activity of PP1 could not be determined due to technical problems (III. 1 III. 2). However, apart from effects on the activity or localization of Glc7, Shp1 was also reported to affect the interactions of Glc7 (Bohm and Buchberger, 2013). Following our observation that holoenzyme formation by newly synthesized PP1 is inhibited by interfering with SPI complex disassembly, we wondered whether the general composition or abundance of PP1 holoenzymes, summarized as the PP1 interactome, is affected in these conditions.

Therefore, we applied two different treatments to suppress SPI complex disassembly, hereafter referred to as “disassembly-deficient conditions”, for an extended duration. First, we tested inhibition of p97 activity for 16 h by NMS-873 and second, we applied our combined strategy for depletion of the SEP domain-containing p97 adapters, which is based on a 48h-RNAi treatment to deplete p37 and UBXN2A in a p47 KO cell line. After both

treatments, we isolated PP1γ by immunoprecipitation and performed MS-based identification and label-free quantification (LFQ) for comparison of co-eluted proteins.

Comparison between the two treatments applied to inhibit SPI complex disassembly in general showed similar intensity changes for most of the established interactors of PP1 (II.5.2). As expected, the interactions with SDS22 and I3 were increased in both conditions. Quantification of I3 by the LFQ method applied here might have underestimated the increase following NMS-873-treatment, which was more clearly observable by Western Blot staining (Figure 23).

Among the interactors that were not reduced by either treatment was NIPP1. This was unexpected, since we had earlier established defects in formation of this holoenzyme with newly synthesized PP1 by both treatments (II.2.3 and II.3.3). Also in the case of MYPT1-PP1, LFQ-based analysis displayed a reduction below the significance threshold. However, Western Blot analysis reproducibly showed less MYPT1 bound to PP1 after depletion of p97 adapters (II.5.2 and data not shown). This could indicate that some shifts are underestimated by this method or our processing of the data.

A general limitation of our approach is that significant changes depend on turnover of PP1 holoenzymes, which might be a slow process considering the long half-life of the catalytic subunit (II.5.1). Furthermore, turnover would only lead to a significant reduction in our approach if the holoenzyme is predominantly replenished by newly synthesized PP1. However, exchange of the catalytic subunit between interactors might occur constantly (Verbinnen et al., 2017), with the potential to keep the overall interactome in balance and to compensate reduced de novo formation of individual holoenzymes by recruitment of the catalytic subunit from other complexes. Another possibility is that the turnover of holoenzymes is also affected in disassembly-deficient conditions, likely as a consequence of decreased cellular metabolic activity, which we detected using a colorimetric assay (MTS assay, Promega, J. Seiler)(Weith et al., 2018). Nevertheless, the data provide valuable hints to investigate further, which pathways might be affected in SPI complex disassembly-deficient conditions and some examples will be discussed in the following.

Among the most strongly reduced interactors of PP1 were SIPP1 (also known as WBP11) and URI1 (or RMP). URI1 has been implicated in nutrient-sensing and TOR kinase signaling (Gstaiger et al., 2003). Together with PP1, it was shown to be involved in setting the threshold for apoptosis as a feedback to growth factor signaling via mTOR (Djouder et al., 2007). On the other hand, URI1 is also a component of the prefoldin-like complex, which cooperates with the Hsp90 co-chaperone R2TP in the assembly of multiprotein complexes such as RNA polymerase II (Boulon et al., 2010), small nucleolar (sno)RNPs, which have RNA-processing functions, as well as small nuclear (sn)RNPs, which form the pre-mRNA splicing machinery (Cloutier et al., 2017). Almost all prefoldin-like complex and R2TP

complex members were identified in our MS experiments and have been reported before as interactors of PP1 in MS-based investigations (Yadav et al., 2017). Roles in response to nutrient starvation or DNA damage have been assigned to the R2TP complex (von Morgen et al., 2015), raising the possibility that the observed changes in its interaction with PP1 are stress-induced. On the other hand, interactions between the R2TP and prefoldin-like complex components and SDS22 were detected in MS experiments (Boldt et al., 2016). Moreover, interactions between Sds22 and Rvb1 and -2, the ATPase subunits of the R2TP complex, were found in a large-scale study and confirmed by pulldown experiments using the N terminus of Sds22 in yeast (Ghosh and Cannon, 2013). Our preliminary results (II.5.4) indicate that a 5 hour treatment with NMS-873 is sufficient to cause reduced interaction of PP1γ with URI1. In sum, a direct connection between SPI complex disassembly and the interaction of PP1 with URI1 might exist but will require further evaluation.

The precise function of SIPP1 is still unknown although it has been linked to PQBP1, a splicing factor with reported roles in neurodegenerative disease (Nicolaescu et al., 2008; Wang et al., 2013). Strikingly, also SIPP1 and PQBP1 were identified as interactors of SDS22 by MS experiments (Boldt et al., 2016). A potential link between SIPP1 and the R2TP/prefoldin-like co-chaperone complex involves the U5 snRNP component of the precatalytic B subcomplex of the spliceosome. While the R2TP members RUVBL1 and -2 interact with the U5 snRNP via ZNHIT2 and may be involved in its recycling between rounds of mRNA splicing (Cloutier et al., 2017), PQBP1 interacts directly with the U5-15 kDa protein subunit of the U5 snRNP (Mizuguchi et al., 2014). Loss of this interaction might be involved in X-linked mental retardation disorders caused by mutants of PQBP1 (Mizuguchi et al., 2014).

We also found increased interactors apart from SDS22 and I3. The most notable among them is I2 (II.5.2), which was implicated as a potential factor during PP1 biogenesis (Verbinnen et al., 2017)(I.3.4). The yeast homolog of I2, Glc8 was shown to be generally required for Glc7 activity or stability (Bharucha et al., 2008; Nigavekar et al., 2002) similar to Sds22 and Ypi1 (I.2.3). Another indication that points to a role of I2 in PP1 biogenesis was found in our pulse-chase experiments. As observed for SDS22 and I3, I2 also seems to bind higher amounts of PP1c* directly after the pulse as compared to the end of a 2 hour chase (II.2.3). It is tempting to speculate that blocking SPI disassembly would stall other processes during PP1 biogenesis, possibly including a step regulated by I2. A different explanation might be that saturation of SDS22 in disassembly-deficient conditions, which has been referred to earlier (III. 3), could lead to channeling of newly synthesized PP1 into other pathways that can stabilize the catalytic subunit. Reports that PP1 can be expressed in *E. coli* by co-expression with I2 are consistent with a stabilizing function of I2 towards PP1 (Hurley et al., 2007). Somewhat contradictory, Böhm and co-workers observed reduced

interaction of Glc7 with Glc8/I2 in Shp1-depleted yeast (Bohm and Buchberger, 2013). However, this inconsistency might be attributable to species-specific differences.
A few other known interactors of PP1 were upregulated as well. They include Aurora A and KPI-2, which interact directly with I2 (Satinover et al., 2004), and a complex containing BRCA1 (II.5.2). However, the processes potentially affected by these changes in the PP1-interactome, such as regulation of centrosomal maturation by Aurora A (Barr and Gergely, 2007), and the DNA damage response by BRCA1, warrant further investigation. Increased interaction with Repo-Man in the SEP domain adapter-depleted condition was consistent with a recent report assigning a role to p37 in limiting the activity of the Repo-Man-PP1 holoenzyme (Lee et al., 2018). In addition, the increased interaction with CReP after NMS-873 treatment might be explained by the recently described role of p97 in facilitating CReP degradation (Hülsmann et al., 2018). These examples illustrate that the results from our mass spectrometry experiments might in part reflect effects that occur independently of SPI complex disassembly.

In sum, the MS-based investigation of the PP1γ interactome provided valuable hints to processes, which might be affected downstream of the biogenesis of PP1. Our MS data do not demonstrate a role in the formation of all holoenzymes. Although we found that two interactors with rather dissimilar cellular localization and function, NIPP1 and MYPT1, both strictly depended on SPI complex disassembly for holoenzyme formation (IV.1), it is possible that they are exceptional cases. Potentially, the catalytic subunit is handed over from the SPI complex only to a specific subset of PP1 interactors, whereas de novo formation of other holoenzymes uses alternative routes of PP1 biogenesis. It is also possible that some PP1 holoenzymes are not formed with the newly synthesized catalytic subunit at all but depend on exchange between holoenzymes as noted before. An interesting possibility is that additional PP1 biogenesis routes could compensate for defective disassembly of the SPI complex. This could be hinted at by our observation that the interaction of PP1 with I2 is increased in disassembly-deficient conditions. Figure 54 summarizes these possibilities.

III. 9 Deficient SPI complex disassembly affects the mitotic function of PP1

A recurrent question in studies regarding the function of SDS22, I3 and their counterparts as well as Shp1 in yeast is whether they are required for the general function of PP1 or more specifically for its nuclear or mitotic roles (I.2.3 and I.3.4). Interestingly, we observed reduced abundance of KNL1 in PP1γ-IP from cells in disassembly-deficient conditions in the MS experiments and by Western Blot (II.5.2). A likely explanation for the reduced interaction with KNL1 is the occupation of the RVxF binding site of the catalytic subunit by I3 in the SPI complex. In our previous publication (Eiteneuer et al., 2014), we reported increased binding of SDS22 to PP1 at its kinetochore-anchor KNL1 upon depletion of I3, consistent with a

direct link between the trimeric complex and the pool of PP1 which is recruited to the kinetochore. In addition to KNL1, two components of the MIS12 kinetochore complex, DSN1 and NSL1 also showed reduced interaction with PP1γ in SEP domain adapter depleted cells (II.5.3). DSN1 is a substrate of PP1 activity at the kinetochore (Eiteneuer et al., 2014; Wurzenberger et al., 2012) and its dephosphorylation is required for stable microtubule attachments (Welburn et al., 2010). Together with reduced interactions with the Astrin/Kinastrin proteins and the kinesin motor KIF14 (II.5.3), these observations indicated potential dysregulation of mitotic events and warranted further investigation of mitosis in SEP domain-adapter depleted cells.

The evaluation of p97-inhibition effects on PP1 mitotic functions is complicated by the role of p97 in extraction of Aurora B (Dobrynin et al., 2011). However, since this function of p97 requires the adapter complex Ufd1-Npl4, the alternative approach by depletion of the three SEP domain-containing adapters allowed us to inhibit p97 activity towards the SPI complex without compromising Aurora B extraction. Applying this approach, we detected increased levels of activated Aurora B on metaphase chromatin (J. Seiler)(Weith et al., 2018) and a roughly 2-fold increased mitotic index in adapter-depleted cells (II.5.5). The direct effect of inhibition of SPI complex disassembly on the KNL1-PP1 interaction can at least partially explain these observations, since decreased recruitment by KNL1 would reduce the amounts of PP1 available at kinetochores to counteract Aurora B. The resulting imbalance might lead to activation of the SAC as shown in SDS22 overexpression conditions (II.1.1) and thereby cause a delay in progression through mitosis, consistent with the observed increase of the mitotic index.

The effect on the mitotic function of PP1 is consistent with yeast data on the effect of Shp1 depletion (Bohm and Buchberger, 2013; Cheng and Chen, 2010). It was also observed that general interference with PP1 function leads to observable effects in mitosis (Winkler et al., 2015). In this line of thought, the observed effect of depleting SEP domain-containing adapters on the mitotic function of PP1 could also be explained by reduced general PP1 activity. Since we could not test the activity of the whole cellular pool of PP1, it remains a matter of speculation whether the supply of newly synthesized, active catalytic subunit is required to maintain the overall active state of the phosphatase. We cannot yet answer whether the SPI complex that supplies the catalytic subunit for interaction with KNL1 is identical to the complex involved in biogenesis. Therefore, a different perspective on the gathered data will be discussed in the following section, which takes into account that the SPI complex may persist or even be formed beyond the biogenesis process that we described here.

III. 10 Potential role of the SPI complex beyond PP1 biogenesis and differential regulation of PP1 holoenzymes

Our data unambiguously show that the process of SPI complex formation and disassembly occurs during PP1 biogenesis, but they also provoke more exploratory questions.

As stated before (III.1), we could not clearly determine which fraction of newly synthesized PP1 depends on formation of the SPI complex during biogenesis. Different pathways of PP1 holoenzyme formation, proceeding either via alternative biogenesis complexes or unassisted cannot be ruled out by our data (Figure 54A). The interesting possibility that I2 might form a complex with newly synthesized PP1 was raised by preliminary observations in pulse-chase experiments (II.2.3) and in MS experiments, which indicated that the interaction of I2 with PP1 was increased in disassembly-deficient conditions (II.5.2, see also III.8).

Under these premises, it would be interesting to further assess which PP1 holoenzymes depend on passage of PP1c* through the SPI complex and which are formed independently of this pathway (Figure 54A).

Another aspect of holoenzyme formation via disassembly of the SPI complex, which has not been sufficiently addressed by our investigations until now, is the role of the individual SEP domain-containing adapters. For example, although p47 was not generally required for normal progression of SPI complex disassembly (II.3.2), it could be imagined that some PP1 holoenzymes specifically require p47 due to its nuclear localization, which distinguishes it from p37 and UBXN2A (I.3.5). As discussed earlier (III.4), regulation of the KNL1-PP1 interaction might represent an interesting case to study differential requirements of the SEP domain adapters (Figure 54A).

In the case of KNL1, it seems unlikely that the holoenzyme is predominantly formed with the newly synthesized catalytic subunit, since the KNL1-PP1 interaction is dynamically regulated during mitosis (I.2.2) and recruitment of PP1 by translation would be very slow. An alternative explanation for the dependency of this interaction on SPI complex disassembly, which was evident in our experiments (II.5.2), would be that PP1 is handed over to KNL1 from a pre-formed SPI complex. As stated before (III.1), it is possible that a certain fraction of the complex formed during PP1 biogenesis persists and could then serve as a reservoir for PP1 holoenzyme formation (Figure 54B, (1) and (4)).

As an experimental approach to generally test for occurrence of the SPI complex outside PP1 biogenesis, it would be interesting to test whether and how strongly the overall amount of the SPI complex is reduced in translation-deficient conditions. We addressed this in a preliminary experiment and observed no reduction of PP1γ in SDS22-IP from cells treated with cycloheximide between 1 h and 6 h (data not shown). This suggests that biogenesis does not account for a large fraction of the overall amount of SPI complex in cells. However, a definite conclusion from such experiments would require to establish that disassembly of

the biogenesis complex proceeds normally and is not inhibited during cycloheximide treatment.

It can also be imagined that the complex is newly formed in a biogenesis-independent manner (Figure 54B (3)). This would fulfill a proposed recycling function in the life cycle of PP1 (Verbinnen et al., 2017), which has already been found in the life cycle of PP2A and serves to rescue the catalytic subunit from stress-induced damage to holoenzymes (Sents et al., 2013). On the other hand, it is also possible that only a subset of PP1 holoenzymes requires this kind of recycling mechanism. It is generally assumed that PP1 holoenzymes can exchange the catalytic subunit stochastically (Heroes et al., 2013)(Figure 54B (3)). However, some PP1-PIP interactions might be too strong for spontaneous release or there might be regulatory demands that are better fulfilled by directed holoenzyme "decomposition". SDS22 is a good candidate to mediate such a process since it has already been observed in trimeric complexes with other PP1 interactors such as KNL1 (Eiteneuer et al., 2014). Potentially, SDS22 in such complexes enforces a conformational shift in PP1 (Lesage et al., 2007), which might subsequently support the replacement of the substrate-specifying interactor by I3 in a "reverse hand-over" mechanism (see also III.7).

Experimentally, formation of the SPI complex in a biogenesis-independent manner could be addressed by a time-course of p97 inhibition in the presence or absence of cycloheximide. Assuming that disassembly of a post-biogenesis SPI complex would show the same dependency on p97, the existence of a different mode of SPI complex formation would presumably lead to its accumulation due to p97 inhibition and without ongoing translation of PP1.

It is tempting to speculate that a post-biogenesis SPI complex would allow further regulatory influence. For example, it could be imagined that kinetochore-localized PP1 is released from such a complex as mentioned above. This would provide a compelling explanation for the apparently increased dependency of the mitotic function of PP1 on p97 activity, compared to other PP1-mediated processes. Presuming the existence of this kind of regulatory mechanism, it would be highly interesting to decipher potentially divergent functions of the SEP domain-containing adapters. In this context, it is worth noting that both p47 as well as p37 have been observed to be phosphorylated by Cdk1 at the onset of mitosis, although this has been previously linked to their roles in membrane fusion processes at the Golgi apparatus and the endoplasmic reticulum (Kaneko et al., 2010; Uchiyama et al., 2003).

Summarizing these ideas, it is possible to propose that apart from the "biogenesis SPI complex", which is well described by our data, a "reservoir SPI complex" and a "recycling SPI complex" could exist. These complex entities could be overlapping or dependent on one another, as illustrated by the notion that a persistent biogenesis SPI complex could become a reservoir SPI complex (Figure 54B). Such roles of the SPI complex might be important levers in the PP1 system and for numerous aspects of cellular physiology.

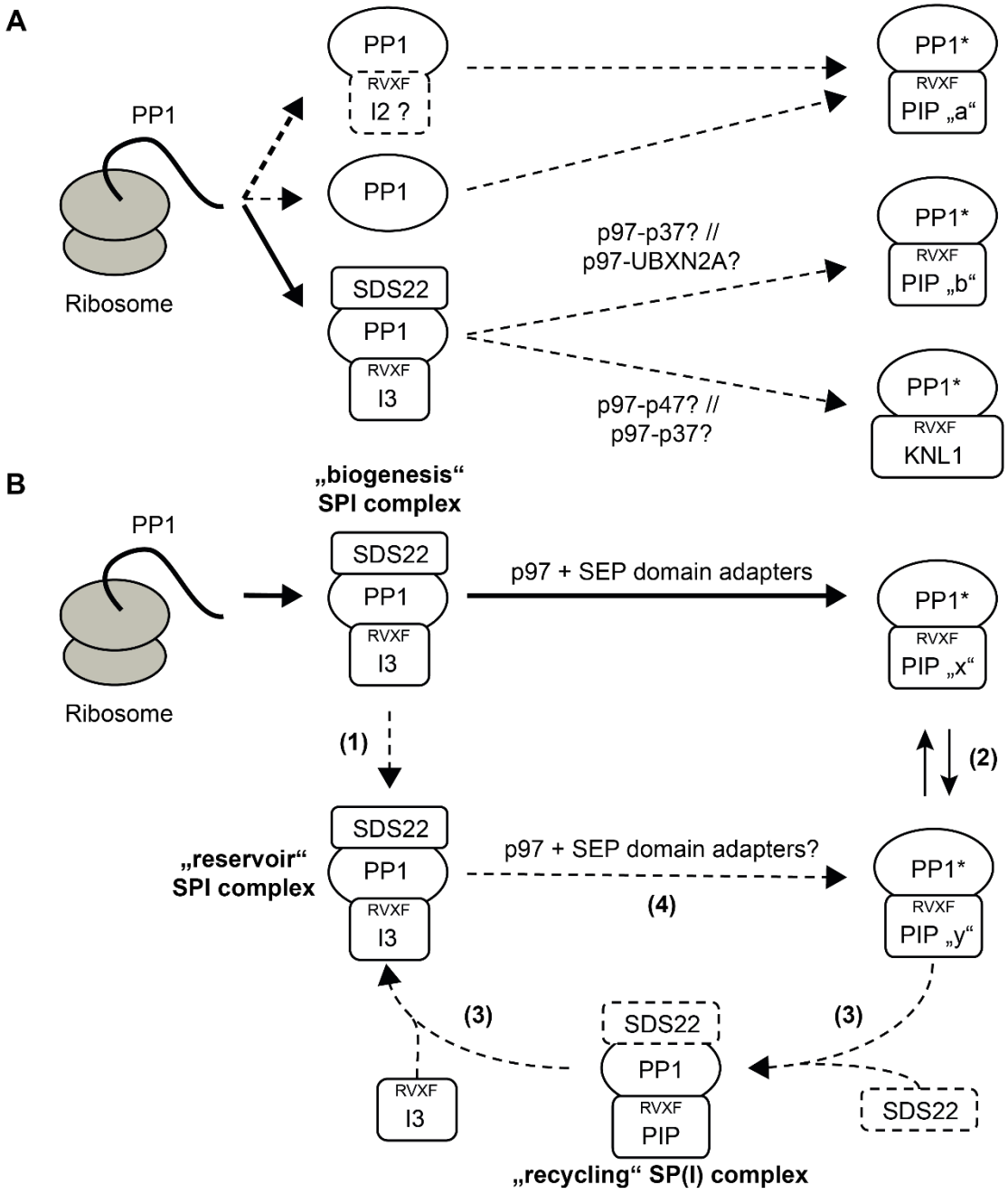

Figure 54: Summary of potential functions of the SPI complex and their regulation by p97.
(**A**) In this thesis, I presented data indicating that the SPI complex forms during PP1 biogenesis (solid arrow). However, which fraction of newly synthesized PP1 passes through this complex is unknown. Direct formation of holoenzymes or alternative biogenesis complexes, as suggested by preliminary data for I2, (III. 8), are possible. The process of holoenzyme formation could differ for individual PIPs (PP1-PIP “a” vs. PP1-PIP “b”). Furthermore, hand-over of PP1, which passes through the SPI complex to individual interactors (PIP “b” vs. KNL1) could depend on p97 together with one specific or a combination of SEP domain adapters, as discussed earlier (III. 9). (**B**) Extended models for potential roles of the SPI complex during and beyond PP1 biogenesis. Strong lines indicate our current understanding of the process of PP1 holoenzyme formation via an intermediate “biogenesis SPI complex”. Other potential instances of occurrence of the SPI complex beyond PP1 biogenesis are indicated in bold. Numbers denote unknown aspects as follows: (**1**) The SPI complex might persist beyond biogenesis. (**2**): Some or all PP1 holoenzymes could exchange the catalytic subunit of PP1 among each other without p97 activity (**3**): An unknown subset of PP1 holoenzymes could depend on a recycling mechanism with participation of the SPI complex. Since SDS22 can form trimeric complexes with other PIPs such as KNL1 (III. 7), it is likely to first make contact to the holoenzyme to be recycled and subsequently recruits I3 to re-establish an SPI complex (“reservoir” complex), which can then serve once more as a source of holoenzyme formation (**4**).

IV Materials and Methods

IV. 1 Cloning

Polymerase chain reactions (PCRs) were performed with Phusion High-Fidelity DNA Polymerase (Thermo Scientific) according to the manufacturer's protocols. Restriction digestions, oligonucleotide dephosphorylation reactions and DNA ligations were done with enzymes from New England Biolabs according to the manufacturer's protocol. For insertion of point mutations into plasmid DNA, the QuickChange site-directed mutagenesis kit (Agilent Technologies) was used. The NucleoSpin® Gel and PCR Clean-up kit (Macherey-Nagel) was used for DNA extraction from agarose gels. For plasmid amplification, chemically competent *E. coli* DH5α or XL1-blue were transformed according to standard procedures. Amplified plasmid DNA was purified using the NucleoSpin® Plasmid kit (Macherey-Nagel) and the NucleoBond® Xtra Maxi kit (Macherey-Nagel). Generated plasmids were verified by control restriction digestion and sequencing (GATC Biotech).

IV. 2 Plasmids and constructs

Table 1: List of plasmids used in this study

Name	**Source**	**Database entry # / location**
pmcherry	database	empty vectors box
pmcherry-SDS22 wt	database	635
pmcherry-SDS22 E192A	database	646
pmcherry-SDS22 W302A	database	647
pcDNA5/FRT/TO	database	empty vectors box
pcDNA5/FRT/TO/cSH/GW	R. Aebersold / M. Varjosalo (Varjosalo et al., 2013)	ORFeome library box
pcDNA5/FRT/TO/GFP-SH	R. Aebersold	838
pcDNA5/FRT/TO/PP1γ-(1x)strep	this study	1183
pcDNA5/FRT/TO/PP1γ-(2x)strep	this Study	1188
pCMV-Sport6-PP1γ	this study	969
peGFP-C1-PP1γ	(Trinkle-Mulcahy et al., 2003)	585
pCMV-Sport6	image clone (see below)	1053

pcDNA5/FRT/TO/PP1γ-(1x)strep and -(2x)strep

The plasmid used to generate the HeLa Flp-In PP1γ-strep cell line contained a twin strep tag ("-(2x)strep") at the C-terminus. In a first step, a single-strep tagged construct was generated as follows: The cDNA encoding PP1γ was amplified by PCR from peGFP-C1-PP1γ (Trinkle-Mulcahy et al., 2003) using a forward primer containing the AflII restriction site (primer 1537)

and an extended reverse primer to integrate a 4 AA (GGGS) linker and a single strep-tag sequence (WSHPQFEK) as well as a stop codon, followed by the XhoI restriction site (primer 1535). This PCR product was inserted by restriction-ligation cloning using enzymes AflII and XhoI into an empty pcDNA5/FRT/TO vector to obtain pcDNA5/FRT/TO-PP1γ-(1x)strep. In a second step, PCR was used to re-amplify this insert but with a shorter reverse primer binding to the strep-tag sequence (primer 1617). An overlapping sequence starting with the same strep-tag sequence (forward primer 1616), followed by a linker (3x GGGS) and a second strep-tag (with nucleotide exchanges but identical AA sequence) was amplified from the plasmid pcDNA5/FRT/TO/SH-GW. The reverse primer (primer 1621) used in this PCR contained a Stop codon (UGA) and the XhoI restriction site. Both PCR products were mixed and used as template for a PCR reaction using only the terminal primers (primers 1537 and 1621) to amplify a hybridized extended sequence containing PP1γ and a C-terminal twin-strep-tag, followed by a Stop codon. This product was finally inserted using enzymes AflII and XhoI into an empty pcDNA5/FRT/TO vector as before.

pCMV-Sport6-PP1γ

The plasmid for expression of PP1γ in rabbit reticulocyte lysate was generated by cloning of human PPP1CC isoform 1 cDNA from peGFP-C1-PP1γ (Trinkle-Mulcahy et al., 2003), extended by its genomic Kozak sequence (“gggaaggcg”, forward primer 1330, reverse primer 1331) into the plasmid pCMV-Sport6 (Xenbase vector, XB-VEC-13583451, derived here from image 4032122) by restriction-ligation cloning using SalI and PstI restriction enzymes. To allow restriction-ligation cloning using PstI, an internal restriction site within the PP1γ coding sequence was modified by site-directed mutagenesis (primers 1328 and 1329), resulting in a silent mutation. The plasmid contained a polyA-signal 3’ prime to the inserted cDNA.

Table 2: DNA primers used in this study

Name	database entry #	Sequence
AflII-PP1γ-fw	1537	GTACCTTGCTTAAGATGGCGGATTTAGATAAACTCAACATC
XhoI-stopp-strep-4AA-linker-PP1G_rev	1535	CTGTCATTCTCGAGTCACTTCTCGAACTGGGGATGGCTCCAAGATCCTCCGCCTTTCTTTGCTTGCTTTGTGATCATAC
strep-rev	1617	CTTCTCGAACTGGGGATGG
strep-for	1616	TGGAGCCATCCCCAGTTC
XhIstp-strp-rv	1621	TAGTACTGCTCGAGTCATTTCTCAAACTGAGGGTGGG
SalI-Kozak-PP1g-fw	1330	CGTATAAAGTCGACGGGAAGGCGATGGCGGATTTAGATAAACTCAAC
PstI-PP1g-rv	1331	CTGATAGACTGCAGCTATTTCTTTGCTTGCTTTGTGATC
PstI-mut_PP1γ_fw	1328	CAGATTTTAAAGCCGGCAGAGAAAAAGAAG
PstI-mut_PP1γ_rv	1329	CTTCTTTTTCTCTGCCGGCTTTAAAATCTG

IV. 3 Antibodies and further reagents

Table 3: List of primary antibodies used for immunofluorescence (IF) or Western blot (WB) staining and immunoprecipitation (IP).
Asterisk (*) denotes antibodies, which were tested in pulse-chase experiments for co-IP of PP1c* (II.1.2II.2.3).

Antigen	Dilution IF / WB / IP	Source	Species of origin	Type	Code, catalog no. / citation
Aurora B	1:500 (IF)	BD biosciences	mouse	monoclonal IgG	611082
Aurora B pT232	1:1000 (IF)	Rockland	rabbit	polyclonal	600-401-677
BubR1	1:1000 (IF)	Millipore	mouse	monoclonal IgG	MAB3612
CREST	1:400 (IF)	Antibody Inc.	human	serum	15-234-0001
PNUTS	1.6 µg (IP)(*)	S.C.	mouse	monoclonal IgG	F-8, sc-271681
Inhibitor-2	1.6 µg (IP)	S.C.	mouse	monoclonal IgG	70.5, sc-130392
NIPP1 for WB	1:1000 (WB)	Sigma	rabbit	polyclonal	HPA027452
NIPP1 for IP	1 µl (IP)	M. Bollen	mouse	monoclonal IgG	272, (Van Dessel et al., 2010)
cyclin B1	1:500 (WB)	Santa Cruz	mouse	monoclonal IgG	GNS-1, sc-245
KNL1	1:1000 (WB)	A. Musacchio	rabbit	polyclonal	(Krenn et al., 2014)
SDS22	1:200 (IF) / 1:1000 (WB) / 1 µg (IP)	Santa Cruz	goat	polyclonal	E-20, sc-162164
p37	1:100 (WB)	J. Seiler / BioGenes	rabbit	polyclonal, affinity-purified	20880, (Kress et al., 2013)
Inhibitor-3	1:1000 (WB) / 5 µl (IP)	J. Seiler / Eurogentec	rabbit	polyclonal, affinity-purified	SA7263, (Eiteneuer et al., 2014)
PP1γ	1:500 (WB) / 1 µg (IP)	Santa Cruz	goat	polyclonal	C-19, sc-6108
MYPT1	1:500 (WB) / 1.6 µg (IP)	Santa Cruz	mouse	monoclonal IgG	C-6, sc-514261
Hsc70	1:10000 (WB)	Santa Cruz	mouse	monoclonal IgG	B-6, sc-7298
p97 for IP	1 µg (IP)	Santa Cruz	mouse	monoclonal IgG	5, sc-57492
URI1 / RMP	1:1000 (WB)	New England Biolabs	rabbit	polyclonal	5844
goat isotype control	used for control-IP	antikoerper online	goat	polyclonal IgG	abin398654
mouse isotype control	used for control-IP	Thermo Fisher Scientific	mouse	polyclonal IgG	10400C
rabbit isotype	used for	Thermo Fisher	rabbit	polyclonal IgG	10500C

control	control-IP	Scientific			
UBXN2A	1:1000 (WB)	J. Seiler / Eurogentec	rabbit	serum	25272, (Weith et al., 2018)
p97	1:5000 (WB)	H. Meyer	rabbit	serum	HME08 (Meyer et al., 2000)
Npl4	1:5000	H. Meyer	rabbit	serum	HME16 (Meyer et al., 2000)
p47	1:1000	H. Meyer	rabbit	serum	HME22 (Meyer et al., 2000)
SIPP1	1:300 (WB), 5 µl (IP)(*)	M. Bollen	rabbit	polyclonal, affinity purified	(Llorian et al., 2004)
Neurabin-II	1.6 µg (IP)(*)	Santa Cruz	mouse	monoclonal IgG	D-7, sc-373974
Synaptopodin	1.6 µg (IP)(*)	Santa Cruz	mouse	monoclonal IgG	D-9, sc-515842
Repo-Man	5 µl (IP)(*)	Sigma	rabbit	polyclonal	HPA030049
KIF18A	1.6 µg (IP)(*)	Santa Cruz	mouse	monoclonal IgG	C-12, sc-390600
KI-67	1.6 µg (IP)(*)	Santa Cruz	mouse	monoclonal IgG	sc-23900
Histone H3 phospho-serine 10		Merck-Millipore	rabbit	polyclonal IgG	06-570
Strep tag		Qiagen	mouse	monoclonal IgG	34850
CDC25A		Thermo Fisher	mouse	monoclonal IgG	DCS-120, MA5-13794

Table 4: List of secondary antibodies used for Western blot and immunofluorescence staining

Antigen	**Coupled fluorophore / enzyme**	**Dilution IF / WB / FACS**	**Source**	**Species of origin**	**Code, catalog no. / citation**
mouse IgG	Alexa 488	1: 500 (IF)	Invitrogen	goat	A11001
mouse IgG	Alexa 633	1: 500 (IF)	-"-	goat	A21052
rabbit IgG	Alexa 633	1: 500 (IF)	-"-	goat	A-21071
rabbit IgG	Alexa 405	1: 500 (FACS)	Abcam	donkey	ab175651
human IgG	Alexa 488	1: 500 (IF)	Invitrogen	goat	A11013
mouse IgG	HRP	1: 10000 (WB)	Bio-Rad	goat	170-6516
rabbit IgG	HRP	1: 10000 (WB)	Bio-Rad	goat	160-6515
goat IgG	HRP	1: 10000 (WB)	Santa Cruz	mouse	sc-2354

NMS-873 (SML1128) was from Sigma, CB-5083 (S8101) was from Selleckchem, MLN7243 (A-1384) was from ChemieTek, MG-132 (474790) was from Merck, cycloheximide was from Sigma (C4859) and ATPγS (NU-406-50) was from Jena Bioscience.

IV. 4 Culture conditions and description of cell lines

Human HeLa cells ("Kyoto" strain) were cultivated in medium consisting of Dulbecco's modified Eagle's medium (DMEM, PAN Biotech), supplemented with 10 % fetal calf serum

(PAN Biotech) and 1 % penicillin/streptomycin (PAN Biotech) in a humidified incubator at 37 °C and 5 % CO2.

For cultivation of the HeLa and HEK293T Flp-In cell lines, standard FCS was replaced by tetracycline-free FCS (PAN Biotech). Furthermore, antibiotics to select for resistance markers were added in the following concentrations to media used to cultivate the stably transfected cell lines: HeLa Flp-In PP1γ-strep cell line: 250 µg/ml Hygromycin B (PAA) and 15 µg/ml Blasticidin S (PAA); HeLa Flp-In GFP-SH cell line: 400 µg/ml Hygromycin B, 4 µg/ml Blasticidin S; HEK293T Flp-In p97 wild-type and - EQ cell lines: 100 µg/ml Hygromycin B and 15 µg/ml Blasticidin S.

For cultivation of the parental HeLa T-REx FRT cell line before generation of HeLa Flp-In PP1γ-strep (see below), 200 µg/ml Zeocin and 15 µg/ml Basticidin S were added to the Flp-In culture medium.

HeLa cell lines with CRISPR/Cas9-mediated genomic knock-out of p47 were established by Jonas Seiler using commercially available plasmids: p47 CRISPR/Cas9 KO Plasmid (h) (Santa Cruz, sc-402328) and p47 HDR Plasmid (h) (Santa Cruz, sc-402328-HDR) for homology-directed repair-based integration of a puromycin-resistance cassette. After transfection, clones were selected for integration of the HDR template by growth in puromycin-supplemented medium. Surviving clonal populations were picked, propagated and tested for loss of p47 expression by Western blot staining (J. Seiler).

IV. 5 Transfection of plasmids for transient expression

HeLa cells were transiently transfected at 40 % - 50 % confluence using the JetPEI transfection reagent (Polyplus) and grown for 24 h before analysis. For experiments in 6-well plates, 0.75 µg plasmid DNA and 3 µl jetPEI transfection reagent were used for transfection according to the manufacturer's instructions. The culture medium was replaced with fresh medium 6 hours after transfection.

IV. 6 Generation of HeLa cell lines using the Flp-In system

A HeLa Kyoto cell line inducibly expressing human PP1γ, fused to a C-terminal twin-strep-tag (HeLa Flp-In PP1γ-strep) was generated based on the Flp-In system (Invitrogen). Parental HeLa T-REx FRT cells, stably expressing the tetracycline repressor (TetR) (a kind gift of Gerhard Müller-Newen, Aachen) were co-transfected with the pOG44 Flp-recombinase plasmid (Invitrogen) and pcDNA5/FRT/TO-PP1γ-(2x)strep in a 9:1 ratio. 24 h post transfection, cells were selected with 250 µg/ml hygromycin B. Single clones were picked, seeded in 96 well plates and expanded. Inducible expression of human PP1γ-strep was verified by Western blotting. The resulting HeLa Flp-In PP1γ-strep cells were maintained as

described above. Transgene expression in all Flp-In cell lines was induced by addition of doxycycline (Sigma-Aldrich) at 1 µg / ml, unless stated otherwise.

IV. 7 RNA interference (RNAi) experiments

For depletion of target proteins in HeLa cells, the intrinsic RNA-interference (RNAi) pathway was induced by transfection of siRNAs using Lipofectamine RNAiMAX (Life Technologies). Cells were transfected either directly together with seeding (reverse transfection) or 24 h after seeding at a confluency of 30 % - 40 %. Transfection was done according to manufacturer's recommendations with final siRNA concentrations of 12 nM (single knock-down experiments) or two times 12 nM (double knock-down experiments), keeping the overall concentration of siRNA constant in each condition of the experiment. In the case of KNL1-RNAi, 60 nM of a mix of two siRNAs were used. Lipofectamine amounts were adjusted to the dish size (3 µl for samples in 6-well plates, 6 µl for 6 cm-, 18 µl for 10 cm-, 36 µl for 15 cm-dishes) and were increased 1.5-fold for double knock-down experiments. Unless otherwise stated, cells were siRNA-treated for 48 h before analysis.

The siRNA oligomers targeting SDS22 (s1: CCAGATCAAGAAGATTGAGAA; s2: AGAGTTCTGGATGAACGACAA) Inhibitor-3 (s1: GUAGAAUGGACAAGUGACATT; s2: CUGCUGTAUUUAUGAGAAATT), NIPP1 (s1: GGAACCTCACAAGCCTCAGCAAATT), p97 (s3: AAGUAGGGUAUGAUGACAUUGTT; s6: GGAGTTCAAAGTGGTGGAAACAGATTT), p47 (s1: AGCCAGCUCUUCCAUCUUATT), p37 (s5: GUGCCGUAAUAUAGAGGAATT; s1: CAGTTTAGATGATGGAGAATT), Ubxn2A (s1: AGAAGAGGUGGACGUUAAATT; s3: GAAAUAUGUUUGUCUACGATT) and a non-targeting control oligomer (CGUACGCGGAAUACUUCGATT) were purchased from Microsynth. A pool of 6 siRNAs targeting all three isoforms of PP1 was purchased from Santa Cruz Biotechnology (sc-43545).

IV. 8 Pulse-chase experiments using metabolic labeling with radioactive amino acids

These experiments were performed with HeLa cells grown to 60 % - 75 % confluency, with or without treatment, in 6 cm- or 10 cm-dishes. Cells were first washed twice and then starved with L-methionine-, L-cystein-free, pH-stabilized medium (gibco DMEM high glucose -Met -Cys, Life Technologies, supplemented with 2 mM L-glutamine, 25 mM HEPES pH = 7.2) for 15 min. Metabolic labeling was achieved by feeding starved cells for 30 min with 100 µCi / ml of ^{35}S-L-methionin and ^{35}S-L-cystein (Hartmann-Analytic, SCIS-103), in 0.8 ml or 2 ml starvation medium for 6 cm- or 10 cm-dishes, respectively. Chase was initiated by a wash step and subsequent addition of medium supplemented with 63 mg/l L-cysteine (Sigma) and 30 mg/l L-methionine (Sigma). Cells were harvested in PBS at indicated times, snap-frozen and stored at -80 °C before being further processed for immunoprecipitation.

Autoradiographs of dried SDS-PAGE gels were recorded on phosphor storage plates (BAS-IP MS 2025 E Multipurpose Standard, Thermo Fisher Scientific) and analysed on a Fujifilm Phosphoimager FLA 3000. For verification of autoradiographic signal identities of gel-separated proteins, specific siRNAs were transfected 14 h prior to metabolic labeling to down-regulate expression of the target proteins.

IV. 9 Preparation of cell extracts

Cells were washed once with PBS at room temperature, collected by scraping into ice-cold PBS and centrifuged into a pellet (500 x g, 4 min, 4 °C), which was either snap-frozen in liquid nitrogen and stored at -80 °C or used directly. For lysis, cell pellets were resuspended in extraction / IP buffer (150 mM KCl, 50 mM Tris pH 7.4; 5 mM $MgCl_2$, 5 % glycerol, 1 % Triton X-100, 2 mM β-mercaptoethanol, supplemented with Roche complete EDTA-free protease inhibitor) and incubated for 20 min. Insoluble material was removed by centrifugation (17000 x g, 15 min, 4 °C). Supernatants were collected and the protein concentration was measured using a bicinchoninic acid (BCA) assay (Interchim).

IV. 10 Immunoprecipitation (IP) and streptactin pull-down experiments

Cell lysis was done using Triton lysis buffer (150 mM KCl, 50 mM Tris pH 7.4, 5 mM MgCl2, 5% glycerol, 1% Triton X-100, 2 mM b-mercaptoethanol supplemented with Roche complete EDTA-free protease inhibitor). Protein content of cleared lysates was determined in a BCA assay (Interchim) and adjusted to 0.3 - 3 mg total protein per sample. In IP experiments, target-specific antibodies or isotype control antibodies were added and lysates were incubated for 1 hour on ice before addition of protein G-coupled beads (Sepharose 4 Fast Flow, GE Healthcare) or protein G-coupled magnetic beads (Dynabeads, Thermo Fisher Scientific). After incubation for 1 hour while rotating at 4 °C, beads were washed 4 times and finally, proteins were eluted from the beads by boiling the samples in SDS sample buffer. For pull-down of strep-tagged proteins, streptactin sepharose beads (IBA) were added to lysates and the suspension was incubated for 2 hours while rotating at 4 °C. Wash and elution steps were identical to those used after immunoprecipitation, except for pull-downs followed by a phosphorylase *a* phosphatase assay IV. 13). Samples were resolved on SDS-PAGE gels, which were then analysed by Western blotting or by drying onto filter paper for autoradiography.

IV. 11 SDS-PAGE and Western blotting

Protein samples were separated by size with standard SDS-PAGE methods using a Tris/glycine/SDS running buffer (200 mM glycine, 25 mM Tris-HCl pH 8.8, 0.1 % SDS) and

the Mini-PROTEAN Tetra Cell system (Bio-Rad). Samples were run at constant current of 10 to 20 mA per gel. The gels were either dried for autoradiography using a heated vacuum gel dryer (Scie Plas, GD4534) for 1.5 h at 80 °C, or used for Western blotting. Western blotting was performed by wet blot in Mini-PROTEAN chambers using Mini-TransBlot modules (Bio-Rad) and a cool-pack to reduce heating. Ice-cold, degassed Towbin buffer (25 mM Tris base, 192 mM glycine, 20 % v/v methanol, 0.1 % SDS) was used. SDS gels were blotted on a nitrocellulose membrane (Hybond-C super, Amersham Biosciences) at a constant voltage of 92 V (250 - 350 mA) for 3 hours and transfer was verified by Ponceau S staining. Membranes were blocked for 1 h at room temperature in 5 % fat free milk in PBS-T (PBS with 0.05 % Tween 20). After blocking, membranes were washed twice for 5 min in PBS-T and incubated in primary antibody dilutions in 3 % BSA in PBS-T or 5 % milk in PBS-T over night at 4 °C. Membranes were then washed 3 times for 5 min in PBS-T before incubating in HRP coupled secondary antibodies diluted in 3 % BSA in PBS-T for 1 h at room temperature. Before detection, membranes were again washed 3 times for 5 min in PBS-T. For detection, membranes were incubated for 3 min with SuperSignal West Pico or ECL Prime chemiluminescence substrates (Thermo Fisher and Amersham, respectively). Light signals were detected on Super RX films (FUJIFILM). Films were developed using a Cawomat 200 IR developing machine (Cawo) and digitalized using a ScanMaker i480 film scanner (Microtek).

IV. 12 Immunofluorescence staining and imaging

For immunofluorescence experiments to test the effect of SDS22 overexpression, HeLa Kyoto cells were grown on 18 mm glass cover slips in 6-well culture dishes and transfected with plasmids as described before (IV. 5). For fixation, cells were washed with PBS and then fixed with 4 % formaldehyde in PBS for 15 min at room temperature. Fixed cells were then washed three times in PBS and permeabilized in 0.1 % Triton X-100 in PBS for 10 min, followed by another two washing steps in PBS. Cells were then incubated in 3 % BSA (Applichem, Albumin Fraction V) in PBS for 30-60 min to block unspecific binding sites. The cover slips were then placed with the cell side down onto drops of 16 µl of primary antibody solution in 3 % BSA in PBS on parafilm in a humidified chamber and incubated for 1.5 hours. Unbound primary antibodies were removed by washing twice in PBS. Afterwards, cells were again incubated in the humid chamber in secondary antibody solution (in 3 % BSA in PBS) for 45 min to 1 h in the dark. Stained cells were washed two times in PBS and once in ddH_2O and finally mounted on glass slides using Mowiol, supplemented with 500 ng / ml DAPI.

Confocal laser scanning microscopy was done on a Leica TCS SP5 AOBS system equipped with PMT and HyD detectors and supported by LASAF software (Leica Microsystems).

Images were acquired using an HCX PL APO 63×/1.4NA oil immersion objective and processed using ImageJ and quantified using CellProfiler software (IV. 17).

IV. 13 Phosphorylase *a*-phosphatase activity assay

HeLa FlpIn cells expressing C-terminally (twin-)strep-tagged PP1γ were induced for 1 hour with 1 µg/ml doxycycline and either directly harvested or treated further by addition of 100 µg/ml cycloheximide together with either DMSO or 5 µM NMS-873 for 1 hour. Non-induced cells as well as HeLa FlpIn cells expressing GFP-SH for 1 hour were harvested in parallel. PP1γ-strep (or GFP-SH) was then isolated in IP buffer using strep-tactin-coupled agarose beads (Strep-tactin Sepharose, IBA). Beads were subsequently washed twice with IP buffer and twice in phosphatase buffer (100 mM NaCl, 50 mM HEPES pH = 7.5, 0.1 % Triton X-100, 1 mM DTT). Isolated proteins were eluted in 3 steps, adding 38 µl phosphatase buffer supplemented with 2.5 mM D(+)-Biotin (BioChemica) each. 35 µl of supernatant was removed in each step, collected and finally centrifuged again to remove residual beads. The supernatant of this centrifugation (~100 µl) was split in two samples, one of which was treated with 0.1 mg/ml trypsin (from bovine pancreas, Sigma) for 5 min at 30 °C. Trypsin activity was blocked by addition of 1 mg/ ml soybean trypsin inhibitor (Sigma) to both samples.

^{33}P-labeled phosphorylase *a* was prepared following a protocol modified from (Liu, 2005). About 1 mg of phosphorylase *b* (from rabbit muscle, Sigma) and a smaller amount (few crystals) of phosphorylase kinase (from rabbit muscle, Sigma) were prepared in separate reaction tubes. A solution of reaction buffer (150 mM Tris-HCl, pH 8.2, 10 mM $MgCl_2$, 0.5 mM $CaCl_2$) was supplemented with 1 mM “cold” ATP and 1 µCi / µl (36 µM) ^{33}P-labeled ATP (Hartmann-Analytic, SRF-301). Phosphorylase *b* was dissolved by adding 50 µl of this solution and pipetting up and down. Phosphorylase kinase was supplemented in 25 µl reaction buffer without radioactive label and was added to the phosphorylase *b* solution. The reaction was incubated for 1 hour at 30 °C. Proteins were then precipitated by addition of 75 µl of a freshly prepared, 90 % saturated solution (prepared from a saturated solution) of ammonium sulfate in water and incubation for 30 min on ice. Precipitated proteins were pelleted by centrifugation (12000 x g, 10 min, 4 °C) and washed four times with an ice-cold, 45 % saturated solution of ammonium sulfate in water. The pellet was resuspended in 130 µl of solubilization buffer (50 mM Tris-HCl, pH 7, 0.1 mM EDTA, 1 mM DTT) and filtered through a Zeba Spin Desalting column (7 K MWCO, Thermo Fisher Scientific) to remove residual ^{33}P-ATP. Aliquots were stored at 4 °C.

1 µl of this phosphorylase *a* solution (230 Bq) was added to isolates of PP1γ-strep (53 µl) and incubated for 15 min at 30 °C, shaking at 600 rpm. The reactions were stopped by addition of 5 µl of a 5 % solution of BSA in PBS and a fresh, saturated solution of trichloroacetic acid (TCA, Sigma) to 10 % final concentration, followed by incubation on ice

for 10 min. Samples were centrifuged (12000 g, 4 °C, 10 min), supernatants were removed and released ^{33}P was measured by scintillation counting using a 300 SL instrument (HIDEX).

IV. 14 Rabbit reticulocyte lysate reactions and dissociation assay

Human PP1γ was expressed in rabbit reticulocyte lysate (RRL, TNT Sp6 System, Promega) from the pCMV-Sport6 plasmid for 1 hour at 30 °C according to manufacturer's instructions with addition of 5 ng/ µl human His-SDS22, purified from insect cells (J. Seiler, see Table 5 for a list of the recombinantly expressed proteins used in these experiments).

The following components (unless indicated otherwise) were used to set up reactions ("dissociation mix") to disassemble the trimeric complex formed in RRL: an ATP-regenerating system, consisting of 2 mM ATP (Sigma), 10 mM creatine phosphate (Sigma) and 10 µg/ ml creatine kinase (Roche), recombinant His-NIPP1 (0.5 µM), recombinant p37 wild-type or mutants (0.2 µM) as indicated, all prepared in HEPES buffer (50 mM HEPES pH 7.5, 150 mM KCl, 1 mM $MgCl_2$, 5% glycerol, 1mM DTT).

Dissociation reactions were started by combining 5 µl of RRL after expression of PP1γ with 5 µl of the dissociation mixes, followed by incubation at 30 °C. At indicated times, reactions were stopped by dilution with 290 µl of cold HEPES buffer supplemented with 1 % Triton X-100 and protease inhibitor cocktail. After centrifugation (17000 g, 4 °C, 15 min), supernatants were removed and SDS22 was immunoprecipitated to analyse the amount of SDS22-PP1γ complex as a surrogate for the trimeric SDS22-PP1γ-I3 complex.

Table 5: List of recombinantly expressed, purified proteins used for *in vitro* reactions. FL: full-length; wt: wild-type.

Construct name	Plasmid backbone	insert	tag	database #	Expression host	Source
His-SDS22	pFH-His	SDS22 FL	His	771	*Trichoplusia ni* Tnao38	Ivana Primorac, Jonas Seiler
His-NIPP1	pET-16b	NIPP1 FL	His	965	*E. coli* BL21	Dana Hönig
p37 wt	pGEX-6P-1	p37 FL	GST (cleaved)	1110	*E. coli* BL21	Jonas Seiler
p37 ΔN	pGEX-6P-1	p37 Δ2-81	GST (cleaved)	1118	*E. coli* BL21	Jonas Seiler
p37 ΔSEP	pGEX-6P-1	p37 Δ140-206	GST (cleaved)	1115	*E. coli* BL21	Jonas Seiler
p37 SHPmut	pGEX-6P-1	p37 F215A/E218A/QKL220-222AAA	GST (cleaved)	1112	*E. coli* BL21	Jonas Seiler

Recombinant proteins were purified by Jonas Seiler (p37 wild-type and mutants, His-SDS22, His-NIPP1) and Ivana Primorac (His-SDS22). Other His-NIPP1 was a kind gift of Dana Hönig.

IV. 15 Fluorescence-activated cell sorting

Native HeLa cells or HeLa p47 KO cells (clone 42) were seeded and transfected with siRNA in 6 cm-dishes. After 48 h, cells were harvested by scraping from the plates and collected by centrifugation (500 x g, 5 min, RT). Pellets were resuspended in cold PBS and centrifuged (500 x g, 5 min, 4 °C). Supernatants were removed to around 50 µl, in which cells were resuspended again. 1 ml of 4 % formaldehyde in PBS was added and cells were fixed for 15 min at RT. After another centrifugation step (500 x g, 4 min, RT), cells were washed twice in PBS, supplemented with 0.1 % Triton X-100 (TX-100) for permeabilization. Pellets after the second wash step were resuspended in blocking solution (1 % BSA / PBS / 0.1 % TX-100) and incubated for 30 min while shaking softly (600 rpm) to block unspecific binding sites. After another centrifugation step, cells were resuspended in a solution of the anti-histone-3 phospho-serine-10 (pH3S10) antibody, diluted 1:1000 in blocking solution and incubated for 1 hour while shaking softly. Cells were then pelleted again by centrifugation and washed twice with PBS / 0.1 % TX-100. Pellets after the second wash step were resuspended in a solution of donkey-anti-rabbit antibody coupled with Alexa fluor 405, diluted 1:500 in blocking solution and incubated for 45 min while shaking softly (in the dark). After centrifugation, cells were washed once with PBS / 0.1 % TX-100 and then resuspended in the same buffer, supplemented with 60 µg/ml RNAse A (Roche) and 40 µg/ml Propidium iodine (Sigma). After 15 min incubation at RT, cells were passed through 100 µm filters and analyzed by fluorescence-activated cell sorting on a MACSquant VYB machine. The results were quantified by FlowJo software (Version 10). Cells were gated for main population of living cells in the forward (FSC-A) against sideward scatter (SSC-A). Cell doublets were gated out by FSC-area against FSC-height intensity. Cells were finally gated by pH3S10 intensity against propidium iodine (PI) intensity and mitotic index was defined by population with high pH3 and high PI intensity.

IV. 16 Mass Spectrometry and label-free quantification

PP1γ interactions were analyzed by mass spectrometry in two different settings: One setting compared interactions of PP1γ in HeLa cells treated with DMSO or 10 µM NMS-873 for 16 hours (MS1). In the second setting, interactions of PP1γ in native HeLa cells, treated with a non-targeting siRNA were compared to those in a HeLa p47 knock-out cell line (clone 42) after RNAi-mediated depletion of p37 (oligo s5) and Ubxn2A (oligo s1) for 48 h (MS2).

The following steps for sample preparation, peptide separation and mass spectrometry analysis were identical in both settings. Immunoprecipitation was performed using goat IgG standard or PP1γ-specific antibodies in at least three biological replicates. Cleared cell lysates, prepared in IP buffer, were supplemented with goat IgG isotype control or goat anti-PP1γ antibody and incubated for 1 h on ice. Protein G-coupled magnetic beads (Dynabeads, Thermo Fisher Scientific) were added for isolation of PP1γ-immune complexes, followed by one wash step in IP buffer and three wash steps in IP buffer without detergent. Proteins were subsequently eluted from the beads by on-bead digestion with LysC. To this end, the beads were resuspended in 50 µl of 8 M Urea, 1 mM DTT and incubated with 1 ng/µl Lys C for 30 min at 37 °C. The supernatants were diluted to reach a final concentration of 1 M Urea using 50 mM ammonium bicarbonate buffer. Reduction and alkylation was achieved by subsequent addition of 5 mM DTT and 10 mM iodoacetamide (IAM) with incubation times of 30 min for each step. To quench excess IAM, more DTT was added to a final concentration of 10 mM. Next, samples were digested overnight with 200 ng/µL trypsin at 37 °C, followed by acidification with formic acid (final concentration 0.5 %).

Acidified tryptic digests were desalted on home-made 2-disc C18 StageTips (Svenja Blaskowski). After elution from the StageTips, samples were dried using a vacuum concentrator (Eppendorf) and the peptides were taken up in 10 µL 0.1 % formic acid solution. Peptides were then separated by reversed phase chromatography and analysed by tandem mass spectrometry on an Orbitrap Elite instrument (Thermo).

Farnusch Kaschani analyzed the obtained spectra using the MaxQuant software and the MaxLFQ algorithm for label-free quantification (LFQ)(Cox et al., 2014). In total, 1871 (MS1) and 1504 (MS2) protein groups were identified. Resulting peptide groups in Perseus v1.5.5.3 (Tyanova et al., 2016) were filtered as follows: removal of proteins, identified only by a post-translationally modified peptide (“only identified by site” in MaxQuant): 11 (MS1) and 76 (MS2) proteins; removal of proteins identified via the reverse part of the decoy database: 18 (MS1) and 14 (MS2) proteins; removal of commonly occurring contaminants (MaxQuant definition): 55 (MS1) and 61 (MS2) proteins. Furthermore, related biological replicates were combined to categorical groups and only those proteins were investigated that were found in at least one categorical group in a minimum of 3 out of 4 biological replicates. In sum, after these filtering steps, 1179 (MS1) and 782 (MS2) protein groups remained.

We further limited our analysis to proteins specifically detected in PP1γ versus control immunoprecipitations (one-sided Student’s t-test, FDR < 0.05, S0 = 2), resulting in sets of 507 (MS1) and 395 (MS2) protein groups, which were then analysed for intensity shifts between the control conditions and those, in which disassembly of the SDS22-PP1-I3 complex was expected to be inhibited (treatment with NMS-873 in MS1 or depletion of p97 adapters in this pathway in MS2). Comparison of protein group quantities (relative

quantification) between different MS runs was based solely on the LFQ results as calculated by MaxQuant (MaxLFQ algorithm)(Cox et al., 2014).

IV. 17 Quantification and statistics

Signal intensities for Aurora B, Aurora B pT232 and BubR1 from IF experiments were quantified using the image analysis software CellProfiler (Carpenter et al., 2006). DAPI and CREST signals were used to identify chromatin and kinetochores, respectively, as primary objects. Aurora B and Aurora B pT232 signals were measured on chromatin, whereas BubR1 signals were measured on kinetochores. Statistical analyses of IF data were done with SigmaPlot software (Systat) applying Mann-Whitney U test on all recorded intensities from the indicated number of replicate experiments to compare between pairs of treatment conditions.

Measured radioactive signal intensities (decays per minute, DPM) resulting from release of ^{33}P-ATP in the phosphorylase *a*-phosphatase assay were first corrected by calculation of half-life corrected values based on the reference date for the radioactive preparation as indicated by the supplier. We performed a One-Way ANOVA test for repeated measures, treating the experiments as “groups”, which were then investigated at different levels of the independent variable, defined by the treatment condition. This increased the statistical power of the test by dividing the total variability into a “within-groups” variability, which reflects the difference in the absolute measures of released radioactivity between different replicates of the same condition, and the actual random error. To correct for multiple testing (at 3 levels of the independent variable), a Bonferroni post-hoc test was performed and calculation of statistical significance was based on this correction.

A similar method was applied to evaluate the effect of combined KO and knock-down of SEP domain adapters on the binding of PP1c* to NIPP1 (II.3.3). In this case, a Two-Way ANOVA test for repeated measures was applied, setting the treatment condition as one factor and the chase time-point as the second factor. Again, the experiments performed on different days were treated as “groups” and investigated at the levels (control vs. depletion; 0, 40 or 120 min) of the independent variables. To correct for multiple testing, we applied a Bonferroni-Holm post-hoc test and based statistical significance calculation on this correction.

For statistical evaluation of the mass spectrometry experiments, calculations were performed using the Perseus software. Pair-wise Student’s t-tests were performed to compare the LFQ intensities of individual protein groups between treatment conditions. Due to the high number of comparisons performed across the data set, Student’s t-test significance evaluation was corrected by a false-discovery rate (FDR, set to 0.05) calculation and by setting minimal difference thresholds (“S0”) as indicated.

For all tests, results meeting the levels of significance of 0.05 (*), 0.01 (**) and 0.001 (***) or lower were considered statistically significant.

References

Alessi, D., MacDougall, L.K., Sola, M.M., Ikebe, M., and Cohen, P. (1992). The control of protein phosphatase-1 by targetting subunits. The major myosin phosphatase in avian smooth muscle is a novel form of protein phosphatase-1. Eur J Biochem *210*, 1023-1035.

Alexandru, G., Graumann, J., Smith, G.T., Kolawa, N.J., Fang, R., and Deshaies, R.J. (2008). UBXD7 binds multiple ubiquitin ligases and implicates p97 in HIF1alpha turnover. Cell *134*, 804-816.

Andreassen, P.R., Lacroix, F.B., Villa-Moruzzi, E., and Margolis, R.L. (1998). Differential subcellular localization of protein phosphatase-1 alpha, gamma1, and delta isoforms during both interphase and mitosis in mammalian cells. J Cell Biol *141*, 1207-1215.

Antoniw, J.F., and Cohen, P. (1975). Separation of two phosphorylase kinase phosphatase activities in rabbit skeletal muscle. Biochem Soc Trans *3*, 83-84.

Baker, T.A., and Sauer, R.T. (2012). ClpXP, an ATP-powered unfolding and protein-degradation machine. Biochimica et biophysica acta *1823*, 15-28.

Barr, A.R., and Gergely, F. (2007). Aurora-A: the maker and breaker of spindle poles. J Cell Sci *120*, 2987-2996.

Barthelme, D., Chen, J.Z., Grabenstatter, J., Baker, T.A., and Sauer, R.T. (2014). Architecture and assembly of the archaeal Cdc48*20S proteasome. Proc Natl Acad Sci U S A *111*, E1687-1694.

Barthelme, D., and Sauer, R.T. (2012). Identification of the Cdc48*20S proteasome as an ancient AAA+ proteolytic machine. Science *337*, 843-846.

Barthelme, D., and Sauer, R.T. (2013). Bipartite determinants mediate an evolutionarily conserved interaction between Cdc48 and the 20S peptidase. Proc Natl Acad Sci U S A *110*, 3327-3332.

Beck, M., Schmidt, A., Malmstroem, J., Claassen, M., Ori, A., Szymborska, A., Herzog, F., Rinner, O., Ellenberg, J., and Aebersold, R. (2011). The quantitative proteome of a human cell line. Mol Syst Biol *7*, 549.

Bella, J., Hindle, K.L., McEwan, P.A., and Lovell, S.C. (2008). The leucine-rich repeat structure. Cell Mol Life Sci *65*, 2307-2333.

Benaroudj, N., Tarcsa, E., Cascio, P., and Goldberg, A.L. (2001). The unfolding of substrates and ubiquitin-independent protein degradation by proteasomes. Biochimie *83*, 311-318.

Bennett, D., and Alphey, L. (2002). PP1 binds Sara and negatively regulates Dpp signaling in Drosophila melanogaster. Nat Genet *31*, 419-423.

Beuron, F., Dreveny, I., Yuan, X., Pye, V.E., McKeown, C., Briggs, L.C., Cliff, M.J., Kaneko, Y., Wallis, R., Isaacson, R.L., *et al.* (2006). Conformational changes in the AAA ATPase p97-p47 adaptor complex. Embo j *25*, 1967-1976.

Bharucha, J.P., Larson, J.R., Gao, L., Daves, L.K., and Tatchell, K. (2008). Ypi1, a positive regulator of nuclear protein phosphatase type 1 activity in *Saccharomyces cerevisiae*. Mol Biol Cell *19*, 1032-1045.

Biggins, S., Severin, F.F., Bhalla, N., Sassoon, I., Hyman, A.A., and Murray, A.W. (1999). The conserved protein kinase Ipl1 regulates microtubule binding to kinetochores in budding yeast. Genes Dev *13*, 532-544.

Black, B.E., and Cleveland, D.W. (2011). Epigenetic centromere propagation and the nature of CENP-a nucleosomes. Cell *144*, 471-479.

Bloecher, A., and Tatchell, K. (1999). Defects in *Saccharomyces cerevisiae* protein phosphatase type I activate the spindle/kinetochore checkpoint. Genes Dev *13*, 517-522.

Blythe, E.E., Olson, K.C., Chau, V., and Deshaies, R.J. (2017). Ubiquitin- and ATP-dependent unfoldase activity of P97/VCP*NPLOC4*UFD1L is enhanced by a mutation that causes multisystem proteinopathy. Proc Natl Acad Sci U S A *114*, E4380-E4388.

Bodnar, N., and Rapoport, T. (2017a). Toward an understanding of the Cdc48/p97 ATPase. F1000Res *6*, 1318.

Bodnar, N.O., Kim, K.H., Ji, Z., Wales, T.E., Svetlov, V., Nudler, E., Engen, J.R., Walz, T., and Rapoport, T.A. (2018). Structure of the Cdc48 ATPase with its ubiquitin-binding cofactor Ufd1-Npl4. Nat Struct Mol Biol.

Bodnar, N.O., and Rapoport, T.A. (2017b). Molecular Mechanism of Substrate Processing by the Cdc48 ATPase Complex. Cell *169*, 722-735.e729.

Bohm, S., and Buchberger, A. (2013). The budding yeast Cdc48(Shp1) complex promotes cell cycle progression by positive regulation of protein phosphatase 1 (Glc7). PLoS One *8*, e56486.

Boldt, K., van Reeuwijk, J., Lu, Q., Koutroumpas, K., Nguyen, T.M., Texier, Y., van Beersum, S.E., Horn, N., Willer, J.R., Mans, D.A., *et al.* (2016). An organelle-specific protein landscape identifies novel diseases and molecular mechanisms. Nat Commun *7*, 11491.

Bollen, M. (2001). Combinatorial control of protein phosphatase-1. Trends Biochem Sci *26*, 426-431.

Bollen, M., Peti, W., Ragusa, M.J., and Beullens, M. (2010). The extended PP1 toolkit: designed to create specificity. Trends Biochem Sci *35*, 450-458.

Bollen, M., and Stalmans, W. (1992). The structure, role, and regulation of type 1 protein phosphatases. Crit Rev Biochem Mol Biol *27*, 227-281.

Borden, K.L., and Freemont, P.S. (1996). The RING finger domain: a recent example of a sequence-structure family. Curr Opin Struct Biol *6*, 395-401.

Boulon, S., Pradet-Balade, B., Verheggen, C., Molle, D., Boireau, S., Georgieva, M., Azzag, K., Robert, M.C., Ahmad, Y., Neel, H., *et al.* (2010). HSP90 and its R2TP/Prefoldin-like cochaperone are involved in the cytoplasmic assembly of RNA polymerase II. Mol Cell *39*, 912-924.

Brautigan, D.L. (2013). Protein Ser/Thr phosphatases--the ugly ducklings of cell signalling. FEBS J *280*, 324-345.

Bruderer, R.M., Brasseur, C., and Meyer, H.H. (2004). The AAA ATPase p97/VCP interacts with its alternative co-factors, Ufd1-Npl4 and p47, through a common bipartite binding mechanism. J Biol Chem *279*, 49609-49616.

Brunger, A.T., and DeLaBarre, B. (2003). NSF and p97/VCP: similar at first, different at last. FEBS Lett *555*, 126-133.

Buchberger, A., Bukau, B., and Sommer, T. (2010). Protein quality control in the cytosol and the endoplasmic reticulum: brothers in arms. Mol Cell *40*, 238-252.

Buchberger, A., Schindelin, H., and Hanzelmann, P. (2015). Control of p97 function by cofactor binding. FEBS Lett *589*, 2578-2589.

Cannon, J.F. (2010). Function of protein phosphatase-1, Glc7, in *Saccharomyces cerevisiae*. Adv Appl Microbiol *73*, 27-59.

Cannon, J.F., Pringle, J.R., Fiechter, A., and Khalil, M. (1994). Characterization of glycogen-deficient glc mutants of *Saccharomyces cerevisiae*. Genetics *136*, 485-503.

Cao, K., Nakajima, R., Meyer, H.H., and Zheng, Y. (2003). The AAA-ATPase Cdc48/p97 regulates spindle disassembly at the end of mitosis. Cell *115*, 355-367.

Carmena, M., Ruchaud, S., and Earnshaw, W.C. (2009). Making the Auroras glow: regulation of Aurora A and B kinase function by interacting proteins. Curr Opin Cell Biol *21*, 796-805.

Carmena, M., Wheelock, M., Funabiki, H., and Earnshaw, W.C. (2012). The chromosomal passenger complex (CPC): from easy rider to the godfather of mitosis. Nat Rev Mol Cell Biol *13*, 789-803.

Carpenter, A.E., Jones, T.R., Lamprecht, M.R., Clarke, C., Kang, I.H., Friman, O., Guertin, D.A., Chang, J.H., Lindquist, R.A., Moffat, J., *et al.* (2006). CellProfiler: image analysis software for identifying and quantifying cell phenotypes. Genome Biol *7*, R100.

Castermans, D., Somers, I., Kriel, J., Louwet, W., Wera, S., Versele, M., Janssens, V., and Thevelein, J.M. (2012). Glucose-induced posttranslational activation of protein phosphatases PP2A and PP1 in yeast. Cell research *22*, 1058-1077.

Ceulemans, H., and Bollen, M. (2004). Functional diversity of protein phosphatase-1, a cellular economizer and reset button. Physiol Rev *84*, 1-39.

Ceulemans, H., De Maeyer, M., Stalmans, W., and Bollen, M. (1999). A capping domain for LRR protein interaction modules. FEBS Lett *456*, 349-351.

Ceulemans, H., Stalmans, W., and Bollen, M. (2002a). Regulator-driven functional diversification of protein phosphatase-1 in eukaryotic evolution. Bioessays *24*, 371-381.

Ceulemans, H., Vulsteke, V., De Maeyer, M., Tatchell, K., Stalmans, W., and Bollen, M. (2002b). Binding of the concave surface of the Sds22 superhelix to the alpha 4/alpha 5/alpha 6-triangle of protein phosphatase-1. J Biol Chem *277*, 47331-47337.

Chan, C.S., and Botstein, D. (1993). Isolation and characterization of chromosome-gain and increase-in-ploidy mutants in yeast.

Chatterjee, J., Beullens, M., Sukackaite, R., Qian, J., Lesage, B., Hart, D.J., Bollen, M., and Kohn, M. (2012). Development of a peptide that selectively activates protein phosphatase-1 in living cells. Angew Chem Int Ed Engl *51*, 10054-10059.

Chen, M.J., Dixon, J.E., and Manning, G. (2017). Genomics and evolution of protein phosphatases. Sci Signal *10*.

Chen, Z.J., and Sun, L.J. (2009). Nonproteolytic functions of ubiquitin in cell signaling. Mol Cell *33*, 275-286.

Cheng, Y.L., and Chen, R.H. (2010). The AAA-ATPase Cdc48 and cofactor Shp1 promote chromosome bi-orientation by balancing Aurora B activity. J Cell Sci *123*, 2025-2034.

Cheng, Y.L., and Chen, R.H. (2015). Assembly and quality control of the protein phosphatase 1 holoenzyme involves the Cdc48-Shp1 chaperone. J Cell Sci *128*, 1180-1192.

Choy, M.S., Page, R., and Peti, W. (2012). Regulation of protein phosphatase 1 by intrinsically disordered proteins. Biochem Soc Trans *40*, 969-974.

Clotet, J., Posas, F., Casamayor, A., Schaaff-Gerstenschlager, I., and Arino, J. (1991). The gene DIS2S1 is essential in *Saccharomyces cerevisiae* and is involved in glycogen phosphorylase activation. Curr Genet *19*, 339-342.

Cloutier, P., Poitras, C., Durand, M., Hekmat, O., Fiola-Masson, E., Bouchard, A., Faubert, D., Chabot, B., and Coulombe, B. (2017). R2TP/Prefoldin-like component RUVBL1/RUVBL2 directly interacts with ZNHIT2 to regulate assembly of U5 small nuclear ribonucleoprotein. Nat Commun *8*, 15615.

Cohen, P.T. (2002). Protein phosphatase 1--targeted in many directions. J Cell Sci *115*, 241-256.

Connor, J.H., Weiser, D.C., Li, S., Hallenbeck, J.M., and Shenolikar, S. (2001). Growth arrest and DNA damage-inducible protein GADD34 assembles a novel signaling complex containing protein phosphatase 1 and inhibitor 1. Mol Cell Biol *21*, 6841-6850.

Costanzo, M., VanderSluis, B., Koch, E.N., Baryshnikova, A., Pons, C., Tan, G., Wang, W., Usaj, M., Hanchard, J., Lee, S.D*., et al.* (2016). A global genetic interaction network maps a wiring diagram of cellular function. Science *353*.

Cox, J., Hein, M.Y., Luber, C.A., Paron, I., Nagaraj, N., and Mann, M. (2014). Accurate proteome-wide label-free quantification by delayed normalization and maximal peptide ratio extraction, termed MaxLFQ. Mol Cell Proteomics *13*, 2513-2526.

Cui, D.Y., Brown, C.R., and Chiang, H.L. (2004). The type 1 phosphatase Reg1p-Glc7p is required for the glucose-induced degradation of fructose-1,6-bisphosphatase in the vacuole. J Biol Chem *279*, 9713-9724.

Dai, R.M., Chen, E., Longo, D.L., Gorbea, C.M., and Li, C.C. (1998). Involvement of valosin-containing protein, an ATPase Co-purified with IkappaBalpha and 26 S proteasome, in ubiquitin-proteasome-mediated degradation of IkappaBalpha. J Biol Chem *273*, 3562-3573.

Dai, R.M., and Li, C.C. (2001). Valosin-containing protein is a multi-ubiquitin chain-targeting factor required in ubiquitin-proteasome degradation. Nat Cell Biol *3*, 740-744.

Damianov, A., Kann, M., Lane, W.S., and Bindereif, A. (2006). Human RBM28 protein is a specific nucleolar component of the spliceosomal snRNPs. Biological chemistry *387*, 1455-1460.

DeLaBarre, B., and Brunger, A.T. (2005). Nucleotide dependent motion and mechanism of action of p97/VCP. Journal of molecular biology *347*, 437-452.

Dinischiotu, A., Beullens, M., Stalmans, W., and Bollen, M. (1997). Identification of sds22 as an inhibitory subunit of protein phosphatase-1 in rat liver nuclei. FEBS Lett *402*, 141-144.

Djouder, N., Metzler, S.C., Schmidt, A., Wirbelauer, C., Gstaiger, M., Aebersold, R., Hess, D., and Krek, W. (2007). S6K1-mediated disassembly of mitochondrial URI/PP1gamma complexes activates a negative feedback program that counters S6K1 survival signaling. Mol Cell *28*, 28-40.

Dobrynin, G., Popp, O., Romer, T., Bremer, S., Schmitz, M.H., Gerlich, D.W., and Meyer, H. (2011). Cdc48/p97-Ufd1-Npl4 antagonizes Aurora B during chromosome segregation in HeLa cells. J Cell Sci *124*, 1571-1580.

Dougan, D.A., Mogk, A., Zeth, K., Turgay, K., and Bukau, B. (2002). AAA+ proteins and substrate recognition, it all depends on their partner in crime. FEBS Lett *529*, 6-10.

Dreveny, I., Kondo, H., Uchiyama, K., Shaw, A., Zhang, X., and Freemont, P.S. (2004). Structural basis of the interaction between the AAA ATPase p97/VCP and its adaptor protein p47. Embo j *23*, 1030-1039.

Drozdetskiy, A., Cole, C., Procter, J., and Barton, G.J. (2015). JPred4: a protein secondary structure prediction server. Nucleic Acids Res *43*, W389-394.

Eiteneuer, A., Seiler, J., Weith, M., Beullens, M., Lesage, B., Krenn, V., Musacchio, A., Bollen, M., and Meyer, H. (2014). Inhibitor-3 ensures bipolar mitotic spindle attachment by limiting association of SDS22 with kinetochore-bound protein phosphatase-1. EMBO J *33*, 2704-2720.

Erales, J., and Coffino, P. (2014). Ubiquitin-independent proteasomal degradation. Biochimica et biophysica acta *1843*, 216-221.

Erzberger, J.P., and Berger, J.M. (2006). Evolutionary relationships and structural mechanisms of AAA+ proteins. Annual review of biophysics and biomolecular structure *35*, 93-114.

Esaki, M., Johjima-Murata, A., Islam, M.T., and Ogura, T. (2018). Biological and Pathological Implications of an Alternative ATP-Powered Proteasomal Assembly With Cdc48 and the 20S Peptidase. Frontiers in molecular biosciences *5*, 56.

Esser, C., Alberti, S., and Hohfeld, J. (2004). Cooperation of molecular chaperones with the ubiquitin/proteasome system. Biochimica et biophysica acta *1695*, 171-188.

Eto, M., Kirkbride, J.A., and Brautigan, D.L. (2005). Assembly of MYPT1 with protein phosphatase-1 in fibroblasts redirects localization and reorganizes the actin cytoskeleton. Cell Motil Cytoskeleton *62*, 100-109.

Eto, M., Kitazawa, T., Matsuzawa, F., Aikawa, S., Kirkbride, J.A., Isozumi, N., Nishimura, Y., Brautigan, D.L., and Ohki, S.Y. (2007). Phosphorylation-induced conformational switching of CPI-17 produces a potent myosin phosphatase inhibitor. Structure *15*, 1591-1602.

Eto, M., Leach, C., Tountas, N.A., and Brautigan, D.L. (2003). Phosphoprotein inhibitors of protein phosphatase-1. Methods Enzymol *366*, 243-260.

Ewing, R.M., Chu, P., Elisma, F., Li, H., Taylor, P., Climie, S., McBroom-Cerajewski, L., Robinson, M.D., O'Connor, L., Li, M.*, et al.* (2007). Large-scale mapping of human protein-protein interactions by mass spectrometry. Mol Syst Biol *3*, 89.

Feng, Z.H., Wilson, S.E., Peng, Z.Y., Schlender, K.K., Reimann, E.M., and Trumbly, R.J. (1991). The yeast GLC7 gene required for glycogen accumulation encodes a type 1 protein phosphatase. J Biol Chem *266*, 23796-23801.

Flynn, J.M., Neher, S.B., Kim, Y.I., Sauer, R.T., and Baker, T.A. (2003). Proteomic discovery of cellular substrates of the ClpXP protease reveals five classes of ClpX-recognition signals. Mol Cell *11*, 671-683.

Foley, E.A., and Kapoor, T.M. (2013). Microtubule attachment and spindle assembly checkpoint signalling at the kinetochore. Nat Rev Mol Cell Biol *14*, 25-37.

Foley, E.A., Maldonado, M., and Kapoor, T.M. (2011). Formation of stable attachments between kinetochores and microtubules depends on the B56-PP2A phosphatase. Nat Cell Biol *13*, 1265-1271.

Francisco, L., Wang, W., and Chan, C.S. (1994). Type 1 protein phosphatase acts in opposition to IpL1 protein kinase in regulating yeast chromosome segregation. Mol Cell Biol *14*, 4731-4740.

Fu, X., Ng, C., Feng, D., and Liang, C. (2003). Cdc48p is required for the cell cycle commitment point at Start via degradation of the G1-CDK inhibitor Far1p. J Cell Biol *163*, 21-26.

Funabiki, H., and Wynne, D.J. (2013). Making an effective switch at the kinetochore by phosphorylation and dephosphorylation. Chromosoma *122*, 135-158.

Garcia-Gimeno, M.A., Munoz, I., Arino, J., and Sanz, P. (2003). Molecular characterization of Ypi1, a novel *Saccharomyces cerevisiae* type 1 protein phosphatase inhibitor. J Biol Chem *278*, 47744-47752.

Ghosh, A., and Cannon, J.F. (2013). Analysis of protein phosphatase-1 and aurora protein kinase suppressors reveals new aspects of regulatory protein function in *Saccharomyces cerevisiae*. PLoS One *8*, e69133.

Golbik, R., Lupas, A.N., Koretke, K.K., Baumeister, W., and Peters, J. (1999). The Janus face of the archaeal Cdc48/p97 homologue VAT: protein folding versus unfolding. Biological chemistry *380*, 1049-1062.

Grallert, A., Boke, E., Hagting, A., Hodgson, B., Connolly, Y., Griffiths, J.R., Smith, D.L., Pines, J., and Hagan, I.M. (2015). A PP1-PP2A phosphatase relay controls mitotic progression. Nature *517*, 94-98.

Grusche, F.A., Hidalgo, C., Fletcher, G., Sung, H.H., Sahai, E., and Thompson, B.J. (2009). Sds22, a PP1 phosphatase regulatory subunit, regulates epithelial cell polarity and shape [Sds22 in epithelial morphology]. BMC Dev Biol *9*, 14.

Gstaiger, M., Luke, B., Hess, D., Oakeley, E.J., Wirbelauer, C., Blondel, M., Vigneron, M., Peter, M., and Krek, W. (2003). Control of nutrient-sensitive transcription programs by the unconventional prefoldin URI. Science *302*, 1208-1212.

Guaitoli, G., Raimondi, F., Gilsbach, B.K., Gomez-Llorente, Y., Deyaert, E., Renzi, F., Li, X., Schaffner, A., Jagtap, P.K., Boldt, K.*, et al.* (2016). Structural model of the dimeric Parkinson's protein LRRK2 reveals a compact architecture involving distant interdomain contacts. Proc Natl Acad Sci U S A *113*, E4357-4366.

Guo, F., Stanevich, V., Wlodarchak, N., Sengupta, R., Jiang, L., Satyshur, K.A., and Xing, Y. (2014). Structural basis of PP2A activation by PTPA, an ATP-dependent activation chaperone. Cell research *24*, 190-203.

Gur, E., and Sauer, R.T. (2008). Recognition of misfolded proteins by Lon, a AAA(+) protease. Genes Dev *22*, 2267-2277.

Hans, F., and Dimitrov, S. (2001). Histone H3 phosphorylation and cell division. Oncogene *20*, 3021-3027.

Hanzelmann, P., and Schindelin, H. (2016). Characterization of an Additional Binding Surface on the p97 N-Terminal Domain Involved in Bipartite Cofactor Interactions. Structure *24*, 140-147.

Hartmann-Petersen, R., Wallace, M., Hofmann, K., Koch, G., Johnsen, A.H., Hendil, K.B., and Gordon, C. (2004). The Ubx2 and Ubx3 cofactors direct Cdc48 activity to proteolytic and nonproteolytic ubiquitin-dependent processes. Curr Biol *14*, 824-828.

Hartwell, L.H., Mortimer, R.K., Culotti, J., and Culotti, M. (1973). Genetic Control of the Cell Division Cycle in Yeast: V. Genetic Analysis of cdc Mutants. Genetics *74*, 267-286.

Hein, M.Y., Hubner, N.C., Poser, I., Cox, J., Nagaraj, N., Toyoda, Y., Gak, I.A., Weisswange, I., Mansfeld, J., Buchholz, F.*, et al.* (2015). A human interactome in three quantitative dimensions organized by stoichiometries and abundances. Cell *163*, 712-723.

Hendrickx, A., Beullens, M., Ceulemans, H., Den Abt, T., Van Eynde, A., Nicolaescu, E., Lesage, B., and Bollen, M. (2009). Docking motif-guided mapping of the interactome of protein phosphatase-1. Chem Biol *16*, 365-371.

Heo, J.M., Livnat-Levanon, N., Taylor, E.B., Jones, K.T., Dephoure, N., Ring, J., Xie, J., Brodsky, J.L., Madeo, F., Gygi, S.P.*, et al.* (2010). A stress-responsive system for mitochondrial protein degradation. Mol Cell *40*, 465-480.

Heroes, E., Lesage, B., Gornemann, J., Beullens, M., Van Meervelt, L., and Bollen, M. (2013). The PP1 binding code: a molecular-lego strategy that governs specificity. FEBS J *280*, 584-595.

Hetzer, M., Meyer, H.H., Walther, T.C., Bilbao-Cortes, D., Warren, G., and Mattaj, I.W. (2001). Distinct AAA-ATPase p97 complexes function in discrete steps of nuclear assembly. Nat Cell Biol *3*, 1086-1091.

Ho, Y., Gruhler, A., Heilbut, A., Bader, G.D., Moore, L., Adams, S.L., Millar, A., Taylor, P., Bennett, K., Boutilier, K.*, et al.* (2002). Systematic identification of protein complexes in *Saccharomyces cerevisiae* by mass spectrometry. Nature *415*, 180-183.

Hombauer, H., Weismann, D., Mudrak, I., Stanzel, C., Fellner, T., Lackner, D.H., and Ogris, E. (2007). Generation of active protein phosphatase 2A is coupled to holoenzyme assembly. PLoS Biol *5*, e155.

Hoppe, T., Matuschewski, K., Rape, M., Schlenker, S., Ulrich, H.D., and Jentsch, S. (2000). Activation of a membrane-bound transcription factor by regulated ubiquitin/proteasome-dependent processing. Cell *102*, 577-586.

Hori, T., Amano, M., Suzuki, A., Backer, C.B., Welburn, J.P., Dong, Y., McEwen, B.F., Shang, W.H., Suzuki, E., Okawa, K.*, et al.* (2008). CCAN makes multiple contacts with centromeric DNA to provide distinct pathways to the outer kinetochore. Cell *135*, 1039-1052.

Hsu, J.Y., Sun, Z.W., Li, X., Reuben, M., Tatchell, K., Bishop, D.K., Grushcow, J.M., Brame, C.J., Caldwell, J.A., Hunt, D.F.*, et al.* (2000). Mitotic phosphorylation of histone H3 is governed by Ipl1/aurora kinase and Glc7/PP1 phosphatase in budding yeast and nematodes. Cell *102*, 279-291.

Hu, K., Li, W., Wang, H., Chen, K., Wang, Y., and Sang, J. (2012). Shp1, a regulator of protein phosphatase 1 Glc7, has important roles in cell morphogenesis, cell cycle progression and DNA damage response in Candida albicans. Fungal genetics and biology : FG & B *49*, 433-442.

Huang, F.L., and Glinsmann, W.H. (1976). Separation and characterization of two phosphorylase phosphatase inhibitors from rabbit skeletal muscle. Eur J Biochem *70*, 419-426.

Huang, H.S., and Lee, E.Y. (2008). Protein phosphatase-1 inhibitor-3 is an *in vivo* target of caspase-3 and participates in the apoptotic response. J Biol Chem *283*, 18135-18146.

Huang, H.S., Pozarowski, P., Gao, Y., Darzynkiewicz, Z., and Lee, E.Y. (2005). Protein phosphatase-1 inhibitor-3 is co-localized to the nucleoli and centrosomes with PP1gamma1 and PP1alpha, respectively. Arch Biochem Biophys *443*, 33-44.

Huang, S., Tang, D., and Wang, Y. (2016). Monoubiquitination of Syntaxin 5 Regulates Golgi Membrane Dynamics during the Cell Cycle. Dev Cell *38*, 73-85.

Hubbard, M.J., and Cohen, P. (1993). On target with a new mechanism for the regulation of protein phosphorylation. Trends Biochem Sci *18*, 172-177.

Hülsmann, J., Kravic, B., Weith, M., Gstaiger, M., Aebersold, R.H., Collins, B.C., and Meyer, H. (2018). AP-SWATH reveals direct involvement of VCP/p97 in integrated stress response signaling through facilitating CReP/PPP1R15B degradation.

Hunter, T. (2007). The age of crosstalk: phosphorylation, ubiquitination, and beyond. Mol Cell *28*, 730-738.

Hurley, T.D., Yang, J., Zhang, L., Goodwin, K.D., Zou, Q., Cortese, M., Dunker, A.K., and DePaoli-Roach, A.A. (2007). Structural basis for regulation of protein phosphatase 1 by inhibitor-2. J Biol Chem *282*, 28874-28883.

Hutchinson, J.A., Shanware, N.P., Chang, H., and Tibbetts, R.S. (2011). Regulation of ribosomal protein S6 phosphorylation by casein kinase 1 and protein phosphatase 1. J Biol Chem *286*, 8688-8696.

Hyer, M.L., Milhollen, M.A., Ciavarri, J., Fleming, P., Traore, T., Sappal, D., Huck, J., Shi, J., Gavin, J., Brownell, J.*, et al.* (2018). A small-molecule inhibitor of the ubiquitin activating enzyme for cancer treatment. Nat Med *24*, 186-193.

Ingebritsen, T.S., and Cohen, P. (1983a). The protein phosphatases involved in cellular regulation. 1. Classification and substrate specificities. Eur J Biochem *132*, 255-261.

Ingebritsen, T.S., and Cohen, P. (1983b). Protein phosphatases: properties and role in cellular regulation. Science *221*, 331-338.

Ingebritsen, T.S., Foulkes, J.G., and Cohen, P. (1980). The broad specificity protein phosphatase from mammalian liver. Separation of the Mr 35 000 catalytic subunit into two distinct enzymes. FEBS Lett *119*, 9-15.

Isono, M., Niimi, A., Oike, T., Hagiwara, Y., Sato, H., Sekine, R., Yoshida, Y., Isobe, S.Y., Obuse, C., Nishi, R.*, et al.* (2017). BRCA1 Directs the Repair Pathway to Homologous Recombination by Promoting 53BP1 Dephosphorylation. Cell Rep *18*, 520-532.

Jackson, M.D., and Denu, J.M. (2001). Molecular Reactions of Protein PhosphatasesInsights from Structure and Chemistry. Chemical Reviews *101*, 2313-2340.

Jagiello, I., Van Eynde, A., Vulsteke, V., Beullens, M., Boudrez, A., Keppens, S., Stalmans, W., and Bollen, M. (2000). Nuclear and subnuclear targeting sequences of the protein phosphatase-1 regulator NIPP1. J Cell Sci *113 Pt 21*, 3761-3768.

Jenni, S., and Harrison, S.C. (2018). Structure of the DASH/Dam1 complex shows its role at the yeast kinetochore-microtubule interface. Science *360*, 552-558.

Jentsch, S., and Rumpf, S. (2007). Cdc48 (p97): a "molecular gearbox" in the ubiquitin pathway? Trends Biochem Sci *32*, 6-11.

Jin, H., Sperka, T., Herrlich, P., and Morrison, H. (2006). Tumorigenic transformation by CPI-17 through inhibition of a merlin phosphatase. Nature *442*, 576-579.

Joglekar, A.P., Bouck, D.C., Molk, J.N., Bloom, K.S., and Salmon, E.D. (2006). Molecular architecture of a kinetochore-microtubule attachment site. Nat Cell Biol *8*, 581-585.

Kaneko, Y., Tamura, K., Totsukawa, G., and Kondo, H. (2010). Phosphorylation of p37 is important for Golgi disassembly at mitosis. Biochem Biophys Res Commun *402*, 37-41.

Katoh, H., Harada, A., Mori, K., and Negishi, M. (2002). Socius is a novel Rnd GTPase-interacting protein involved in disassembly of actin stress fibers. Mol Cell Biol *22*, 2952-2964.

Kennedy, M.J., Hughes, R.M., Peteya, L.A., Schwartz, J.W., Ehlers, M.D., and Tucker, C.L. (2010). Rapid blue-light-mediated induction of protein interactions in living cells. Nat Methods *7*, 973-975.

Kloppsteck, P., Ewens, C.A., Forster, A., Zhang, X., and Freemont, P.S. (2012). Regulation of p97 in the ubiquitin-proteasome system by the UBX protein-family. Biochimica et biophysica acta *1823*, 125-129.

Klumpp, S., and Krieglstein, J. (2009). Reversible phosphorylation of histidine residues in proteins from vertebrates. Sci Signal *2*, pe13.

Kobe, B., and Kajava, A.V. (2001). The leucine-rich repeat as a protein recognition motif. Curr Opin Struct Biol *11*, 725-732.

Koller, K.J., and Brownstein, M.J. (1987). Use of a cDNA clone to identify a supposed precursor protein containing valosin. Nature *325*, 542-545.

Komander, D. (2009). The emerging complexity of protein ubiquitination. Biochem Soc Trans *37*, 937-953.

Kondo, H., Rabouille, C., Newman, R., Levine, T.P., Pappin, D., Freemont, P., and Warren, G. (1997). p47 is a cofactor for p97-mediated membrane fusion. Nature *388*, 75-78.

Kong, M., Ditsworth, D., Lindsten, T., and Thompson, C.B. (2009). Alpha4 is an essential regulator of PP2A phosphatase activity. Mol Cell *36*, 51-60.

Kothe, M., Ye, Y., Wagner, J.S., De Luca, H.E., Kern, E., Rapoport, T.A., and Lencer, W.I. (2005). Role of p97 AAA-ATPase in the retrotranslocation of the cholera toxin A1 chain, a non-ubiquitinated substrate. J Biol Chem *280*, 28127-28132.

Krecic, A.M., and Swanson, M.S. (1999). hnRNP complexes: composition, structure, and function. Curr Opin Cell Biol *11*, 363-371.

Krenn, V., Overlack, K., Primorac, I., van Gerwen, S., and Musacchio, A. (2014). KI motifs of human Knl1 enhance assembly of comprehensive spindle checkpoint complexes around MELT repeats. Curr Biol *24*, 29-39.

Kress, E., Schwager, F., Holtackers, R., Seiler, J., Prodon, F., Zanin, E., Eiteneuer, A., Toya, M., Sugimoto, A., Meyer, H.*, et al.* (2013). The UBXN-2/p37/p47 adaptors of CDC-48/p97 regulate mitosis by limiting the centrosomal recruitment of Aurora A. J Cell Biol *201*, 559-575.

Krick, R., Bremer, S., Welter, E., Schlotterhose, P., Muehe, Y., Eskelinen, E.L., and Thumm, M. (2010). Cdc48/p97 and Shp1/p47 regulate autophagosome biogenesis in concert with ubiquitin-like Atg8. J Cell Biol *190*, 965-973.

Krishna, S.S., Majumdar, I., and Grishin, N.V. (2003). Structural classification of zinc fingers: survey and summary. Nucleic Acids Res *31*, 532-550.

Kunda, P., Rodrigues, N.T., Moeendarbary, E., Liu, T., Ivetic, A., Charras, G., and Baum, B. (2012). PP1-mediated moesin dephosphorylation couples polar relaxation to mitotic exit. Curr Biol *22*, 231-236.

Lampson, M.A., and Cheeseman, I.M. (2011). Sensing centromere tension: Aurora B and the regulation of kinetochore function. Trends Cell Biol *21*, 133-140.

Latterich, M., Frohlich, K.U., and Schekman, R. (1995). Membrane fusion and the cell cycle: Cdc48p participates in the fusion of ER membranes. Cell *82*, 885-893.

Le, L.T., Kang, W., Kim, J.Y., Le, O.T., Lee, S.Y., and Yang, J.K. (2016). Structural Details of Ufd1 Binding to p97 and Their Functional Implications in ER-Associated Degradation. PLoS One *11*, e0163394.

Lee, B.H., Schwager, F., Meraldi, P., and Gotta, M. (2018). p37/UBXN2B regulates spindle orientation by limiting cortical NuMA recruitment via PP1/Repo-Man. J Cell Biol *217*, 483-493.

Lesage, B., Beullens, M., Pedelini, L., Garcia-Gimeno, M.A., Waelkens, E., Sanz, P., and Bollen, M. (2007). A complex of catalytically inactive protein phosphatase-1 sandwiched between Sds22 and inhibitor-3. Biochemistry *46*, 8909-8919.

Li, H., Rokavec, M., Jiang, L., Horst, D., and Hermeking, H. (2017). Antagonistic Effects of p53 and HIF1A on microRNA-34a Regulation of PPP1R11 and STAT3 and Hypoxia-induced Epithelial to Mesenchymal Transition in Colorectal Cancer Cells. Gastroenterology *153*, 505-520.

Li, J.M., Wu, H., Zhang, W., Blackburn, M.R., and Jin, J. (2014). The p97-UFD1L-NPL4 protein complex mediates cytokine-induced IkappaBalpha proteolysis. Mol Cell Biol *34*, 335-347.

Lim, H.H., Zhang, T., and Surana, U. (2009). Regulation of centrosome separation in yeast and vertebrates: common threads. Trends Cell Biol *19*, 325-333.

Linding, R., Jensen, L.J., Diella, F., Bork, P., Gibson, T.J., and Russell, R.B. (2003). Protein disorder prediction: implications for structural proteomics. Structure *11*, 1453-1459.

Littlepage, L.E., Wu, H., Andresson, T., Deanehan, J.K., Amundadottir, L.T., and Ruderman, J.V. (2002). Identification of phosphorylated residues that affect the activity of the mitotic kinase Aurora-A. Proc Natl Acad Sci U S A *99*, 15440-15445.

Liu, D., Vleugel, M., Backer, C.B., Hori, T., Fukagawa, T., Cheeseman, I.M., and Lampson, M.A. (2010). Regulated targeting of protein phosphatase 1 to the outer kinetochore by KNL1 opposes Aurora B kinase. J Cell Biol *188*, 809-820.

Liu, H., Krizek, J., and Bretscher, A. (1992). Construction of a GAL1-regulated yeast cDNA expression library and its application to the identification of genes whose overexpression causes lethality in yeast. Genetics *132*, 665-673.

Liu, Y. (2005). Analysis of posttranslational regulations in the Neurospora circadian clock. Methods Enzymol *393*, 379-393.

Llorian, M., Beullens, M., Andres, I., Ortiz, J.M., and Bollen, M. (2004). SIPP1, a novel pre-mRNA splicing factor and interactor of protein phosphatase-1. Biochem J *378*, 229-238.

Logan, M.R., Nguyen, T., Szapiel, N., Knockleby, J., Por, H., Zadworny, M., Neszt, M., Harrison, P., Bussey, H., Mandato, C.A.*, et al.* (2008). Genetic interaction network of the *Saccharomyces cerevisiae* type 1 phosphatase Glc7. BMC Genomics *9*, 336.

London, N., Ceto, S., Ranish, J.A., and Biggins, S. (2012). Phosphoregulation of Spc105 by Mps1 and PP1 regulates Bub1 localization to kinetochores. Curr Biol *22*, 900-906.

Loubery, S., Daeden, A., Seum, C., Holtzer, L., Moraleda, A., Damond, N., Derivery, E., Schmidt, T., and Gonzalez-Gaitan, M. (2017). Sara phosphorylation state controls the dispatch of endosomes from the central spindle during asymmetric division. Nat Commun *8*, 15285.

MacKelvie, S.H., Andrews, P.D., and Stark, M.J. (1995). The *Saccharomyces cerevisiae* gene SDS22 encodes a potential regulator of the mitotic function of yeast type 1 protein phosphatase. Mol Cell Biol *15*, 3777-3785.

Magnaghi, P., D'Alessio, R., Valsasina, B., Avanzi, N., Rizzi, S., Asa, D., Gasparri, F., Cozzi, L., Cucchi, U., Orrenius, C.*, et al.* (2013). Covalent and allosteric inhibitors of the ATPase VCP/p97 induce cancer cell death. Nat Chem Biol *9*, 548-556.

Marquina, M., Queralt, E., Casamayor, A., and Arino, J. (2012). Lack of the Glc7 phosphatase regulatory subunit Ypi1 activates the morphogenetic checkpoint. Int J Biochem Cell Biol *44*, 1862-1871.

McKelvey, A.C., Lear, T.B., Dunn, S.R., Evankovich, J., Londino, J.D., Bednash, J.S., Zhang, Y., McVerry, B.J., Liu, Y., and Chen, B.B. (2016). RING finger E3 ligase PPP1R11 regulates TLR2 signaling and innate immunity. Elife *5*.

Meadows, J.C., Shepperd, L.A., Vanoosthuyse, V., Lancaster, T.C., Sochaj, A.M., Buttrick, G.J., Hardwick, K.G., and Millar, J.B. (2011). Spindle checkpoint silencing requires association of PP1 to both Spc7 and kinesin-8 motors. Dev Cell *20*, 739-750.

Meyer, H., Bug, M., and Bremer, S. (2012). Emerging functions of the VCP/p97 AAA-ATPase in the ubiquitin system. Nat Cell Biol *14*, 117-123.

Meyer, H., and Popp, O. (2008). Role(s) of Cdc48/p97 in mitosis. Biochem Soc Trans *36*, 126-130.

Meyer, H.H., Kondo, H., and Warren, G. (1998). The p47 co-factor regulates the ATPase activity of the membrane fusion protein, p97. FEBS Lett *437*, 255-257.

Meyer, H.H., Shorter, J.G., Seemann, J., Pappin, D., and Warren, G. (2000). A complex of mammalian ufd1 and npl4 links the AAA-ATPase, p97, to ubiquitin and nuclear transport pathways. Embo j *19*, 2181-2192.

Meyer, H.H., Wang, Y., and Warren, G. (2002). Direct binding of ubiquitin conjugates by the mammalian p97 adaptor complexes, p47 and Ufd1-Npl4. Embo j *21*, 5645-5652.

Minshull, J., Murray, A., Colman, A., and Hunt, T. (1991). *Xenopus* oocyte maturation does not require new cyclin synthesis. J Cell Biol *114*, 767-772.

Mita, P., Savas, J.N., Ha, S., Djouder, N., Yates, J.R., 3rd, and Logan, S.K. (2013). Analysis of URI nuclear interaction with RPB5 and components of the R2TP/prefoldin-like complex. PLoS One *8*, e63879.

Mizuguchi, M., Obita, T., Serita, T., Kojima, R., Nabeshima, Y., and Okazawa, H. (2014). Mutations in the PQBP1 gene prevent its interaction with the spliceosomal protein U5-15 kD. Nat Commun *5*, 3822.

Moir, D., Stewart, S.E., Osmond, B.C., and Botstein, D. (1982). Cold-sensitive cell-division-cycle mutants of yeast: isolation, properties, and pseudoreversion studies. Genetics *100*, 547-563.

Moorhead, G.B., De Wever, V., Templeton, G., and Kerk, D. (2009). Evolution of protein phosphatases in plants and animals. Biochem J *417*, 401-409.

Morello, L.G., Coltri, P.P., Quaresma, A.J., Simabuco, F.M., Silva, T.C., Singh, G., Nickerson, J.A., Oliveira, C.C., Moore, M.J., and Zanchin, N.I. (2011). The human nucleolar protein FTSJ3 associates with NIP7 and functions in pre-rRNA processing. PLoS One *6*, e29174.

Moura, M., Osswald, M., Leça, N., Barbosa, J., Pereira, A.J., Maiato, H., Sunkel, C.E., and Conde, C. (2017). Protein Phosphatase 1 inactivates Mps1 to ensure efficient Spindle Assembly Checkpoint silencing. In eLife.

Muller, J.M., Shorter, J., Newman, R., Deinhardt, K., Sagiv, Y., Elazar, Z., Warren, G., and Shima, D.T. (2002). Sequential SNARE disassembly and GATE-16-GOS-28 complex assembly mediated by distinct NSF activities drives Golgi membrane fusion. J Cell Biol *157*, 1161-1173.

Musacchio, A. (2015). The Molecular Biology of Spindle Assembly Checkpoint Signaling Dynamics. Curr Biol *25*, R1002-1018.

Nasa, I., and Kettenbach, A.N. (2018). Coordination of Protein Kinase and Phosphoprotein Phosphatase Activities in Mitosis. Front Cell Dev Biol *6*, 30.

Nasa, I., Rusin, S.F., Kettenbach, A.N., and Moorhead, G.B. (2018). Aurora B opposes PP1 function in mitosis by phosphorylating the conserved PP1-binding RVxF motif in PP1 regulatory proteins. Sci Signal *11*.

Nicolaescu, E., Beullens, M., Lesage, B., Keppens, S., Himpens, B., and Bollen, M. (2008). Nature of the nuclear inclusions formed by PQBP1, a protein linked to neurodegenerative polyglutamine diseases. Eur J Cell Biol *87*, 817-829.

Nigavekar, S.S., Tan, Y.S., and Cannon, J.F. (2002). Glc8 is a glucose-repressible activator of Glc7 protein phosphatase-1. Arch Biochem Biophys *404*, 71-79.

Novoyatleva, T., Heinrich, B., Tang, Y., Benderska, N., Butchbach, M.E., Lorson, C.L., Lorson, M.A., Ben-Dov, C., Fehlbaum, P., Bracco, L.*, et al.* (2008). Protein phosphatase 1 binds to the RNA recognition motif of several splicing factors and regulates alternative pre-mRNA processing. Hum Mol Genet *17*, 52-70.

Ogura, T., and Wilkinson, A.J. (2001). AAA+ superfamily ATPases: common structure--diverse function. Genes to cells : devoted to molecular & cellular mechanisms *6*, 575-597.

Ohkura, H., Kinoshita, N., Miyatani, S., Toda, T., and Yanagida, M. (1989). The fission yeast dis2+ gene required for chromosome disjoining encodes one of two putative type 1 protein phosphatases. Cell *57*, 997-1007.

Ohkura, H., and Yanagida, M. (1991). *S. pombe* gene sds22+ essential for a midmitotic transition encodes a leucine-rich repeat protein that positively modulates protein phosphatase-1. Cell *64*, 149-157.

Pakos-Zebrucka, K., Koryga, I., Mnich, K., Ljujic, M., Samali, A., and Gorman, A.M. (2016). The integrated stress response. EMBO Rep *17*, 1374-1395.

Pantazopoulou, M., Boban, M., Foisner, R., and Ljungdahl, P.O. (2016). Cdc48 and Ubx1 participate in a pathway associated with the inner nuclear membrane that governs Asi1 degradation. J Cell Sci *129*, 3770-3780.

Papadopoulos, C., Kirchner, P., Bug, M., Grum, D., Koerver, L., Schulze, N., Poehler, R., Dressler, A., Fengler, S., Arhzaouy, K.*, et al.* (2017). VCP/p97 cooperates with YOD1, UBXD1 and PLAA to drive clearance of ruptured lysosomes by autophagy. Embo j *36*, 135-150.

Parisi, E., Yahya, G., Flores, A., and Aldea, M. (2018). Cdc48/p97 segregase is modulated by cyclin-dependent kinase to determine cyclin fate during G1 progression. Embo j.

Patel, S., and Latterich, M. (1998). The AAA team: related ATPases with diverse functions. Trends Cell Biol *8*, 65-71.

Pedelini, L., Marquina, M., Arino, J., Casamayor, A., Sanz, L., Bollen, M., Sanz, P., and Garcia-Gimeno, M.A. (2007). YPI1 and SDS22 proteins regulate the nuclear localization and function of yeast type 1 phosphatase Glc7. J Biol Chem *282*, 3282-3292.

Peggie, M.W., MacKelvie, S.H., Bloecher, A., Knatko, E.V., Tatchell, K., and Stark, M.J. (2002). Essential functions of Sds22p in chromosome stability and nuclear localization of PP1. J Cell Sci *115*, 195-206.

Peng, J., Schwartz, D., Elias, J.E., Thoreen, C.C., Cheng, D., Marsischky, G., Roelofs, J., Finley, D., and Gygi, S.P. (2003). A proteomics approach to understanding protein ubiquitination. Nat Biotechnol *21*, 921-926.

Peng, Z.Y., Trumbly, R.J., and Reimann, E.M. (1990). Purification and characterization of glycogen synthase from a glycogen-deficient strain of *Saccharomyces cerevisiae*. J Biol Chem *265*, 13871-13877.

Peters, C., Andrews, P.D., Stark, M.J., Cesaro-Tadic, S., Glatz, A., Podtelejnikov, A., Mann, M., and Mayer, A. (1999). Control of the terminal step of intracellular membrane fusion by protein phosphatase 1. Science *285*, 1084-1087.

Peters, J.M., Walsh, M.J., and Franke, W.W. (1990). An abundant and ubiquitous homo-oligomeric ring-shaped ATPase particle related to the putative vesicle fusion proteins Sec18p and NSF. Embo j *9*, 1757-1767.

Peti, W., Nairn, A.C., and Page, R. (2013). Structural basis for protein phosphatase 1 regulation and specificity. FEBS J *280*, 596-611.

Pickart, C.M. (1997). Targeting of substrates to the 26S proteasome. FASEB journal : official publication of the Federation of American Societies for Experimental Biology *11*, 1055-1066.

Pinsky, B.A., Kotwaliwale, C.V., Tatsutani, S.Y., Breed, C.A., and Biggins, S. (2006). Glc7/protein phosphatase 1 regulatory subunits can oppose the Ipl1/aurora protein kinase by redistributing Glc7. Mol Cell Biol *26*, 2648-2660.

Posch, M., Khoudoli, G.A., Swift, S., King, E.M., Deluca, J.G., and Swedlow, J.R. (2010). Sds22 regulates aurora B activity and microtubule-kinetochore interactions at mitosis. J Cell Biol *191*, 61-74.

Poulsen, M., Lukas, C., Lukas, J., Bekker-Jensen, S., and Mailand, N. (2012). Human RNF169 is a negative regulator of the ubiquitin-dependent response to DNA double-strand breaks. J Cell Biol *197*, 189-199.

Qian, J., Lesage, B., Beullens, M., Van Eynde, A., and Bollen, M. (2011). PP1/Repo-man dephosphorylates mitotic histone H3 at T3 and regulates chromosomal aurora B targeting. Curr Biol *21*, 766-773.

Rabouille, C., Kondo, H., Newman, R., Hui, N., Freemont, P., and Warren, G. (1998). Syntaxin 5 is a common component of the NSF- and p97-mediated reassembly pathways of Golgi cisternae from mitotic Golgi fragments *in vitro*. Cell *92*, 603-610.

Rabouille, C., Levine, T.P., Peters, J.M., and Warren, G. (1995). An NSF-like ATPase, p97, and NSF mediate cisternal regrowth from mitotic Golgi fragments. Cell *82*, 905-914.

Ragusa, M.J., Dancheck, B., Critton, D.A., Nairn, A.C., Page, R., and Peti, W. (2010). Spinophilin directs protein phosphatase 1 specificity by blocking substrate binding sites. Nat Struct Mol Biol *17*, 459-464.

Ramadan, K., Bruderer, R., Spiga, F.M., Popp, O., Baur, T., Gotta, M., and Meyer, H.H. (2007). Cdc48/p97 promotes reformation of the nucleus by extracting the kinase Aurora B from chromatin. Nature *450*, 1258-1262.

Raman, M., Sergeev, M., Garnaas, M., Lydeard, J.R., Huttlin, E.L., Goessling, W., Shah, J.V., and Harper, J.W. (2015). Systematic proteomics of the VCP-UBXD adaptor network identifies a role for UBXN10 in regulating ciliogenesis. Nat Cell Biol *17*, 1356-1369.

Ramaswamy, N.T., Li, L., Khalil, M., and Cannon, J.F. (1998). Regulation of yeast glycogen metabolism and sporulation by Glc7p protein phosphatase. Genetics *149*, 57-72.

Rape, M., Hoppe, T., Gorr, I., Kalocay, M., Richly, H., and Jentsch, S. (2001). Mobilization of processed, membrane-tethered SPT23 transcription factor by CDC48(UFD1/NPL4), a ubiquitin-selective chaperone. Cell *107*, 667-677.

Ravindran, R., Polk, P., Robinson, L.C., and Tatchell, K. (2018). New ubiquitin-dependent mechanisms regulating the Aurora B-protein phosphatase 1 balance in *Saccharomyces cerevisiae*. J Cell Sci *131*.

Rebelo, S., Santos, M., Martins, F., da Cruz e Silva, E.F., and da Cruz e Silva, O.A. (2015). Protein phosphatase 1 is a key player in nuclear events. Cell Signal *27*, 2589-2598.

Renvoise, B., Querol, G., Verrier, E.R., Burlet, P., and Lefebvre, S. (2012). A role for protein phosphatase PP1gamma in SMN complex formation and subnuclear localization to Cajal bodies. J Cell Sci *125*, 2862-2874.

Rezvani, K., Teng, Y., Pan, Y., Dani, J.A., Lindstrom, J., Garcia Gras, E.A., McIntosh, J.M., and De Biasi, M. (2009). UBXD4, a UBX-containing protein, regulates the cell surface number and stability of alpha3-containing nicotinic acetylcholine receptors. The Journal of neuroscience : the official journal of the Society for Neuroscience *29*, 6883-6896.

Riemer, A., Dobrynin, G., Dressler, A., Bremer, S., Soni, A., Iliakis, G., and Meyer, H. (2014). The p97-Ufd1-Npl4 ATPase complex ensures robustness of the G2/M checkpoint by facilitating CDC25A degradation. Cell cycle (Georgetown, Tex) *13*, 919-927.

Ritz, D., Vuk, M., Kirchner, P., Bug, M., Schutz, S., Hayer, A., Bremer, S., Lusk, C., Baloh, R.H., Lee, H.*, et al.* (2011). Endolysosomal sorting of ubiquitylated caveolin-1 is regulated by VCP and UBXD1 and impaired by VCP disease mutations. Nat Cell Biol *13*, 1116-1123.

Robinson, L.C., Phillips, J., Brou, L., Boswell, E.P., and Tatchell, K. (2012). Suppressors of ipl1-2 in components of a Glc7 phosphatase complex, Cdc48 AAA ATPase, TORC1, and the kinetochore. G3 (Bethesda) *2*, 1687-1701.

Rodrigues, N.T., Lekomtsev, S., Jananji, S., Kriston-Vizi, J., Hickson, G.R., and Baum, B. (2015). Kinetochore-localized PP1-Sds22 couples chromosome segregation to polar relaxation. Nature *524*, 489-492.

Rogers, S., Fey, D., McCloy, R.A., Parker, B.L., Mitchell, N.J., Payne, R.J., Daly, R.J., James, D.E., Caldon, C.E., Watkins, D.N.*, et al.* (2016). PP1 initiates the dephosphorylation of MASTL, triggering mitotic exit and bistability in human cells. J Cell Sci *129*, 1340-1354.

Rosenberg, J.S., Cross, F.R., and Funabiki, H. (2011). KNL1/Spc105 recruits PP1 to silence the spindle assembly checkpoint. Curr Biol *21*, 942-947.

Rost, B., Yachdav, G., and Liu, J. (2004). The PredictProtein server. Nucleic Acids Res *32*, W321-326.

Roy, J., and Cyert, M.S. (2009). Cracking the phosphatase code: docking interactions determine substrate specificity. Sci Signal *2*, re9.

Ryu, J.K., Min, D., Rah, S.H., Kim, S.J., Park, Y., Kim, H., Hyeon, C., Kim, H.M., Jahn, R., and Yoon, T.Y. (2015). Spring-loaded unraveling of a single SNARE complex by NSF in one round of ATP turnover. Science *347*, 1485-1489.

Sang, T.K., and Ready, D.F. (2002). Eyes closed, a Drosophila p47 homolog, is essential for photoreceptor morphogenesis. Development (Cambridge, England) *129*, 143-154.

Sassoon, I., Severin, F.F., Andrews, P.D., Taba, M.R., Kaplan, K.B., Ashford, A.J., Stark, M.J., Sorger, P.K., and Hyman, A.A. (1999). Regulation of *Saccharomyces cerevisiae* kinetochores by the type 1 phosphatase Glc7p. Genes Dev *13*, 545-555.

Satinover, D.L., Leach, C.A., Stukenberg, P.T., and Brautigan, D.L. (2004). Activation of Aurora-A kinase by protein phosphatase inhibitor-2, a bifunctional signaling protein. Proc Natl Acad Sci U S A *101*, 8625-8630.

Sauer, R.T., Bolon, D.N., Burton, B.M., Burton, R.E., Flynn, J.M., Grant, R.A., Hersch, G.L., Joshi, S.A., Kenniston, J.A., Levchenko, I.*, et al.* (2004). Sculpting the proteome with AAA(+) proteases and disassembly machines. Cell *119*, 9-18.

Scazzari, M., Amm, I., and Wolf, D.H. (2015). Quality control of a cytoplasmic protein complex: chaperone motors and the ubiquitin-proteasome system govern the fate of orphan fatty acid synthase subunit Fas2 of yeast. J Biol Chem *290*, 4677-4687.

Schirmer, E.C., Glover, J.R., Singer, M.A., and Lindquist, S. (1996). HSP100/Clp proteins: a common mechanism explains diverse functions. Trends Biochem Sci *21*, 289-296.

Schmidt, J.C., Kiyomitsu, T., Hori, T., Backer, C.B., Fukagawa, T., and Cheeseman, I.M. (2010). Aurora B kinase controls the targeting of the Astrin-SKAP complex to bioriented kinetochores. J Cell Biol *191*, 269-280.

Schuberth, C., and Buchberger, A. (2008). UBX domain proteins: major regulators of the AAA ATPase Cdc48/p97. Cell Mol Life Sci *65*, 2360-2371.

Schuberth, C., Richly, H., Rumpf, S., and Buchberger, A. (2004). Shp1 and Ubx2 are adaptors of Cdc48 involved in ubiquitin-dependent protein degradation. EMBO Rep *5*, 818-824.

Seifried, A., Schultz, J., and Gohla, A. (2013). Human HAD phosphatases: structure, mechanism, and roles in health and disease. FEBS J *280*, 549-571.

Sents, W., Ivanova, E., Lambrecht, C., Haesen, D., and Janssens, V. (2013). The biogenesis of active protein phosphatase 2A holoenzymes: a tightly regulated process creating phosphatase specificity. FEBS J *280*, 644-661.

Sharma, K., D'Souza, R.C., Tyanova, S., Schaab, C., Wisniewski, J.R., Cox, J., and Mann, M. (2014). Ultradeep human phosphoproteome reveals a distinct regulatory nature of Tyr and Ser/Thr-based signaling. Cell Rep *8*, 1583-1594.

Shibata, Y., Oyama, M., Kozuka-Hata, H., Han, X., Tanaka, Y., Gohda, J., and Inoue, J. (2012). p47 negatively regulates IKK activation by inducing the lysosomal degradation of polyubiquitinated NEMO. Nat Commun *3*, 1061.

Shimada, M., and Nakanishi, M. (2013). Response to DNA damage: why do we need to focus on protein phosphatases? Front Oncol *3*, 8.

Silva, J.V., Freitas, M.J., and Fardilha, M. (2014). Phosphoprotein phosphatase 1 complexes in spermatogenesis. Curr Mol Pharmacol *7*, 136-146.

Sivakumar, S., Janczyk, P.L., Qu, Q., Brautigam, C.A., Stukenberg, P.T., Yu, H., and Gorbsky, G.J. (2016). The human SKA complex drives the metaphase-anaphase cell cycle transition by recruiting protein phosphatase 1 to kinetochores. Elife *5*.

Smith, D.M., Chang, S.C., Park, S., Finley, D., Cheng, Y., and Goldberg, A.L. (2007). Docking of the proteasomal ATPases' carboxyl termini in the 20S proteasome's alpha ring opens the gate for substrate entry. Mol Cell *27*, 731-744.

Smolka, M.B., Albuquerque, C.P., Chen, S.H., and Zhou, H. (2007). Proteome-wide identification of *in vivo* targets of DNA damage checkpoint kinases. Proc Natl Acad Sci U S A *104*, 10364-10369.

So, J.S., Cho, S., Min, S.H., Kimball, S.R., and Lee, A.H. (2015). IRE1alpha-Dependent Decay of CReP/Ppp1r15b mRNA Increases Eukaryotic Initiation Factor 2alpha Phosphorylation and Suppresses Protein Synthesis. Mol Cell Biol *35*, 2761-2770.

Sollner, T., Whiteheart, S.W., Brunner, M., Erdjument-Bromage, H., Geromanos, S., Tempst, P., and Rothman, J.E. (1993). SNAP receptors implicated in vesicle targeting and fusion. Nature *362*, 318-324.

Solyom, S., Aressy, B., Pylkas, K., Patterson-Fortin, J., Hartikainen, J.M., Kallioniemi, A., Kauppila, S., Nikkila, J., Kosma, V.M., Mannermaa, A.*, et al.* (2012). Breast cancer-associated Abraxas mutation disrupts nuclear localization and DNA damage response functions. Sci Transl Med *4*, 122ra123.

St-Denis, N., Gupta, G.D., Lin, Z.Y., Gonzalez-Badillo, B., Veri, A.O., Knight, J.D.R., Rajendran, D., Couzens, A.L., Currie, K.W., Tkach, J.M.*, et al.* (2016). Phenotypic and Interaction Profiling of the Human Phosphatases Identifies Diverse Mitotic Regulators. Cell Rep *17*, 2488-2501.

Stach, L., and Freemont, P.S. (2017). The AAA+ ATPase p97, a cellular multitool. Biochem J *474*, 2953-2976.

Starita, L.M., Lo, R.S., Eng, J.K., von Haller, P.D., and Fields, S. (2012). Sites of ubiquitin attachment in *Saccharomyces cerevisiae*. Proteomics *12*, 236-240.

Stone, E.M., Yamano, H., Kinoshita, N., and Yanagida, M. (1993). Mitotic regulation of protein phosphatases by the fission yeast sds22 protein. Curr Biol *3*, 13-26.

Stralfors, P., Hiraga, A., and Cohen, P. (1985). The protein phosphatases involved in cellular regulation. Purification and characterisation of the glycogen-bound form of protein phosphatase-1 from rabbit skeletal muscle. Eur J Biochem *149*, 295-303.

Sudakin, V., Ganoth, D., Dahan, A., Heller, H., Hershko, J., Luca, F.C., Ruderman, J.V., and Hershko, A. (1995). The cyclosome, a large complex containing cyclin-selective ubiquitin ligase activity, targets cyclins for destruction at the end of mitosis. Mol Biol Cell *6*, 185-197.

Sullivan, M., and Morgan, D.O. (2007). Finishing mitosis, one step at a time. Nat Rev Mol Cell Biol *8*, 894-903.

Swingle, M.R., Honkanen, R.E., and Ciszak, E.M. (2004). Structural basis for the catalytic activity of human serine/threonine protein phosphatase-5. J Biol Chem *279*, 33992-33999.

Tang, P.M., Bondor, J.A., Swiderek, K.M., and DePaoli-Roach, A.A. (1991). Molecular cloning and expression of the regulatory (RG1) subunit of the glycogen-associated protein phosphatase. J Biol Chem *266*, 15782-15789.

Teng, Y., Rezvani, K., and De Biasi, M. (2015). UBXN2A regulates nicotinic receptor degradation by modulating the E3 ligase activity of CHIP. Biochemical pharmacology *97*, 518-530.

Terrak, M., Kerff, F., Langsetmo, K., Tao, T., and Dominguez, R. (2004). Structural basis of protein phosphatase 1 regulation. Nature *429*, 780-784.

Thoms, S. (2002). Cdc48 can distinguish between native and non-native proteins in the absence of cofactors. FEBS Lett *520*, 107-110.

Tomko, R.J., Jr., Funakoshi, M., Schneider, K., Wang, J., and Hochstrasser, M. (2010). Heterohexameric ring arrangement of the eukaryotic proteasomal ATPases: implications for proteasome structure and assembly. Mol Cell *38*, 393-403.

Tresse, E., Salomons, F.A., Vesa, J., Bott, L.C., Kimonis, V., Yao, T.P., Dantuma, N.P., and Taylor, J.P. (2010). VCP/p97 is essential for maturation of ubiquitin-containing autophagosomes and this function is impaired by mutations that cause IBMPFD. Autophagy *6*, 217-227.

Trinkle-Mulcahy, L., Andrews, P.D., Wickramasinghe, S., Sleeman, J., Prescott, A., Lam, Y.W., Lyon, C., Swedlow, J.R., and Lamond, A.I. (2003). Time-lapse imaging reveals dynamic relocalization of PP1gamma throughout the mammalian cell cycle. Mol Biol Cell *14*, 107-117.

Tung, H.Y., Wang, W., and Chan, C.S. (1995). Regulation of chromosome segregation by Glc8p, a structural homolog of mammalian inhibitor 2 that functions as both an activator and an inhibitor of yeast protein phosphatase 1. Mol Cell Biol *15*, 6064-6074.

Tyanova, S., Temu, T., Sinitcyn, P., Carlson, A., Hein, M.Y., Geiger, T., Mann, M., and Cox, J. (2016). The Perseus computational platform for comprehensive analysis of (prote)omics data. Nat Methods *13*, 731-740.

Uchiyama, K., Jokitalo, E., Kano, F., Murata, M., Zhang, X., Canas, B., Newman, R., Rabouille, C., Pappin, D., Freemont, P.*, et al.* (2002). VCIP135, a novel essential factor for p97/p47-mediated membrane fusion, is required for Golgi and ER assembly *in vivo*. J Cell Biol *159*, 855-866.

Uchiyama, K., Jokitalo, E., Lindman, M., Jackman, M., Kano, F., Murata, M., Zhang, X., and Kondo, H. (2003). The localization and phosphorylation of p47 are important for Golgi disassembly-assembly during the cell cycle. J Cell Biol *161*, 1067-1079.

Uchiyama, K., Totsukawa, G., Puhka, M., Kaneko, Y., Jokitalo, E., Dreveny, I., Beuron, F., Zhang, X., Freemont, P., and Kondo, H. (2006). p37 is a p97 adaptor required for Golgi and ER biogenesis in interphase and at the end of mitosis. Dev Cell *11*, 803-816.

van den Boom, J., and Meyer, H. (2018). VCP/p97-Mediated Unfolding as a Principle in Protein Homeostasis and Signaling. Mol Cell *69*, 182-194.

van den Boom, J., Wolf, M., Weimann, L., Schulze, N., Li, F., Kaschani, F., Riemer, A., Zierhut, C., Kaiser, M., Iliakis, G.*, et al.* (2016). VCP/p97 Extracts Sterically Trapped Ku70/80 Rings from DNA in Double-Strand Break Repair. Mol Cell *64*, 189-198.

Van Dessel, N., Beke, L., Gornemann, J., Minnebo, N., Beullens, M., Tanuma, N., Shima, H., Van Eynde, A., and Bollen, M. (2010). The phosphatase interactor NIPP1 regulates the occupancy of the histone methyltransferase EZH2 at Polycomb targets. Nucleic Acids Res *38*, 7500-7512.

Van Dessel, N., Boens, S., Lesage, B., Winkler, C., Gornemann, J., Van Eynde, A., and Bollen, M. (2015). Protein phosphatase PP1-NIPP1 activates mesenchymal genes in HeLa cells. FEBS Lett *589*, 1314-1321.

Varjosalo, M., Sacco, R., Stukalov, A., van Drogen, A., Planyavsky, M., Hauri, S., Aebersold, R., Bennett, K.L., Colinge, J., Gstaiger, M.*, et al.* (2013). Interlaboratory reproducibility of large-scale human protein-complex analysis by standardized AP-MS. Nat Methods *10*, 307-314.

Verbinnen, I., Ferreira, M., and Bollen, M. (2017). Biogenesis and activity regulation of protein phosphatase 1. Biochem Soc Trans *45*, 89-99.

Vereshchagina, N., Bennett, D., Szoor, B., Kirchner, J., Gross, S., Vissi, E., White-Cooper, H., and Alphey, L. (2004). The essential role of PP1beta in Drosophila is to regulate nonmuscle myosin. Mol Biol Cell *15*, 4395-4405.

Virshup, D.M., and Shenolikar, S. (2009). From promiscuity to precision: protein phosphatases get a makeover. Mol Cell *33*, 537-545.

Voges, D., Zwickl, P., and Baumeister, W. (1999). The 26S proteasome: a molecular machine designed for controlled proteolysis. Annual review of biochemistry *68*, 1015-1068.

von Morgen, P., Horejsi, Z., and Macurek, L. (2015). Substrate recognition and function of the R2TP complex in response to cellular stress. Front Genet *6*, 69.

Wakula, P., Beullens, M., Ceulemans, H., Stalmans, W., and Bollen, M. (2003). Degeneracy and function of the ubiquitous RVXF motif that mediates binding to protein phosphatase-1. J Biol Chem *278*, 18817-18823.

Wan, C., Borgeson, B., Phanse, S., Tu, F., Drew, K., Clark, G., Xiong, X., Kagan, O., Kwan, J., Bezginov, A.*, et al.* (2015). Panorama of ancient metazoan macromolecular complexes. Nature *525*, 339-344.

Wang, H., and Brautigan, D.L. (2002). A novel transmembrane Ser/Thr kinase complexes with protein phosphatase-1 and inhibitor-2. J Biol Chem *277*, 49605-49612.

Wang, Q., Moore, M.J., Adelmant, G., Marto, J.A., and Silver, P.A. (2013). PQBP1, a factor linked to intellectual disability, affects alternative splicing associated with neurite outgrowth. Genes Dev *27*, 615-626.

Wang, W., Stukenberg, P.T., and Brautigan, D.L. (2008). Phosphatase inhibitor-2 balances protein phosphatase 1 and aurora B kinase for chromosome segregation and cytokinesis in human retinal epithelial cells. Mol Biol Cell *19*, 4852-4862.

Warren, G. (1993). Membrane partitioning during cell division. Annual review of biochemistry *62*, 323-348.

Waterhouse, A., Bertoni, M., Bienert, S., Studer, G., Tauriello, G., Gumienny, R., Heer, F.T., de Beer, T.A.P., Rempfer, C., Bordoli, L.*, et al.* (2018). SWISS-MODEL: homology modelling of protein structures and complexes. Nucleic Acids Res *46*, W296-W303.

Watkins, G.R., Wang, N., Mazalouskas, M.D., Gomez, R.J., Guthrie, C.R., Kraemer, B.C., Schweiger, S., Spiller, B.W., and Wadzinski, B.E. (2012). Monoubiquitination promotes calpain cleavage of the protein phosphatase 2A (PP2A) regulatory subunit alpha4, altering PP2A stability and microtubule-associated protein phosphorylation. J Biol Chem *287*, 24207-24215.

Weber-Ban, E.U., Reid, B.G., Miranker, A.D., and Horwich, A.L. (1999). Global unfolding of a substrate protein by the Hsp100 chaperone ClpA. Nature *401*, 90-93.

Weith, M., Seiler, J., Van den Boom, J., Kracht, M., Hülsmann, J., Primorac, I., del Pino-Garcia, J., Kaschani, F., Kaiser, M., Musacchio, A.*, et al.* (2018). Ubiquitin-independent disassembly by a p97 AAA-ATPase complex drives PP1 holoenzyme formation. Mol Cell *under revision*.

Welburn, J.P., Grishchuk, E.L., Backer, C.B., Wilson-Kubalek, E.M., Yates, J.R., 3rd, and Cheeseman, I.M. (2009). The human kinetochore Ska1 complex facilitates microtubule depolymerization-coupled motility. Dev Cell *16*, 374-385.

Welburn, J.P., Vleugel, M., Liu, D., Yates, J.R., 3rd, Lampson, M.A., Fukagawa, T., and Cheeseman, I.M. (2010). Aurora B phosphorylates spatially distinct targets to differentially regulate the kinetochore-microtubule interface. Mol Cell *38*, 383-392.

Wendler, P., Ciniawsky, S., Kock, M., and Kube, S. (2012). Structure and function of the AAA+ nucleotide binding pocket. Biochimica et biophysica acta *1823*, 2-14.

Wilson, W.A., Wang, Z., and Roach, P.J. (2005). Regulation of yeast glycogen phosphorylase by the cyclin-dependent protein kinase Pho85p. Biochem Biophys Res Commun *329*, 161-167.

Winkler, C., De Munter, S., Van Dessel, N., Lesage, B., Heroes, E., Boens, S., Beullens, M., Van Eynde, A., and Bollen, M. (2015). The selective inhibition of protein phosphatase-1 results in mitotic catastrophe and impaired tumor growth. J Cell Sci *128*, 4526-4537.

Wojcik, C., Yano, M., and DeMartino, G.N. (2004). RNA interference of valosin-containing protein (VCP/p97) reveals multiple cellular roles linked to ubiquitin/proteasome-dependent proteolysis. J Cell Sci *117*, 281-292.

Wordeman, L. (2010). How kinesin motor proteins drive mitotic spindle function: Lessons from molecular assays. Semin Cell Dev Biol *21*, 260-268.

Wurzenberger, C., Held, M., Lampson, M.A., Poser, I., Hyman, A.A., and Gerlich, D.W. (2012). Sds22 and Repo-Man stabilize chromosome segregation by counteracting Aurora B on anaphase kinetochores. J Cell Biol *198*, 173-183.

Xiao, L., Chen, Y., Ji, M., Volle, D.J., Lewis, R.E., Tsai, M.Y., and Dong, J. (2011). KIBRA protein phosphorylation is regulated by mitotic kinase aurora and protein phosphatase 1. J Biol Chem *286*, 36304-36315.

Xu, Y., Anderson, D.E., and Ye, Y. (2016). The HECT domain ubiquitin ligase HUWE1 targets unassembled soluble proteins for degradation. Cell discovery *2*, 16040.

Yadav, L., Tamene, F., Goos, H., van Drogen, A., Katainen, R., Aebersold, R., Gstaiger, M., and Varjosalo, M. (2017). Systematic Analysis of Human Protein Phosphatase Interactions and Dynamics. Cell Syst *4*, 430-444 e435.

Yang, S.D., Vandenheede, J.R., and Merlevede, W. (1981). Identification of inhibitor-2 as the ATP-mg-dependent protein phosphatase modulator. J Biol Chem *256*, 10231-10234.

Yang, Y., Primrose, D.A., Leung, A.C., Fitzsimmons, R.B., McDermand, M.C., Missellbrook, A., Haskins, J., Smylie, A.S., and Hughes, S.C. (2012). The PP1 phosphatase flapwing regulates the activity of Merlin and Moesin in Drosophila. Dev Biol *361*, 412-426.

Ye, Y. (2006). Diverse functions with a common regulator: ubiquitin takes command of an AAA ATPase. Journal of structural biology *156*, 29-40.

Ye, Y., Meyer, H.H., and Rapoport, T.A. (2001). The AAA ATPase Cdc48/p97 and its partners transport proteins from the ER into the cytosol. Nature *414*, 652-656.

Ye, Y., Meyer, H.H., and Rapoport, T.A. (2003). Function of the p97-Ufd1-Npl4 complex in retrotranslocation from the ER to the cytosol: dual recognition of nonubiquitinated polypeptide segments and polyubiquitin chains. J Cell Biol *162*, 71-84.

Yuan, X., Simpson, P., McKeown, C., Kondo, H., Uchiyama, K., Wallis, R., Dreveny, I., Keetch, C., Zhang, X., Robinson, C.*, et al.* (2004). Structure, dynamics and interactions of p47, a major adaptor of the AAA ATPase, p97. EMBO J *23*, 1463-1473.

Zhang, H., Wang, Q., Kajino, K., and Greene, M.I. (2000a). VCP, a weak ATPase involved in multiple cellular events, interacts physically with BRCA1 in the nucleus of living cells. DNA and cell biology *19*, 253-263.

Zhang, J., Zhang, L., Zhao, S., and Lee, E.Y. (1998). Identification and characterization of the human HCG V gene product as a novel inhibitor of protein phosphatase-1. Biochemistry *37*, 16728-16734.

Zhang, J., Zhang, Z., Brew, K., and Lee, E.Y. (1996). Mutational analysis of the catalytic subunit of muscle protein phosphatase-1. Biochemistry *35*, 6276-6282.

Zhang, L., Qi, Z., Gao, Y., and Lee, E.Y.C. (2008). Identification of the interaction sites of Inhibitor-3 for protein phosphatase-1. Biochem Biophys Res Commun *377*, 710-713.

Zhang, M., Chang, H., Zhang, Y., Yu, J., Wu, L., Ji, W., Chen, J., Liu, B., Lu, J., Liu, Y.*, et al.* (2012). Rational design of true monomeric and bright photoactivatable fluorescent proteins. Nat Methods *9*, 727-729.

Zhang, S., Guha, S., and Volkert, F.C. (1995). The Saccharomyces SHP1 gene, which encodes a regulator of phosphoprotein phosphatase 1 with differential effects on glycogen metabolism, meiotic differentiation, and mitotic cell cycle progression. Mol Cell Biol *15*, 2037-2050.

Zhang, X., Gui, L., Zhang, X., Bulfer, S.L., Sanghez, V., Wong, D.E., Lee, Y., Lehmann, L., Lee, J.S., Shih, P.Y.*, et al.* (2015). Altered cofactor regulation with disease-associated p97/VCP mutations. Proc Natl Acad Sci U S A *112*, E1705-1714.

Zhang, X., Shaw, A., Bates, P.A., Newman, R.H., Gowen, B., Orlova, E., Gorman, M.A., Kondo, H., Dokurno, P., Lally, J.*, et al.* (2000b). Structure of the AAA ATPase p97. Mol Cell *6*, 1473-1484.

Zhao, M., Wu, S., Zhou, Q., Vivona, S., Cipriano, D.J., Cheng, Y., and Brunger, A.T. (2015). Mechanistic insights into the recycling machine of the SNARE complex. Nature *518*, 61-67.

Zhou, H.J., Wang, J., Yao, B., Wong, S., Djakovic, S., Kumar, B., Rice, J., Valle, E., Soriano, F., Menon, M.K.*, et al.* (2015). Discovery of a First-in-Class, Potent, Selective, and Orally Bioavailable Inhibitor of the p97 AAA ATPase (CB-5083). J Med Chem *58*, 9480-9497.

Abbreviations

aa	amino acid
AAA	ATPases associated with diverse cellular activities
AAA-ATPase	ATPase associated with various cellular activities
APC/C	anaphase promoting complex / cyclosome
ATP	adenosine 5‘-triphosphate
ATPase	adenosine 5‘-triphosphatase
AurB	Aurora B
BCA	bicinchoninic acid
BiSTriP	bipartite docking site of Sds22 that interacts with the α4/α5/α6 triangular region of PP1
BS1	binding site 1
BUB	budding uninhibited by benomyl
BUBR1	Bub-related 1
CCAN	constitutive centromere-associated network
Cdc	cell division cycle
CDK	Cyclin-dependent kinase
cDNA	coding DNA
CENP	centromere protein
CHX	cycloheximide
CPC	Chromosomal passenger complex
CSF	cytostatic factor
DAPI	4',6-diamidino-2-phenylindole
ddH2O	water,deionized and sterile-filtered
DMEM	Dulbecco's Modified Eagle Medium
DNA	deoxyribonucleic acid
DOX	doxycycline
DTT	dithiothreitol
DUB	deubiquitinating enzyme
EC	error correction
ECL	enhanced chemiluminescence
EDTA	ethylenediaminetetraacetic acid
EM	electron microscopy
EMCCD	Electron-multiplying Charge-coupled Device
ER	Endoplasmic Reticulum
ERAD	ER-associated degradation
FCS	fetal calf serum
FDR	false discovery rate
GFP	green fluorescent protein
Glc	GLyCogen
GST	*Glutathione* S-transferase
H	histone
HA	hemagglutinin epitope tag
HAD	haloacid dehalogenase
HEK 293	Human Embryonic Kidney 293 cells
HeLa	Henrietta Lacks human cervical carcinoma cell line

HEPES	4-(2-hydroxyethyl)-1-piperazineethanesulfonic acid
HSC	heat shock cognate protein
HSP	heat shock protein
I2	Inhibitor-2
I3	Inhibitor-3
IDoHA	I2 docking site for the hydrophobic and acidic grooves
IDP	intrinsically disordered protein
IF	immunofluorescence
INCENP	inner centromere protein
IP	immunoprecipitation
Ipl1	Increase in PLoidy 1
K_D	dissociation constant
KD	RNAi-mediated knockdown
KMN	KNL1, Mis12, Ndc80
KNL1	kinetochore null protein 1
KO	knockout
LRR	leucine-rich repeats
Luc	luciferase
MAD	mitotic arrest deficient
MCC	mitotic checkpoint complex
Mis12	missegregation 12
Mps1	monopolar spindle protein1
mRNA	messenger RNA
MTS	3-(4,5-dimethylthiazol-2-yl)-5-(3-carboxymethoxyphenyl)-2-(4-sulfophenyl)-2H-tetrazolium)
MyPhoNE	myosin phosphatase N-terminal element
MYPT1	myosin phosphatase-targeting subunit 1
Ndc80	nuclear division cycle 80
NIPP1	Nuclear Inhibitor of PP1
NLS	nuclear localization signal
Npl4	nuclear protein localization protein 4
NSF	N-ethylmaleimide sensitive fusion protein
NuMA	nuclear mitotic apparatus protein
PAGE	polyacrylamide gel electrophoresis
pAurB	Aurora B, phosphorylated at threonine-232
pBPA	p-benzoylphenylalanine
PBS	phosphate-buffered saline
PCR	polymerase chain reaction
PDB	Protein Data Bank
PFA	paraformaldehyde
PI	propidium iodine
PIP	PP1-interacting protein
pNPP	para-nitrophenylphosphate
PP1	Protein phosphatase-1
PP1c*	PP1 catalytic subunit, newly synthesized, including all isoforms
PP2A	protein phosphatase-2A

PPM	metal-dependent protein phosphatase
PPP	phosphoprotein phosphatase
PPP1R	phosphoprotein phosphatase 1 regulatory subunit
pT232	phospho-threonine-232
PTP	protein tyrosine phosphatase
PTPA	PP2A phosphatase activator
PUB	peptide N-glycosidase / ubiquitin-associated
PUL	PLAA, Ufd3 and Lub1
Repo-Man	Recruits PP1 Onto Mitotic Chromatin at Anaphase
RNA	ribonucleic acid
RNAi	RNA interference
RRL	rabbit reticulocyte lysate
RT	room temperature
S. cerevisiae	*Saccharomyces cerevisiae*
S. pombe	*Schizosaccharomyces pombe*
s.e.m.	standard error of the mean
SAC	spindle assembly checkpoint
SD	standard deviation
SDS	sodium dodecyl sulfate
SDS22	suppressor of Dis2 mutant 2
SEP	Shp1, eyes closed and p47
SH	Strep-HA
Shp1	suppressor of high-copy PP1
siRNA	small interfering RNA
SLIM	short linear motif
SNARE	soluble NSF attachment protein receptor
SPI	SDS22-PP1-I3 complex
SpiDoC	spinophilin docking site for the C-terminal groove
SRH	second region of homology
Strep	streptavidin affinity tag
T232	Threonine-232
TE	Tris EDTA
Tris	Tris(hydroxymethyl)-aminomethan
Ub	ubiquitin
UBA	ubiquitin-associated
UBX	ubiquitin-regulatory X
UBXD	UBX domain-containing protein
Ufd1	ubiquitin fusion degradation protein 1
UPR	unfolded protein response
UPS	ubiquitin-proteasome system
UPS	ubiquitin-proteasome system
VBM	VCP-binding motif
VCP	valosin containing protein
VIM	VCP-interacting motif
wt	wild-type
XEE	*Xenopus laevis* egg extract
Ypi1	Yeast phosphatase inhibitor 1

Acknowledgements

I would like to thank, first and foremost, Hemmo Meyer for the opportunity and his trust in my work on this project. His support allowed me to develop and refine ideas, while his guidance kept the project on the best possible track. I am also grateful for his help in expanding my scientif hoirzon by fostering collaborations outside Essen.

My colleague, Jonas Seiler and former colleague, Annika Eiteneuer were incredibly supportive during my early days in Hemmo's lab. I want to thank you for sharing your experience in this project and for your time spent in discussions and for the great collaboration. Jonas was a constant support till the end of my thesis and I am glad he stayed with us during this time.
I am thankful to Johannes van den Boom for sharing valuable experience with various methods, great advice and for his wonderful work on figures. Most of all, thank you for critical reading of this thesis.
Furthermore, Julia Hülsmann and Matthias Kracht were wonderful colleagues and I am happy to have worked with you in the last years.
During my thesis I had the oppurtunity to meet great people outside our lab and first of all, I would like to thank Mathieu Bollen for the support and scientific discussions at several stages of my thesis. His advice was of great value for our project and my thesis. I am also grateful for discussion and communication with Javier del Pino Garcia, who added valuable insight.
There were many more colleagues who supported me in this project. With apologies to all who I do not include here, I would like to thank Nina Schulze for introduction and continous support with microscopy, Ivana Primorac and Dana Hönig for their expertise on protein purification and Marc Schuster for his help with flow cytometry.
This thesis would look different if it was not for our technical assistant Sabine Effenberger, whose contribution was indispensable. I would also like to thank Miram Schmidt an Christina Kamp-Meltzer for organizational support.

My friends and family were a never ending source of motivation and support. I am happy to have been supported by great parents who always helped with their love and guidance.
My wife Tara is the person I have to thank most of all for supporting me in this time. The time spent with you in these years is the best I can remember. Hamishe movasebbe hamdigar bemanim! Dooset daram.

Der Lebenslauf ist in der Online-Version aus Gründen des Datenschutzes nicht enthalten.

Affidavits / Erklärungen

Erklärung:

Hiermit erkläre ich, gem. § 6 Abs. (2) f) der Promotionsordnung der Fakultäten für Biologie, Chemie und Mathematik zur Erlangung des Dr. rer. nat., dass ich das Arbeitsgebiet, dem das Thema „“ zuzuordnen ist, in Forschung und Lehre vertrete und den Antrag von Matthias Weith befürworte und die Betreuung auch im Falle eines Weggangs, wenn nicht wichtige Gründe dem entgegenstehen, weiterführen werde.

Essen, den _____ _____

Unterschrift eines Mitglieds der Universität Duisburg-Essen

Erklärung:

Hiermit erkläre ich, gem. § 7 Abs. (2) c) + e) der Promotionsordnung der Fakultäten für Biologie, Chemie und Mathematik zur Erlangung des Dr. rer. nat., dass ich die vorliegende Dissertation selbständig verfasst und mich keiner anderen als der angegebenen Hilfsmittel bedient habe.

Essen, den _____ _____

Unterschrift des/r Doktoranden/in

Erklärung:

Hiermit erkläre ich, gem. § 7 Abs. (2) d) + f) der Promotionsordnung der Fakultäten für Biologie, Chemie und Mathematik zur Erlangung des Dr. rer. nat., dass ich keine anderen Promotionen bzw. Promotionsversuche in der Vergangenheit durchgeführt habe und dass diese Arbeit von keiner anderen Fakultät/Fachbereich abgelehnt worden ist.

Essen, den _____ _____

Unterschrift des/r Doktoranden/in